



**HAL**  
open science

# Severe osmotic compression of the yeast *Saccharomyces cerevisiae*

Agnès Miermont

► **To cite this version:**

Agnès Miermont. Severe osmotic compression of the yeast *Saccharomyces cerevisiae*. Biophysics. Université Paris-Diderot - Paris VII, 2013. English. NNT: . tel-00864602

**HAL Id: tel-00864602**

**<https://theses.hal.science/tel-00864602>**

Submitted on 23 Sep 2013

**HAL** is a multi-disciplinary open access archive for the deposit and dissemination of scientific research documents, whether they are published or not. The documents may come from teaching and research institutions in France or abroad, or from public or private research centers.

L'archive ouverte pluridisciplinaire **HAL**, est destinée au dépôt et à la diffusion de documents scientifiques de niveau recherche, publiés ou non, émanant des établissements d'enseignement et de recherche français ou étrangers, des laboratoires publics ou privés.

Pour obtenir le grade de DOCTEUR DE L'UNIVERSITÉ PARIS DIDEROT

Spécialité : Biophysique

Ecole doctorale Interdisciplinaire Européenne Frontières du Vivant (ED 474)

Laboratoire Matière et Systèmes Complexes

# Severe osmotic compression of the yeast *Saccharomyces cerevisiae*

présentée par :

---

**Agnès MIERMONT**

Soutenue le 8 Février 2013 devant le jury composé de:

Emmanuelle Fabre	Directeur de Recherche, CNRS	Présidente du jury
Damien Baigl	Professeur Université Paris 6, CNRS	Rapporteur
Frédéric Devaux	Professeur Université Paris 6, CNRS	Rapporteur
Sébastien Léon	Chargé de Recherche, CNRS	Examineur
Francesc Posas	Professeur, Universitat Pompeu Fabra, Espagne	Examineur
Pietro Cicuta	Lecturer, Cambridge University, Angleterre	Examineur
Pascal Hersen	Chargé de Recherche, CNRS	Directeur de thèse



## ACKNOWLEDGEMENTS

*J'ai décidé d'écrire mes remerciements en anglais et en français ayant eu la chance de travailler et d'interagir avec des personnes de différentes nationalités.*

*I first would like to deeply thank all the members of my Ph.D. committee, Damien Baigl, Frédéric Devaux, Emmanuelle Fabre, Sébastien Léon, Francesc Posas and Pietro Cicuta. I am heartily grateful to all of them for having accepted to be part of my Ph.D. committee, for the time spent on my manuscript and for the time taken to travel to Paris, or simply to Paris Diderot.*

*Je remercie énormément Pascal Hersen de m'avoir encadré pendant ces trois dernières années. Merci pour ta patience à m'inculquer quelques bases de physique, pour tes nombreux encouragements qui m'ont aidé à avancer dans les moments difficiles et merci pour ta grande disponibilité malgré tes absences singapouriennes. En tant que première doctorante, je sais que cet encadrement a pu être source de stress et je crois pouvoir dire que j'ai bénéficié d'une attention particulière. J'espère avoir la chance de pouvoir toujours travailler avec des personnes aussi ouvertes, humaines et compréhensives.*

*Merci à Samuel Bottani pour son implication dans ce projet. Merci pour ton écoute, nos discussions, tes nombreux conseils et soutiens que ce soit au sein du laboratoire ou de l'école doctorale.*

*Merci à Sébastien Léon pour son aide et soutien tout au long de ma thèse. Merci d'avoir pris de ton temps pour m'apprendre les bases de la levure, pour nous avoir dépanné de si nombreuses fois en matière de souches ou de plasmides et pour m'avoir souvent accueillie au sein de ton laboratoire que ce soit pour des discussions ou la réalisation d'expériences.*

*Merci à Gilles Charvin qui a été un tuteur excellent malgré la distance. Merci pour nos discussions, pour tes conseils et ton aide précieuse de par l'aspect interdisciplinaire du projet. Merci aussi pour m'avoir accueillie à Strasbourg et pour m'avoir aidée dans mes préparations de conférences.*

*To Megan McClean who welcome me in her laboratory. Thank you very much for letting me dispose of your laboratory as I wished. Thank you also for your availability, your listening and support despite the limited time you had available at that time.*

*To Shiqiong Hu who teach me so much during my stay in Singapore. Thank you for your patience, your help, your support when I started writing my thesis but also thank you a lot for being so joyful, for your huge generosity and for initiating me to the so good Asiatic culinary culture.*

*Merci à Jannis Uhlendorf et Clément Vulin pour votre aide, vos idées, vos conseils, votre bonne humeur et soutien au quotidien. Merci aussi d'avoir toujours été là pour les dépannages de dernières minutes sur le microscope ou pour bricoler une manip.*

*Merci à François Whaharte pour ton aide précieuse sur l'aspect microscopie du projet. Merci aussi pour ta patience à répondre à mes nombreux mails, à m'expliquer et me réexpliquer des principes de microscopie ou des modèles mathématiques, et enfin merci pour ton intérêt pour le projet malgré des levures souvent récalcitrantes !*

*Merci aussi à Carole Barache, Nadine Beyer, Lucie Bouchu et Danielle Champeau qui s'occupaient de la comptabilité et de l'administration.*

*Merci à Laurent Réa qui a fait les pièces métalliques de la manip.*

*Un grand merci à toutes les personnes qui ont été là au quotidien et grâce à qui ces années ont été géniales : Jannis Uhlendorf mon camarade de HOG, Clément Vulin qui m'a fait rêver avec son projet de tour Eiffel en levure, Fanny Evenou et nos parties endiablées de fléchettes, Kelly Aubertin et ses petits gâteaux remonte-moral, Alain Richert pour nos escapades au magasin de l'IJM et bien sur Loudjy Chevry pour nos arrachages de cheveux sur Word mais surtout pour nos nombreux fous rires.*

*Merci aussi au bureau 756A pour sa bonne humeur, ses petits déjeuners du vendredi matin, ses pauses café et ses papotages à toutes heures.*

*Un grand merci à ma famille, merci pour votre soutien malgré la distance.*

*Enfin un merci tout particulier à Vincent. Merci d'avoir toujours été là pour me supporter, m'encourager et me conseiller.*

# TABLE OF CONTENTS

TABLE OF CONTENTS	5
RÉSUMÉ	7
CONTEXT	9
CHAPTER 1.	
INTRODUCTION	13
<b>1. Macromolecular crowding</b>	<b>14</b>
<i>In vitro</i> approaches	15
<i>In vivo</i> approaches	18
Cell volume and optimal molecular crowding?	21
<b>2. Challenging macromolecular crowding through cell volume compression</b>	<b>26</b>
The mechanism of osmosis	26
Osmotic behavior of biological membrane	30
Physiological response to osmotic stress	34
Mechanisms of cell volume regulations	35
<b>3. Signaling osmostress in yeast</b>	<b>39</b>
MAP Kinase pathways in yeast	39
The HOG pathway	44
<b>4. The HOG pathway as a systems biology model</b>	<b>50</b>
A word on microfluidics	50
Frequency response of the HOG pathway	52
OBJECTIVES	57
CHAPTER 2.	
OSMOTIC COMPRESSION SLOWS DOWN THE HOG PATHWAY	59
<b>5. Cellular compression triggers a slow-down of the HOG pathway</b>	<b>60</b>
Hog1 nuclear localization kinetics	60
Hog1 phosphorylation kinetics	64
Comparing phosphorylation and nuclear import of Hog1	65
Cell volume decrease as a function of osmotic stress	66
Hog1 diffusion kinetics	69
<b>6. Discussion</b>	<b>76</b>

CHAPTER 3.	
GLOBAL EFFECT OF MACROMOLECULAR CROWDING ON INTRACELLULAR DYNAMICS	81
<b>7. Other processes slow down caused by cellular compression</b>	<b>82</b>
Msn2, Yap1, Crz1 and Mig1 nuclear translocation dynamics	82
Crz1 and Msn2 nuclear imports are independent of the HOG pathway	86
<b>8. Cytoplasmic diffusion under compression</b>	<b>88</b>
Citrine, YFP and Ura1-GFP diffusion in yeast	88
GFP diffusion in the human cell lines	89
<b>9. Endocytosis and other active processes</b>	<b>91</b>
<b>10. Jamming recovery after a short period of intense compression</b>	<b>93</b>
<b>11. Discussion</b>	<b>95</b>
CONCLUSION AND PERSPECTIVES	99
APPENDIX	107
<b>12. Supplementary Results</b>	<b>108</b>
Hog1 dynamics at very severe stress	108
Pre-stressing the cells improves their adaptation to compression	109
The cells sense the rate of increase of the input intensity	110
Cell death after long periods of severe stresses	113
<b>13. Supplementary Data</b>	<b>114</b>
Bionumbers	114
Osmotic Pressure: order of magnitude	114
<b>14. Materials and Methods</b>	<b>115</b>
Yeast strains	115
Culture conditions and media	115
Strains list	116
Mammalian cell lines	117
Inverted fluorescent microscopy	118
FRAP and FLIP microscopy	118
Western blot	119
Images analyses / Quantification of the relative nuclear localization	120
Quantification of the cellular volume	122
FRAP and FLIP analysis	123
Quantification of the diffusion coefficient	123
BIBLIOGRAPHY	125
Appended Articles	141

## RÉSUMÉ

Les cellules ont développé plusieurs voies de signalisation et de réponses transcriptionnelles pour réguler leur taille et coordonner leur croissance et leurs divisions cellulaires. L'intérieur des cellules est naturellement surchargé par des macromolécules. Cet encombrement macromoléculaire, appelé *crowding*, a été intensément étudié *in vitro* et est connu pour affecter la cinétique des réactions. Cependant, l'étude des effets d'encombrement *in vivo* est plus difficile en raison du haut niveau de complexité et d'hétérogénéité à l'intérieur d'une cellule. Au cours de cette thèse, nous nous sommes intéressés aux effets de changement du volume cellulaire sur la cinétique de réactions biochimiques chez la levure *Saccharomyces cerevisiae*. Pour cela, nous avons induit des stress osmotiques pour comprimer la cellule et étudier l'impact du *crowding* sur les cinétiques de signalisation. La réduction du volume cellulaire augmente la viscosité interne et peut retarder le fonctionnement de plusieurs voies de signalisation et de processus cellulaires. En augmentant progressivement le niveau de compression, on observe un ralentissement des processus biologiques jusqu'à un point où l'adaptation cellulaire est abolie. Ceci a été observé pour la translocation nucléaire de facteurs de transcription (Hog1, Msn2, Crz1, Mig1 et Yap1) ainsi que pour la mobilité des protéines Abp1 et Sec7. Nous montrons aussi que la compression altère la capacité de plusieurs protéines à diffuser dans le cytoplasme de différents types cellulaires. Nous proposons que ces altérations cinétiques induites par l'augmentation de la viscosité intracellulaire ne soient pas sans rappeler une transition vitreuse. Ces résultats suggèrent l'importance d'un encombrement macromoléculaire optimal permettant aux cellules de fonctionner correctement.



## CONTEXT

This thesis starts with a simple observation: living cells are densely packed with macromolecules. Their interior is said to be crowded and is very different from a dilute environment. In terms of magnitude, macromolecules occupy an important fraction of the cytoplasm of living cells – which may be as high as 30-40% of the total cell volume [1]. The aspect of a biological interior was nicely illustrated by Goodsell: proteins and cytoskeleton structures are entangled and fill the whole cytoplasm (Figure 1). This can also be seen on an electron tomography image of the crowded cytoplasm of *Dictyostelium discoideum* cells [2] (Figure 1). Those observations of a dense cytoskeleton composed of a complex mesh of actin filaments support the idea that the cell interior is densely filled with heterogeneous and multi-scaled structures. There is apparently little space available for proteins to move freely in the cytoplasm.

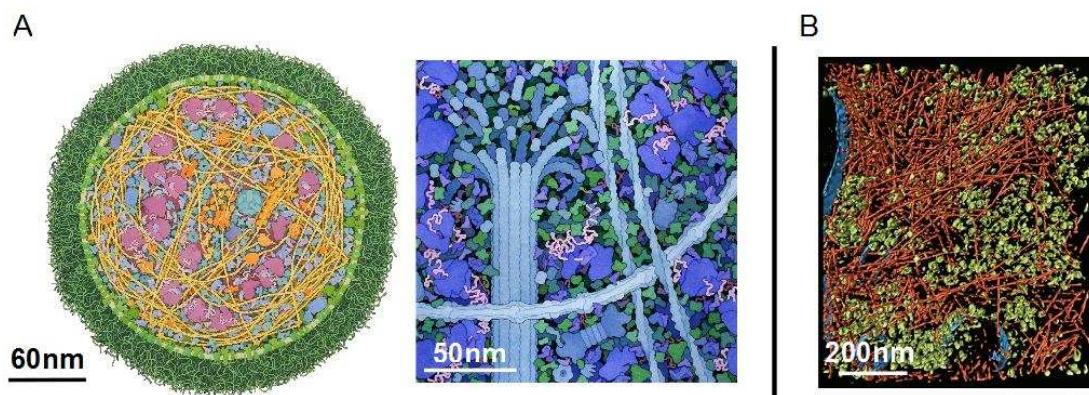


Figure 1. (A) Representation of internal cellular environments. (Left) Section of a *Mycoplasma mycoides* cell showing DNA (yellow filaments), DNA polymerases (yellow round shape molecules) and ribosomes (purple molecules). (Right) Portion of an eukaryotic cytoplasm showing the cytoskeleton filaments and the ribosomes. (D.S. Goodsell, the Scripps Research Institute). (B) Electron tomography visualization of the sub-cellular structures of a *Dictyostelium discoideum* cell. Actin filaments are shown in red, ribosomes and other macromolecules in green and membrane parts in blue (from Medalia *et al.*[2]).

However, proteins do move in the cytoplasm and their mobility is crucial for many biochemical reactions to occur and thus for a proper cell activity. Chemical solutions with a high volume fraction of molecules create what is called a crowded environment. The term concentrated is not really appropriate here, because, as it is the case in a cellular context, single molecules or proteins may not be present at high

## Context

concentrations. Instead, it is the sum of many low-concentrated macromolecules species that gives rise to a crowded interior [1, 3]. Macromolecular crowding has been studied for years, mostly *in vitro*. It is generally expected to alter the thermodynamics and kinetics of biochemical reactions when compared to the case of a dilute solution [4]. While macromolecular crowding may enhance some reactions by increasing the encounter frequency between chemical partners because of a smaller distance between molecules, the rate of protein encounters may also decrease due to the difficulty for proteins to move around. It comes through that crowding affects biochemical reactions depending on their rate-limited step [5, 6]. Hence, predicting the impacts of crowding is not a trivial task. Although, macromolecular crowding has been studied in numerous *in vitro* experiments, its impact in a cellular context has been mostly overlooked. A few studies have measured the chemical properties of proteins and kinetics of some biochemical reactions *in vivo* and compared it to what was known *in vitro*. Notably, differences were observed for protein stability [7] and protein diffusion rate [8].

In turn, we can wonder what would happen if the cell volume was reduced, and thus the intracellular concentrations and macromolecular crowding were further increased. Indeed, the cell volume can be altered by multitude parameters linked to osmosis deregulations. To give a few examples: in ischemia, the impairment of Na<sup>+</sup>K<sup>+</sup>ATPase channel leads to NaCl accumulation and cell swelling [9]. Hormones, like glucagon or insulin in hepatocytes trigger the abnormal motion of electrolytes across the plasma membrane leading to volume deregulation [10]. Metabolic reactions can also alter the cellular volume. For instance, muscle cells accumulate lactate after exercise, increasing the intracellular osmolarity and triggering cell swelling. Modification of the extracellular concentration, and thus of the external osmotic pressure, also leads to volume changes. The kidney medullary cells<sup>1</sup> are naturally exposed to high concentration of salt (NaCl) and urea due to the concentrating action of the urinary system [11]. It is important to note that osmotic

---

<sup>1</sup> The renal medulla is the innermost part of the kidney. The renal medulla contains the structures of the nephrons which is responsible for maintaining the salt and water balance of the blood. The interstitium of the renal medulla is hypertonic, providing osmotic gradient for water reabsorption.

stress also alters various biological processes. For example, hyper-osmotic stress triggers cytoskeleton disintegration [12], endocytosis impairment [13] and alterations of the nucleo-cytoplasmic transport [14]. Cells have evolved different mechanisms to cope with osmotic challenges, and the genetic network and signaling pathways at play are usually well characterized. However, the relations between osmotic challenges, the induced molecular crowding and the cell functioning are mostly unexplored.

We are left with numerous interrogations regarding the importance of molecular crowding in cells and how it is linked with the physiological response to osmotic stress. The aim of this thesis is precisely to explore this link by quantifying the dynamics of several cellular processes in live cells immediately after hyper-osmotic compression.

I will use the yeast *Saccharomyces cerevisiae* as a model organism. This classic eukaryotic model has the advantages to be easily imaged by microscopy and genetically manipulated through homologous recombination. Many of its cellular processes are well understood, at least mechanistically. It is also a perfect model for quantitative studies, and it has been used as such by several groups working at the interface between physics, computational biology and biology.

Yeast cells detect, signal and adapt to a hyper-osmotic stress through the HOG pathway (High Osmolarity Glycerol). HOG is viewed as a canonical pathway for signal processing in living cells and has received considerable attention these past 10 years. A key feature of the HOG cascade is the phosphorylation and nuclear translocation of the protein Hog1 upon hyper-osmotic stresses. Its nuclear import occurs usually after a few minutes, is very reproducible and has been used as a robust output of the HOG cascade.

My PhD started with a counter-intuitive observation: the HOG cascade activation kinetics was slower after a severe osmotic stress than after a mild one. I expected to observe a stronger response, which would have allowed the cell to better adapt to a harsher environment. I then postulated that this change of dynamics could be due to the increased macromolecular crowding in the cytoplasm and designed a set of

## Context

experiments to test that hypothesis. Before describing these experiments in details, I will first briefly review what is known on macromolecular crowding. I will then focus on the description of the volume regulatory mechanisms in yeast, including a description of the HOG cascade. I will then show that osmotic compression leads to a progressive slow-down of the phosphorylation, the nuclear translocation and the mobility of the key protein Hog1. In the last chapter we will see that a qualitatively similar effect is obtained with other dynamical processes (nuclear translocation of transcription factors and protein diffusion). The final discussion will outline the relation between our findings and the glassy-like phase transition that occurs in colloidal systems and progressively leads to a jammed system when the colloid density increases.

## CHAPTER 1.

### INTRODUCTION

<b>1. Macromolecular crowding</b>	<b>14</b>
<i>In vitro</i> approaches	15
<i>In vivo</i> approaches	18
Cell volume and optimal molecular crowding?	21
<b>2. Challenging macromolecular crowding through cell volume compression</b>	<b>26</b>
The mechanism of osmosis	26
Osmotic behavior of biological membrane	30
Physiological response to osmotic stress	34
Mechanisms of cell volume regulations	35
<i>Solutes transport</i>	37
<i>Organic solutes transport</i>	38
<b>3. Signaling osmostress in yeast</b>	<b>39</b>
MAP Kinase pathways in yeast	39
The HOG pathway	44
<b>4. The HOG pathway as a systems biology model</b>	<b>50</b>
A word on microfluidics	50
Frequency response of the HOG cascade	52

## 1. Macromolecular crowding

As we briefly discussed, the intracellular medium is said to be *crowded*, *confined* or *volume occupied*. Crowding and confinement have slightly different definitions although inducing similar effects. While macromolecular crowding refers to the situations resulting from interactions of one soluble molecule to another, macromolecular confinement points out the effect of the physical sequestration of soluble molecules by fixed boundaries [15]. In other words, confinement occurs when large particles are constrained to small compartments or pores with dimensions comparable to the size of macromolecules. Macromolecular crowding and confinement are interdependent and based on steric effects. Their joint actions impact the thermodynamics and kinetics of reactions. In the bacteria *Escherichia coli*, the cytoplasmic macromolecular total concentration is about 300-400 g/L [16].

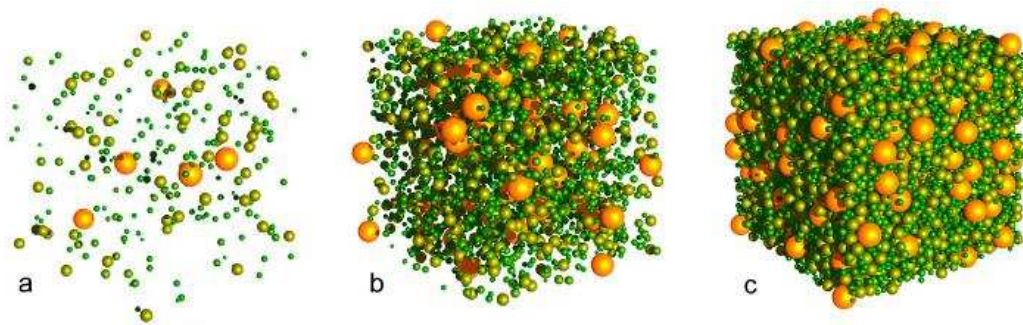


Figure 2. Virtual cytoplasm in which the volume fraction occupies respectively 1% (a), 10% (b), and 50% (c) of the overall volume. Figure from Ridgway *et al.* [17].

In *Saccharomyces cerevisiae* the density of macromolecules is about the same. It can be estimated<sup>2</sup> around 330 g/L. This means that typically 30% of the yeast cell volume is physically occupied by macromolecules and organelles. Similarly, Lanni *et al.* estimated the intracellular density of mammalian cells around 200-300 g/L by using refractive index measurement [18]. As reviewed by Fulton in 1982, 17 to 35% of the total volume of most living cells is physically occupied by macromolecules [1] which means that the cell interior is very crowded, and far from the case of dilute

---

<sup>2</sup> The mean volume of a cell ( $V=37 \mu\text{m}^3$ ; [197]) and the cell density ( $\eta=1.1 \text{ g/ml}$ ; [200]), gives a total cell mass ( $m_T$ ) around  $40.7 \mu\text{g}$ . The fraction of cell mass occupied by water is 60% [199]. Therefore, the dry mass ( $m_d$ ) represents 40% of the wet mass, that is  $16 \mu\text{g}$ . The cell wall represents 24.5% of the dry mass [201]. Consequently, the protein mass inside the cell ( $m_p$ ) is  $12 \mu\text{g}$ . As the mean volume of a cell is  $37 \mu\text{m}^3$ , the density of macromolecules inside *S. cerevisiae* roughly is 330 g/L.

solution studied *in vitro* (1-10 g/L). In Figure 2, the situation with different volume fractions are represented and give an appreciable view of how *crowded* the intracellular medium can be. The total occupancy of molecules may impact the equilibrium thermodynamics and kinetics of biological reactions when compared to *in vitro* kinetics in a diluted environment. Macromolecular crowding is simply due to the mutual impenetrability of molecules caused by steric repulsion. Steric repulsion is always present for molecules whatever the others repulsive or attractive interactions. From steric repulsion emerges the existence of an excluded volume representing the part of the total volume that cannot be filled by another macromolecule. This excluded volume depends on the number, size and shape of the molecules present in the solution (Figure 3).

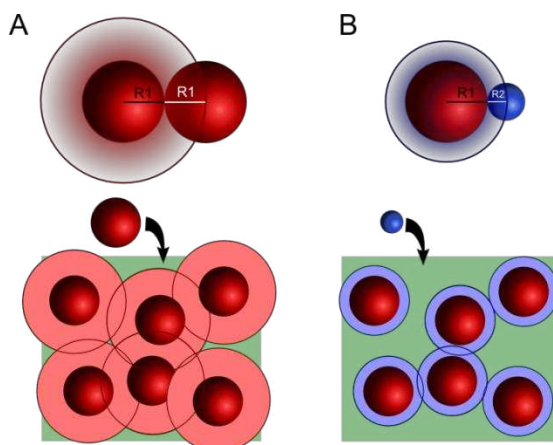


Figure 3. Representation of the excluded volume. The minimal distance a particle can approach another is defined by the radius of the smallest particle (top panel). Hence, if a particle is added to a finite system containing particles of the radius  $R_1$ , the available volume (shown in green) would be higher for a smaller particle (blue) than a particle of the same radius. Reproduced from Rivas *et al.* and Minton *et al.* [6, 19].

### *In vitro* approaches

Since the 60's, macromolecular crowding has been studied in the context of deciphering its effects on the thermodynamic equilibrium of chemical reactions, macromolecules stability and association rates. Macromolecular crowding is studied *in vitro* by the addition of a crowding agent to a set of test molecules. The crowding agent is usually chosen with a molecular mass between 50 and 200 kDa and does not interact with the tested proteins so that it only increases the excluded volume and changes steric repulsion between molecules [20]. Common macromolecular agents are polyethylene glycol [21], polyvinyl alcohol [22], dextrans [5], ovalbumin, albumin or haemoglobin [23]. The thermodynamic stability of protein folding,

## Chapter 1. Introduction

molecules association, enzyme kinetics or stability of protein oligomers are frequent subjects of investigations (Table 1). Ogston and Laurent were among the firsts to describe experimentally the physical chemistry effects of macromolecular crowding. They showed that the addition of crowding agents to serum albumin *in vitro* influenced the thermodynamic activities of the solution. They proposed that the impenetrability of particles, and so volume exclusion, can explain the effects observed when increasing the macromolecular crowding. Subsequent studies mainly involved the coupling of mathematical models with *in vitro* experiments. The Minton group [3, 4] extended the work of Ogston and Laurent and theoretically demonstrated the importance of volume exclusion on the thermodynamics effects of crowding. Their model described the effects of macromolecular crowding as a shift in the thermodynamic equilibrium in favor of the more compact structure. Several groups have also studied macromolecular crowding and confinement using theoretical approaches. For instance, the Zhou group combined modeling and experimentation to describe the effect of macromolecular agent like dextran on proteins folding and interactions stability [24]. In general, macromolecular crowding is predicted to stabilize compact states relative to less compact unfolded states. For instance, macromolecular crowding is seen to alter the refolding of reduced lysozyme and triggers aggregation *in vitro*. Yet, aggregation can be prevented by the action of molecular chaperones [25, 26]. Aggregation, in contrast to polymerization, involves proteins in non-native conformations and is irreversible. Amyloid fibrils are insoluble fibrous structured associate with numerous pathologies. The use of crowding agents like random coil polymers, cross-linked polymers, and native proteins accelerates the rate of amyloid fibers formations as observed for alpha-synuclein<sup>3</sup> [27]. In addition, macromolecular crowding enhances protein association. Among others, it promotes the association of ribosomal subunits [28] and favors fibrous protein formation through polymerization like hemoglobin [23], F-actin [21] and fibrin gels [29]. Finally, macromolecular crowding has also been shown to facilitate the association of DNA with its targeting proteins

---

<sup>3</sup> Alpha-synuclein is a soluble protein that is prominently expressed in the central nervous system. In pathological conditions, alpha-synuclein aggregates to form insoluble fibrils that are hallmarks of some neurodegenerative diseases (synucleinopathies).

and to enhance or favor DNA compaction [30]. Crowding effects on the kinetics of reactions are also non-negligible. Leduc *et al.* in 2012 analyzed *in vitro* the effect of macromolecular crowding on the motion of molecular motor on cytoskeleton filaments. They postulated that molecular motors have evolved to operate in crowded cellular environments. However, by increasing the concentration of the motor protein kinesins above physiological conditions, they observed a decrease in its velocity [31]. Similarly, *in vitro* diffusion of globular proteins are lower in a crowded solution of either hydrophilic polymers [32] or hydrogels [33].

Table 1. Effects of macromolecular crowding; reproduced and modified from [39].

<b>Macromolecular crowding effects on association equilibria</b>	
<b>Dextran 10K</b>	Enhances the formation of a decamer of bovine pancreatic trypsin inhibitor
<b>Bovine Serum Albumin (BSA) or ovalbumin</b>	Increases the binding affinity of replication protein RepA for specific DNA sequences
<b>Protein RNase A</b>	Promotes the dimerization of tracer apomyoglobin
<b>Reported effects of macromolecular crowding on protein stability with respect to denaturation</b>	
<b>Dextran 30K</b>	Stabilizes the molten globule conformation of apomyoglobin at pH 2 with respect to heat and cold-induced unfolding
<b>PEG 20K</b>	Refolding rate of Rd-apocyt b562 increases by 30% at 30°C
<b>PEG 4K</b>	Increases the melting temperature $T_m$ for thermal denaturation of DNase I
<b>Reported effects of macromolecular crowding on enzyme activity</b>	
<b>PEG 6K</b>	Increases enzyme activity of <i>Escherichia coli</i> AspP
<b>Polymeric crowding agents</b>	Enzymatic activity increases and then decreases with increasing concentration of protein crowding agents
<b>PEG 4K to 20K</b>	Enhances activity of DNase I and S1 nuclease, does not significantly affect activity of exonuclease III, and decreases activity of exonuclease I
<b>Reported effects of macromolecular confinement on protein stability and conformation</b>	
<b>Polyacrylamide gels</b>	Increases the melting temperature $T_m$ of several proteins
<b>Mesoporous silica and addition of 0.4 M urea</b>	Confinement of glucose isomerase increases specific activity
<b>Cavity of GroEL/GroES</b>	Confinement of several proteins accelerates or decelerates rate of refolding in a size-dependent manner

## Chapter 1. Introduction

Despite the diversity of experimental conditions (crowding agents, particles concentration, molecular weight) the results evidence that there are quantitatively significant differences between a crowded environment and a dilute solution. It is however difficult to extrapolate from those studies since they are performed in ideal minimalist conditions far from actual biological conditions.

### ***In vivo* approaches**

Cells are not only densely filled with macromolecules. They are also composed of many different, interacting proteins moving in a heterogeneous, compartmentalized structure. The effects of macromolecular crowding alone on biochemical and biophysical cellular reactions are thus difficult to investigate in living cells. Yet, some groups managed to study these effects on protein stability and folding. For instance, the group of Oas analyzed the stability of the protein  $\lambda_{6-85}$  in *E. Coli*. Their method is based on the detection by MALDI<sup>4</sup> mass spectrometry of the amide hydrogen exchange as a marker of the protein folding stability. While the hydrogens are usually protected from exchange upon native conformation of the protein, unfolded state exposed them to the solvent and led to their release. The authors compared the stability measured *in vivo* with previous *in vitro* data and concluded that increasing crowding *in vivo* enhances the protein stability [7]. The group of Gierasch developed a method to tag the cellular retinoic acid-binding protein I (CRABP). They observed that the folding behavior and properties observed of the protein in *E. coli* was consistent with *in vitro* studies [34]. Moreover, the 3D visualization with high resolution of complex physiological environment is now possible using cryo-electron tomography [2]. Also, cell organelles and protein mobility can be efficiently observed using microfluidic techniques coupled to microscopy [35]. In particular, diffusion of proteins is expected to decrease in a crowded environment. This can be checked at the single cell level using

---

<sup>4</sup> The Matrix-Assisted Laser Desorption/Ionization (MALDI) technique is a mass spectrometry method that increased the upper mass limit of classical analyses of biomolecules to over 300,000 Da.

Fluorescence Recovery After Photobleaching (FRAP)<sup>5</sup> or Fluorescence Correlation Spectroscopy (FCS)<sup>6</sup>. In 2004, Weiss and collaborators analyzed by FCS the diffusion of fluorescent dextran in the cytoplasm of HELA cells [8]. They observed an abnormal sub-diffusion process<sup>7</sup> of dextran polymers. Using computer simulations, they demonstrated that macromolecular crowding is implicated in this process. Kao *et al.* measured the diffusion of fluorescent particle in Swiss 3T3 fibroblasts. They observed a decrease in the cytoplasmic diffusion of the small fluorescent probe BCECF upon cell volume reduction (Figure 4A) [36].

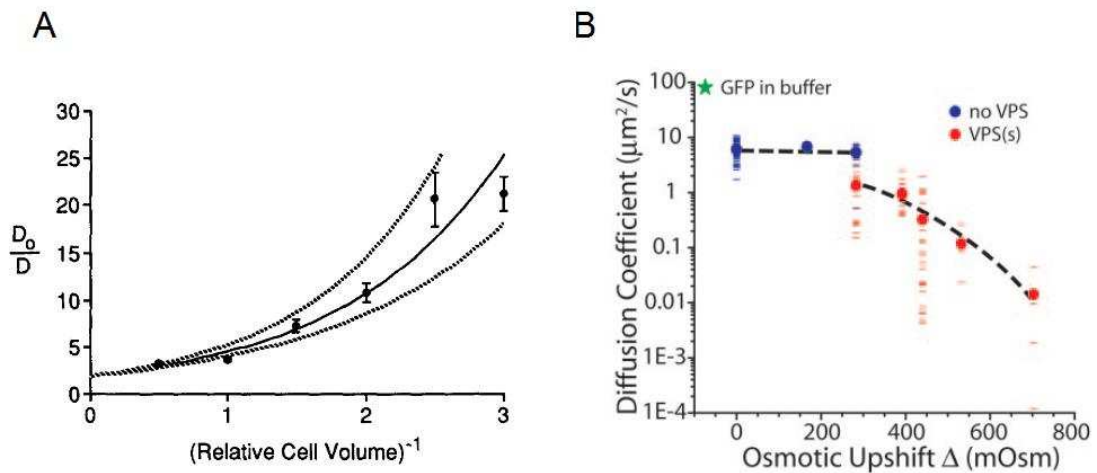


Figure 4. *In vivo* effects of increasing macromolecular crowding on proteins diffusion. (A) Diffusion of BCECF inside 3T3 fibroblasts measured as a function of the inverse of the relative cell volume ( $V_0/V$ ). The diffusion of the fluorescent probe BCECF is decreased upon volume reduction. Data are represented as the mean  $\pm$  standard error of the mean for three to seven measurements. Taken from Kao *et al.* [36]. (B) GFP diffusion in *E. coli* plotted in function of osmotic up-shift. The authors observed the apparition of Visible Plasmolysis Spaces (VPSs) above 280 mOsm/L that correlates the rapid decrease of GFP diffusion. Taken from Konopka *et al.* [37].

<sup>5</sup> Fluorescence Recovery After Photobleaching (FRAP) is a method for measuring the dynamics of 2D or 3D molecular mobility such as diffusion or transport. A defined region is photobleached and the recovery of fluorescence is monitored. The time of recovery is given by the motion of the remaining fluorescence particles.

<sup>6</sup> Fluorescence Correlation Spectroscopy (FCS) is a technique in which spatial fluctuations of the fluorescence intensity are measured in a microscopic volume of about  $10^{-15}$  L (1 femtoliter) defined by a focused laser beam.

<sup>7</sup> Sub-diffusion processes are characterized by deviations from the classical Brownian diffusion. The mean square displacement of a subdiffusive particle increases sublinearly with time. The degree of this abnormality depends on the size and conformation of the traced particle and on the total protein concentration of the solution.

## Chapter 1. Introduction

Similarly, Konopka *et al.* performed FRAP experiments in *E. coli*. FRAP is more difficult to achieve with bacteria than in mammalian cells due to their small size ( $\sim 2 \mu\text{m}$ ). Nevertheless, the authors managed to quantify a decrease in diffusion of the GFP protein when the osmotic stress was increased, and thus the cell size was decreased (Figure 4B) [37]. This is an important result, since it suggests that the cells dynamics can be altered upon volume compression, as we hypothesized in the introduction.

Indeed, applying a hyper-osmotic stress triggers the cell shrinkage and the densification of its intracellular environment. Hence, it increases the level of macromolecular crowding. Hyper-osmotic stress is known to have several physiological consequences on intracellular organization, notably on organelles. For example, osmotic stress induces the transient disintegration of both actin and microtubule cytoskeleton [12]. It also affects the vacuoles morphology in *S. cerevisiae*. Vacuoles are the most prominent organelle in yeast and have a central role in osmoregulation due to their capacity to stock water. After an osmotic stress, the vacuoles divide in numerous smaller vacuole fragments [38]. In another study, the impact of osmotic stress on the size and morphology of the nucleus in mammalian cells has been computed. The authors predicted that the nucleus shrinks proportionally to the cell size [39]. Petelenz-Kurdziel *et al.* confirmed these results by measuring in *S. cerevisiae* the size of both the cell and the nucleus upon various NaCl concentrations [40]. In agreement with modeling, they observed a linear variation of the nucleus size with the overall cell compression notably at low concentration (100 mM NaCl). However, the nuclear volume recovered the osmotic stress faster than the whole cell size, especially at high concentrations ( $> 400 \text{ mM NaCl}$ ). Despite those known macrostructures alterations, it is not easy to discriminate between a biological-physiological response and the crowding effect due to the increase of the excluded volume.

## Cell volume and optimal molecular crowding?

As previously mentioned, the volume fraction occupied by macromolecules may be as high as 30 to 40%. Most eukaryotes present a similarly high crowded intracellular environment even though their typical dimensions vary between 5 and 100  $\mu\text{m}$  (Figure 5 and Table 2).

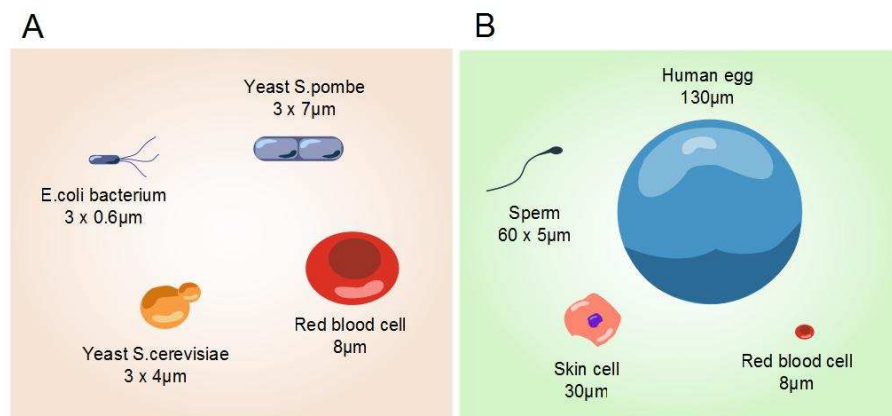


Figure 5. Cell size heterogeneity. (A) Comparison of cell sizes between different species. (B) Comparison of cell sizes in same organism (human). Reproduced from: <http://learn.genetics.utah.edu/>.

Table 2. Dimensions rates are taken from [41–43].

Species	Dimensions			Reactions rates	
	Diameter ( $\mu\text{m}$ )	Volume ( $\mu\text{m}^3$ )	Genome (Mbp)	Diffusion of proteins ( $\mu\text{m}^2\cdot\text{s}^{-1}$ )	Cell cycle (min)
<i>Escherichia coli</i>	0.7-2	0.5-5	5	7.7	20-40
<i>Saccharomyces cerevisiae</i>	3-6	20-160	12	15	70-140
<i>Schizosaccharomyces pombe</i>	3.7-5	92	13.8	-	90-180
<b>Animal cells</b>	10-100	100-10,000	2000-3000	27	900-1800

To explain the apparent conservation of such a high intracellular density, Dill *et al.* in 2011 postulated that it has been selected through evolution so that biochemical reaction rates are optimal [44]. They took into account the competitive effects of molecular crowding on diffusion and collision rates of proteins. Decreasing protein diffusion may limit the rate of biochemical processes, while increasing the probability of protein encounters may increase the same biochemical rates. Since

## Chapter 1. Introduction

both effects depend on molecular crowding, there should be an optimal of protein density for which the biochemical rates are maximum. In their theoretical framework, they only took into account diffusion-limited reaction. The rate of reaction,  $r_d$ , of a stationary reactant of radius  $a$  with a mobile particle was approximated to be proportional to the concentration  $c$  and the diffusion constant  $D$  of the mobile particle:

$$r_d = 4\pi acD \quad (1)$$

The authors used the fact that  $c$  varies like the volumic fraction  $\Phi$ . Increasing  $\Phi$  increases the frequency of particle encounter but on the meantime decreases their diffusion. Therefore the two effects can equilibrate each other. To link the diffusion to the molecular crowding, they first expressed the cytoplasm viscosity by:

$$\eta = \eta_0 \left(1 - \frac{\Phi}{\Phi_g}\right)^{-2} \quad (2)$$

$\eta_0$  being the viscosity of water, and  $\Phi_g \sim 0.58$  the volume fraction where the glass transition occurs. Assuming that the diffusion coefficient,  $D$ , varies like the inverse of the cytoplasm viscosity,  $(1/\eta)$ , the diffusion rate is given by:

$$r_d \sim cD \sim \Phi \left(1 - \frac{\Phi}{\Phi_g}\right)^2 \quad (3)$$

To find the maximum rate, and so the optimal one, the authors set the derivative of this equation to zero:

$$\frac{dr_d}{d\Phi} = \left(1 - \frac{\Phi}{\Phi_g}\right)^2 - 2 \left(1 - \frac{\Phi}{\Phi_g}\right) \left(\frac{\Phi}{\Phi_g}\right) = 0 \quad (4)$$

The maximum rate is obtained when  $\Phi = \Phi_g/3$ . As previously mentioned,  $\Phi_g = 0.58$ . Thus, the predicted optimal macromolecular density is  $\Phi = 0.19$ . This estimated value is close to the actual cellular volume fraction ( $\Phi \approx 0.2$ ) [18, 45]. This optimum, if it exists, corresponds to a fine tuning between the cell size and the intracellular macromolecular content. Above the optimal volume fraction, the diffusion coefficient significantly decreases and affects all diffusion-limited reactions. Rapid

protein association is an example of diffusion-limited reactions. In contrast, reactions can also be limited by the rate of conversion of an intermediate. Such reactions are referred to as transition-state or chemically rate-limited. Note that molecular crowding is expected to decrease the rate of diffusion-limited reaction while possibly enhancing chemically rate-limited reactions (Figure 6).

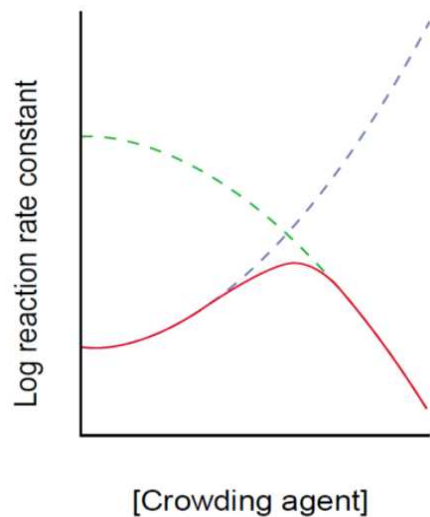


Figure 6. Representation of reactions rate in function of the molecular crowding. The dashed green line represents diffusion-limited rate constant, proportional to the frequency of encounter of the two reactants. The dashed blue line depicts chemistry-limited rate constant. Finally the solid red line corresponds to the overall rate constant. Taken from Ellis [45].

In this simple description, Dill *et al.* did not take into account the intracellular complexity. The authors disregarded chemically rate-limited reactions and assumed that the intracellular species behave like hard spheres, a crude approximation. Yet a soft colloid framework is more appropriate to describe the cell interior [46]. Colloids are particles of nano- or micro-meter size that are dispersed in a liquid, forming a suspension. Colloidal particles can be either solid (rigid) like glass or plastic, or soft (deformable) like vesicles or micelles and are respectively called hard and soft colloids. These colloidal particles, when present at high density, may alter the ability of the liquid to flow as in a dilute case, ultimately undergoing what is called a glassy transition: the system becomes jammed. Near this transition, the motion of the particles in the suspension becomes slow enough that it can be considered as frozen. In a very recent study, Zhou *et al.* showed that eukaryotic cells interiors behave as soft colloids upon compression [47]. More precisely, they showed that the cytoplasmic viscosity increased exponentially with the macromolecular volume fraction, a characteristic reminiscent from a soft glassy transition (Figure 7).

## Chapter 1. Introduction

Fragility, defined as the derivative of the logarithm of the viscosity with respect to the volume fraction, is used to characterize the behavior of such glassy transition and in particular the ability of a colloidal system to support small perturbations of density [48]. The relaxation time of non-deformable hard colloidal particles is highly sensitive to a change in density which defined them as fragile liquid. On the contrary, soft colloids are deformable particles and are able to go beyond simple contact with surrounding particles. Their glassy transition is more progressive than for rigid particles. They are said to be non-fragile liquids. As shown in Figure 7, the intracellular viscosity is drastically increased when the crowding is increased. Although this model of the viscosity of the cytoplasm is closer to reality than the elementary one used by Dill *et al.*, their conclusion remains valid: increasing the protein density and thus the molecular crowding inside the cytoplasm increases the cytoplasm viscosity and thus decreases the diffusion coefficients of proteins, thereby decreasing their biochemical reaction rates.

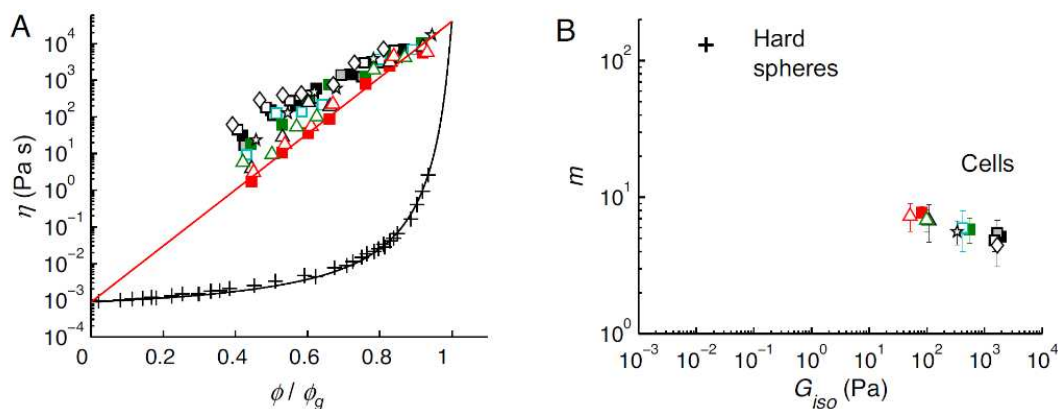


Figure 7. Cells behave as soft colloid under compression. (A) The viscosity of different mammalian cells is estimated in function of the relative volume fraction of macromolecules. Cells present an exponential distribution contrasting with the sharp transition observed for hard sphere (black cross). (B) The fragility  $m$  is plotted in function of the isotonic stiffness. Figure taken from Zhou *et al.*[47].

As we have just discussed, cell volume compression induced by osmotic perturbations allows the investigation of diverse biological processes including protein stability and folding [7, 34], sub-cellular diffusion rate [8, 36, 37], or membrane mechanical properties [47]. Importantly, we can wonder how signal transduction mechanisms are affected by macromolecular crowding. Only few groups have analyzed the impact of macromolecular crowding on signaling pathways. Eide and coworker used a computational simulation to investigate the

coupling of ligands to the dedicated receptor in the T lymphocytes [49]. Lipkow *et al.* studied the impacts of macromolecular crowding on the chemotaxis activity of *E. coli*. They analyzed the diffusion of the protein CheY from the receptors to the flagella motors. When they introduced macromolecular confinement to their simulations, the authors observed a decrease in CheY diffusion [50]. Even if a variety of modeling approaches could be used for such investigation [17, 51], computing the effects of crowding remains difficult [52]. Some studies approached experimentally this question. Rohwer *et al.* measured *in vitro* the rate of transfer of a chemical group along a series of carriers [53]. They analyzed a classical bacteria group-transfer pathway called phosphoenolpyruvate (PEP): carbohydrate phosphotransferase system (PTS). Upon glucose uptake by *E. coli*, a phosphoryl group is transferred along four PTS proteins. The authors measured a decrease in the flux of phosphoryl transfer under macromolecular crowding. Even if this investigation has been successfully conducted *in vitro*, transferring such analysis *in vivo* is not trivial. To our knowledge, Van Wuytswinkel *et al.* are the only one to show a direct macromolecular crowding effects on signal transduction although their study was very preliminary and not conducted in the purpose of investigating the effects of crowding [54]. The authors applied osmotic shocks to the yeast *S. cerevisiae* and analyzed intermediate reactions kinetics of the High Osmolarity Glycerol (HOG)<sup>8</sup> MAPK pathway. For a severe stress (1.4 M NaCl), they observed that the HOG cascade was apparently slower than for a gentle stress (0.4 M NaCl). They did not provide any reasonable explanation for this. Volume compaction due to osmotic stresses and the increased in macromolecular crowding is a possible explanation of this counter intuitive effect. In this thesis, we will further explore this and use osmotic compression to study the links between induced molecular crowding and signaling in yeast. However, it is important first to characterize what the effects of osmotic stress are in the cellular context, and then to describe precisely the way the budding yeast cope with it.

---

<sup>8</sup> The High Osmolarity Glycerol (HOG) MAPK pathway is activated by increased environmental osmolarity and results in a rise of the cellular glycerol concentration to adapt the intracellular osmotic pressure.

## 2. Challenging macromolecular crowding through cell volume compression

### The mechanism of osmosis

Let's consider a perfect semi-permeable membrane, that is a membrane permeable to solvent, in our case water, but impermeable to solutes. If the concentrations of solutes are not identical on both sides of the membrane, one observes motion of water through the semi-permeable membrane to equilibrate solutes concentrations on both sides. This results in the creation of a pressure acting on the membrane. The osmotic pressure,  $\pi$ , measured in Pascal (Pa), is defined as the pressure that one needs to apply externally to counteract the net flow of water (Figure 8).

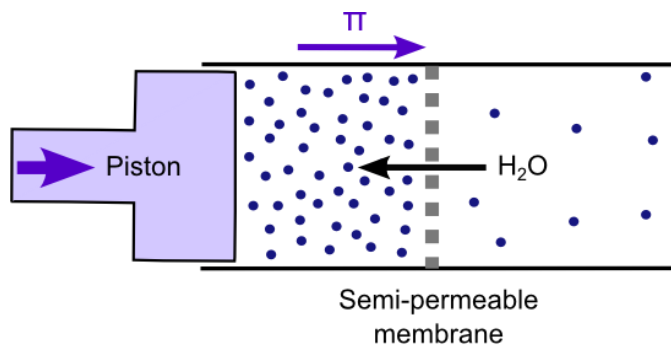


Figure 8. Osmosis equilibration triggered by water flow through a semi-permeable membrane. Water flows from the area of low solute concentration (blue dots; right chamber) to the area of high solute concentration (left chamber). If a pressure is applied to the plunger, the flow of water is reduced. The pressure necessary to stop the water flow corresponds to the osmotic pressure,  $\pi$ . Reproduced from Strange *et al.*[55].

The Van't Hoff relation states that the osmotic pressure that is due to the presence of a solute in ideal solution is given by:

$$\pi = RT \frac{n}{V} = RT C_i \quad (5)$$

$R$  is the perfect gas constant (8.31 J/K.mol),  $T$  the absolute temperature (in kelvin),  $n$  is the number of osmotically active moles,  $V$  is the volume ( $\text{m}^3$ ) and  $C_i$  the molar concentration of solute  $i$ . Accordingly, increasing the number of solute molecules in a solution increases its osmotic pressure. If one mole of electrolyte dissociates into several ions, it results in a greater osmotic pressure than in the case of the addition of a simple compound. The osmolarity of the medium is higher. The number of mole has to be multiplied by the number of ions after dissolution (ex: 1 mole of

CaCl<sub>2</sub> = 3 osmol). The osmol concentration of a solution can be described either in term of osmolality or osmolarity. Osmolality indicates the total number or moles present in a kilogram of solution, while osmolarity is related to the number of moles present in one liter of solution. Osmometers are dedicated tools for measuring the osmotic pressure. Membrane osmometers are made with a chamber connected to a column and filled with high concentrated solutes (Figure 9). A semi-permeable membrane separates this chamber from the solvent. Due to the differences in osmolarity of the two solutions, water flows inside the chamber and the level of liquid rises inside the column: the level of liquid in the column rises above the level of solvent. The osmotic pressure is equilibrated by the hydrostatic pressure due to gravity.

$$\pi = \rho gh \quad (6)$$

in which  $h$  is the level difference between the column and the solvent chamber,  $\rho$  is the volumic mass of the solution and  $g$  the gravity acceleration. Measuring  $h$  is a direct measurement of the osmotic pressure. Alternatively, the osmotic pressure can be measured directly by a pressure transducer [56].

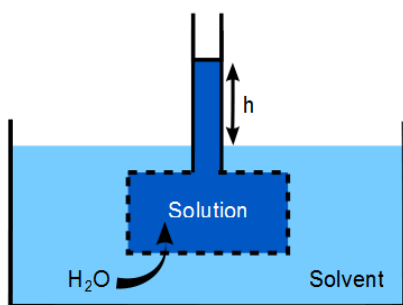


Figure 9. Basic representation of a membrane osmometer. A solution (dark blue) is separated from the solvent (light blue) by a semi-permeable membrane. The equilibration of the sum of osmotic pressures and hydrostatic pressure leads to a difference of water levels that can easily be measured.

In terms of thermodynamics, the osmotic equilibrium is reached when the chemical potentials of the solvents are identical on both sides of the membrane. The chemical potential is defined as the change of enthalpy ( $\Delta G$ ) of a system if some particles are added or removed to a solution when the number of moles of other compounds, the temperature and the pressure stay constant:

## Chapter 1. Introduction

$$\mu_i = \left( \frac{dG}{dn_i} \right)_{T,P,n_j} \quad (7)$$

For the case of an ideal gas, the chemical potential is then given by:

$$\mu_i = \mu_i^0 + RT \cdot \ln \frac{P_i}{P_0} \quad (8)$$

$\mu_i^0$  is the chemical potential under the standard conditions and depends on the temperature only, while  $P_i$  is the partial pressure of the species  $i$ . Similarly the chemical potential for a solute in an ideal, dilute solution is expressed as:

$$\mu_i = \mu_i^0 + RT \cdot \ln \frac{C_i}{C_0} \quad (9)$$

$C_i$  is the concentration of molecule  $i$ . Yet, real solutions differ from ideal situations due to interactions between molecules of solute species  $i$  and all other solute and solvent molecules in the solution. To account for this, the chemical potential is then expressed as:

$$\mu_i = \mu_i^0 + RT \cdot \ln a_i \quad (10)$$

$a$  is called the thermodynamic activity and is given by:

$$a_i = \gamma_i \cdot \frac{C_i}{C_0} \quad (11)$$

$\gamma_i$  is the activity coefficient. In ideal situation,  $\gamma_i=1$  and the effective concentration  $a_i$  is identical to the concentration. When the concentration increases, the solution is no more in ideal conditions and the activity coefficient decreases due to solute-solute interactions. This is in particular the case when studying highly crowded solutions. On the previous equation, one sees that the Van't Hoff relation is analogous to the law of the ideal gas. With the same analogy one can relate the osmotic pressure to the chemical potential and get a definition even in the case of crowded environments for which the Van't Hoff relation does not hold anymore:

Considering the situation of a semi-permeable membrane that separates a diluted solution from a pure solvent, the osmotic equilibrium can be written as,

$$\mu_w^0(p) = \mu_w^0(p + dp) + RT \cdot \ln a_w \quad (12)$$

where  $\mu_w^0(p)$  is the chemical potential on the side of the pure solvent (water) and  $\mu_w^0(p + dp) + RT \cdot \ln a_w$  the chemical potential on the solute side, where the pressure is augmented by the osmotic pressure  $dp$ . We can then write that

$$\mu_w^0(p + dp) = \mu_w^0(p) + dp \frac{\partial \mu_w^0}{\partial p} \quad (13)$$

and

$$\frac{\partial \mu_w^0}{\partial p} = V_m \quad (14)$$

$V_m$  is the molar volume, that is to say the volume occupied by a mole of solute. By combining the last equations and knowing that the pressure differences,  $dp$ , is the osmotic pressure,  $\pi$ , we obtain:

$$\pi = -\frac{RT}{V_m} \cdot \ln a_w \quad (15)$$

For diluted solutions, the activity can be written as  $a_w = 1 - x_i$  with  $x_i$  the proportion of solute relative to the number of total moles. In highly diluted solutions,  $x_i$  is small compared to 1 and one can approximate the  $\ln(1-x_i) \sim -x_i$ . Therefore, the osmotic pressure can be expressed as:

$$\pi = \frac{RT}{V_m} \cdot x_i \quad (16)$$

By definition,  $x_i$  is equal to the ratio of the number of mole of solute,  $n_i$ , on the number of total moles,  $n_{tot}$ . For a dilute solution, it is close to the number of mole of solvent,  $n_w$ . Since  $V_m \cdot n_w$  is the total volume of solvent,  $V$ , we find the Van't Hoff law for a diluted solution:

$$\pi = \frac{RT}{V} \cdot n_i = RTCi \quad (17)$$

## Osmotic behavior of biological membrane

Osmotic equilibration often occurs in a cellular context. However, cell membranes are far from the ideal semi-permeable membranes previously described. For instance, water motion directed by osmotic gradients may be enhanced by the presence of water channels, the aquaporins<sup>9</sup> [57]. Moreover, biological membranes are permeable to electrolytes. Apart from small molecules that diffuse spontaneously, transport through the membrane can be achieved actively through ions channels and carriage processes [58]. Similarly to water, electrolytes move toward their lower concentration and this transport is at play when concentrations on both sides of the cytoplasmic membrane are unbalanced. This is indeed why cells spend some of their energy to maintain concentration of key ions despite their external concentration by constantly pumping them in or out. Note that an ionic flow ultimately helps to decrease the difference of osmotic pressure. Staverman, in 1951, improved the model of cellular osmosis by including the membrane permeability to solute  $i$  [59] and introducing the reflection coefficient,  $\sigma_i$ .

$$\sigma_i = \frac{\Delta\pi_{obs}}{\Delta\pi_{th}} \quad (18)$$

$\Delta\pi_{obs}$  is the observed osmotic pressure and  $\Delta\pi_{th}$  is the osmotic pressure for an ideal semi-permeable membrane. The reflection coefficient ranges from 0 to 1. When the solute is entirely impermeable to the membrane,  $\sigma_i=1$ . On the contrary, if the solute is entirely permeable to the membrane, the reflection coefficient is equal to zero. This reflection coefficient term is added to the primary osmotic pressure equation.

$$\Delta\pi_{eff} = \sigma_i RT \Delta C_i \quad (19)$$

Taking into account the membrane permeability to solutes, the flow of water,  $J_v$ , driven by hydrostatic ( $\Delta P$ ) and osmotic ( $\Delta\pi$ ) pressure differences, can be defined as:

---

<sup>9</sup> Aquaporins are water channels involved in the control of the water content of cells [208]. Although aquaporins are water specific, they may also be permeable to small molecules like glycerol or urea. In the yeast *S. cerevisiae*, there are two aquaporins, named AQY1 and AQY2. Yeast strains deleted for aquaporin genes, most notably AQY2, show a stronger resistance to rapid osmotic changes [208]. However, many yeast strains, including the parental strains we are using in this study, have a genetic mutation for aquaporin genes and express non-functional aquaporins [209].

$$J_v = L_p(\Delta P - \sigma_i \Delta \pi_{th}) \quad (20)$$

$L_p$  corresponds to the hydraulic conductivity of the cell membrane. It defines the permeability of the membrane to water. Most cells do not actively maintain an osmotic pressure difference through their membrane, although they use their channels and pumps to control the ionic content of their cytoplasm. However, organisms surrounded by a rigid cell wall like plant cells, yeast or bacteria, maintain a significant pressure difference, called turgor pressure [60]. The turgor pressure has an essential role for growth, cell structure and membrane transport. The cell wall surrounding the membrane of such cells is a rigid and dynamic organelle that notably protects cells against external mechanical stresses, including osmotic stress. The turgor pressure is due to the mechanical rigidity of the cell wall. The turgor pressure is measured as the difference between the internal ( $\pi_{int}$ ) and the external ( $\pi_{ext}$ ) total pressure exerted on the cell.

$$\Delta \pi_t = \pi_{int} - \pi_{ext} \quad (21)$$

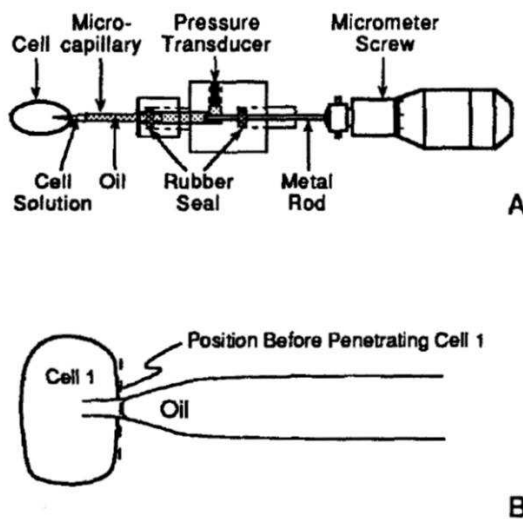


Figure 10. Diagram of a pressure probe and its utilization on cell. (A) Pressure probes are composed of a micro-capillary, pressure transducer and spaced filled with oil (represented shaded). (B) The penetration of the micro-capillary in the cell triggers the formation of a meniscus at the interface between the cell medium and the micropipette oil. The pressure is measured by positioning the meniscus, thanks to the metal rod, to its location before inserting the micro-capillary. Taken from Boyer [61].

Several methods have been used to estimate the turgor pressure of cell-wall organisms (Table 3). In plants, turgor pressure of single cells was measured experimentally using pressure probes (Figure 10). The device, initially developed for large single algal cells, is essentially composed of a pressure transducer and a micro-capillary filled with oil. The tip of the micro-capillary is inserted inside a cell

## Chapter 1. Introduction

and the turgor pressure corresponds to the necessary pressure to stop the flow out of water [61]. However, such method is rarely used in single cell due to the technical difficulty of targeting a specific cell; instead it is applied for whole plant tissues.

The small size of micro-organisms such as bacteria or yeast prevents the use of pressure probes. In prokaryotes, organelles called intracellular gas vesicles are used for turgor estimations [62]. Gas vesicles are intracellular compartments filled with air and impermeable to water. They are found in prokaryotes like cyanobacteria, halophilic archaeo bacteria and some eubacteria. These gas vesicles do not absorb light in the visible spectra but instead they scatter light. Under pressure, the gas vesicles collapse, decreasing the amount of light scattered. Ultimately, the turgor can be measured through quantification of this decline in function of the pressure applied. However, this technique cannot be applied to every cell-walled organism since only some prokaryotes present gas vesicles. Minc and coworkers developed a microfluidic device to extract the mechanical properties of the yeast *Schizosaccharomyces pombe* [63]. Other technical approaches exist but are usually not very precise [64, 65]. It is indeed a challenge to measure an osmotic pressure in a complex system, densely packed with proteins and macromolecules such as a cytoplasm. The presence of the turgor cell wall that can sustain a difference of osmotic pressure between the internal and external environment is a considerable limitation to internal osmotic pressure estimation. In the budding yeast, there is no experimental method for direct measurement of the turgor pressure. Instead, several studies estimated the turgor value indirectly [65, 66] but unfortunately obtained values that did not compare very well (Table 3). According to the Van't Hoff relation the cell volume and the external osmotic pressure are inversely proportional. Yet, because of the turgor pressure, this equation cannot be applied directly. Under compression, the turgor pressure decreases as the osmotic stress increases and three regimes can be distinguished [66]. During the first one, called the transient phase, the turgor pressure decreases but still presents positive values (Figure 11, left). When the turgor pressure reaches a null value, volume reduction enters the second phase, the steady-state phase. In this case, the cell shrinks in a manner inversely proportional to the external osmolarity (Figure 11). The turgor

pressure is null and the internal and external pressures are equal. From this, the turgor pressure can be estimated [65]. Recently, Schaber *et al.* made a mathematical model of cell-wall organisms under compression [67]. They compiled four experiments conducted on *S. cerevisiae* in which cell volume variations were measured over a range of osmotic stress. By fitting their model on their experimental data, they extracted a turgor pressure of 0.6 MPa. Such value is supported by previous estimation of yeast turgor in stationary growth phase [68]. After the steady-state phase, the volume reaches a plateau. During this plateau, the cell undergoes plasmolysis which is the physical dissociation of the cell wall from the membrane [67].

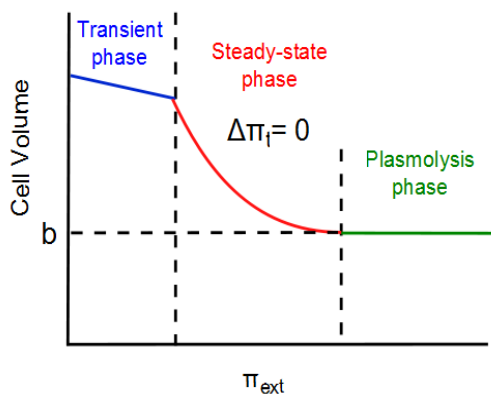


Figure 11. Cell volume and osmotic pressure relationship in cell-walled organisms. (A) Cell volume reduction in function of increasing external pressure ( $\pi_{\text{ext}}$ ) can be subdivided in three phases. In the transient phase, the turgor pressure decreases but stays positive. In the steady-state phase, the turgor pressure ( $\Delta\pi_t$ ) reaches a null value and the cell volume variation follows the Van't Hoff law. Under extreme osmotic pressure, the cell reaches a minimal volume for which plasmolysis occurs.  $b$  corresponds to the smallest possible size and is referred as the non-osmotic volume (NOV).

Table 3. Turgor pressure measurements and methods used.

Organisms	Turgor pressures (MPa)	Techniques	References
<i>Arabidopsis</i> Epidermal root cells	0.65	Pressure probe	[69]
Bacteria <i>Ancylobacter aquaticus</i>	0.187	Intracellular gas vesicles	[70]
Yeast <i>S. pombe</i>	0.85	Microfluidic chamber	[63]
Bacteria <i>Bacillus subtilis</i>	1.9	Van't Hoff relationship	[65]
Yeast <i>S. cerevisiae</i>	0.05 - 2.9	Van't Hoff relationship	[71, 72]
Yeast <i>S. cerevisiae</i>	0.6	Mathematical model	[67]

## Physiological response to osmotic stress

In iso-osmotic conditions, cells are, by definition at an osmotic equilibrium (Figure 12, middle). Whenever a change in osmolarity occurs, a flow of water and electrolytes spontaneously appears, leading to a change of cell volume and a novel mechanical equilibrium, in which the osmotic pressures and the turgor pressure are balanced. One talks about hypo-osmotic stress when the extracellular environment is diluted compared to the iso-osmotic conditions for the cell. Such dilution triggers a net flow of water inside the cell. Consequently, the cell swells. The cell membrane is stretched and this can eventually lead to the rupture of the cell membrane (haemolysis in red blood cells). Cell-walled organisms are more resistant to bursting because of the cell wall that can resist expansion (Figure 12, left) [73]. In such situation, cells are said to be turgid. In contrast, hyper-osmotic stress corresponds to the change from an iso-osmotic to a concentrated extracellular environment. It leads to the loss of cytoplasmic water and the shrinkage of the cells. Consequently, the cell membrane wrinkles and for a too strong stress, plasmolysis appears (Figure 12, right).

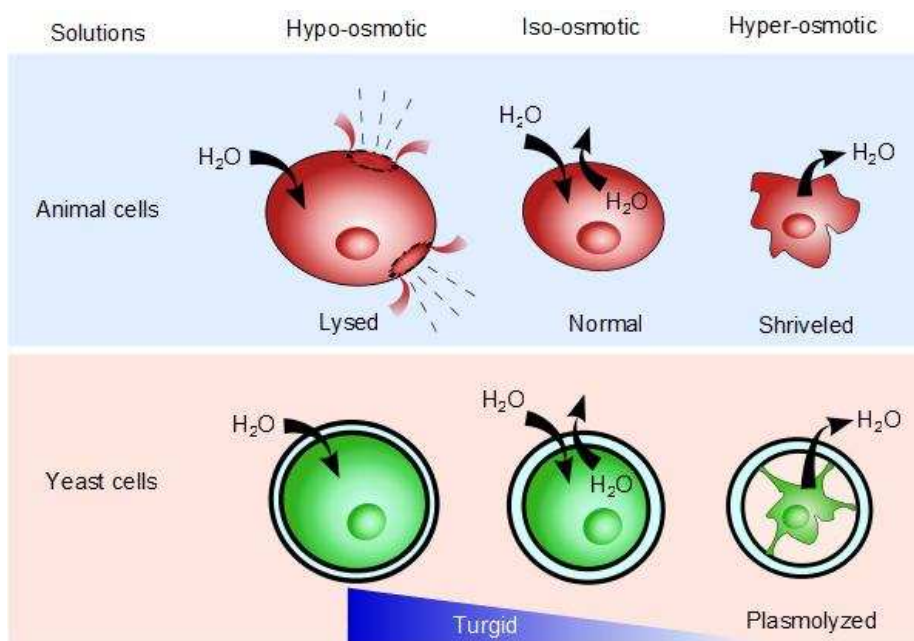


Figure 12. Comparison of hyper-osmotic, hypo-osmotic and iso-osmotic conditions in animal (top panel) versus cell-walled organisms (bottom panel). In hypo-osmotic solution (left), water flows in and triggers the cell to swell. At high hypo-osmotic condition, cells could eventually lyse. In hyper-osmotic condition (right), water flows out leading to cell shrinkage. The cell membrane ultimately invaginates. In cell-walled organisms, plasmolysis occurs.

## Mechanisms of cell volume regulations

We have previously discussed the effect of changing the external osmotic pressure on the cell volume and the cell mechanical integrity. Mammalian organisms usually maintain their cells in a controlled environmental fluid with limited osmotic fluctuations. However, some specialized cells, like the kidney inner medullary cells [11] or chondrocytes cells [74] are subject to rapid and strong variation in their intracellular or extracellular concentration and need dedicated volume regulatory mechanisms [75]. In plant, osmosis has essential functions for cell growth and nutrients uptake by the roots. During these processes, plant cells swell until they become turgid due to the high pressure exerted on their cell wall [60]. Such stress leads to an abnormal cell physiology that may impact the proper functioning of biological processes. Cells should be able to adapt to such stress so as to recover a normal cell size. There are several regulation mechanisms depending on the cell type and their usual ionic environment. For micro-organisms, the predominant strategy for osmoregulation is the production and accumulation of a compatible osmolyte. For instance, *E. coli* can synthesize glycine betaine as an osmoprotectant [76]. This osmolyte is said to be compatible as it does not alter, *a priori*, the intracellular properties even at high concentrations. Other micro-organisms living in extreme environments like halophilic bacteria or archaea, have developed a “salt-in” strategy [77]. As those organisms are constantly challenged by strong osmotic stress, they can maintain a high intracellular salt concentration.

In its natural environment, *S. cerevisiae* is exposed to sucrose and hexoses concentrations ranging from 0.1 to 1.5 M [78]. In laboratories, 1 M sorbitol corresponds to the typical concentration to induce an osmotic stress for *S. cerevisiae*. Many micro-organisms are adapted to extreme environments such as high osmotic conditions, acidic pH, or low temperatures. Organisms that are able to grow under constant stressful conditions are called extremophile. The capacity of a species to grow under low availability of water is termed osmotolerance<sup>10</sup>, xerotolerance<sup>11</sup>,

---

<sup>10</sup> Osmotolerance is the ability to resist a wide range of osmotic pressures.

<sup>11</sup> Xerotolerance is the ability to grow in conditions with low water availabilities.

## Chapter 1. Introduction

halophilism<sup>12</sup> or osmophilism<sup>13</sup> [79, 80]. The first term is more generally applied for yeast. Osmotolerant yeasts cannot be separated in two categories but rather present a range of tolerances [80]. Yeasts are among the best studied micro-organism for osmoregulation. This is mainly motivated by industrial interests such as the improvement of fermentation performance or the determination of adaptation limits for food preservation. A few yeast species are able to grow in moderate salt conditions such as *D. hansenii* which maximally grow in the presence of 0.25 - 0.5 M NaCl. Although osmotolerant cells are able to grow in extreme environment, their growth rate is generally slower than osmosensitive cells (Figure 13). Indeed the mean generation time for osmotolerant yeast strains is about 4 to 8 hours while non-osmotolerant strains divided every 90–120 minutes [80, 81].

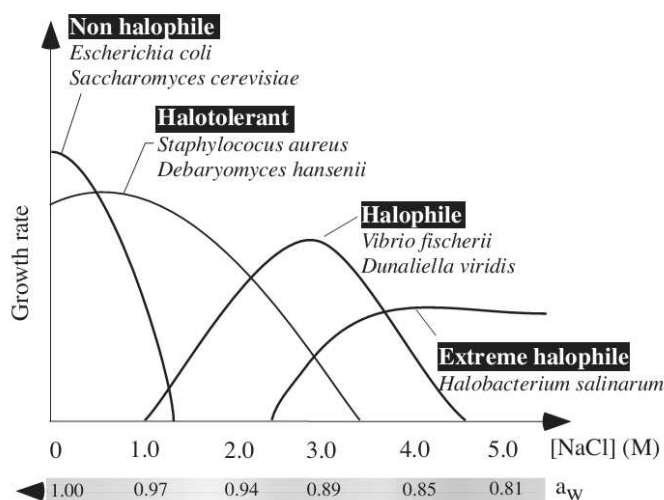


Figure 13. Representation of growth rate capacity of various osmotolerant micro-organisms in function of the external osmolarity. The osmotolerant yeasts *Zygosaccharomyces rouxii* or *Debaryomyces hansenii* are able to grow under 4 M sodium chloride while *Saccharomyces cerevisiae* reaches its limit around 1.7 M NaCl [82]. This graph is adapted from Horikoshi and Grant [81], and Madigan *et al.* [83].

<sup>12</sup> Halophilism is the requirement of high salt (NaCl) concentrations for growth of microorganisms.

<sup>13</sup> Osmophilism is the requirement of high osmotic pressure for growth of microorganisms.

### *Solutes transport*

Osmoregulation mechanisms involve ionic or organic molecules accumulation and transports through the cell membrane. In mammalian cells, electrolytes are the first solutes to be mobilized after osmotic alterations. The major ions species implicated are  $K^+$ ,  $Na^+$ ,  $Ca^{2+}$  and  $Cl^-$ . Ion transport is done by channels and carrier-type transporters. Channels ensure the diffusion of electrolytes downhill to their gradient through passive transport. Transporters include exchangers ( $Na^+/Ca^{2+}$ ), co-transporters ( $K^+/Cl^-$ ), and active ion pumps. The last one uses ATP to trigger the transport of electrolytes opposite to their gradient direction ( $Na^+/K^+$ -ATPase). Those gradients are essential for vital cellular functions like the production of electrical signals in neurons or for signal transduction pathways activation. As the cell accumulates essential materials, like proteins or metabolites, the export of electrolytes allows the maintenance of concentrations balance. Therefore, the concentration of electrolytes is usually slightly lower inside than outside the cell. The volume maintenance is essentially achieved through the  $Na^+/K^+$ -ATPase pump. Potassium is also required within the cell to activate a variety of processes, whereas high intracellular sodium concentrations are inhibitory. Intracellular potassium is also required for the exclusion of the ion chloride  $Cl^-$  thanks to the co-transporter  $K^+/Cl^-$  (Figure 14A).

In *S. cerevisiae*, ion transport mechanisms consist of six plasma membrane transporters: the potassium uptake channels Trk1 and Trk2, the potassium channel Tok1, the Pi-Na symporter Pho89, and the efflux systems Ena ( $Na^+$ -ATPases) and Nha1 ( $Na^+/H^+$  anti-porter) (Figure 14B). In *S. cerevisiae*, applying NaCl stress may be deleterious for cells due to the accumulation of intracellular  $Na^+$ . To limit its toxicity,  $Na^+$  is either excluded from the cell through the Nha1 channel or sequestered in a pre-vacuolar compartment [84].

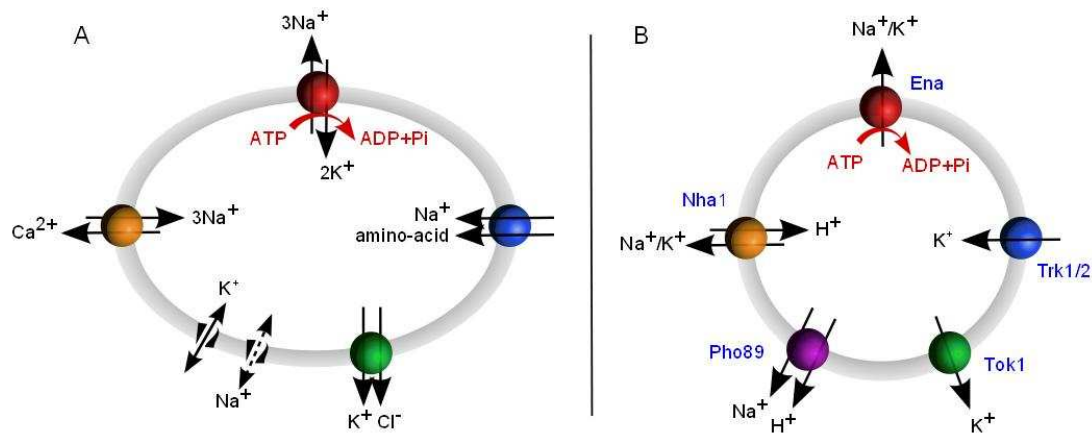


Figure 14. (A) Representation of major ion channels in mammalian cells. the Na<sup>+</sup>/K<sup>+</sup>-ATPase (red, top), the Na<sup>+</sup>/Ca<sup>2+</sup> exchanger (yellow, left), K<sup>+</sup> and Na<sup>+</sup> ion channels (black), the K<sup>+</sup>/Cl<sup>-</sup> cotransporter (green, bottom) and the Na<sup>+</sup> amino acid cotransporter (blue, right) are the principal channels assuring ion transports. (B) Representation of major ion transport systems in *S. cerevisiae*.

### *Organic solutes transport*

Electrolytes recruitment occurs on short timescales but longer hyper-osmotic exposition leads to the accumulation of compatible organic osmolytes. Those osmolytes may be present at high concentration inside the cytoplasm (10 to 100 mM) and play key roles in cell volume regulation. Three major classes of osmolytes exist in eukaryotes: polyalcohols (*e.g.* sorbitol, inositol, glycerol), methylamines (*e.g.* betaine) and amino acids plus derivatives (*e.g.* glycine, glutamate). Their accumulation is mediated either by active transport through dedicated channels or by *de novo* synthesis. To detect osmotic changes, mammalian cells use different signaling mechanisms such as p38<sup>14</sup>, ERK<sup>15</sup> and JNK<sup>16</sup>. In the budding yeast, our model of study, the central system for osmo-adaptation is the HOG pathway, of the family of the Mitogen Activated Protein Kinases (MAPK).

<sup>14</sup> The p38 signaling transduction pathway plays an essential role in regulating many cellular processes including inflammation, osmotic stress, cell differentiation, cell growth and apoptosis.

<sup>15</sup> The Extracellular Signal-Regulated Kinase (ERK) cascade functions in cellular proliferation, differentiation, and survival.

<sup>16</sup> The c-Jun NH2-terminal Kinase (JNK) pathway becomes activated after exposure to inflammatory cytokines as well as to diverse stress inputs including UV irradiation or heat shock. It also plays a role in neural development and apoptosis.

### 3. Signaling osmostress in yeast

#### MAP Kinase pathways in yeast

The MAPK pathways are specialized eukaryotic signaling cascades involved in a wide range of cellular processes. They respond to various stimuli, such as growth factor, stress or nutrient conditions [85]. MAPK cascades dedicated in stress-response stimulations are called Stress-Activated Protein Kinase (SAPK) [86]. MAPKs contain a module of three protein kinases that act in series and are successively activated by phosphorylation (Figure 15). A set of dedicated membrane proteins sense specific stimulation and activate the first actor called a MAP kinase kinase kinase (MAPKKK) protein. This kinase will in turn phosphorylate (activate) the MAP kinase kinase (MAPKK) protein on its serine and threonine domains, itself phosphorylating the MAP kinase (MAPK) protein on its threonine (or serine) and tyrosine residues (Thr/Ser-X-Tyr). This last phosphorylation can induce the translocation of the MAPK into the nucleus. There, it phosphorylates transcription factors on conserved serine/threonine residues. After the MAPK pathways have performed their signaling and the transcriptional regulation has occurred, the cascade activity can be shut-down by various feedback mechanisms. In particular, several proteins phosphatases can act either on MAPKK or MAPK (serine-threonine phosphatases) or only on MAP kinase (tyrosine phosphatases) proteins [87].

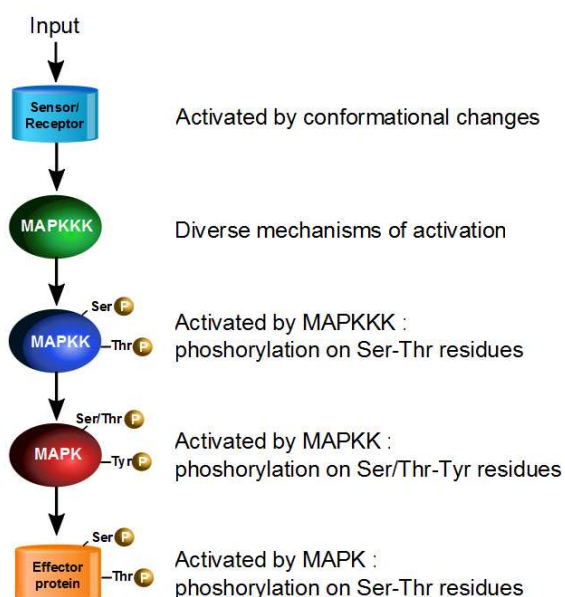


Figure 15. Representation of a MAPK pathway. MAPK cascades are composed by proteins kinases that are activated successively by phosphorylation on conserved residues. Reproduced from Rodríguez de Mier [88].

In *S. cerevisiae*, Mitogen Activated Protein Kinases (MAPK) pathways are very well described. *S. cerevisiae* contains five MAPK pathways. The spore wall assembly pathway is specific to diploid cells and occurs when they undergo meiosis [89]. We will not describe it further here. The four others pathways are the following:

**The Pseudohyphal growth pathway** is induced in diploid cells by nitrogen starvation and in haploid cells by carbon starvation. It triggers cell elongation and invasive growth. This signaling pathway involves many but not all of the components used in the pheromone response pathway (see below) [90]. The scaffold protein Ste5 is probably responsible for pathways insulation (

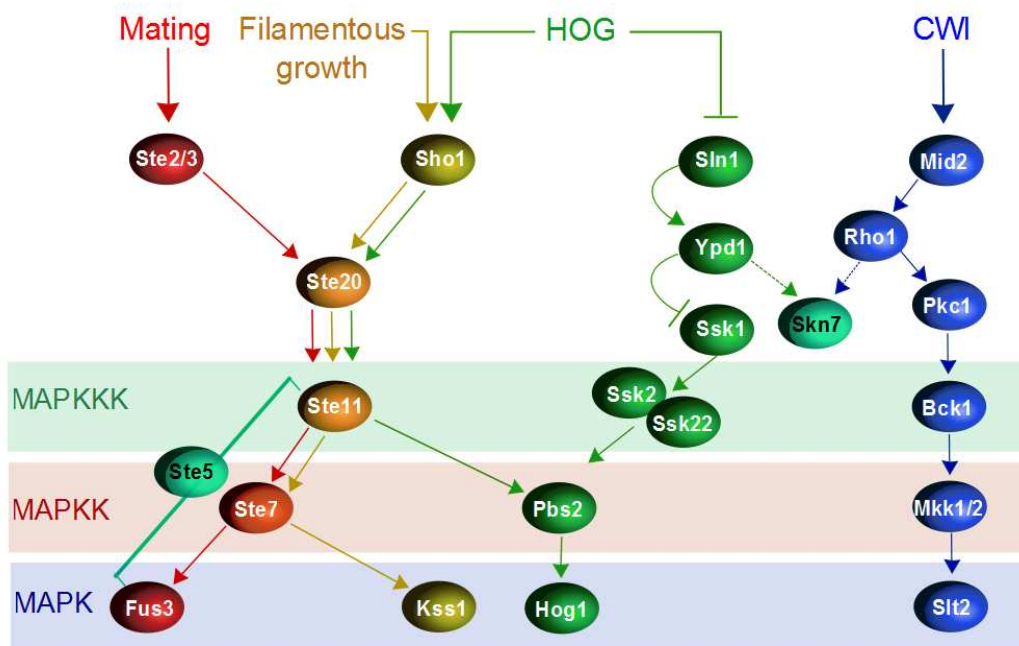


Figure 16, left). By tethering actors of the pathway, Ste5 form a complex that direct the signal to the appropriate MAPK [91].

**The Pheromone pathway** mediates the interaction between two haploid cells of different sex type (*a* or  $\alpha$  cells) which mating gives a diploid cell. This pathway is initiated by pheromone molecules released by the haploids of the opposite cell type. Response to pheromone includes polarized growth towards a mating partner, cell cycle arrest in G1, and increased expression of proteins needed for cell adhesion.

The **Cell Wall Integrity (CWI) pathway** is initiated by hypo-osmotic stress, as well as situations in which the cell wall integrity is compromised [92]. This cascade is not only activated after a stress of the cell wall, but also in normal physiological conditions, notably during cell growth and cell wall remodeling. During cell division or mating, the membrane can be under tension and/or deformed. Such morphological changes are assumed to be handled by the CWI pathway.

Finally, the **High Osmolarity Glycerol (HOG) pathway** is involved in hyper-osmotic stress response. The HOG pathway is one of the best understood osmo-responsive systems in eukaryotes [93]. Together with the pheromone pathways, they are considered as models to study the quantitative aspect of MAPK cascades. The HOG pathway presents several easy and observable readouts. Several studies analyzed its dynamics and predicted their behavior by modeling approaches [94–96]. We will come back in details on its description and functioning.

As shown on

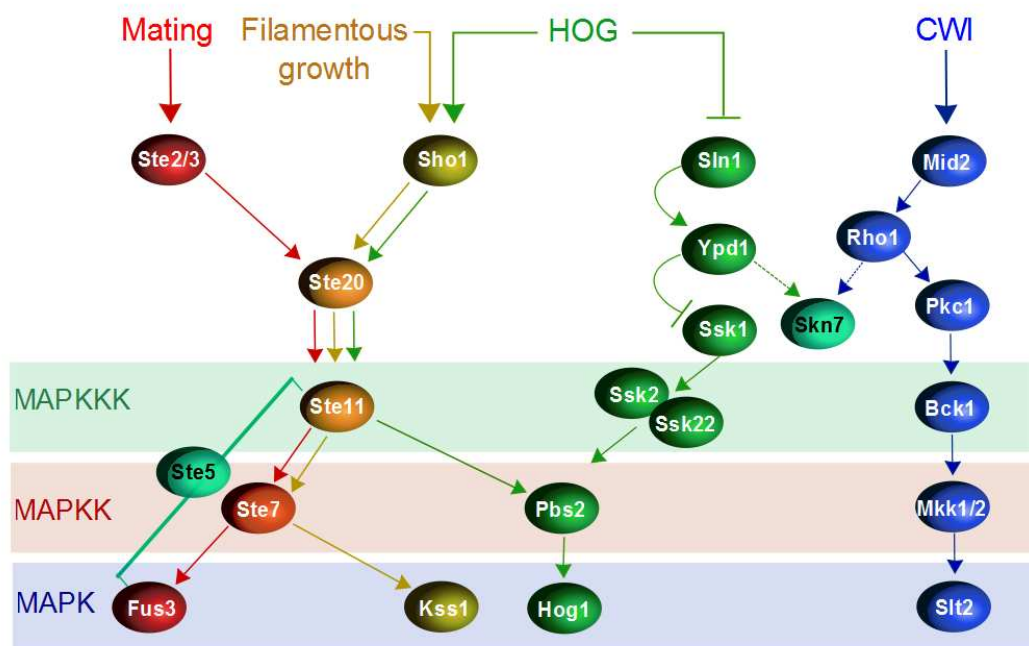


Figure 16, the MAPK pathways often share components, but cross-activation, although possible in principle, is not usually observed [97]. For example, the mechanism which maintains the response specificity between the HOG and the pheromone pathways is debated. While McClean *et al.* described mutual

## Chapter 1. Introduction

inactivation mechanisms between pathways (cross-inhibition) [98], Patterson *et al.* proposed instead that the confinement of shared proteins ensure insulation of both pathways [99]. It is less clear how the HOG and the CWI pathway interact. The HOG and the CWI pathways are mutually exclusive in their expressional response [100] which suggests the implication of a common actor. A possible candidate is the oxidative stress-response kinase Skn7. Indeed, this factor is controlled by sensors which are acting on both the HOG pathway [101] and the CWI pathway [102] (

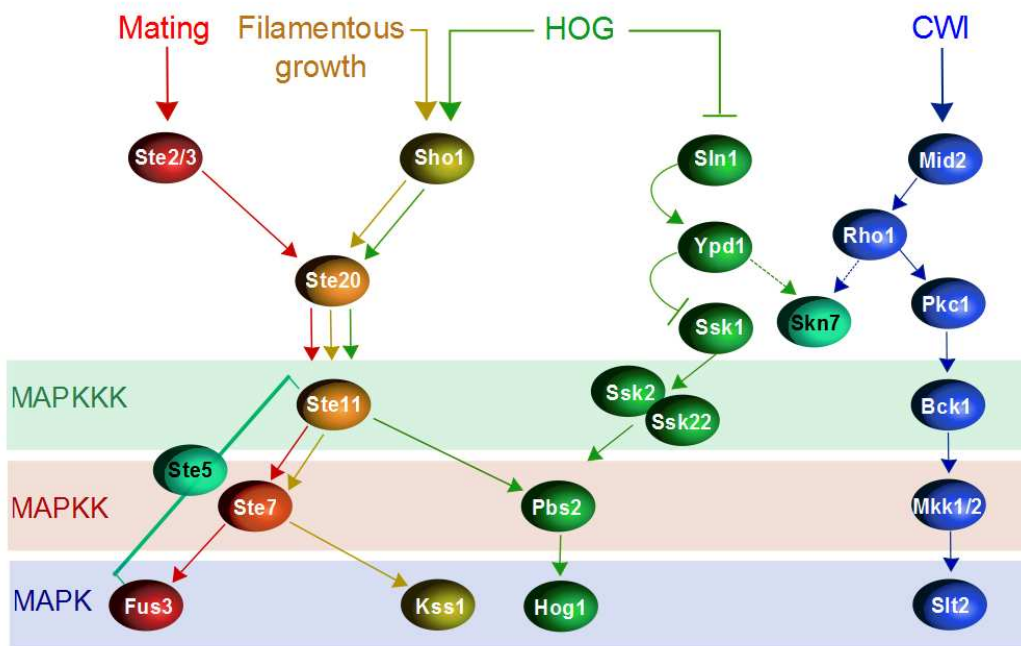


Figure 16).

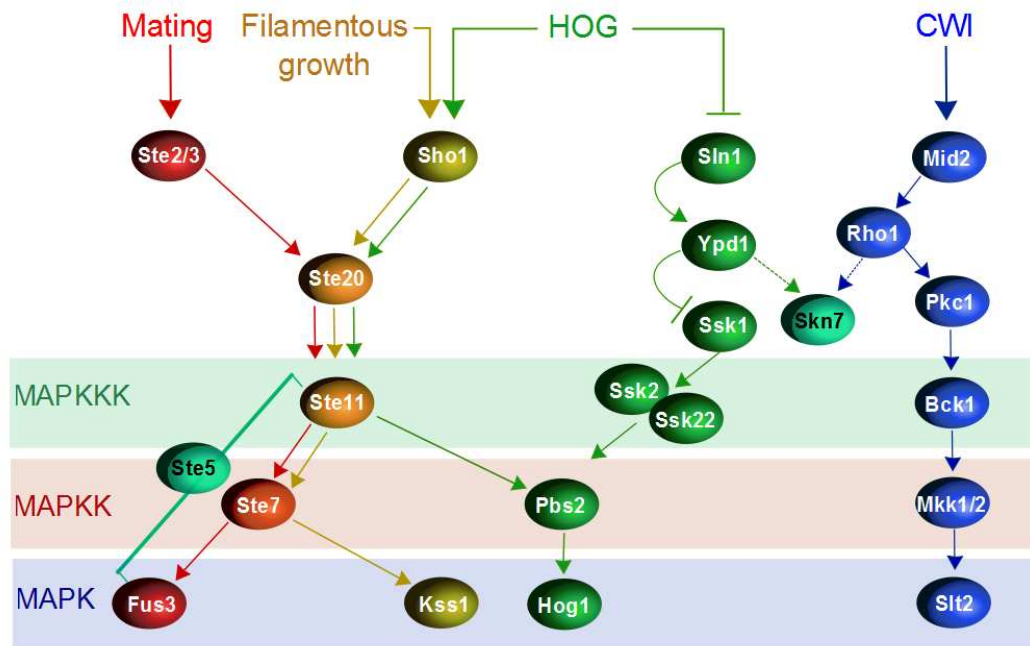


Figure 16. Schematic representation of the four MAPK pathways operating in growing yeast. Regulation and cross-talks are shown for the mating response (left), the filamentous growth and the HOG pathway (middle). Skn7 convergent node is a possible candidate for the mutual exclusion of the HOG and the CWI pathways (right).

## The HOG pathway

The HOG pathway is activated by hyper-osmotic stress, caused for example by high external concentration of NaCl, sorbitol [92], KCl, glucose [103] or glycerol [104]. In the past years, several studies showed that the HOG pathway can respond to other variation of its environment. The HOG cascade seems to be activated by oxydation [105], heat stress [106] or the presence of arsenite [107]. An overview of the HOG pathway steps and dynamics are sketched in Figure 17 and the typical timescales of the different steps occurring after a hyper-osmotic stress are given in Table 4.

Table 4. Timescales of the HOG pathway upon the induction of a moderate hyper osmotic stress

Structural changes and processing	Timescales	References
Cell shrinkage	~10 sec	[108]
Hog1 phosphorylation	1-2 min	[54, 109, 110]
Hog1 nuclear import	2-5 min	[54, 109, 110]
Gene expression	15 min	[100]
Glycerol production	20-30 min	[111]
Hog1 dephosphorylation/export	20-30 min	[111]

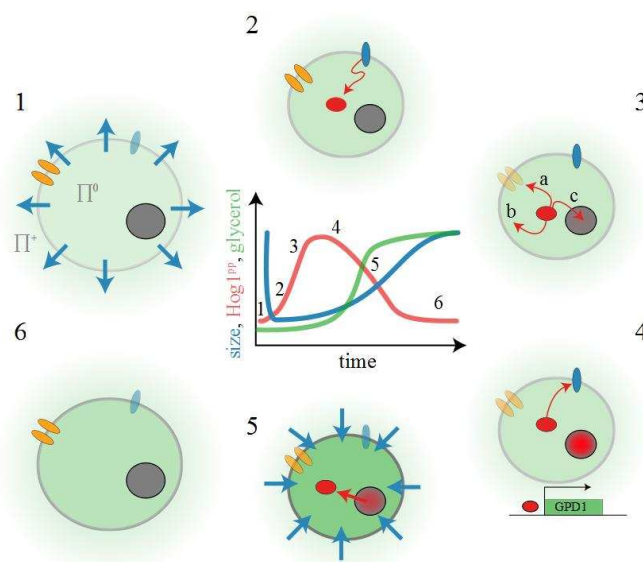


Figure 17. Response of a yeast cell to a hyper-osmotic shock. (1) Upon osmotic shock, water rushes out of the cells. (2) Change in membrane pressure triggers the HOG pathway activation leading, through signal processing, to the phosphorylation of the transcriptional factor Hog1 (represented in red). (3) Once phosphorylated, Hog1 has various actions in the cytoplasm (a). It seems indirectly involved in Fps1 glycerol efflux channel closure, leading to glycerol retention (b). Hog1 phosphorylated is also strongly imported inside the nucleus (c). (4) Hog1 nuclear triggers the transcriptional regulation of several genes, leading to glycerol synthesis. (5-6) Glycerol accumulation induces water to flow inside the cell, forcing the cell to swell. Feedback loops trigger the export of Hog1 and the opening of the Fps1 channel.

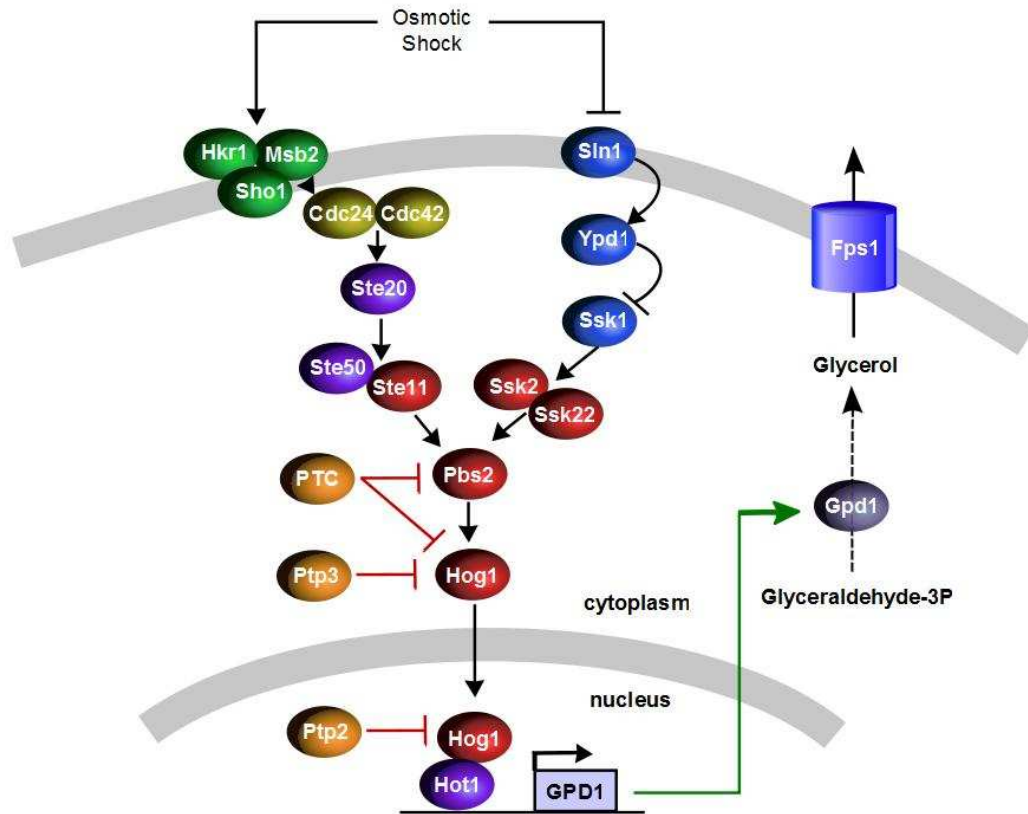


Figure 18. Representation of the HOG pathway in the yeast *S. cerevisiae*. The HOG cascade consists of two input branches. The phosphorelay branch SLN1 and the enzymatic branch SHO1, converge and trigger the phosphorylation of Pbs2. Activated Pbs2 phosphorylates Hog1. Hog1 activated is then imported inside the nucleus and leads to the synthesis of glycerol. Once the cell is adapted, phosphatases lead to the dephosphorylation of the MAPK Hog1 and its nuclear export. Reproduced from Rodríguez de Mier [88].

When subjected to a moderate hyper-osmotic stress, the cell shrinks in few seconds due to rapid loss of water. Membrane sensory receptors detect a signal leading to the HOG pathway activation (Figure 18).

How cells sense osmotic variation is still not well understood. Until now, three mechanisms have been proposed [112]. Protein sensors could either detect the increase in macromolecular crowding, the change of pH or the concentration of some solutes and the mechanical alteration of the plasma membrane. It is also possible that one or several sensing mechanisms are involved at the same time. Tamas *et al.* suggested that change in membrane rigidity and more particularly in turgor pressure is the signal sensed by the HOG cascade [104]. They observed that glycerol, used as an osmotic stress agent, is more likely to trigger an osmotic

## Chapter 1. Introduction

response than when using ethanol which is known to alter protein hydration. This argues in favor of a sensing mechanism at the level of the membrane or cell wall mechanical properties.

After the sensing process, the signal is transduced to downstream actors. The HOG MAPK pathway is composed on two redundant upstream branches that converge for the activation of the MAPKK protein Pbs2. (Figure 19). The SLN1 branch is a phosphorelay system, similar to the two-component phosphorelay present in bacteria. It is composed by three successive proteins kinase Sln1-Ypd1-Ssk1 and is a negative regulator of the HOG cascade [113] (Figure 19A). The second branch, SHO1 requires Sho1, the G-protein Cdc42, the Ste20 p21-activated kinase, the MAPKKK Ste11, and the Ste11-binding protein Ste50. Upstream, Sho1 binds to other trans-membrane proteins, Msb2, Hkr1 and Opy2. This branch is also partially implicated in the pheromone response and the filamentous growth pathways [97]. To prevent signaling cross-talk, Pbs2 acts as a scaffold protein of the SHO1 branch. By interacting with both the upstream protein Sho1 and the downstream MAPKKK Ste11, Pbs2 mediates a specific hyper-osmotic signaling (Figure 19B). The role of Sho1 as an osmosensor has been recently reconsidered and it seems more likely to act as a facilitator of modules assembly. Other trans-membranes proteins linked to Sho1, such as the proteins Hkr1 and Msb2 are osmosensor candidates [114].

Both SLN1 and SHO1 branches lead to the phosphorylation of their respective MAPKKKs (Figure 19). The SHO1 branch induces the activation of the MAPKKK Ste11 while the SLN1 branch triggers the phosphorylation of Ssk2/Ssk22 redundant MAPKKKs activations. The MAPKKK Ste11 is activated by dual phosphorylation on its serine and threonine residues while Ssk2 is activated by the unphosphorylated form of Ssk1. The MAPKKKs Ste11 and Ssk2/22 both can activate the MAPKK Pbs2 by phosphorylation on its Ser514 and Thr518 [115]. Finally, activated Pbs2 phosphorylates the MAPK Hog1 on its Thr174 and Tyr176 residues [116].

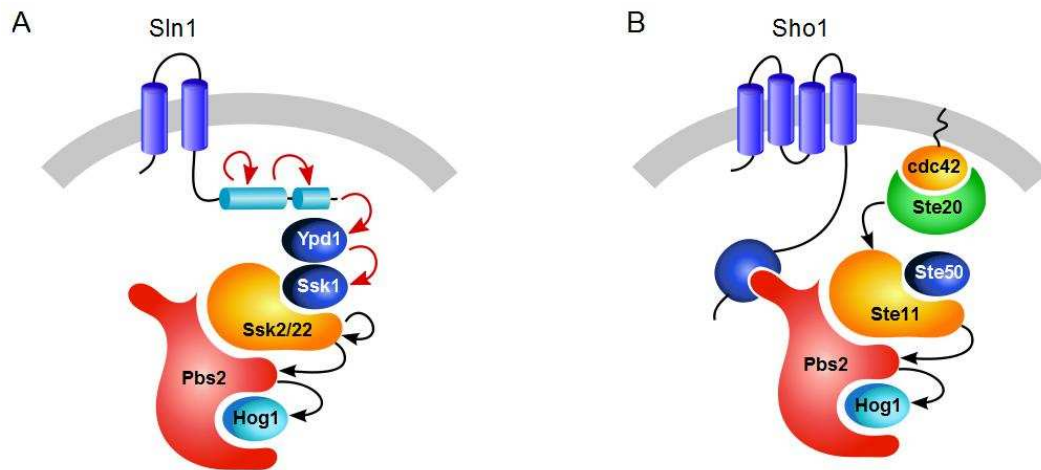


Figure 19. Representation of the respective SLN1 (A) and SHO1 (B) branches of the HOG pathway. (A) In iso-osmotic conditions, Sln1 is activated by auto-phosphorylation on His576. The phosphate is then transferred on the Asp1144 of its own receiver domain, and is then relocated on the Ypd1-His64. Finally the phosphate is recruited on Ssk1-Asp554. The phosphorylation of Ssk1 prevents the interaction of Ssk1 with the MAPKKKs Ssk2/Ssk22. In hyper-osmotic conditions, Sln1 is inhibited, leading to the de-phosphorylation of Ssk1. Ssk1 activated will then interact with downstream actors. (B) Under hyper-osmotic conditions, Sho1 recruits and links directly Pbs2 to its SH3 domain. Then, Ste50 anchors the set of three proteins Sho1-Ste11-Pbs2 to the proteins cdc42 and Opy2 leading to Ste11 activation. The black arrows represent serine, threonine or tyrosine phosphorylation while red arrows represent phosphotransfer events in iso-osmotic conditions. In hyper-osmotic conditions, the MAPKKKs Ssk2/22 and Ste11 (yellow proteins) are activated by their respective branches leading to the phosphorylation of the MAPKK Pbs2 (red protein), itself phosphorylating the MAPK Hog1 (light blue protein). Reproduced from O'Rourke and Herskowitz [117].

Both Hog1 and Pbs2 are essential actors of the HOG pathway as deletion of one or both genes leads to osmo-sensitivity [118]. Once activated, the MAPK Hog1 triggers several actions in both the cytoplasm and the nucleus. In the cytoplasm, Hog1 participates in the cell cycle arrest in either G1 or G2 phases through the respective activation of the CDK-inhibitor protein Sic1 [119], and the checkpoint kinase Hsl1 [120]. Once the cell overcomes the osmotic stress, the progression through the cell cycle is restored. Active cytoplasmic Hog1 is also involved in ionic regulation through the nuclear membrane essential for proteins-chromatin binding. Indeed, due to cell volume reduction, the nucleus shrinks and this triggers inter-chromatin pores enlargement. This process facilitates electrolyte accumulation and leads to the dissociation of most proteins from the chromatin. In order to restore this ionic equilibrium, Hog1 targets and activates the Tok1 potassium channel and the Nha1 Na<sup>+</sup>/H<sup>+</sup> antiporter [121]. Cytoplasmic Hog1 also triggers a decrease in translation through the activation of the kinase Rck2 [122]. In addition, cytoplasmic active Hog1 seems to indirectly control the Fps1 glycerol channel closure that allows

## Chapter 1. Introduction

intracellular accumulation of glycerol [123]. Even if the cytoplasmic role of Hog1 has non-negligible effects, it has long been thought to be insufficient for complete osmoregulation. Yet, restricting Hog1 into the cytoplasm by sequestering it at the membrane is sufficient for survival after short, gentle osmotic stimulations [124, 125]. This process is independent of Fps1 closure as cytoplasmic anchored Hog1 cells for which *FPS1* is deleted still survive. Westfall *et al.* proposed that Hog1 enhances the activity of enzymes implicated in glycerol metabolism [124]. Although cytoplasmic Hog1 is sufficient for osmotolerance on short period of time, the nuclear action of Hog1 remains essential for long-periods or strong osmotic stresses [125]. Indeed, after a hyper-osmotic stress, Hog1 is also rapidly transported in the nucleus by the karyopherin Nmd5 [109]. Since no NLS<sup>17</sup> or NES<sup>18</sup> sequences have been found in Hog1, the details of its nucleo-cytoplasmic transport remains unclear [116]. Hog1 nuclear activates several transcription factors. Hot1 [126], Msn1 [126] the bZIP<sup>19</sup> protein Sko1 [127] and the MADS box<sup>20</sup> protein Smp1 [128] are the direct transcription factors target of Hog1 recruited after hyper-osmotic shocks. However, other stress response factors are also involved, such as the two redundant zinc-finger binding domain proteins Msn2/Msn4 that drive the general stress response in yeast [129]. The control of those different factors by Hog1 leads to the differential expression of several genes [130]. This transcriptional modification is transient and targets approximately 5% of all yeast genes [100]. The transcription of 186 genes is up-regulated to 3-fold higher, while the transcription of around 100 genes is down-regulated by a factor of 1.5. The genes that are down-regulated encode essentially cyclins, ribosomal proteins and other translational factors. The decrease in expression of those genes is linked to the transient growth and division arrest [131]. An important fraction of up-regulated genes are involved in cell

---

<sup>17</sup> Nuclear Localization Signal (NLS) is a short sequence that is used to target the protein to the cell nucleus through the Nuclear Pore Complex.

<sup>18</sup> Nuclear Export Signal (NES) is a short sequence that targets proteins for export from the cell nucleus to the cytoplasm through the Nuclear Pore Complex.

<sup>19</sup> Basic Leucine Zipper (bZIP) is a domain found in DNA binding eukaryotic transcriptional factors. One part of the domain contains a basic region that directly interacts with DNA and a leucine zipper that mediates dimerization through contact with a protein partner.

<sup>20</sup> The MADS box is a highly conserved sequence motif found in a family of transcription factors. Most MADS domain factors play important roles in developmental processes.

protection such as chaperones or oxidative protectors as well as in cell wall protection and synthesis through lipid expression. Around 30 genes, specifically targeted by Hog1, are involved in the carbohydrate metabolism, essential for glycerol synthesis. The glycerol-3-phosphate dehydrogenase and the glycerol-3-phosphatase are critical actors of this production. Two similar isogenes, *GPD1* plus *GPD2* [132] and *GPP1* plus *GPP2* [133] respectively encode those enzymes. Glycerol is a polyol naturally synthesized by yeast as a source of carbon and energy. It is also the only osmolyte synthesized by *S. cerevisiae* upon hyper-osmotic stress. The glycerol accumulation increases the intracellular osmolarity. This forces water to flow back inside the cell to equilibrate osmotic pressures. The cell can eventually recover its physiological size. The Figure 20 summarizes the actions of Hog1 in both the cytoplasm and the nucleus.

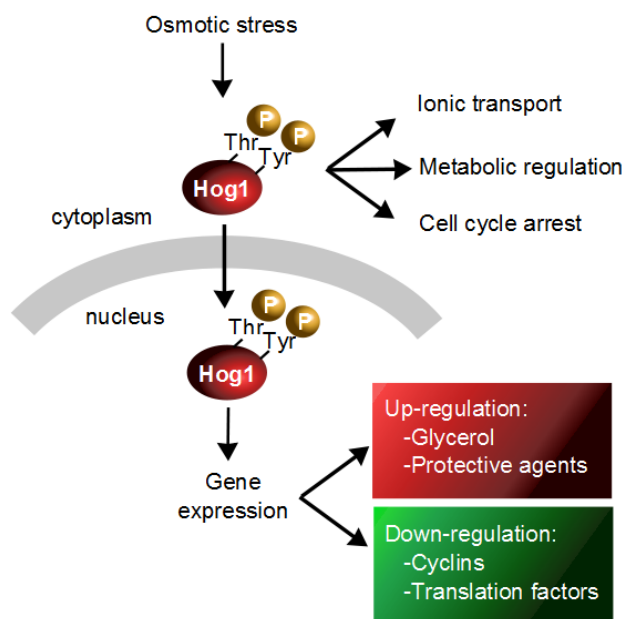


Figure 20. Hog1 physiological roles in both the cytoplasm and the nucleus. In the cytoplasm, Hog1 triggers various actions, like electrolytes flow regulation, metabolic or translational regulation. On long-term, nuclear Hog1 triggers more efficient transcriptional responses, leading to glycerol synthesis. Reproduced from Rodríguez de Mier [88].

About 30 min after a hyper-osmotic shock, concomitant with the onset of glycerol production, Hog1 is dephosphorylated and exported from the nucleus via the karyopherin Xpo1 [109]. In yeast, three classes of protein phosphatases are known to down-regulate MAPK pathways. The dual specificity phosphatases (DSPs) dephosphorylate both phosphotyrosine (pY) and phosphothreonine (pT), the protein tyrosine phosphatases (PTPs) dephosphorylate only tyrosine residues while the protein phosphatases type 2C (PTC) dephosphorylate threonine, serine, and sometimes tyrosine residues [87]. For the HOG pathway, the serine-threonine

phosphatases Ptc1, Ptc2, and Ptc3 [134, 135] act on both Pbs2 and Hog1, while the tyrosine phosphatases, Ptp2 and Ptp3 strictly target Hog1 [135, 136]. Ptp2 is predominantly localized in the nucleus, Ptp3 in the cytoplasm, while the protein phosphatases types 2C are located both in the cytoplasm and in the nucleus (Figure 18). Previous studies suggest that phosphatases are constitutively active in order to constantly counteract pathway activation rather than providing an intrinsic feedback mechanism [96, 137].

## 4. The HOG pathway as a systems biology model

### A word on microfluidics

Various groups have analyzed [96] the characteristics of the HOG pathway such as its kinetics [138], cross-talks [98] and feedbacks processes [125]. To carry out such investigations quantitatively, one needs to control precisely the osmotic stress stimulation (duration, intensity) and to observe living yeast cells with high spatiotemporal resolution. Microfluidic devices can be designed to meet these requirements. Micro-chambers can be made to entrap a limited population of cells precisely fed through channels conveying nutrient and environmental fluids. Temporal variation of the cells' environment can also be applied while recording the response through microscopy at the single cell level. Many microfluidic devices varying in complexity have been designed and used for many applications in biology such as long-term cells imaging in a controlled environment [139], cDNA analyses through PCR [140, 141] and cell-based screening assays for drug discovery [142]. Several techniques are available for manufacturing microfluidic devices like micromachining [143] or soft lithography [144] to cite but a few examples. Soft lithography, is a cheap, rapid, simple method, and is widely used in quantitative biology laboratories (Figure 21).

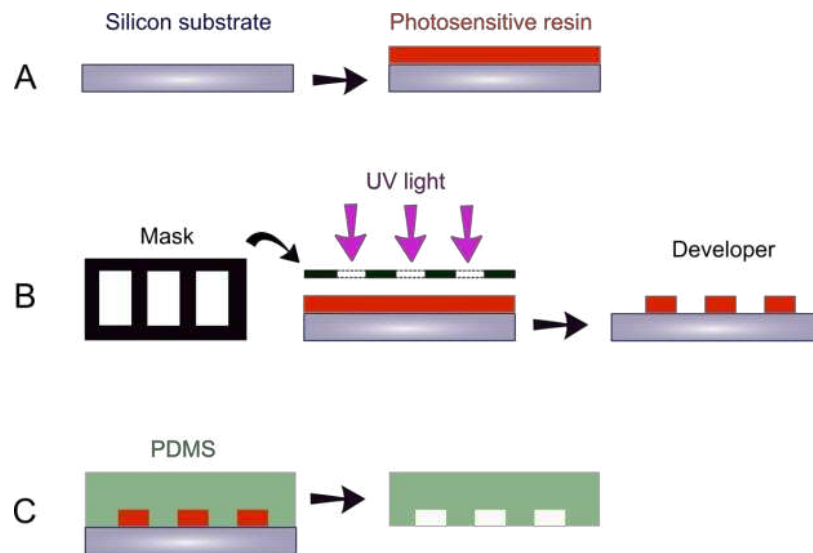


Figure 21. Representation of the soft lithography technique used in this study. (A) A silicon substrate is homogeneously coated with a thin layer of photo-sensitive resin. In this representation the resin is photo-negative meaning that it polymerizes under UV exposure. (B) UV is applied to the resin through a mask on which the patterns have been previously printed. After raising away undeveloped photoresin, the UV exposed resin forms the specific patterns. (C) PDMS is poured on the previous template and is mixed with curing agent and heated in order to solidify. The master template can then be re-used for PDMS molding. Reproduced from Weigl *et al.*[145].

It is based on the use of a positive or a negative photosensitive resin that polymerizes respectively with or without UV radiation. The patterning is done by spreading the resin homogeneously on a flat wafer, laying down a transparency mask and shining through the mask with UV light. This cures the photoresist according to the transparency pattern printed on the mask. The photoresist resin is then developed to remove the uncured resin (Figure 21A-B). This wafer is used as a master template that can be re-used almost indefinitely. A polymer, usually polydimethylsiloxane (PDMS), is mixed with a curing agent, cast on the master pattern and cured by heating (Figure 21C). Once the PDMS has been cured and peeled of the template, it can be used as a microfluidic chip. Holes are punched in the PDMS block at the location of the inlets and outlets. Its surface is then treated by oxydation in a plasma oven which facilitates its binding to a glass coverslip. Pumps connected to valves or pressure controllers are then used to generate and control a fluid flow.

The small dimensions of microfluidic devices and the typical flow rates used in such devices usually means that the flows are laminar [146]. Indeed, the Reynolds

number,  $R_e = \frac{uL}{\nu}$ , ( $u$  is the mean velocity of the fluid,  $L$  the typical dimension of the device and  $\nu$  the fluid kinematic viscosity) is always very small, a hallmark of laminar flows. The Reynolds number is a dimensionless number that compares inertial effects to viscous effects in a flowing fluid, so that for low Reynolds, the viscous effects are dominant. This confers the advantage of flow compartmentalization inside a unique channel (Figure 22). Indeed, in this case, the streams flow parallel to each other, with minimal mixing by diffusion at the interface.

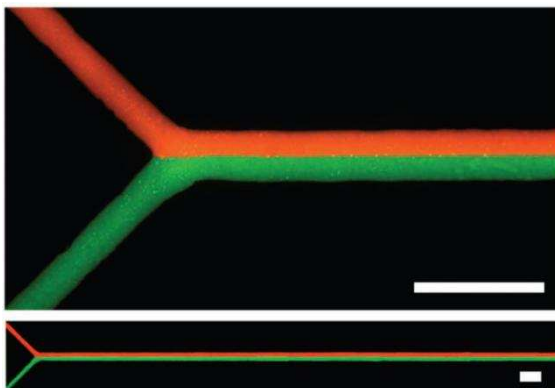


Figure 22. Fluorescent microscopy image of a laminar co-flow inside a straight microfluidic channel. Two fluorescent fluids (red and green dyes) meet at a Y junction and then flow side by side. The scale bars represent 0.5 mm. Taken from Therriault *et al.* [147].

### Frequency response of the HOG pathway

Using laminar coflows, Hersen *et al.* designed a fast binary switch to repeatedly change the environment of single yeast cells between two osmotic conditions [138]. Two fluids of different osmolarities were flowing side by side on yeast cells attach to the glass bottom of the microfluidic channel. Varying the pressure of one inlet moves the interface between the two fluids laterally, thus quickly changing the osmolarities of yeast cells near the interface. The extracellular osmolyte concentration was varied periodically to create square-wave inputs. Using this microfluidic device, they recorded the dynamic of nuclear accumulation of the protein Hog1 in function of the period of the osmotic stimulation. Hersen *et al.* characterized the pathway frequency response and its bandwidth. At frequencies lower than the cut off frequency of the HOG cascade, the cells nicely tracked the period of the applied shock and responded faithfully to it by displaying a periodic localization of the Hog1 protein. However, above this cut off frequency, the systems couldn't follow anymore the period of the stimulus, but instead integrated the input

as if it were one steady stress of lower magnitude (Figure 23). They also studied the difference between the two upstream branches of the pathway. They showed that SLN1, as a rapid acting branch is able to sense frequency at a level that the SHO1 branch cannot.

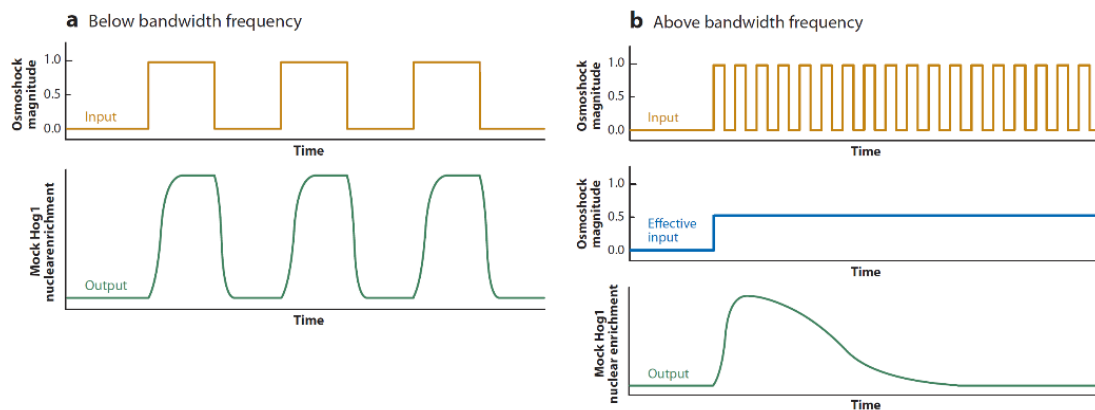


Figure 23. Representation of the frequency response of the HOG pathway. (a) The Hog1 nuclear localization (output, green) follows the osmotic stimulation (input, yellow) when the input frequency is low enough. (b) At high frequency (yellow), the HOG cascade cannot sense the temporal variation. Instead it responds as if there were a single osmotic input (blue input, green output). Taken from Muzzey and Van Oudenaarden [35].

Mettetal *et al.* in 2008 coupled experimentation and mathematical modeling to describe the feedback loops dynamics of the HOG pathway [125]. They developed a similar device than Hersen *et al.* and recorded the nuclear fluorescence accumulation of Hog1. In addition to Hersen *et al.* who measured the oscillatory capacity of Hog1 between the nucleus and the cytoplasm, Mettetal *et al.* measured the phase shift of Hog1 oscillations. Based on that, they characterized two feedback mechanisms: A fast cytoplasmic action occurring on short timescale involving Hog1 as a metabolism inductor, and a slower nuclear one leading to a transcriptional feedback. They confirmed this hypothesis by inhibiting de novo gene expression and observing similar Hog1 nuclear translocation response. Westfall *et al.* reached the same conclusions by physically tethering Hog1 at the plasma membrane which prevented it to translocate inside the nucleus. In contrast with a *hog1Δ* strain, this strain was still able to overcome osmotic stress, showing the importance of Hog1 cytoplasmic actions upon gentle osmotic stress [124].

## Chapter 1. Introduction

Based on the response-kinetics of the HOG pathway, quantitative models of the cascade have been developed. The most complete one has been developed by Klipp *et al.* [96]. They not only computed the HOG pathway, but integrated the overall glycerol metabolism as well as gene expression modification of enzymes involved in osmoadaptation. They also added to their model the closure of the membrane glycerol transporter Fps1 and the feedback loops leading to Hog1 dephosphorylation through phosphatases activity. Their model reproduced accurately the transient behavior of the overall HOG system through simple stimulation. It involved both Pbs2 and Hog1 activation, but also Hog1 nuclear import, glycerol production and cell size recovery. A similar but simplified version of this model [148] allowed the prediction of the Hog1 nuclear translocation behavior through different scenarios of input like simple step increase, periodic pulses or up-staircase increases of osmotic stress. A recent study by Uhlendorf *et al.*, in which I have taken part, proposed a different investigation that used the HOG pathway as an inducible promoter system (Appended Article #2). The HOG osmoregulation system in yeast was used to implement a biological control of the transcription of a fluorescent reporter [149]. We used a microfluidic device for long-term cell imaging, and recorded the expression of yECitrine placed under the control of the glycerol proton symporter Stl1 promoter. This system was coupled to a Model Predictive Controller (MPC)<sup>21</sup> that estimated the fluorescence of either a population or a single cell and adjusted the optimal osmotic input necessary to maintain a constant expressional level of yEcitrine. By applying osmotic pulse of 5 to 8 minutes with relaxation intervals of minimum 20 minutes, they were able to force the transcriptional response to a constant value for 15 hours.

---

<sup>21</sup> **Model Predictive Control (MPC)** is a mathematical method in which the current control action is obtained by solving, at each sampling instant, an optimal control problem for which errors, namely the difference between the predicted output and the desired reference, is minimized over a future horizon. Once the results of the manipulations are predicted, the controller applies a stimulation to the variable that produces the desired output.

## Chapter 1. Introduction

To make a long story short, the mechanistic details of the HOG cascade are indeed very well known. In the scope of our project this is an important pathway since we will compress cells using osmotic stress. It is also a very complex system with many partners, and it is probably now clearer to the reader why molecular crowding effects are not easily studied in live cells, where proteins activation depends on so many actors. Nevertheless, we will discuss the possibility to use osmotic compression as a way to modulate molecular crowding in the cytoplasm and observe its effects on the dynamics of several cellular processes.



## OBJECTIVES

The main objective of this thesis is to characterize the effects of increasing macromolecular crowding on the dynamics of signal transductions. I used hyper-osmotic stress to compress *S. cerevisiae* cells and increase the macromolecular crowding, while observing by microscopy the dynamics of several cellular processes. In the first part of this thesis, I describe the effects of increased macromolecular crowding on the kinetics of the HOG pathway. I base this analysis on the measurements of the phosphorylation, the cytoplasmic diffusion ability and the nuclear translocation of its transcriptional factor Hog1. While, it is well known that a moderate hyper-osmotic shock triggers a quick nuclear translocation of Hog1 (2-5 min), I investigate how increasing molecular crowding alters this process. In a second part, I ask whether the observed effects are specific to the HOG signaling. To this end, I analyze other biological processes in yeast and in higher eukaryotic cells. I focus on the nuclear translocation of alternatives transcriptional factors such as Msn2, Crz1, Yap1 and Mig1 upon osmotic compression. I also study other processes than signaling such as endocytosis and protein mobility. The diffusion of Hog1-GFP, Ura1-GFP, citrine and YFP is investigated in *S. cerevisiae* while the diffusion of GFP is analyzed in human cell lines. I finally discuss the adaptability of cells to severe osmotic compression and discuss further how our data can be interpreted in terms of molecular crowding and its effect on the dynamics of cellular processes.



## CHAPTER 2.

# OSMOTIC COMPRESSION SLOWS DOWN THE HOG PATHWAY

<b>5. Cellular compression triggers a slow-down of the HOG pathway</b>	<b>60</b>
Hog1 nuclear localization kinetics	60
Hog1 phosphorylation kinetics	64
Comparing phosphorylation and nuclear import of Hog1	65
Cell volume decrease as a function of osmotic stress	66
Hog1 diffusion kinetics	69
<b>6. Discussion</b>	<b>76</b>

## 5. Cellular compression triggers a slow-down of the HOG pathway

### Hog1 nuclear localization kinetics

We started our investigation by looking at the effects of cellular compressions on the HOG cascade. Volume compression was achieved by using sorbitol as a hyperosmotic stress agent. We used two different experimental devices. The first one is an improved version of the Y-shape microfluidic chip previously used in our lab for the characterization of the HOG pathway frequency response [138]. This device has a main channel of 50  $\mu\text{m}$  high and 500  $\mu\text{m}$  wide with two inlets on one side and one outlet at the opposite side (Figure 24A). One inlet is fed with an isotonic medium, the Synthetic Complete (SC) medium, and the other with the same culture medium supplemented with sorbitol. As we said previously in the case of laminar flows, fluids do not mix but flow side by side [146]. The position of the fluids interface is set by the applied pressure at the inlets. A difference in refractive indices between the media allows the visualization of the fluids position by phase contrast. The flow in the channel is controlled via a pressure controller system called Microfluidics Flow Control Systems (MFCS, Fluigent). Changing the pressure difference displaces the interface laterally in less than a second. Cell adhesion inside the chamber is achieved by functionalizing the glass coverslip with concanavalin A (2 mg/ml): a lectin protein which binds specifically to mannosyl and glucosyl residues of the yeast cell wall. The concanavalin A solution is injected inside the chamber and incubated for 10 min. Cells, previously grown in SC medium are then added to the chamber and given some time to bind to the lectins.

The second system is a simple perfusion chamber called gaskets (Figure 24B). The chamber size is much larger, 19 mm x 6 mm, with a volume capacity of about 85  $\mu\text{l}$ . They are made in silicone and can adhere to glass coverslips naturally. Their dual-access ports allow to quickly flowing reagents (< 10 sec, including manual operation). Liquid is added manually by using a micropipette at one side and by aspirating at the other access port by capillarity with a paper towel. As for the Y-

## Chapter 2. Osmotic compression slows down the HOG pathway

shape microfluidic device, cell adhesion is also achieved by coating the glass cover slip with concanavalin A.

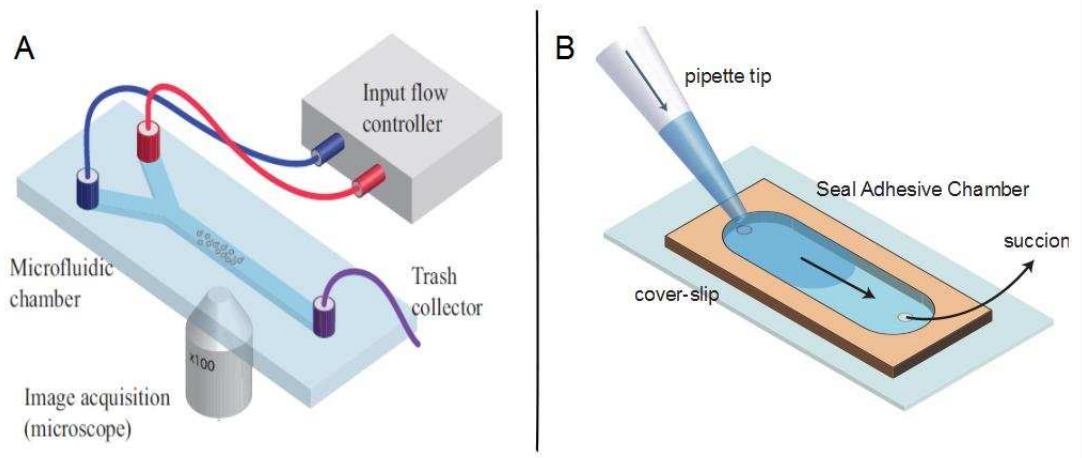


Figure 24. Representation of the microfluidic devices used in this study. (A) The Y-shape device is composed of two inlets and one outlet. One of the inlets is fed with iso-osmotic medium and the other with hyper-osmotic medium (sorbitol). The cells bind to concanavalin A previously coated on the coverslip. By applying pressure differences in the inlets, the environment of cells can be controlled temporally and spatially. The microfluidic device is set-up on an inverted microscope for the time-lapse observation of protein behavior under osmotic stimulation. (B) Illustration of water flowing inside a perfusion chamber gasket. The chamber, on his down side, is composed of rubber which adheres to coverslips. The media is then introduced without leaking by pipetting in one side and aspirating the other side.

We focused our analyses on Hog1 nuclear accumulation upon hyper-osmotic stimulation using a strain in which *HOG1* has been tagged by a green fluorescent protein and the histone *HTB2* by a red fluorescent protein (*HOG1-GFP*; *HTB2-mCherry*). The first observations were performed using the fast-switching media microfluidic device coupled with time-lapse microscopy. Bright-field, GFP and mCherry images were acquired at each time point. The position of the nucleus was measured thanks to Htb2-mCherry acquisitions which were then used to quantify the amount of Hog1-GFP in the nucleus. The measured output of the HOG activation was defined as the ratio of nuclear Hog1 versus its cytoplasmic level (see the appendix for material and methods).

Using such method, we were able to generate very fast osmotic stimulation and to study the dynamics of Hog1 at the single cell level (Figure 25). For instance, applying a sudden and unique osmotic stress (Figure 25A) of gentle magnitude (1 M sorbitol), gave the expected response of the HOG pathway. We could similarly

## Chapter 2. Osmotic compression slows down the HOG pathway

observe the frequency response of the nuclear import of Hog1 using periodic square pulses of sorbitol (Figure 25B). The Y-shape microfluidic device is indeed particularly suitable for the generation of such repetitive stimulations [138]. Up-staircase input of osmotic stress is another example of inputs for which the re-stimulation of Hog1 after adaptation could be observed (Figure 25C). The gaskets were more practical in this latter case since the Y-shape device was restricted to two possible inputs only.

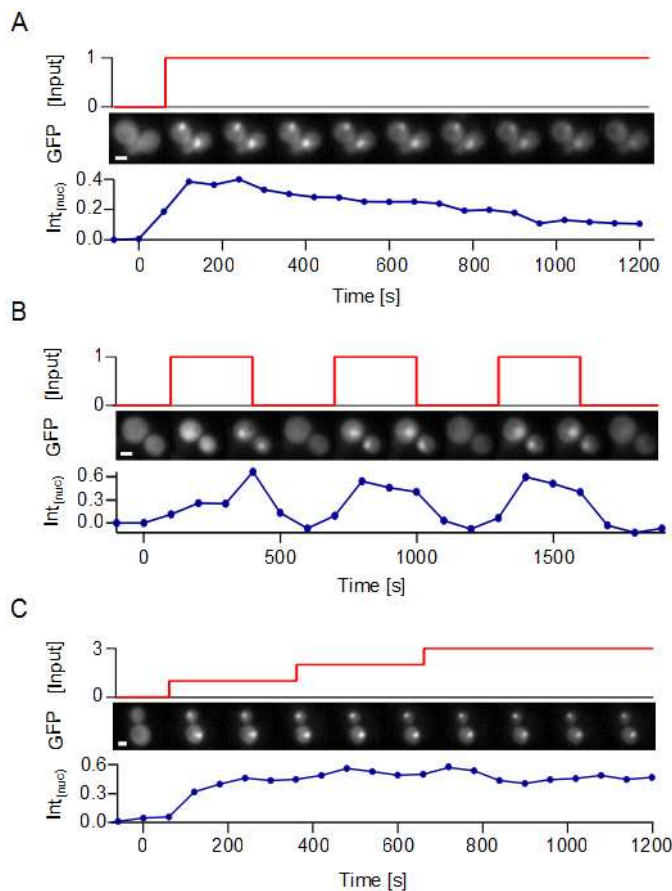


Figure 25. Examples of input-output experiments conducted in this study. The induced input (sorbitol) can either be a single step input (A), periodic pulses (B) or up-staircase increase signal (C). The nuclear localization of Hog1 ( $Int_{(nuc)}$ ) is induced by sorbitol input (red curve) and measured by the ratio of GFP nuclear ( $Int_{GFPnuc} - Int_{GFPcell}$ ) to the whole GFP fluorescence ( $Int_{GFPcell}$ ) (blue curve and points). The scale bars represent 2  $\mu m$ .

When we applied a single step shock (Figure 25A) of a gentle osmotic stress (1 M sorbitol), we observed a rapid cell shrinkage (< 30 sec) followed by the nuclear import of Hog1, reaching a maximum 3 to 5 minutes after the stress. Concomitant to Hog1 nuclear import, the cell volume progressively increased. As the cell almost recovered its initial size, Hog1 was slowly exported, taking around 20 to 30 min to come back to its initial cytoplasmic level (Figure 26). This result was consistent with previous analyses showing a rapid and transient Hog1 nuclear import after a gentle stress [54, 109].

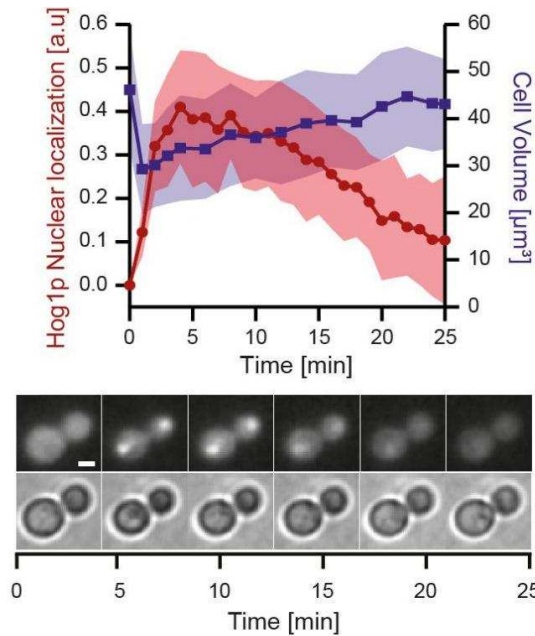


Figure 26. Effect of moderate osmotic stress on Hog1 nuclear accumulation. Cell shrinkage followed by Hog1 nuclear enrichment occurs rapidly upon 1 M sorbitol induction. Bottom panel: GFP (Hog1) and bright-field (volume) images of 1 M sorbitol experiment over time. The scale bar represents 2  $\mu\text{m}$ .

Similar results were obtained with osmotic shock ranging from 0.5 to 1 M. The maximum nuclear localization occurs around 3 to 5 min after the stress. However, applying a sorbitol concentration of 1.2 M led to a slightly slower response, with a maximum nuclear import 9 min after the stress. A stress with 1.5 M sorbitol triggers a maximum translocation  $\sim 17$  min after the stress. The effect becomes more and more visible with increasing sorbitol concentration. At the concentration of 1.75 M sorbitol, the maximum localization time was around 50 min (Figure 27). Above 2.2 M, no more nuclear localization was observed (Figure A1). There was a progressive slow-down of Hog1 nuclear accumulation when the osmotic compression was increased.

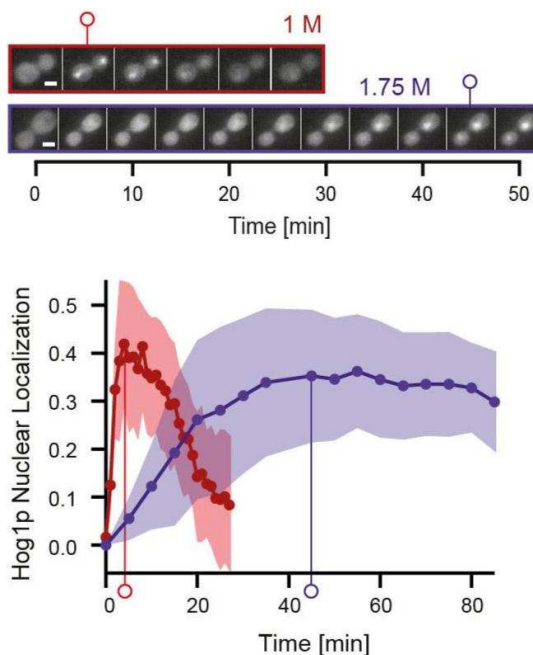


Figure 27. Increasing osmotic stress slows down the ability of Hog1 to translocate in the nucleus. Top panel: Time-lapse imaging of Hog1 nuclear translocation upon 1 M sorbitol (red) or 1.75 M (blue) stimulation. The scale bars represent 2  $\mu\text{m}$ . Bottom panel: The rate of Hog1 nuclear translocation is plotted in function of time. The time of maximal nuclear localization is recorded for both 1 M (red line, 5 min) and 1.75 M (blue line, 45 min) sorbitol induction.

## Chapter 2. Osmotic compression slows down the HOG pathway

This was consistent with the fact that a frequency response study of the HOG cascade to a severe osmotic stress (2 M sorbitol) showed that the cascade was not able to follow faithfully the signal even for low frequency. Several questions arose from our observations. We can first wonder if it is the osmotic stress or the volume compression that is responsible for this slow-down. Does this effect occur transiently? How progressive is it? In order to address these questions, we started a quantitative study of the Hog1 dynamics over a range of sorbitol concentrations.

### **Hog1 phosphorylation kinetics**

We measured Hog1 phosphorylation kinetics upon single osmotic stress up-shift by western blots (see the appendix for material and methods). Under 1 M sorbitol, the maximum activation occurred rapidly, around 2 min after the stress as reported by previous analyses [54, 109, 110]. At 1.5 M sorbitol, Hog1 phosphorylation occurred from 2 min to 30 min after the stress with a phosphorylation peaking at 10 min. Applying 1.8 M sorbitol led to a phosphorylation between 30 min to 2 hours after the shock with a peak at 30 min. Finally with a stress made with 2 M sorbitol, Hog1 activation was delayed from 30 min to 3 hours peaking at 1 hour. At the concentration of 2.5 M, no more phosphorylation was detected (Figure 28). For each concentration, we performed a control by incubating the blots with antibody against the constitutive protein Phosphoglycerate Kinase (PGK)<sup>22</sup>. PGK presented a homogeneous expression for each concentration and timescale confirming the specificity of Hog1 phosphorylation in response to hyper-osmotic shocks (Figure A7). From these results, we concluded that the phosphorylation of Hog1 was slowed down and that it remained phosphorylated longer for stronger hyper-osmotic stresses.

---

<sup>22</sup> 3-Phosphoglycerate Kinase (PGK) catalyzes during glycolysis the transfer of a high-energy phosphoryl group from the acyl phosphate of 1,3-diphosphoglycerate to ADP to produce ATP.

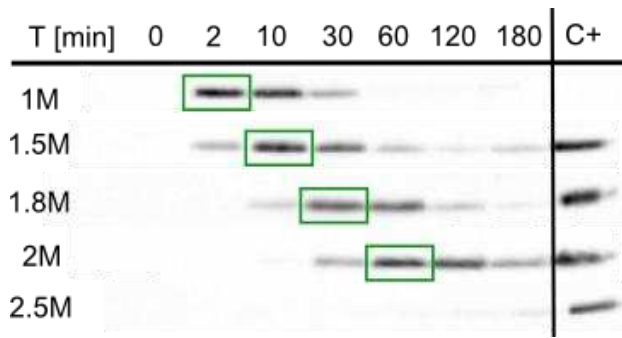


Figure 28. Hog1 phosphorylation kinetics. The maximum of Hog1 phosphorylation (boxed by green rectangles) is delayed when increasing stress. At 2.5 M sorbitol, no more activation is observable. The positive control (C+) corresponds to the 2 min peak of Hog1 phosphorylation at 1 M sorbitol.

### Comparing phosphorylation and nuclear import of Hog1

We also quantitatively measured the maximum of Hog1 nuclear localization over a range of osmotic stress. To do so, we used the simple gasket system as it was not useful to create time varying signal for this study. The timescale of activation profiles of both Hog1 phosphorylation and its nuclear accumulation were compared by plotting their maximum induction time in function of the stress intensity. There was a good correlation, which was expected since both processes are linked (Figure 29). Indeed, Hog1 phosphorylation is necessary and sufficient to trigger its nuclear import.

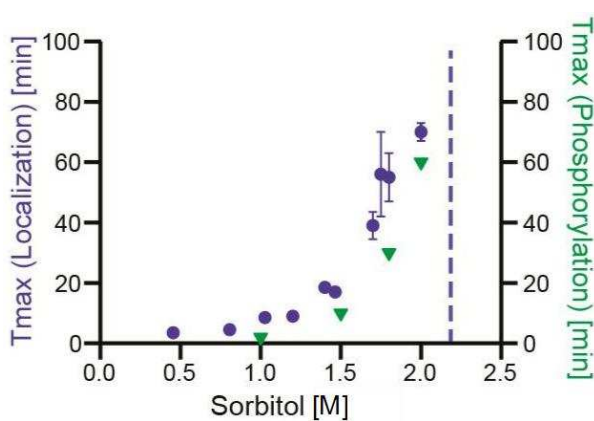


Figure 29. Comparison of Hog1 activation and nuclear accumulation characteristic timescales as a function of sorbitol concentration. The dynamics of Hog1 phosphorylation (green inverted triangles) and nuclear translocation (blue circles) are similarly decreased with increasing compression. The blue dashed bar represents the limit sorbitol concentration of cell responsiveness (2.2 M).

Increasing the osmotic compression and thus the intracellular macromolecular crowding triggered a progressive slow-down of both the phosphorylation and the nuclear accumulation of the protein Hog1. Those data are consistent with the previous observation made by Van Wuytswinkel *et al.* [54]. As we mentioned in the introduction, in their study, the authors compared the effect of a mild (0.4 M) and a

## Chapter 2. Osmotic compression slows down the HOG pathway

severe (1.4 M) NaCl stress on Hog1 activation and nuclear translocation. Upon severe osmotic shock (1.4 M) they observed a delay in the response and longer activation duration compared to a mild stress (0.4 M). They also showed that Hog1 nuclear localization delay was correlated with a delay in the expression of stress-responsive genes.

### Cell volume decrease as a function of osmotic stress

To go on with our hypothesis that the slow-down of Hog1 was related to increased molecular crowding due to volume compression, we measured the cell volume before ( $V_{max}$ ) and after ( $V$ ) the stress. The cell volume decreased with increasing osmotic stresses. The final cell volume reached a minimum at ~2 M sorbitol corresponding to ~40% of the initial cell volume (

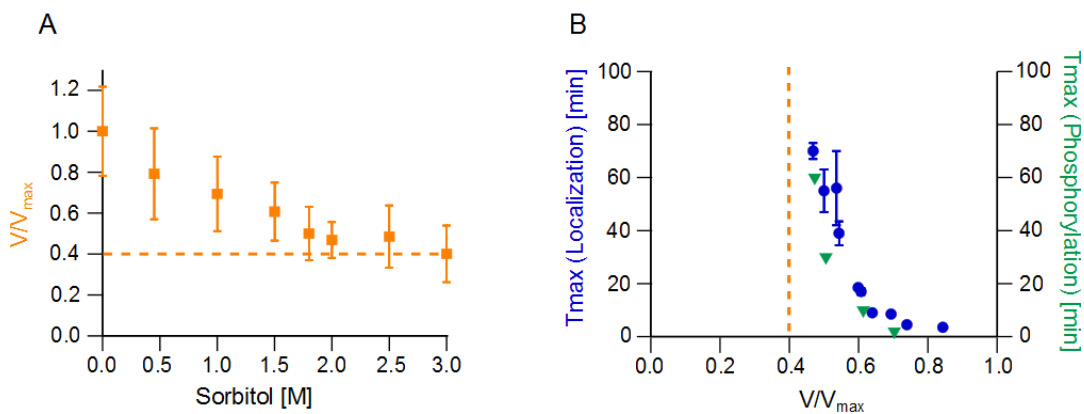


Figure 30A). This value is close to the minimum cell volume calculated by previous authors which is of about 50% of the initial cell volume [40, 67, 71].

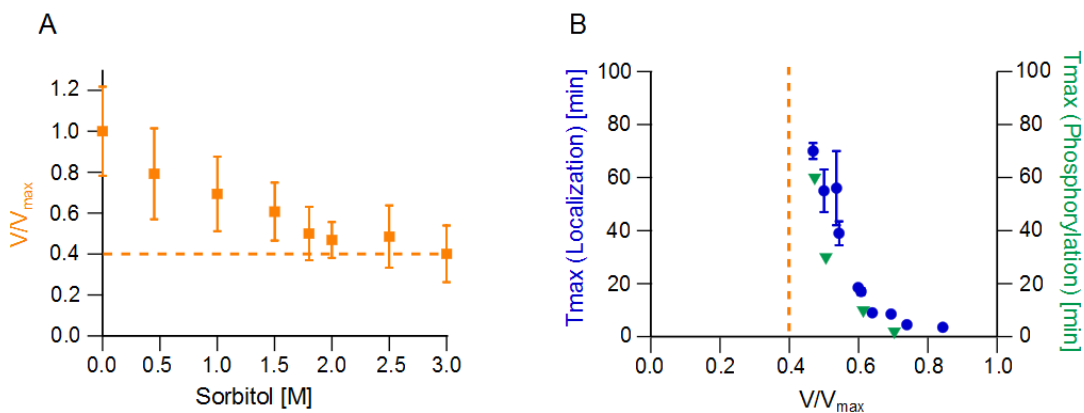


Figure 30B shows the kinetics of the nuclear translocation and phosphorylation of Hog1 as a function of the relative cell volume. It can be seen that the slow-down for

## Chapter 2. Osmotic compression slows down the HOG pathway

both Hog1 activation and nuclear import is more and more pronounced for larger cell compression that is small  $V/V_{\max}$ .

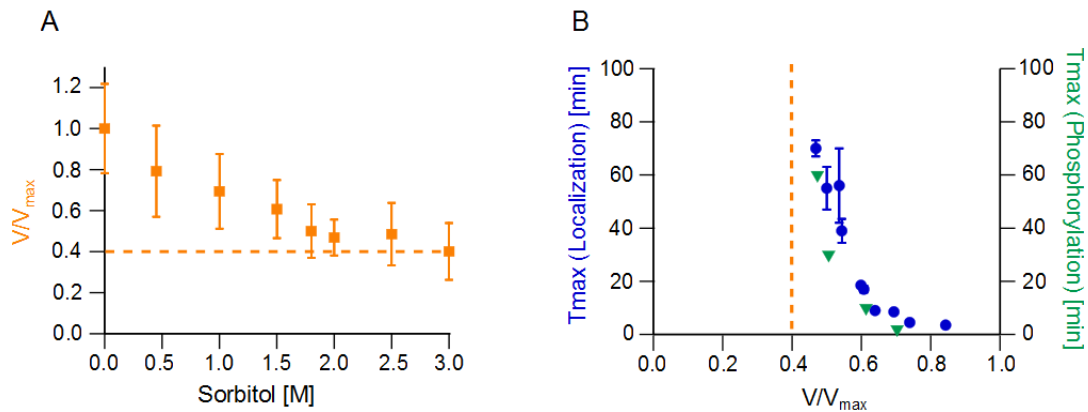


Figure 30. Cell volume reduction and Hog1 slow-downs. (A) The relative cell volume in function of the sorbitol concentration shows a rapid decrease. A plateau is reached around 2 M sorbitol and corresponds to a minimal cell volume of 40%. (B) The times for maximum Hog1 activation and nuclear localization are plotted in function of the relative cell volume reduction. Those maxima increase significantly with cell size compression.

Experiments conducted with NaCl as an osmotic agent confirmed these findings. Hog1 nuclear translocation was analyzed over concentrations ranging from 0.25 M to 1.4 M NaCl. Applying the concentrations of 0.25 M and 0.5 M triggers similar dynamics with a maximum nuclear accumulation 3 to 5 min after the stress. Increasing the concentration to 1 M induces a nuclear import peaking at 13 min, while the maximum import upon 1.4 M NaCl occurs ~67 min after the stress. Note that since NaCl dissociates in two ions when dissolved ( $\text{Na}^+$  and  $\text{Cl}^-$ ), the osmolarity of a 1 M NaCl solution is, in first approximation, equivalent to a 2 M sorbitol solution. To illustrate this, the NaCl concentration axis is scaled with a factor two compared to the sorbitol axis (Figure 31A).

Chapter 2. Osmotic compression slows down the HOG pathway

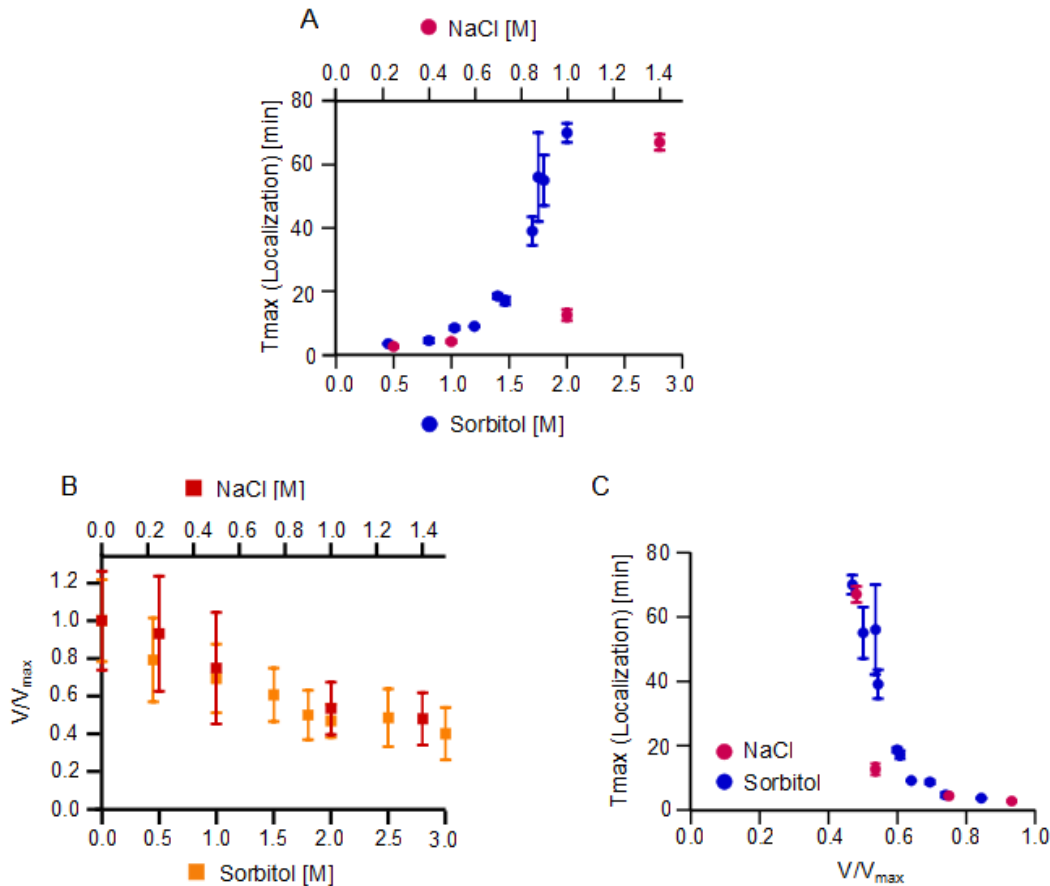


Figure 31. Comparison of both NaCl and sorbitol effects on the kinetics of Hog1. (A) The graph shows the maximum time of Hog1 nuclear localization for both sorbitol (blue circles) and NaCl (red circles) in function of their concentrations. To illustrate the difference of osmolarity between sorbitol and NaCl, the top axis is scaled by a factor two compared to the bottom axis. (B) The relative cell volume is plotted in function of sorbitol (yellow squares) and NaCl (red squares) concentrations. (C) Both NaCl and sorbitol trigger similar delays of the HOG cascade when plotted in function of the cell volume reduction.

We nevertheless observed that there were still differences between Hog1 response to NaCl and sorbitol. Indeed, the maximum time of Hog1 nuclear accumulation triggered with NaCl occurs more progressively than with sorbitol. Another interesting observation is their different signaling capacities. Cells subjected to NaCl 1.4 M, approximately equivalent to a 2.8 M sorbitol, were still triggering the import of Hog1 while cells stimulated by sorbitol were not responding anymore above 2.2 M (Figure A1). Thus, the comparison of the dynamics for the two osmotic agents is not straight forward. Interestingly, both sorbitol and NaCl stresses lead to similar volume reduction (Figure 31B) and their effects on Hog1 dynamics are similar when the dynamics are plotted in function of the cell volume reduction (Figure 31C). These results further suggest that Hog1 dynamics impairment is not dependent on

the osmotic agents used or its osmolarity but on its action on the cell volume reduction.

### Hog1 diffusion kinetics

Macromolecular crowding is known to alter the diffusion of molecules. Several groups observed a progressive decrease in protein diffusion both *in vitro* [30, 32] and *in vivo* [36, 37]. I previously showed that the dynamics of the HOG cascade (activation and nuclear translocation) are altered by volume compression. A possible reason for this decrease may be the densification of the cytoplasm that leads to slower diffusion of proteins, including Hog1. A method for measuring the transport of fluorescent particles inside cells is the Fluorescence Recovery After Photobleaching (FRAP) technique. FRAP was initially used as a method for measuring diffusion in cellular membranes [150] but has been largely extended for the study of intracellular dynamics such as cytoskeleton dynamics, vesicle transport, protein recycling or signal transduction [151].

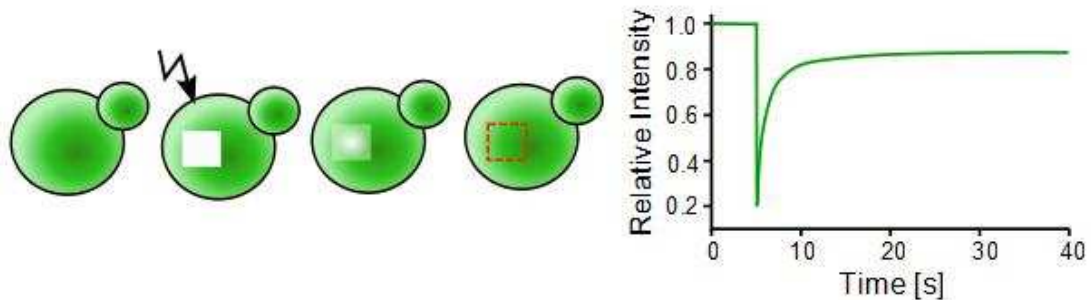


Figure 32. Principle of Fluorescence Recovery After Photobleaching (FRAP). A region of interest is bleached with an intense laser beam for a short period of time and the fluorescence recovery is measured over time.

FRAP experiments consist in applying a high intensity laser pulse to a small area of a cell for a short period of time. This exposition causes an irreversible photochemical bleaching of the fluorophores at that particular time and location. The bleached particles cannot contribute to the fluorescence of the region anymore. Fluorescent proteins from the other cell locations eventually diffuse inside the bleached zone and one observes a recovery in fluorescence (Figure 32). This recovery is recorded at low laser power to avoid extra photobleaching.

## Chapter 2. Osmotic compression slows down the HOG pathway

The fraction of molecules that induces the fluorescence restoration is called the mobile fraction ( $Mf$ ) whereas the fraction that cannot restore the fluorescence is the immobile fraction ( $If$ ). Measuring the recovery rate resulting from the transport of fluorescent particles on the bleach region allows the determination of those fractions (Figure 33). It is obtained by the ratio of the pre-bleach ( $I_i$ ) to the post-bleach fluorescence ( $I_\infty$ ).

$$Mf = \frac{I_\infty - I_0}{I_i - I_0} \quad (22)$$

$I_0$  is the minimum fluorescence value after the bleach. The speed of recovery to half the plateau ( $I_\infty$ ) is the half time of fluorescence recovery ( $\tau_{1/2}$ ) (Figure 33).

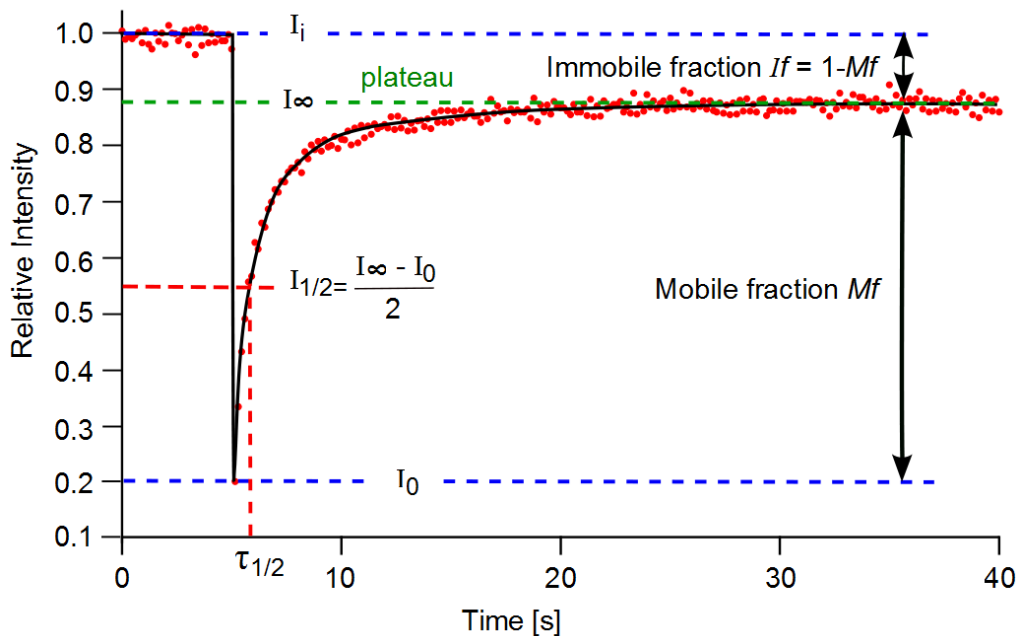


Figure 33. Representation of a FRAP recovery curve. After bleaching a defined region of the cell, the initial intensity ( $I_i$ ) drops to a minimal low value ( $I_0$ ). With time the fluorescence recovers and reaches a plateau ( $I_\infty$ ). From the recovery curve several parameters are extracted such as the mobile and immobile fraction but also the half time ( $\tau_{1/2}$ ) of recovery from the intensity of half recovery ( $I_{1/2}$ ).

Difference in the mobile versus immobile fraction can also give clues about the intracellular processes at play such as interactions between particles or complexes. However, the mobile fraction can also be affected by other parameters such as intracellular barriers preventing free diffusion of the interest protein. Multiple

kinetics models have been developed allowing rapid and consistent extraction of those FRAP features [152].

Using FRAP method, I analyzed the effect of increasing macromolecular crowding on the diffusion capacity of cytoplasmic Hog1-GFP. I used a strain *HOG1-GFP; pbs2Δ* to prevent the activation of Hog1 leading to its nuclear accumulation. In the *pbs2Δ* background, the HOG cascade is genetically disrupted and Hog1 cannot be phosphorylated and imported in the nucleus. Instead, Hog1 remains present homogeneously in the cytoplasm for all the tested stress conditions. FRAP experiments were done on cells in iso-osmotic and in 1 M, 1.5 M and 2 M sorbitol. Each osmotic condition was repeated on 6 to 10 cells. The experiments were conducted on a Total Internal Reflection Fluorescence (TIRF)<sup>23</sup> microscope from the Curie Imaging Center. A smallest possible spot of typically 2 μm diameter was photo-bleached and the recovery in fluorescence recorded during 5 sec (see the appendix for material and methods). Due to the small size of yeast (4 μm), the bleached area fills half of the cell. Since a large proportion of molecules were bleached, the total fluorescence of the cell decreased and induced a reduction of the apparent mobile fraction on recovery curves.

We first investigated the fluorescence recovery of cells in iso-osmotic environment. This showed a rapid and complete fluorescence recovery after the bleach, in typically less than one second. When FRAP was performed on yeast exposed to gentle hyper-osmotic shock (1 M sorbitol), the fluorescence restoration was observed around 4-5 sec after the bleach. Upon higher sorbitol concentrations (1.5 M and 2 M), no fluorescence recovery was observed (Figure 34). These results showed that increasing macromolecular crowding through osmotic compression triggers a slow-down of the cytoplasmic diffusion of Hog1-GFP.

From the recovery curves of iso-osmotic and gentle stress conditions (1 M sorbitol), we estimated a coefficient of diffusion using the 2D-diffusion model of Braga *et al.* [153]. By plotting the transverse section of the average photobleached area, called

---

<sup>23</sup> Total Internal Reflection Fluorescence Microscopy (TIRFM) uses an evanescent wave to excite fluorophores in a restricted region of the specimen immediately adjacent to the interface between two media of different refractive indices.

## Chapter 2. Osmotic compression slows down the HOG pathway

the fluorescent intensity profile, parameters such as the radius ( $\omega_m$ ) and depth ( $k_m$ ) of the bleached region can be extracted by fitting a Gaussian curve. Using those parameters, the characteristic time of diffusion  $\tau_D$  is obtained from the fit of the fluorescence recovery curve (Figure A12). It is defined as the necessary time for a molecule to explore the bleached region area. The coefficient of diffusion can then be estimated knowing the radius of the bleached area  $\omega_m$ .

$$D = \frac{\omega_m^2}{4 \tau_D} \quad (23)$$

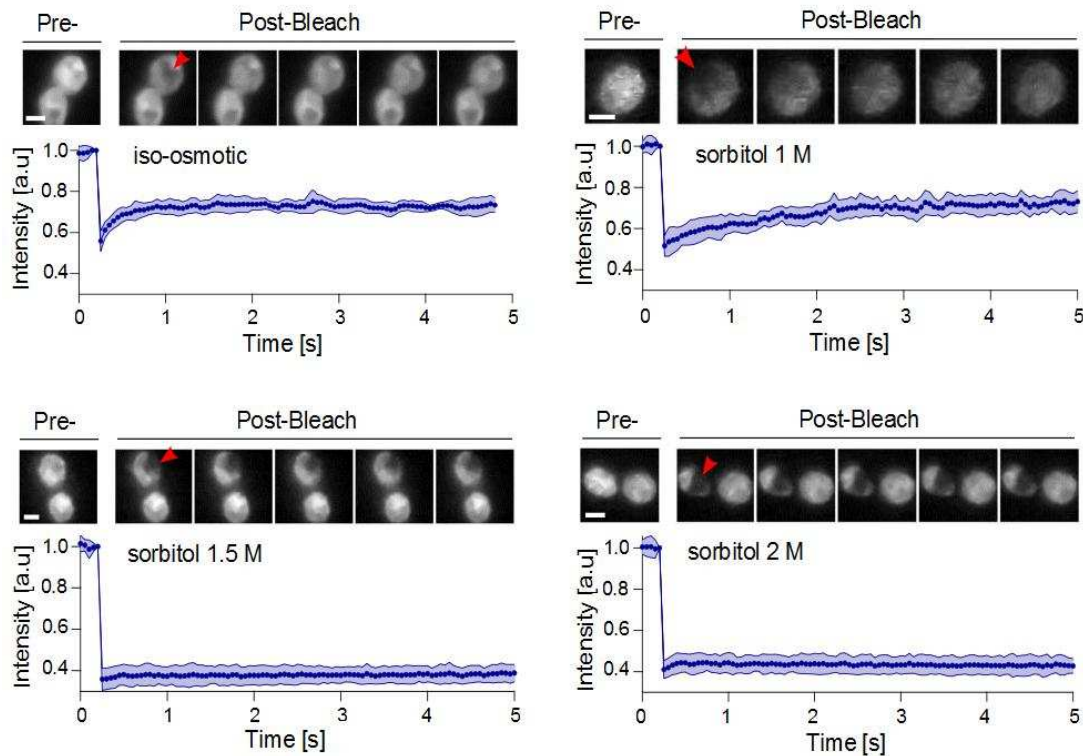


Figure 34. FRAP experiments conducted on yeast *HOG1-GFP; pbs2Δ* in four different crowding conditions: iso-osmotic, 1 M, 1.5 M and 2 M sorbitol. Image sequences of the FRAP experiments are shown for each condition. The applied laser beam is represented by a red arrow. The fluorescence restoration of the bleached area is measured for 6 to 10 cells per each osmotic stress and the data are represented as the mean  $\pm$  one standard deviation (blue curves). Top: In iso-osmotic medium (SC), the recovery is rapid, ( $< 1$  sec) while in sorbitol 1 M the recovery is delayed and occurred 4-5 sec after the bleach. Bottom: Higher crowding induction (1.5 M and 2 M) prevents fluorescence recovery. The scale bars represent  $2 \mu\text{m}$ .

Although the half-time of recovery  $\tau_{1/2}$  is regularly used instead of the characteristic time  $\tau_D$ , those parameters are usually unrelated. Yet some models define a direct relationship between those factors that depends on a photobleaching parameter  $K$  such as  $\tau_{1/2} = K\tau_D$  [154]. From the Equation 23, we obtained in iso-osmotic condition a diffusion coefficient for Hog1-GFP of  $15 \mu\text{m}^2 \cdot \text{s}^{-1}$ . Other studies have estimated a

diffusion coefficient for GFP around  $27 \mu\text{m}^2.\text{s}^{-1}$  in Chinese Hamster Ovary (CHO) cells [155] and  $6.1 \mu\text{m}^2.\text{s}^{-1}$  in bacteria [37]. Although the protein Hog1-GFP may diffuse differently than GFP alone due to a higher molecular weight, their order of magnitude is similar. For moderate osmotic stress condition (sorbitol 1 M), the diffusion coefficient of Hog1-GFP was of  $\sim 1.7 \mu\text{m}^2.\text{s}^{-1}$ , that is 1/10 of the diffusion in iso-osmotic conditions (Table 5). Hence, osmotic compression seems to significantly impact diffusion, even for a gentle stress. Note that, in such a case, the nuclear localization of Hog1 still occurs rapidly (3-5 min). This is consistent with the fact that with such a diffusion coefficient of  $1.7 \mu\text{m}^2.\text{s}^{-1}$ , molecules explore a  $4 \mu\text{m}$ -radius cell in about 9 sec ( $\langle x^2 \rangle / D$ ). Note that, as majority of biological processes (e.g. protein synthesis) range on longer scales (several minutes), this decrease in diffusion should not yet be a limiting factor for the kinetics of diffusion-limited reactions. However stronger stresses definitely prevented molecules to diffuse around.

Table 5. Comparison of the coefficients of diffusion obtained in this study with previous diffusion analyses.

Osmotic conditions	Organisms	Diffusion	References
Iso-osmotic	Chinese Hamster Ovary cells	$27 \mu\text{m}^2.\text{s}^{-1}$	[155]
Iso-osmotic	<i>E. coli</i>	$6.1 \mu\text{m}^2.\text{s}^{-1}$	[37]
Iso-osmotic	<i>S.cerevisiae</i>	$15 \mu\text{m}^2.\text{s}^{-1}$	This study
Sorbitol 1 M	<i>S.cerevisiae</i>	$1.7 \mu\text{m}^2.\text{s}^{-1}$	This study

The diffusion reduction measured with FRAP can be confirmed by another photobleaching method called the Fluorescence Loss In Photobleaching (FLIP). FLIP is a technique complementary to FRAP used to analyze the mobility of particles inside the whole intracellular medium. It is particularly useful for deciphering the connection between compartments such as the Golgi with the endoplasmic reticulum. In the FLIP technique, the same region is continuously bleached, thereby preventing its fluorescence recovery (Figure 35). Ultimately the bleached particles diffuse in their compartment and decrease the cellular fluorescence elsewhere in the cell. The loss in fluorescence is measured by recording the intensity in a different region than the bleached area. The loss in fluorescence in that region constitutes the mobile fraction while the remaining fluorescence in the cell corresponds to immobilized molecules.

## Chapter 2. Osmotic compression slows down the HOG pathway

FLIP experiments were conducted on the *HOG1-GFP; pbs2Δ* strain. Each experiment was performed on 6 to 10 cells and lasted 5 sec. For this set of experiments, we only compared two osmotic conditions, iso-osmotic and sorbitol 2M. We first performed FLIP experiments on cells in iso-osmotic condition and observed a rapid loss of the entire fluorescence in the cytoplasm, in about 3 sec (Figure 36, left). This showed that Hog1-GFP was a very mobile protein, diffusing everywhere in the cytoplasm.

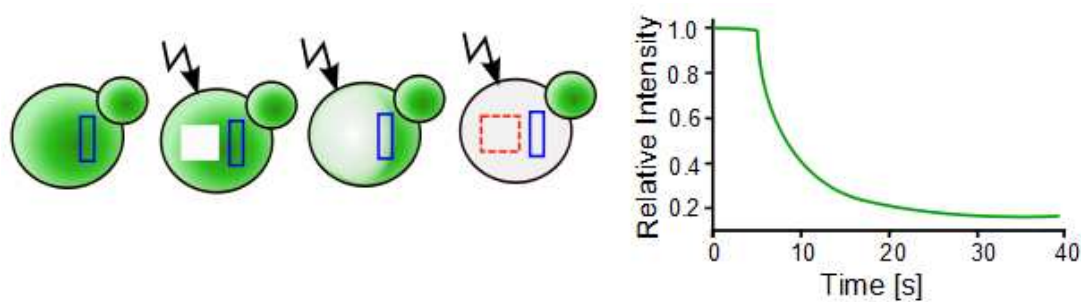


Figure 35. Principle of FLIP. FLIP experiments are done by continuously bleaching a defined cell area preventing any fluorescence recovery. The bleached particles diffuse inside their whole compartment and trigger a global decrease of the cell fluorescence. This loss is determined by measuring the intensity in a region outside the bleached area (blue rectangle). Quantitative information about the particle motility can then be extracted from the fluorescence loss curve.

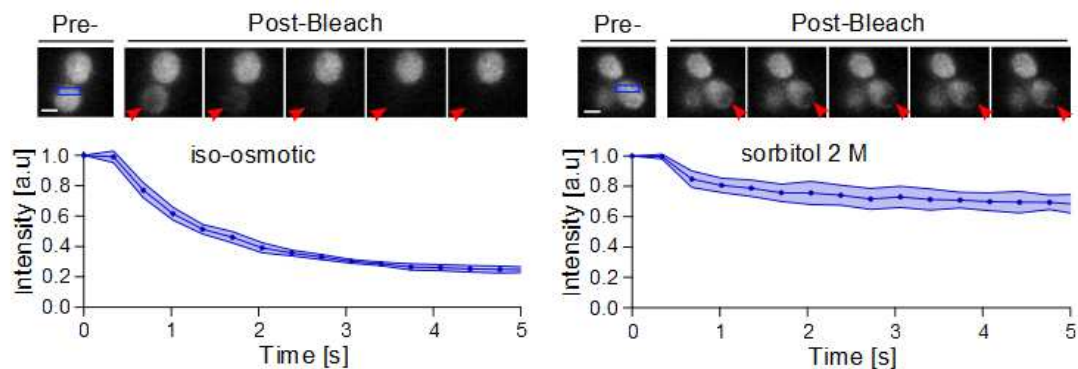


Figure 36. FLIP experiments conducted on yeast *HOG1-GFP; pbs2Δ* in two different crowding conditions: iso-osmotic and 2 M sorbitol. Images of cells before and after the bleach are shown for each condition in function of time. The applied laser beam is represented by a red arrow and the recorded region by a blue rectangle. The fluorescence restoration of the bleached area is measured for 6 to 10 cells for each osmotic stress and the data are represented as the mean  $\pm$  one standard deviation (blue curves). The scale bars represent 2  $\mu\text{m}$ .

In contrast, cells subjected to a severe osmotic stress showed a much slower decrease of fluorescence and conserved a high level of fluorescence after 5 sec of stress in some regions of the cells (Figure 36, right). Those results confirmed that Hog1-GFP in highly crowded environment is much less diffusive than in isotonic condition. Another interesting observation is the homogeneous fluorescence loss of

## Chapter 2. Osmotic compression slows down the HOG pathway

the whole cell in iso-osmotic condition. It means that the observed decrease may not be an effect of increase protein restriction to a particular location but more likely an impairment of diffusion in the whole cell.

## 6. Discussion

In this chapter, I showed that volume compression induced by hyper-osmotic shocks affects the kinetics of the HOG pathway. I notably observed a progressive slow-down of the phosphorylation and nuclear translocation of Hog1. These two mechanisms present similar alterations of their kinetics. Since both processes are correlated, the direct effect of osmotic stress on nuclear translocation is not clear. The import delay can either be the direct effect of phosphorylation alteration or triggered by a combination of nuclear transport and activation reduction. The effects of hyper-osmotic stresses on the nucleo-cytoplasmic transport have been the subject of numerous studies but the established results are often contradictory. Indeed, Kelley and Paschal applied a gentle hyper-osmotic stress on mammalian cells and observed a reduced nuclear transport ability of a NLS-tagged fluorescent reporter protein, GST-GFP-NLS [156]. On the contrary, Finan *et al.* observed in mammalian cells an increase in nuclear transport of 10 kDa dextran, which is about 5 times smaller than the protein Hog1 (48 kDa) [14]. In yeast, the protein Gsp1 associated to the nucleo-cytoplasmic import doesn't seem to be affected by gentle osmotic stress while other nuclear proteins such as the shuttling RNA binding protein Npl3 is abnormally exported [157]. Even if moderate osmotic stresses give rise to different nucleo-cytoplasmic shuttling behaviors, which may depend on the molecules sizes or shuttling mechanisms, we cannot exclude yet that strong hyper-osmotic stress disrupts more systematically the nucleo-cytoplasmic transports of proteins.

In any case, both the activation and the nuclear translocation delay correlate with the cell volume reduction. Indeed, using NaCl as alternative osmotic agent, we also obtained a progressive delay in the nuclear translocation of Hog1 upon increasing concentrations. In contrast with sorbitol treated cells, cells osmotically stressed with NaCl present a faster nuclear translocation and an increased signaling capacity to severe stress, at least if we assume that NaCl and sorbitol osmolarities can be compared based on their concentrations. In yeast, NaCl intracellular accumulation is deleterious. Therefore Na<sup>+</sup> is exported through dedicated channels or sequestered in a pre-vacuolar compartment. However, the initial Na<sup>+</sup> accumulation may be sufficient to reduce the effect of volume compression and explain the faster osmotic

response and the enhanced signaling capacity. Importantly, when plotted in function of the cell volume reduction, sorbitol and NaCl trigger identical kinetics for Hog1 nuclear accumulation. This supports the idea that the main regulator of the Hog1 activation slow-down is mainly the cellular volume reduction and not the nature of the osmotic agent.

Finally we observed a decrease of the diffusion of the protein Hog1-GFP with increasing hyper-osmotic stresses. We measured the coefficient of lateral diffusion for both iso-osmotic and sorbitol 1 M conditions and respectively obtained  $15 \mu\text{m}^2.\text{s}^{-1}$  and  $1.7 \mu\text{m}^2.\text{s}^{-1}$ . Even if these values seem consistent with previous published values, they need to be handled with care. Indeed, the diffusion model of Braga *et al.* assumes an infinite system and neglects boundary effects. Although this model is optimally implemented for large mammalian cells, it is not the case for yeast in which diffusion is limited due to the small size of cells. Another issue of those FRAP experiments came from the cell size reduction upon hyper-osmotic stress. Consequently, the ratio of the bleached area to the whole cell size increases with increasing the stress and could impact the determination of the diffusion coefficient. From the literature, it is known that increasing the size of the bleached area leads to an overestimation of the coefficient of diffusion [158, 159]. In condition of moderate hyper-osmotic stress (1 M sorbitol) for which the relative size of the bleached area is enlarged, we obtained a 10 times decrease of the diffusion coefficient. Therefore, our estimation upon moderate hyper-osmotic stress may be overestimated and the diffusion coefficient may be even lower. But, and this is what is important here, our results are in agreement with the fact that Hog1 signaling is delayed upon volume compression because of an increase of the cytoplasmic density, and thus its viscosity, which in turn decreases diffusion.

As we already mentioned in the introduction, Dill *et al.* highlighted the relation between the typical biochemical reaction rates and the diffusion coefficient of a protein inside the cytoplasm. Here, we observed a nonlinear increase of the typical timescale of activation of the HOG cascade when compressing yeast cells osmotically. Increasing volume compression raises its intracellular density and led to a decrease in diffusion, in agreement with our observations. But we would like to

## Chapter 2. Osmotic compression slows down the HOG pathway

go further and discuss the nature of this nonlinear increase and to link it with the study of Zhou *et al.* that we briefly presented in the introduction.

Following their argument, we propose that the progressive delay of both Hog1 activation and nuclear translocation is reminiscent of a soft colloidal glassy-like transition. These authors advanced that, in first approximation, the cytoskeleton of mammalian cells are composed of deformable particles and behave as soft colloids. They showed that in such a case, the viscosity of the medium  $\eta$  scales exponentially with the volume fraction of macromolecules  $\Phi$  and is expressed as,

$$\eta = \eta_0 e^{\alpha\Phi} \quad (24)$$

In our case we cannot measure the viscosity directly, but we can try to link it with the diffusion coefficient in the cytoplasm. We can indeed assume that the diffusion in the cytoplasm is inversely proportional to the viscosity consistently with the Stokes-Einstein equation,

$$D = \frac{k_B T}{6\pi\eta a} \quad (25)$$

$k_B$  being the Boltzmann constant,  $T$  the temperature and  $a$  the radius of a spherical particle. Therefore the diffusion will vary as,

$$D \sim e^{-\alpha\Phi} \quad (26)$$

As previously stated, the reaction rate of a biochemical reaction limited by diffusion is given by,

$$r_D = 4\pi a c D \quad (27)$$

Since the concentration,  $c$ , varies as the volume fraction,  $\Phi$ , we can write that the typical reaction rate varies as the macromolecular volume fraction times the diffusion coefficient. The typical timescale of a diffusion limited reaction,  $T_{\max}$ , defined as the inverse of the diffusion rate then scales as,

$$T_{max} \sim \frac{1}{\phi} e^{\alpha\phi} \quad (28)$$

We can test this basic model that links our results to that of Zhou *et al.* through simple scaling arguments. As shown on Figure 37, it fits well our data of cell under compression. In line with Zhou *et al.*, those results suggest that osmotically compressed yeast cells also behave as soft colloids. The observed slow-down and its nonlinear fast increase for large compression can then be interpreted as cells undergoing a colloidal glassy-like transition.

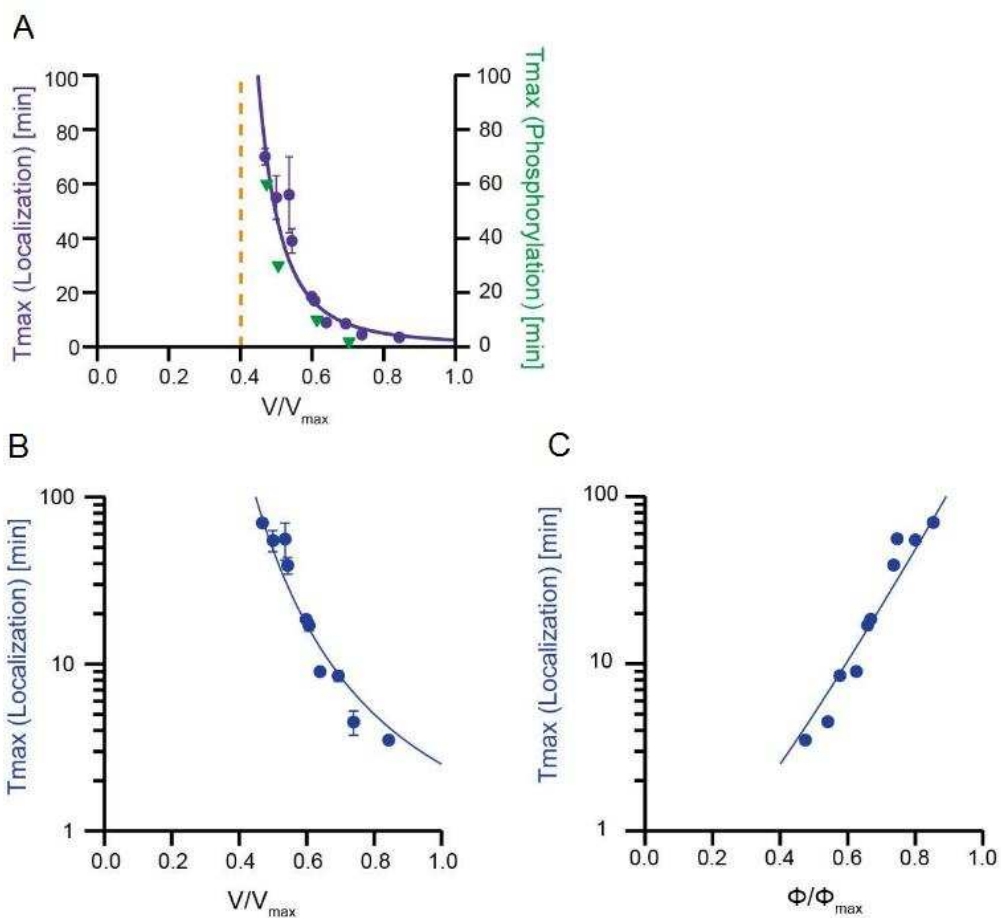


Figure 37. Cell volume compression and Hog1 dynamics in log coordinates. (A) The times of maximum Hog1 activation and nuclear localization in function of the relative cell volume reduction. These maxima increase with cell size compression. The blue line is a fit consistent with what is expected for a soft colloid glassy-like transition,  $T_{max} = T_0 \frac{V}{V_{max}} e^{\alpha V_{max}/V}$ ;  $T_0 = 0.065$  and  $\alpha = 3.6$ . (B) The time of maximum Hog1 nuclear localization is shown in logarithmic scale and is fitted in function of the relative volume variation  $V/V_{max}$ . (C) Log of  $T_{max}$  is now plotted as a function of the relative protein density. The protein relative density,  $\Phi / \Phi_{max}$ , is defined as the inverse of  $V/V_{max}$  and normalized so that its maximum is 1 (arbitrary choice).

## Chapter 2. Osmotic compression slows down the HOG pathway

We thus conclude that the kinetics alterations of the HOG pathway are a consequence of the intracellular viscosity increase. As the density increases, intracellular diffusion is decreased and leads to the slow-down of the HOG cascade, to the point where the HOG cascade is stalled. If this is true, then we can think of several experiments that should give similar results, and in particular other, unrelated signaling and dynamical processes should be similarly slowed down by osmotic compression. This is the subject of the next part of this thesis.

## CHAPTER 3.

# GLOBAL EFFECT OF MACROMOLECULAR CROWDING ON INTRACELLULAR DYNAMICS

<b>7. Other processes slow down caused by cellular compression</b>	<b>82</b>
Msn2, Yap1, Crz1 and Mig1 nuclear translocation dynamics	82
Crz1 and Msn2 nuclear imports are independent of the HOG pathway	86
<b>8. Cytoplasmic diffusion under compression</b>	<b>88</b>
Citrine, YFP and Ura1-GFP diffusion in yeast	88
GFP diffusion in the human cell lines	89
<b>9. Endocytosis and other active processes</b>	<b>91</b>
<b>10. Jamming recovery after a short period of intense compression</b>	<b>93</b>
<b>11. Discussion</b>	<b>95</b>

## 7. Other processes slow down caused by cellular compression

### **Msn2, Yap1, Crz1 and Mig1 nuclear translocation dynamics**

In the previous chapter, we analyzed the dynamics of the HOG pathway under cellular compression and suggested that the observed slow-down is due to volume compression and the increase in intracellular density. As this cause is generic, acting on the whole cellular volume is expected to have consequences on other pathway than HOG. To check our hypothesis, we analyzed the dynamics of different signaling cascades under volume compression. We selected four distinct proteins chosen to have functional differences with the MAPK Hog1 (Table 6).

Msn2 is a zinc-finger protein negatively controlled by the cAMP-PKA pathway and involved in the general stress response such as heat, osmotic shock, oxidative stress, low pH or glucose starvation [160–162]. After a hyper-osmotic stress, Msn2 is hyper-phosphorylated and imported into the nucleus where it binds to stress responsive elements (STREs) located upstream of their target genes. Yet the transduction mechanisms responsible for Msn2 activation remain unclear. Despite independent activation mechanisms, both Hog1 and Msn2 proteins are sensitive to hyper-osmotic stress and can establish cooperative interactions [103].

The transcription factor Yap1 is a bZIP DNA-binding protein of the AP-family. It is activated by the glutathione peroxidase (GPx)-like enzyme Gpx3 under oxidation [163]. Yap1 activation leads to its accumulation inside the nucleus where it triggers the expression of anti-oxidants proteins. In normal environment, the protein Crm1 binds to the Yap1 NES sequence and triggers its export. Under the addition of 300  $\mu$ M hydrogen peroxide ( $H_2O_2$ ), the creation of disulfide bonds modifies the NES sequence and embeds it in the carboxy-terminal domain [164, 165]. Ultimately, Yap1 continuous export is inhibited and it accumulates inside the nucleus.

Crz1, is a calcineurin-responsive zinc-finger protein activated by calcium input [166]. Without stimulation, Crz1 is phosphorylated and localizes in the cytoplasm. Upon calcium addition, calcineurin triggers its dephosphorylation and its import into the nucleus [167, 168]. Crz1 nuclear binds to sequences called calcineurin-

dependent response element (CDRE) and turns on a variety of genes involved in ion homeostasis [166, 169].

The last protein we studied is Mig1, a transcriptional factor involved in glucose repression. When the main carbon source is glucose, the Reg1-Glc7 protein phosphatase complex dephosphorylates Mig1 which triggers its nuclear import [170, 171]. In the nucleus, Mig1 binds to the promoters of glucose-repressed genes, notably affecting the GAL gene expression [172].

Table 6. Characteristics of the selected transcriptional factors.

TFs	Types	Inputs	Activators	Activations	Importers	Exporters	References
<b>Hog1</b>	MAPK	Hyper-osmotic	Pbs2	Phosphorylation (P)	Nmd5	Xpo1	[109, 173]
<b>Msn2</b>	Zinc-finger	General stress	-	Hyper-P	-	Msn5	[160, 161, 174]
<b>Crz1</b>	Zinc-finger	Calcium	Calcineurin	De-P	Nmd5	Msn5	[166–168]
<b>Yap1</b>	Leucine zipper	Oxidation	Gpx3	Oxydation	Pse1/ Kap121	Xpo1	[163, 164, 175]
<b>Mig1</b>	Zinc-finger	Glucose	Reg1-Glc7	De-P	-	Msn5	[170–172]

We analyzed the nuclear translocation dynamics of these four transcriptional factors under increasing compression. We applied single osmotic stress of increasing sorbitol concentrations to compress the cells, and recorded the time to reach the maximum nuclear translocation for each protein. Msn2, like Hog1, is sensitive to osmotic stress. However, Crz1, Yap1 and Mig1 activations depend on other inputs. For studying their dynamics upon compression, we combined an osmotic stress with their respective stimulus in order to induce cellular compression in parallel to their activation (Figure 38). The intensity of their stimulation was set at a constant value between experiments.

### Chapter 3. Global effect of macromolecular crowding on intracellular dynamics

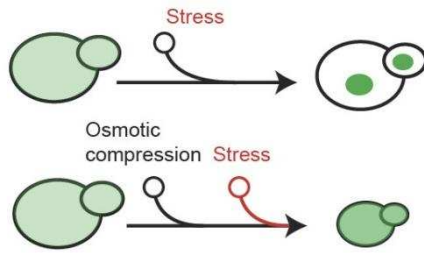


Figure 38. Sketch illustrating the difference between a single stimulation and a dual stimulation with osmotic compression. The latter is expected to slow down cell dynamics.

We first investigated the nuclear accumulation dynamic of Msn2 using different concentrations of sorbitol alone. After a gentle stress (0.5 M sorbitol), Msn2 maximally translocated in 3 min and was then rapidly exported. Restoration of normal Msn2 cytoplasmic concentration was achieved after typically 20-30 min. Upon a stronger osmotic stress (1.4 M sorbitol), its nuclear localization took much more time and occurred after 30 min, while after a severe stress (1.75 M sorbitol) it took more than 60 min (Figure 39A). Therefore, as for the HOG cascade, there was a progressive, nonlinear slow-down of Msn2 dynamics upon cellular compression.

Using the double stimulation previously described (Figure 38), the nuclear translocation dynamics of the three others transcriptional factors was then investigated. From the literature, we know that Crz1 is activated by 200 mM CaCl<sub>2</sub>. In such conditions, Crz1 accumulates in the nucleus in a few minutes. Based on that, we supplemented the solution of 200 mM CaCl<sub>2</sub> with increasing concentration of sorbitol. We observed that after a gentle osmotic compression (0.5 M sorbitol), Crz1 localized inside the nucleus after 5-6 min. Increasing the hyper-osmotic compression to 1.4 M sorbitol led to a maximum nuclear import 90 min after the stress. Those results suggested that Crz1 dynamics is also slowed down by osmotic compression. Although no connection between the HOG pathway and Crz1 is known, applying a hyper-osmotic stress alone also triggered a nuclear accumulation of Crz1 (Figure 39B). And in agreement with our hypothesis, the nuclear translocation was slower with increasing hyper-osmotic stress.

Yap1 and Mig1 were investigated the same way. While Yap1 is known to translocate rapidly upon 300  $\mu$ M H<sub>2</sub>O<sub>2</sub>, Mig1 import occurs when its carbon source is switched from galactose to glucose (20 g/L). We stimulated those factors with their respective

inputs alone and observed a maximal nuclear localization about 10 min after induction. Once their respective inputs were supplemented with sorbitol to compress the cells, we obtained a progressive decrease of their nuclear translocation dynamics (Figure 39C-D). Therefore, increasing compression slows down the signaling dynamics of four unrelated transcriptional factors.

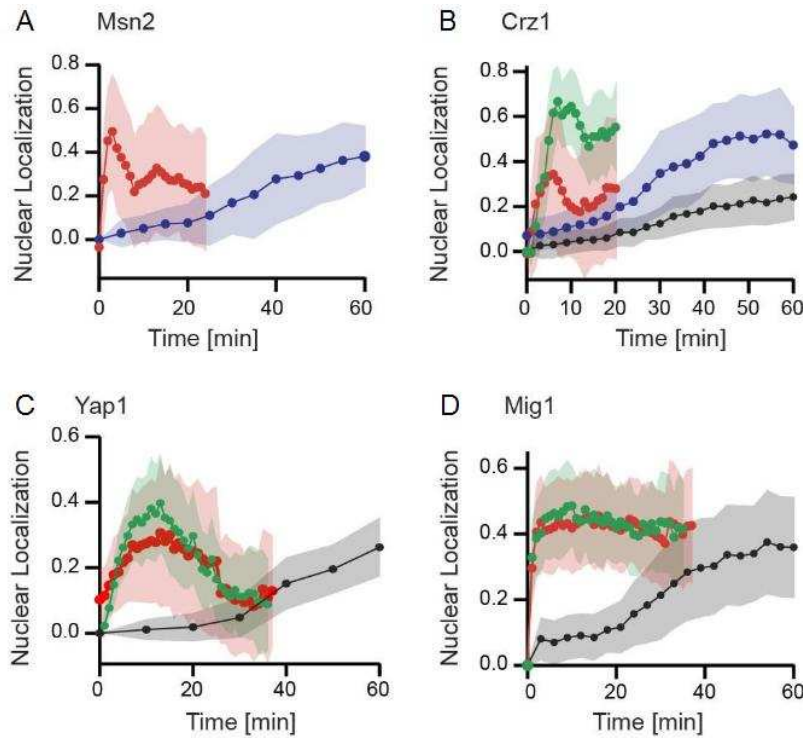


Figure 39. Cellular compression triggers nuclear imports slow-downs of four transcriptional factors. (A) Msn2 nuclear localization subjected to either a gentle osmotic shock (sorbitol 0.5 M, red) or a strong osmotic stress (sorbitol 1.75 M, blue). (B) Crz1 nuclear translocation induced by calcium stimulation alone (CaCl<sub>2</sub> 200 mM, green), CaCl<sub>2</sub> plus gentle osmotic stress (CaCl<sub>2</sub> + sorbitol 0.5 M, red), CaCl<sub>2</sub> plus strong osmotic stress (CaCl<sub>2</sub> + sorbitol 1.4 M, black) or sorbitol alone (sorbitol 1.75 M, blue). (C) Yap1 nuclear translocation after an oxidative stimulation alone (H<sub>2</sub>O<sub>2</sub> 300 μM, green), oxidative stress plus gentle osmotic stress (H<sub>2</sub>O<sub>2</sub> + sorbitol 0.5 M, red), or oxidation plus strong osmotic stress (H<sub>2</sub>O<sub>2</sub> + sorbitol 1.4 M, black). (D) Mig1 nuclear translocation after glucose stimulation (glucose 20 g/L, green), glucose plus a gentle osmotic stress (glucose + sorbitol 0.5 M, red), or glucose plus a strong osmotic stress (glucose + sorbitol 1.4 M, black). Yeast cells have been pre-grown on galactose medium. Data are represented as the mean over many cells (N>20) +/- one standard deviation.

We compared the nuclear translocation dynamics of those four factors by studying their maximal nuclear localization time in function of the sorbitol concentration (Figure 40A). They all displayed a nonlinear behavior with an apparent divergence for strong compression. Similarly to our conclusion on Hog1 and the hypothesis of

the existence of a soft colloid glassy-like transition, these dynamics are nicely fitted

using the equation  $T_{max} = T_0 \frac{V}{V_{max}} e^{\alpha V_{max}/V}$  (Figure 40B).

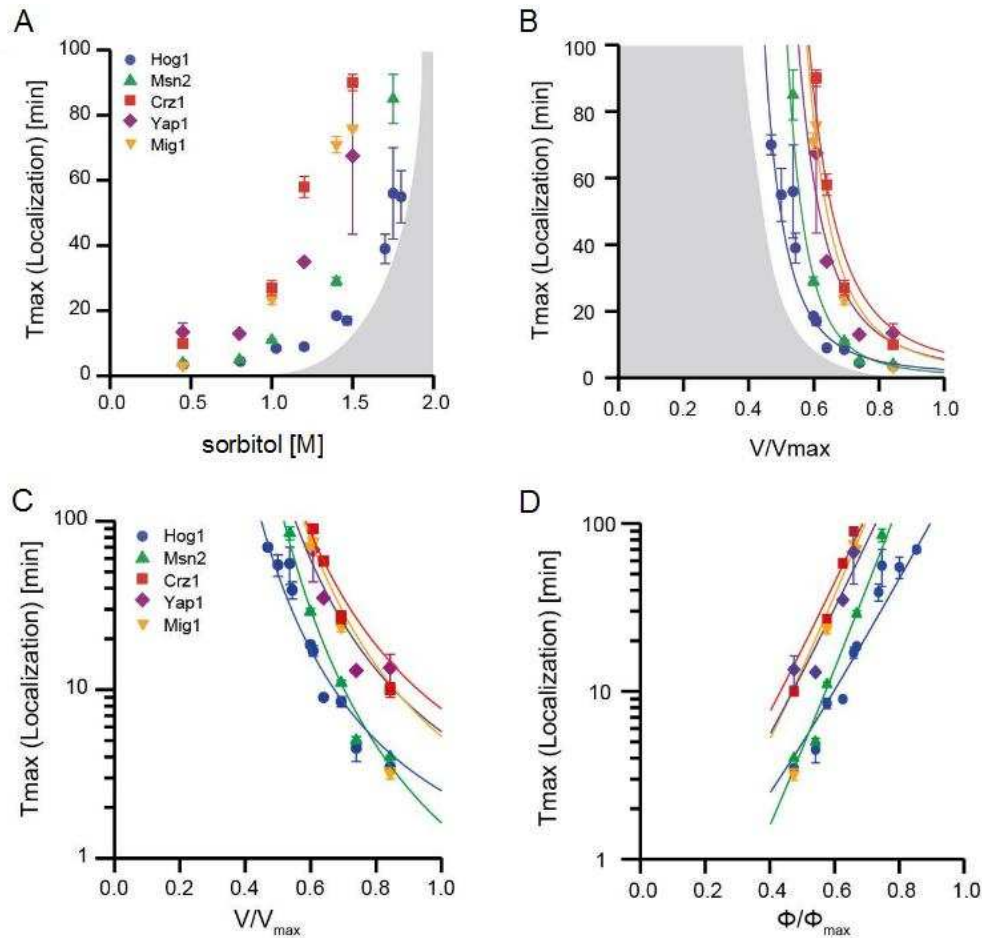


Figure 40. Maximum nuclear localization timescale measured for Msn2 (sorbitol), Yap1 (sorbitol + 300  $\mu$ M  $H_2O_2$ ), Crz1 (sorbitol + 200 mM  $CaCl_2$ ), Mig1 (sorbitol + glucose 20 g/L) compared to the kinetics of Hog1 (sorbitol) in function of the sorbitol concentration (A) or the relative cell volume (B). The curves are the fits of the function  $T_{max} = T_0 \frac{V}{V_{max}} e^{\alpha V_{max}/V}$  that model the behavior of a soft colloid near its glass transition. For Msn2,  $T_0 = 0.035$  and  $\alpha = 3.9$ ; for Crz1,  $T_0 = 0.096$  and  $\alpha = 4.4$ ; for Yap1,  $T_0 = 0.077$  and  $\alpha = 4.3$ ; for Mig1,  $T_0 = 0.043$  and  $\alpha = 4.8$ . (C) For each transcriptional factor, the time of maximum nuclear localizations is plotted in logarithmic scale and is fitted in function of the relative volume variation  $V/V_{max}$ . (D) Log of the  $T_{max}$  is plotted as a function of the relative protein density. The protein relative density,  $\Phi / \Phi_{max}$ , is defined as the inverse of  $V/V_{max}$  and normalized so that its maximum is 1 (arbitrary choice).

### Crz1 and Msn2 nuclear imports are independent of the HOG pathway

Crz1 and Msn2 are sensitive to hyper-osmotic stress alone. It is known that a cooperative interaction between Hog1 and Msn2/4 is at play upon osmotic stress.

We cannot exclude that Msn2 nuclear recruitment depends on the activity of Hog1.

Therefore, the delay in the nuclear localization of Msn2 upon compression could be a secondary effect of the HOG pathway alterations. Since Crz1 was also found to be activated by hyper-osmotic stress alone, the possible implication of the HOG pathway in the dynamics modification of both Msn2 and Crz1 nuclear import needed to be investigated. In order to characterize if the HOG cascade was involved, the same experiments were reproduced in *hog1Δ* strains. As the HOG pathway is nonfunctional in the strains *CRZ1-GFP; hog1Δ* and *MSN2-GFP; hog1Δ*, Msn2 and Crz1 nuclear accumulation may be directly related to the reduction of volume. We indeed observed a progressive slow-down for both factors upon hyper-osmotic stress increase. These results are in good agreement with previous studies showing a nuclear import of Msn2 even in absence of Hog1 [103, 160]. Note that, for the same sorbitol concentrations, the strains deleted for *HOG1* present longer times of maximum nuclear localization than the wild-type strains (Figure 41A-B). Yet, when their translocation dynamics are plotted in function of the relative cell volume, both the wild-type and *hog1Δ* strains dynamics overlap (Figure 41C-D). Those observations confirm that Msn2 and Crz1 nuclear localization delays are more likely triggered by cell volume reduction than by the dynamics alterations of the HOG pathway.

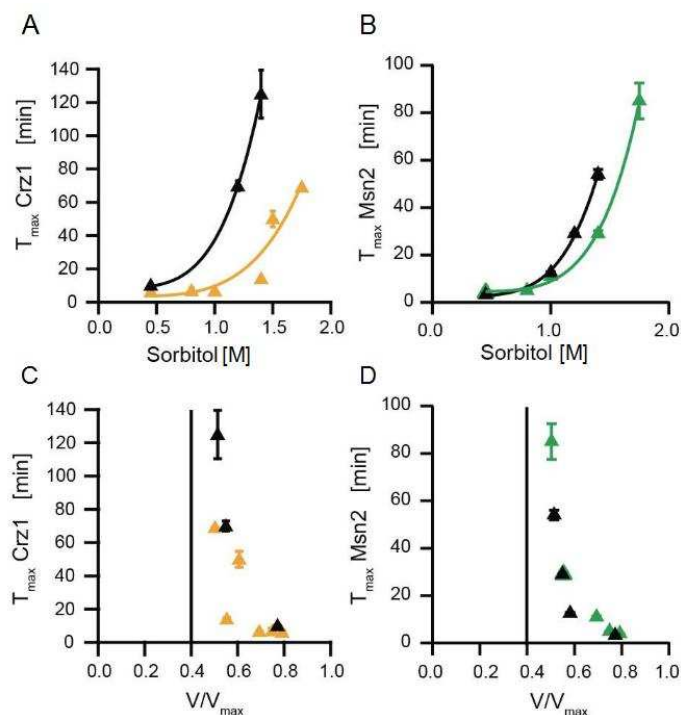


Figure 41. Nuclear translocation dynamics of the transcriptional factors Crz1 (A,C) and Msn2 (B,D) in a *hog1Δ* background (black triangle) compared to their respective wild-type strains (Crz1-GFP yellow and Msn2-GFP green). The time of maximum nuclear localization of the strains *MSN2-GFP; hog1Δ* and *CRZ1-GFP; hog1Δ* are plotted in function of the sorbitol concentration (A,B) or the relative cell volume (C,D).

## 8. Cytoplasmic diffusion under compression

### Citrine, YFP and Ura1-GFP diffusion in yeast

In the previous chapter, we observed that volume compression not only altered the activation and nuclear import of Hog1 but also its diffusion dynamics. To strengthen our argument and gain in generality, we performed FRAP analyses on three other yeast strains: Two strains expressing the fluorochromes yCitrine and YFP under the respective promoters ACT1 and ADH1 and the third one expressing the protein Ura1-GFP. We performed these FRAP experiments on a Spinning disk confocal microscope<sup>24</sup> from the Mechanobiology Institute of the National University of Singapore. Unlike the strain *HOG1-GFP; pbs2Δ* previously used for Hog1 diffusion experiments, the three strains *pACT1-citrine*, *pADH1-YFP* and *URA1-GFP* present a functional HOG cascade. Since these cells adapt to mild and moderate stress and recover their volume soon after the stress, the normal diffusion of proteins might be restored rapidly. Therefore, the real diffusion impairment may be underestimated. As we preferred to avoid such unpredictable situations, we studied only two experimental conditions, iso-osmotic versus severe hyper-osmotic stress (2 M sorbitol) (Figure 42). Each experiment was repeated on 5 to 10 cells. We first analyzed the recovery of fluorescence in iso-osmotic conditions. For each protein tested, we observed a recovery, although with various rates. While Ura1-GFP recovered as fast as the protein Hog1-GFP (< 1 sec), citrine and YFP recoveries took longer time (> 5 sec). But, and this is a crucial point, upon a severe osmotic stress (2 M sorbitol), all three proteins did not recover their fluorescence at the bleached area (Figure 42). Therefore, even if the three proteins citrine, YFP and Ura1-GFP have different diffusion rates in iso-osmotic conditions, their diffusion is strongly decreased, and even jammed by severe cellular compression. This is in the line with our hypothesis that cellular compression induces a general decrease of protein diffusion.

---

<sup>24</sup> Spinning disk confocal microscopes use a series of moving pinholes on a disc to scan spots of light. It allows the acquisition of multiple points simultaneously rather than scanning a single point at a time. In this way, the images are obtained at very high frame rates with minimum illumination of the samples.

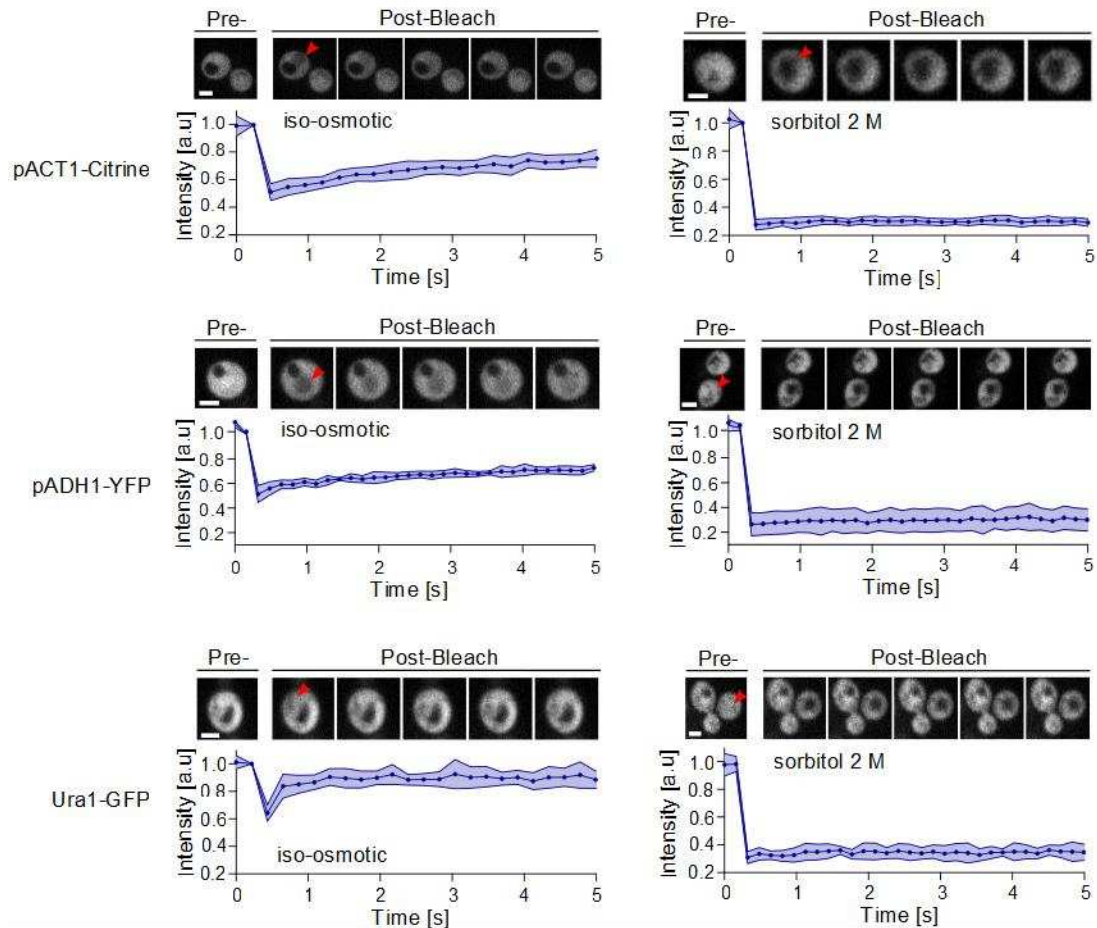


Figure 42. FRAP experiments conducted on the three yeast strains *pACT1-citrine*, *pADH1-YFP* and *URA1-GFP*. Two conditions were applied: iso-osmotic (left graphs) and 2 M sorbitol (right graphs). Image sequences of the FRAP experiments are shown for each condition. The vacuoles are observed inside some cells due to their absence of fluorescence staining. The red arrows represent the location of the applied laser beam. The fluorescence restoration of the bleached area is measured for 5 to 10 cells for each osmotic situation and the data are represented as the mean  $\pm$  one standard deviation (blue curves). For each strain, the recovery in iso-osmotic condition is observed while no recovery is detectable upon severe osmotic stress. The scale bars represent 2  $\mu$ m.

### GFP diffusion in the human cell lines

Consistently with our central hypothesis, the effect of volume compression should affect diffusion processes not only in yeast cells but also in other species. Thus, we also investigated the diffusion of proteins in the cytoplasm of higher eukaryotic cells subjected to volume compression. We used two different human epithelial cell lines MCF-7 and A549 that both expressed constitutively the protein GFP. We used the polymer polyethylene glycol (PEG) 400, as it is classically done in mammalian cells, to induce osmotic stresses. It was prepared at 40% w/w, which is approximately equivalent to a concentration of 1 M. The experiments were conducted on the same

spinning disk than the previous yeast analyses. For each osmotic condition, the experiments were repeated on 5 to 6 cells. In iso-osmotic conditions, similar GFP diffusion recovery was observed for both cell lines in less than 2 sec after the bleaches (Figure 43, left panel). Upon compression by 40% PEG, neither MCF-7 nor A549 recovered from the bleaching (Figure 43, right panel). Strikingly, and as it is the case for yeast, in such conditions, the bleached area remained visible by the naked eye for the duration of the FRAP experiment. This is another experimental evidence that cellular compression leads to a decrease in protein diffusion, and eventually jamming for too strong compression, in different cell types. Other FRAP analyses reported in the literature on mammalian cells [36] and bacteria [37] are in the same line of results and provide additional evidences for an universal decrease in diffusion upon volume reduction.

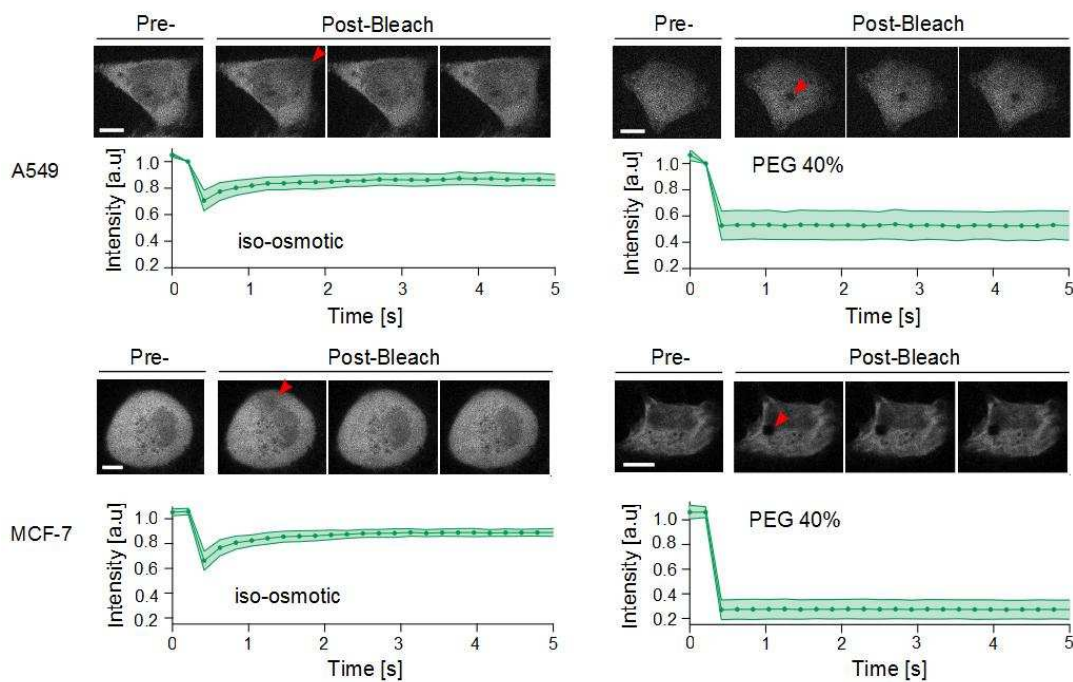


Figure 43. FRAP experiments conducted on two human epithelial cell lines, A549 and MCF-7 constitutively expressing GFP. Two conditions were applied: iso-osmotic (left graphs) versus 40% PEG 400 (right graphs). Image sequences of the FRAP experiments are shown for each condition. The red arrows represent the applied laser beam. The fluorescence restoration of the bleached area was measured for 5 to 6 cells per condition and data are represented as the mean  $\pm$  one standard deviation (green curves). For each cell line, the recovery in iso-osmotic condition was quick ( $< 2$  sec) while no recovery was detectable upon severe osmotic stress. The scale bars represent  $15 \mu\text{m}$ .

## 9. Endocytosis and other active processes

There are obviously, other active, dynamics processes in cells that can be studied after volume compression. We choose first to look at endocytosis to provide a different approach and further insight into the effect of osmotic compression on the dynamics of cellular processes *in vivo*. Endocytosis is the process by which external substances are imported inside cells by membrane invagination followed by intracellular vesicles formation. This biological function is essential in many regulatory processes, like plasma membrane recycling [176], protein trafficking [177] or cell-surface receptors uptake [178]. Since this process involves intracellular transport, we hypothesized it could also be slowed down under cell compression. We first investigated the endocytosis dynamics using the fluorescent dye FM4-64 as a tracer of bulk endocytosis. FM4-64 is a lipophilic styryl membrane-selective dye that intercalates into the plasma membrane and is precisely internalized with vesicles. We applied FM4-64 to cells in iso-osmotic condition and observed, as expected, the dynamics of formation of fluorescent vesicles. In contrast, cells compressed by a severe osmotic stress (3 M sorbitol) showed no more vesicle formation and a labeling restricted to the plasma membrane even after 70 min of incubation (Figure 44A).

Another process that can be easily monitored is the mobility of the protein Abp1. This protein is an actin binding protein which connects the actin cytoskeleton to endocytic sites [179]. In normal condition, Abp1 presents a punctiform distribution at the membrane. It is a very mobile protein as its spots are seen to move around near the membrane, and to appear and disappear in less than a minute [180]. We investigated the effect of cellular compression on the motility of Abp1 patches using high sorbitol concentrations of 1.5 M and 2 M. The motion of Abp1 patches was recorded first in iso-osmotic environment and then we replaced the environment by a high osmolarity medium. Abp1 patches abruptly stopped their random, diffusive like motion and appeared as if frozen or jammed. The freezing transition is easily observed on the spatiotemporal view of the Figure 44B.

Finally, we looked at one last protein related to vesicle dynamics in yeast. Sec7 encodes a guanine nucleotide exchange factor (GEF) for ADP ribosylation factors

### Chapter 3. Global effect of macromolecular crowding on intracellular dynamics

and regulates the formation of coated vesicles in intracellular trafficking, more particularly in intra-Golgi and ER-to-Golgi transport [181]. Using the same experimental strategy, we recorded Sec7 motion upon a sudden change in osmolarity. As observed for Abp1, Sec7 patches abruptly stopped their motion after a 1.5 M or 2 M osmotic stress (Figure 44C).

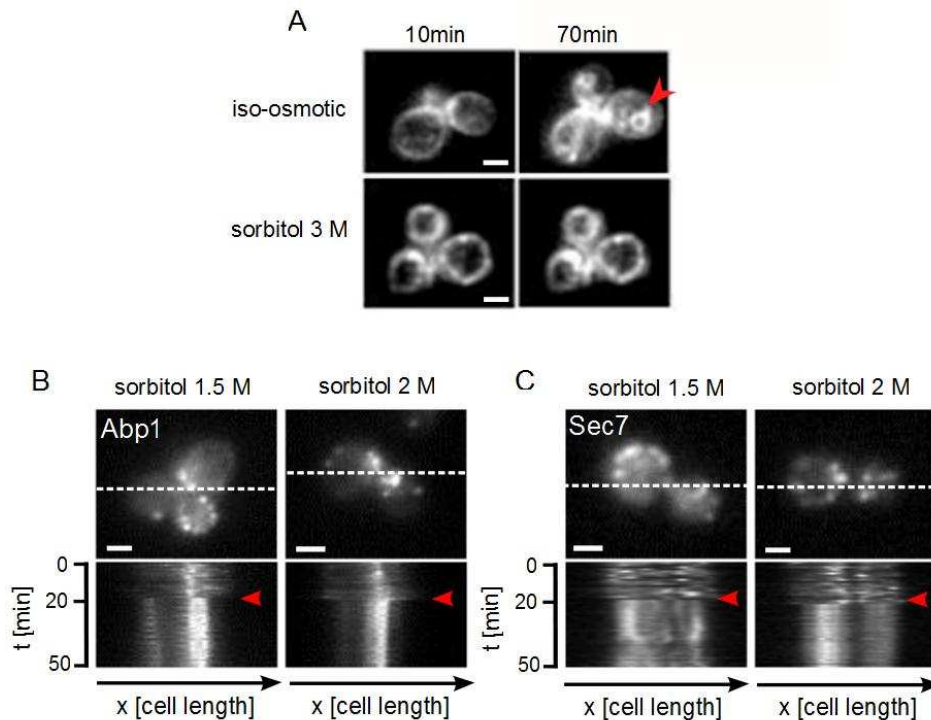


Figure 44. Endocytosis dynamics upon cellular compression. (A) FM4-64 staining comparison between iso-osmotic and severe osmotic conditions (sorbitol 3 M) at two different time points after the dye addition (10 and 70 min). The red arrow points the apparition of a vesicle. (B) Abp1-GFP images in iso-osmotic condition and orthogonal views of the transition between iso-osmotic condition and 1.5 M or 2 M sorbitol stress. (C) Sec7-mCherry images in iso-osmotic condition and orthogonal views of the transition between iso-osmotic condition and 1.5 M or 2 M sorbitol stress. The white dashed lines indicate the position in the cell which has been used for constructing the spatiotemporal view. The red arrows point out the time (20 min after the stress) for which the environment is switched from an iso-osmotic to a hyper-osmotic medium. The scale bars represent 2  $\mu\text{m}$ .

## 10. Jamming recovery after a short period of intense compression

As we have shown, when the stress is severe enough, several signaling dynamics and dynamical processes are drastically slowed down or jammed. In agreement with our hypothesis, if the main reason for this dynamical arrest is the sudden cell compression, and the increase in viscosity, then such dynamics should recover if the cell volume is restored. Therefore, we analyzed the cell ability to recover in terms of nuclear import of transcriptional factors once its cell size is restored. The experiment consisted in applying a transient severe osmotic stress followed by a gentle osmotic stimulation (Figure 45).

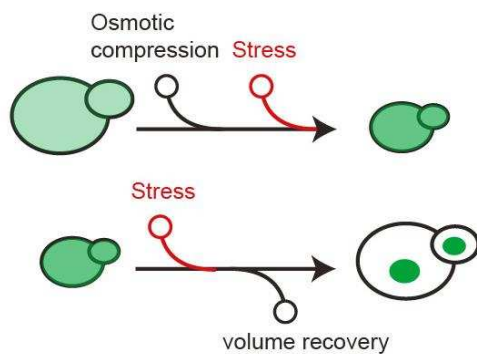


Figure 45. Principle of signaling activation by volume recovery. Cells are stressed and at the same time osmotically compressed by a severe osmotic stress (3 M sorbitol). Thus, cells are first stalled and cannot respond to the chemical stress. The osmotic compression is then relaxed by a return to an isotonic stressful condition and we observed if cells are able to detect and respond to the chemical stress which is still present in the cells' environment.

This two-step stimulation is performed for every transcriptional factor previously tested, that is to say Hog1, Msn2, Crz1, Yap1 and Mig1. We first investigated Hog1 and Msn2 responses (Figure 46). 3 M sorbitol was applied for 5 minutes and then replaced by sorbitol 1 M. The environment was not switched back to an iso-osmotic medium since our measured output was the nuclear accumulation of Hog1 or Msn2 that does not occur in an isotonic environment. For both factors, cells were not responding during the first 5 min, but once the osmotic compressive constraint was released, the nuclear transport of the proteins rapidly occurred in every recorded cell.

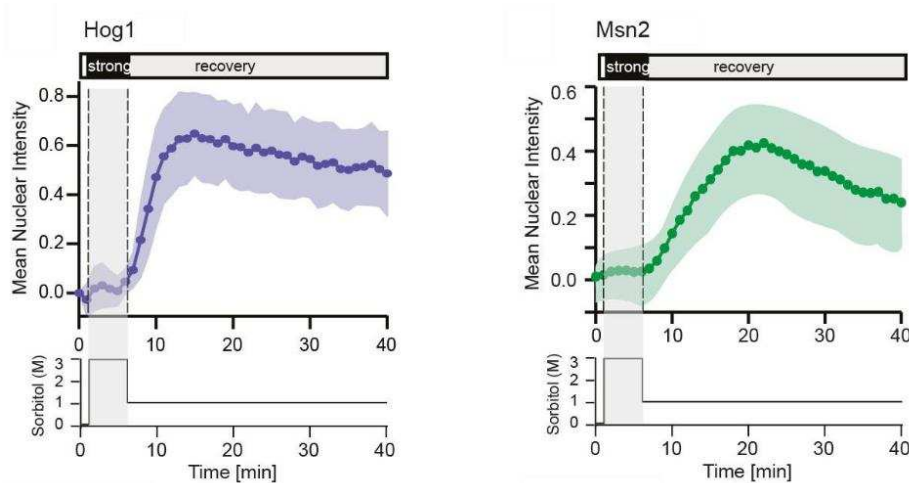


Figure 46. Two-step stimulation is applied to the transcriptional factors Hog1 and Msn2. A strong osmotic stress (3 M sorbitol) is first applied for 5 minutes and then replaced by a gentle osmotic stimulation (1 M sorbitol). The nuclear localization capacity of proteins is recorded through time. For both Hog1 and Msn2, the nuclear localization is observed as soon as the transition from 3 M to 1 M sorbitol occurs.

The reversibility of the system was similarly tested for Crz1, Yap1 and Mig1. Crz1 was first stressed with 3 M sorbitol supplemented with  $\text{CaCl}_2$  200 mM for 5 min and the medium was then replaced by a solution of  $\text{CaCl}_2$  200 mM (Figure 47). We applied similar stimulation to Yap1 using  $\text{H}_2\text{O}_2$  300  $\mu\text{M}$  and Mig1 with glucose 20 g/L. These three factors all recovered their activity after the volume clamp was released. Indeed, during the 5 min of severe stress, the cells were non-responsive but once the cells recovered a normal size, the nuclear import was rapidly observed. The responses, in term of maximum nuclear localization time and rate were close to that of a single stimulation.

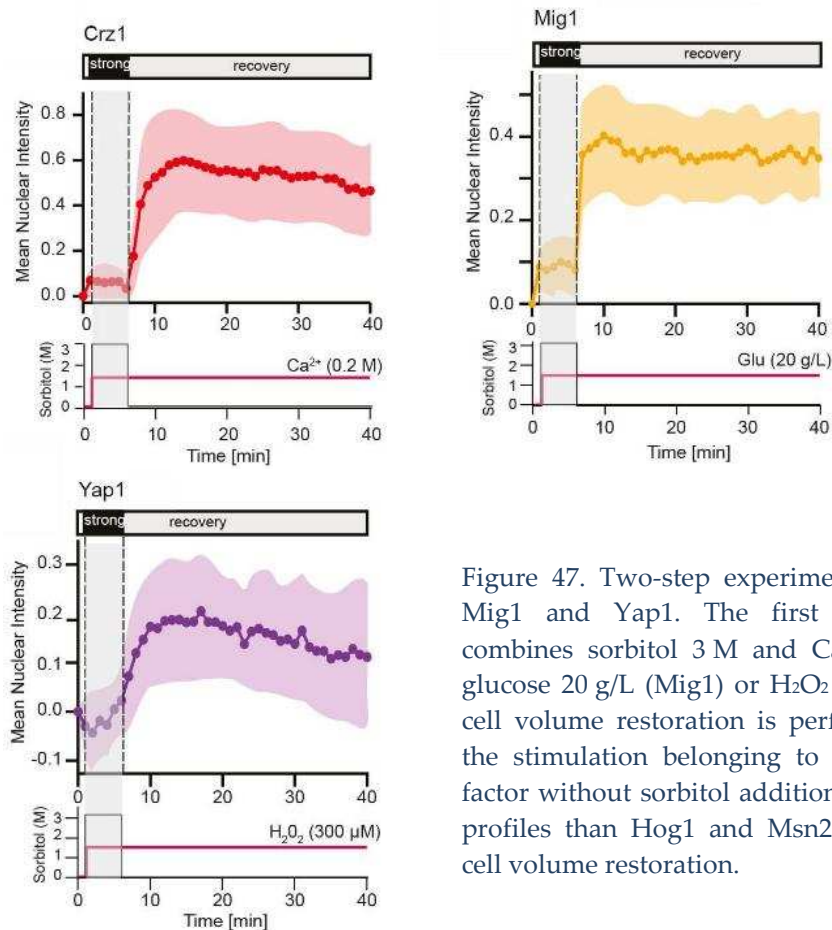


Figure 47. Two-step experiment applied to Crz1, Mig1 and Yap1. The first severe stimulation combines sorbitol 3 M and CaCl<sub>2</sub> 200 mM (Crz1), glucose 20 g/L (Mig1) or H<sub>2</sub>O<sub>2</sub> 300 μM (Yap1). The cell volume restoration is performed by applying the stimulation belonging to each transcriptional factor without sorbitol addition. Similar restoration profiles than Hog1 and Msn2 are obtained upon cell volume restoration.

## 11. Discussion

The Chapter 2 was focused on the HOG pathway response to hyper-osmotic stress and on its slow-down by volume compression. Increased intracellular viscosity due to reduced volume could explain the observed jamming. This chapter pushed further this argument and focused on the consequences of volume reduction on other cellular processes than the HOG pathway. Indeed, if the macromolecular crowding hypothesis is valid, then the same kinetics effects should occur for other proteins and motion in yeast but also for other eukaryotic cells. In the first part of this chapter, we investigated the kinetics of different processes upon volume reduction. The nuclear imports of Msn2, Crz1, Yap1 and Mig1 were shown to be slowed down upon increasing hyper-osmotic stresses and thus to present similar behaviors than Hog1. In this context, transient stress experiments were useful to determine what happen when the cell recover a normal volume due to release of the

### Chapter 3. Global effect of macromolecular crowding on intracellular dynamics

stress. According to our hypothesis, all processes should recover. Indeed, when the cells were transiently subjected to severe osmotic stress (5 min) followed by a release of the volume constraint, all cells were able to trigger a rapid nuclear import of any of these transcription factors.

Apart from signal transduction, we also observed endocytosis and vesicles transport arrest upon strong hyper-osmotic stress. Finally, using the same FRAP technique, we extended the diffusion alterations observed for Hog1-GFP to YFP, citrine and Ura1-GFP. In contrast to iso-osmotic conditions for which the fluorescence of those proteins recovered quickly, no fluorescence recovery was detected upon 2 M sorbitol induction. Yet, in iso-osmotic condition, we observed different rates of fluorescence restoration for those proteins. While the recovery of the protein Ura1-GFP and Hog1-GFP was fast, the recovery of the proteins YFP and citrine took more than 5 sec. The fluorophores GFP, YFP and citrine belong to the same family and have identical molecular weight. Therefore, these proteins should have similar diffusion properties. A possible interpretation is the presence of vacuoles which may enhance the effects of macromolecular confinement and interfere with the diffusion of proteins. In these three strains, we noticed that their vacuoles sizes may vary from one cell to another. In the strain *HOG1-GFP; pbs2Δ* from which we estimated the coefficients of diffusion, only small vacuoles were observed compared to the wild-type strains. Since the vacuoles are implicated in osmoadaptation, disrupting the HOG pathway could have consequences on the vacuoles morphologies and/or proportions. Therefore, due to the absence of vacuoles in this *pbs2Δ* strain, the calculated diffusion coefficients are certainly more accurate than if obtained in a wild-type strain.

The diffusion of proteins is not only altered in yeast but also in higher eukaryotic cells. Indeed, for the two human cell lines MCF-7 and A549, the diffusion of GFP is affected upon severe osmotic stress. We conclude that cellular compression induces kinetics slow-down of several, unrelated dynamical processes, in frame with theoretical considerations on the nonlinear slow-down of relaxation dynamics observed in a glassy transition of a colloid. However, several aspects of macromolecular crowding need to be further discussed. First of all, volume

reduction may prevent the intracellular import of activator molecules by changing the permeability of the membrane. Indeed, Mig1, Crz1 and Yap1 activation seems to depend on the intracellular location of their respective stimulus. Exposure to high temperature, prolonged mating pheromone or changes in extracellular ions triggers intracellular calcium increase and Crz1 activation [182]. While glucose uptake seems essential for Mig1 activation [183], intracellular reactive oxygen species (ROS) lead to Yap1 activation [163]. Consequently, the signaling delays could be the consequence of the uptake alteration of the activator molecules. Yet, we can show that Crz1 delay is not caused by calcium uptake impairment. Indeed, we observed that hyper-osmotic stress alone triggered Crz1 activation and that Crz1 kinetics is slowed down after a severe osmotic compression when stimulated by sorbitol only (Figure 48). Al-Mohanna *et al.* and Lange *et al.* described, in the cytoplasm of respectively human neutrophils and hamster insulinoma (HIT) cells, the capacity of actin to store calcium. They notably observed that calcium may be released upon actin depolymerization [184, 185]. It has also been observed that hyper-osmotic stress is linked to calcium release in chondrocytes [186]. Since hyper-osmotic stress is known to induce actin cytoskeleton depolymerization in *S. cerevisiae* [12], the unspecific activation of Crz1 may be related to actin dissociation and calcium release in the cytoplasm. In this case, calcium is already intracellular and the increase in macromolecular crowding is likely to be involved in the nuclear translocation delay that we observed for Crz1. However, for Yap1 or Mig1, it is not possible to conclude, although we can note that H<sub>2</sub>O<sub>2</sub> and glucose are small molecules that should diffuse easily across the plasma membrane.

From the beginning of this thesis, we proposed macromolecular crowding as a candidate for the observed alterations in the kinetics of reactions. However, other processes may be involved. For instance, maintenance of a constant intracellular pH is essential for the activity of numerous enzymes, ion channels functioning or cell cycle and proliferation capacity. Decreasing the pH is seen to affect the efficiency of a wide range of cellular processes such as glycolysis, protein synthesis, DNA synthesis or endocytosis [187]. Even if the intracellular acidification may damage the kinetics of reactions, it has no reason to alter the diffusion of several proteins unspecifically. The decrease in the rate of diffusion is more naturally explained by

steric effects of volume compression such as macromolecular crowding or confinement.

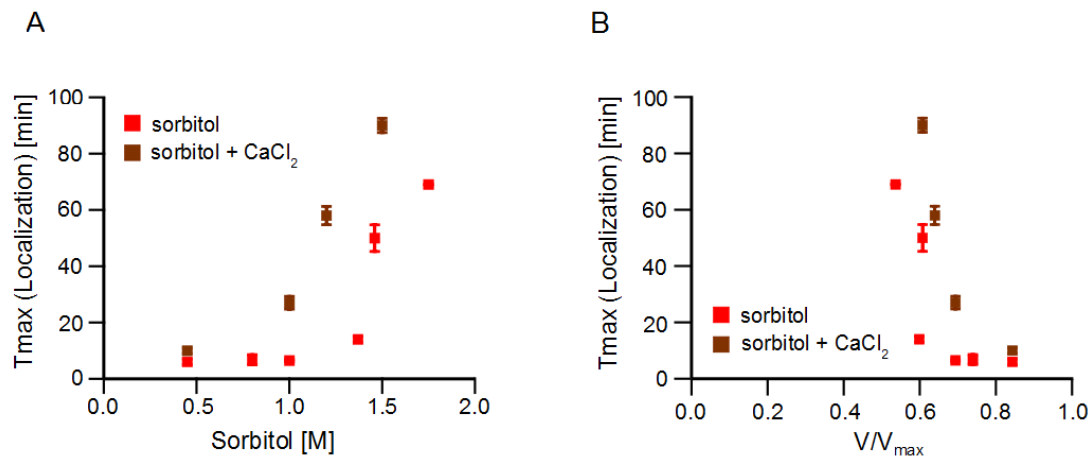


Figure 48. Kinetics of the nuclear localization of Crz1 upon hyper-osmotic stress alone (red squares) or with the coupling of hyper-osmotic stress and  $CaCl_2$  200 mM (brown squares). The times of maximum nuclear import are plotted in function of the sorbitol concentration (A) or the relative cell volume reduction (B).

As explained in the introduction, confinement concerns the effect of molecules organized in networks (*e.g.* cytoskeleton, membranes) that leads to the physical sequestration of proteins within bounded structures such as channels, interstices or pores [15]. This situation favors aggregation and protein binding. Confinement could enhance protein binding equilibria and reduce the rate of diffusion in a manner similar to what we observed. Yet, crowding and confinement are not mutually exclusive and could be both implicated.

## CONCLUSION AND PERSPECTIVES

In this thesis, I have analyzed the effects of cell volume reduction on the dynamics of reactions in live cells. For this purpose, I used hyper-osmotic stress in the yeast *Saccharomyces cerevisiae* to progressively compress the cell and analyze the effects on the kinetics of the HOG pathway. I observed that the activation and the nuclear translocation of the dedicated transcriptional factor Hog1 are progressively slowed down upon increasing hyper-osmotic stresses. I correlated those alterations with a decrease in the cytoplasmic diffusion of the protein Hog1. The nuclear imports of unrelated factors, namely Msn2, Crz1, Yap1 and Mig1, present similar kinetics impairments. Not only signal transduction processes but also endocytosis and vesicles formations displayed alterations of their dynamics. Finally we extended the diffusion impairment observed for Hog1-GFP to the diffusion of Ura1-GFP, citrine and YFP in *S. cerevisiae* and GFP in the human epithelial cell lines, A549 and MCF-7. From those results, we concluded that cellular compression triggers a global diffusion alteration that affects a wide range of processes kinetics. Macromolecular crowding is a suitable candidate for this diffusion decrease. Applying a severe cellular compression leads to a global arrest of several reactions but, once the cell size is restored, reactions can occur normally. In line with Dill *et al.*, we proposed that evolution has maximized reaction rates by an adjustment of the cell size to the molecular density [44]. Macromolecular crowding enhances the rate of protein association but at the same time, decreases diffusion. Therefore, a shift in the equilibrium would either affect the encounter probability of molecules if the media is diluted or instead decrease the diffusion of protein in a too crowded environment. In any case it would result in a modification of reaction rates. Reactions are not abruptly stopped upon mild or moderate hyper-osmotic stresses but instead present a range of volume compressions for which they are delayed. By progressively increasing the osmolarity, the intracellular density is progressively increased. This change leads to an exponential decline of the dynamics with respect to the cytoplasmic density increase similarly to what is observed for soft colloidal glassy-like transitions [47].

## Conclusion and Perspectives

In this thesis, I showed several evidences suggesting that macromolecular crowding is a key player during osmotic stress and that osmoregulation acts primarily to counterbalance its negative consequences. Further experiments would be welcome to test and extend the quantitative analysis that we proposed. For instance, we could only measure the diffusion coefficients for three hyper-osmotic conditions on the osmosensitive strain (*pbs2Δ*) and one condition on the wild-type strains providing us only estimations of the diffusion rates. Being more quantitative with a higher resolution would make possible to study the effect of diffusion in a crowding *in vivo* environment and then better relate our measurements with theoretical predictions.

Microscopy techniques may also be improved for better precision of diffusion measurement. Indeed, the FRAP technique used in this study is not optimal when applied on small cells due to the important size of the bleached area compared to the total size of the cell. Moreover, applying a hyper-osmotic stress reduces the cell size and ultimately increases the proportion of the bleached area. Consequently, the measured diffusion coefficients can only be regarded as estimations. In order to improve diffusion measurements, other possible techniques could be used. Single Molecule Tracking (SMT) is a method for tracking a fluorescent molecule over time. The trajectory of the molecule motion is plotted in function of time and a coefficient of diffusion can be obtained. However, with such method, the molecules are difficult to visualize *in vivo* due to background fluorescence of the cytoplasm. Another possible single molecule tracking method is the Fluorescence Correlation Spectroscopy (FCS) approach. As previously described, FCS method has been used inside HELA cells for the determination of dextran diffusion upon increasing macromolecular crowding [8]. Despite the encountered difficulties of using FRAP in this study, this method remains a technique of choice for determining the mobility of molecules *in vivo*.

We could also extend this work by addressing if other processes in cell are similarly slowed down upon compression or if instead differences exist and why. For instance, in the endocytosis analysis, I observed differences in recovery between Abp1 and Sec7 patches motion. While Sec7 patches recovered their motion after ~15 minutes of 1.5 M sorbitol stress, Abp1 patches were still jammed. Abp1 motion

depends on the actin cytoskeleton which is not the case of Sec7 [188, 189]. Knowing that the cytoskeleton disassembles upon osmotic compression, it can result in a longer recovery of Abp1 patches motion compared to Sec7. Once again, using the SMT technique, we could improve the quantification of those observations and maybe extend this observation to the direct analysis of the cytoskeleton upon osmotic stress.

Cell volume reduction is linked to the intracellular density and its accurate measurement is essential. However, the cell volumes have been calculated from 2D pictures and the smallest cell size was recorded 1 min after the stress. As the cell size variation occurs in ~10 sec, we may underestimate the actual smallest cell size and our calculation can only be regarded as an estimation. Using confocal microscopy, 3D pictures of yeast could be obtained on shorter timescale (15-30 sec) and would give accurate spatiotemporal measurements of the cell size modifications upon compressions.

In this thesis, we not only have been interested in the effects of volume compression on different biological processes or organisms, but we also addressed the limit of cellular adaptation to compression and how cell could possibly adapt to severe stress (see the appendix for supplementary results). All along this study, we used sudden and unique osmotic stress. In these conditions, cells are not able to adapt to stress above 2.2 M sorbitol (Figure A1). However, cells in the wild may overcome diverse stimulations with different rates of variation. As a preliminary study, we analyzed the adaptability of cells to severe osmotic stress upon different time varying stimulations (see the appendix). We first noticed that cells preparation through pre-centrifugation enhances their adaptability to severe osmotic stress (Figure A2). The principle of acquiring a resistance to specific stress is well known in yeast. Sensing early sign of fluctuation prepares the cell for environmental change and may confer an evolutionary advantage in the wild. However, in our case, the centrifugation may involve different sensing mechanisms than osmotic shocks and it could be interesting to address what are the mechanisms implicated. Cell response to hypergravity has been rarely studied even though this process is intensively used for molecular and cellular biology protocols. Yet, Hoson *et al.*, observed that

## Conclusion and Perspectives

prolonged hypergravity modified the cell wall of plant cells by making it rigid and thick [190]. In our case, prior centrifugation improves the cell ability to import Hog1 inside the nucleus upon severe osmotic stress without changing its kinetics. Those results show that a stimulation of physical nature increases cells resistance to hyper-osmotic stress. However, the mechanism by which centrifugation prepare cells is unclear. Hog1 is not involved since centrifugation alone does not trigger its activation or its nuclear localization (Figure A2, A-C points zero). Soto *et al.* observed that hypergravity triggered the activation of the MAPKs Sty1 and Pmk1 which are respective effectors of the stress-activated protein kinase pathway and the cell-integrity pathway in *S. pombe* [191]. Therefore, in *S. cerevisiae*, centrifugation may activate parallel mechanisms of cellular protection such as the transcriptional factor Msn2. Further investigation could be conducted to characterize the mechanisms involved in this process.

We also tried to vary the rate at which the osmolarity of the environment was changed and looked at the HOG pathway kinetics (Figure A3-Figure A4). When a severe osmotic stress is applied slowly (2-3 min to switch media), the nuclear import of Hog1 does occur as it would in the case of a sudden (few seconds) gentle stress. Consequently, the absolute stress intensity has no deleterious effects on Hog1 nuclear import if the input rate is slow enough compared to the nuclear transport of the protein. In contrast with a gentle osmotic stress for which Hog1 is exported 20-30 min after the shock, the slow increase of the input up to an intensity of 3 M sorbitol prevents its export (Figure A3). It is possible that delaying the compression allows rapid reactions such as the Hog1 nuclear import to be processed while the volume compression is still not too strong, but blocks downstream steps of the pathway later on. It could then be interesting to study gene expression ability of cells after sudden or slow osmotic compression.

We also noticed that in contrast with short periods of strong stresses, longer periods lead to a progressive increase in cell mortality (Figure A5). Both the intensity of the stress and the duration of the stress are enhancers of mortality, consistently with previous studies [192, 193]. Silva *et al.* observed that severe hyper-osmotic stresses trigger mitochondria alterations leading to apoptosis in yeast. However, the

primary cause of cell death upon compression is not clear. Plasmolysis may correspond to the transition above which jamming is irreversible. From the model developed by Schaber *et al.*, plasmolysis may occur at 4 Osm/L. In our study, the higher concentration used is 3 M sorbitol, equivalent to 3 Osm/L. Consequently, our range of osmotic conditions is lower than the predicted plasmolysis concentration. Moreover plasmolysis is not necessarily related to cell mortality since a majority of plant cells or bacteria stay viable [194, 195]. We have previously showed that jamming can be reversed when cells are subjected to severe stress (3 M sorbitol) for a short period of time (5 min). Therefore, plasmolysis, if it occurs in our experiments, may be reversed, at least for short timescales.

We observed that cells subjected to severe stress seem to enter a frozen state. It would be interesting to investigate the actual state of the cells under compression using electron microscopy for example. The use of a viability dye would also give an estimation of the state of the cell. Yet, the possible cessation of molecules uptake due to severe compression may prevent the import of the viability dye. Consequently the dye would stay extracellular whether the cell is dying or not and give rise to false negative results. FUN-1 is a two-color fluorescent probe for which the staining changes when cells die. While metabolically active cells present red-fluorescent structures, the dead cells show diffuse yellow-green fluorescence. Using this dye, the direct and accurate characterization of the yeast viability upon strong hyper-osmotic conditions may be established. This characterization would allow the study of the dormant state of cells upon long exposure of stress. Whether the cells are programmed to enter a quiescent state for long term survival or are brutally jammed should be addressed and better understood.

In addition to those quantifications improvements, alternative investigations could be conducted. In this PhD work, I focused on signal transduction in yeast. We may wonder if the dynamics of other mechanisms are similarly delayed upon compression. Further investigations could be performed on other processes such as gene expression, protein phosphorylation and associations or on the structure and rigidity of the cytoskeleton.

## Conclusion and Perspectives

Moreover, the volume compression effects could be investigated in other species. Indeed, yeasts are small cells surrounded by a cell wall and increasing hyper-osmotic stress strongly affects membrane stiffness. Therefore, we may wonder if the effect of volume compression may vary with different cell morphologies. Studying the effect of compression between different cell types would allow a better understanding of the *in vivo* biochemistry. I have previously shown that severe compressions inhibit the diffusion of GFP proteins into the cytoplasm of mammalian cells. Yet the analysis is not quantitative enough to be compared with our previous diffusion analysis on yeast. Once again, this study could be improved by applying intermediary hyper-osmotic shocks and analyzing the diffusion of alternative proteins. The effects of compression on signal processing could also be a parameter of comparison. In mammalian cells, osmotic regulation mechanisms are complex and implicate not only p38 (Hog1 homolog) but also the JNK (C-Jun N-terminal Kinases) and ERK (extracellular regulated kinases) pathways. The nuclear translocation of their respective factors could be analyzed upon increasing compression and compared with the yeast kinetics.

We may also complete this study by investigating the effects of volume compression on different yeast species. Indeed, if differences in reaction rates exist, we could address if it is because of different cell morphologies or different adaptations to osmotic stress. It can be investigated by comparing the adaptation limits of *S. cerevisiae* with different osmotolerant yeasts. In this study, we observed that *S. cerevisiae* limit of adaptation is about 2 M sorbitol. Yet, different osmotolerant species may behave differently to sudden stimulations and therefore present different resistances to severe stresses.

Another possible investigation may concern the cellular damages resulting from increasing macromolecular crowding. We have observed that long periods of severe osmotic stresses lead to apoptosis. But how cell compressions lead to cell death is not much documented. Are the deleterious effects of macromolecular crowding start immediately upon any level of compression? Or is it a threshold above which alterations occur? Processes related to aging such as ROS accumulation,

## Conclusion and Perspectives

mitochondria activity or cell cycle progression could be analyzed through volume reduction and give clue about the mechanisms at play.

In the end, this PhD work raises questions related to the evolutionary conservation of intracellular densities. Indeed, we may wonder if cells do indeed use macromolecular crowding as a master regulator of their biochemical reaction rates. We previously discuss about an optimum of reactions dynamics accounting for molecular crowding. Do cells select for some intracellular optimality conditions? Is there a net adjustment of cell sizes and expressional rates in order to regulate intracellular densities? Even if those questions remain unsolved, it seems that most eukaryotic cells present a crowded intracellular environment that may account for a universal mechanism which has been selected by evolution.



## APPENDIX

<b>12. Supplementary Results</b>	<b>108</b>
Hog1 dynamics at very severe stress	108
Pre-stressing the cells improves their adaptation to compression	109
The cells sense the rate of increase of the input intensity	110
Cell death after long periods of severe stresses	113
<b>13. Supplementary Data</b>	<b>114</b>
Bionumbers	114
Osmotic Pressure: order of magnitude	114
<b>14. Materials and Methods</b>	<b>115</b>
Yeast strains	115
Culture conditions and media	115
Strains list	116
Mammalian cell lines	117
Inverted fluorescent microscopy	118
FRAP and FLIP microscopy	118
Western blot	119
Images analyses / Quantification of the relative nuclear localization	120
Quantification of the cellular volume	122
FRAP and FLIP analysis	123
Quantification of the diffusion coefficient	123

## 12. Supplementary Results

### Hog1 dynamics at very severe stress

Our observations were limited to a range of stimulations for which the cells are able to adapt. In order to go deeper in our understanding of cell resistance to severe stress, we measured the percentage of cells able to import Hog1 into the nucleus, even after very long time. At the concentration of 1.8 M, around 90% of the cells triggered a nuclear import of Hog1 while at 2.2 M, 100% of the cells were not responsive even after 3 hours of stimulation. Fitting the data with a sigmoid gives a transition around 2 M sorbitol for which 50% of the cells were not responsive anymore (Figure A1). This should be compared to our phosphorylation result showing that Hog1 was not phosphorylated anymore at 2.5 M sorbitol.

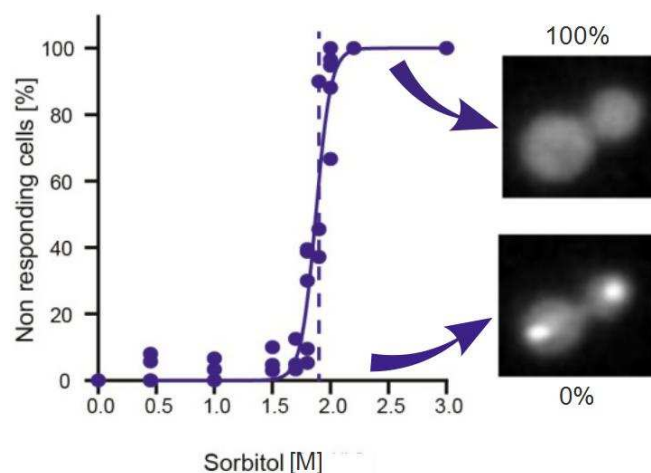


Figure A1. Determination of the cells adaptability to volume compression. For a moderate osmotic stress (< 1.5 M sorbitol) all cells trigger a Hog1 nuclear localization. Increasing the sorbitol concentration leads to a decrease in the quantity of responsive cells. The transition is sharp and occurs at 2 M. Above this transition, almost 100% of cells are not importing Hog1 into the nucleus.

It is known that hyper-osmotic stresses trigger, through the activation of Hog1, the arrest in either G1 or G2 states of the cell cycle. It will eventually re-start once the osmotic homeostasis is restored. When cells were exposed to a constant stress of 1.8 M sorbitol, they showed the ability to resume budding after 3 to 5 hours of stress. Above this concentration, no or few divisions were observed even after 14 hours. In such situations, the cell interior is jammed, preventing any possible reaction to occur.

### **Pre-stressing the cells improves their adaptation to compression**

We usually used sudden osmotic stimulations to compress the cells. In such conditions, the cells were able to adapt to sorbitol concentrations lower than 2M. However, alternative stress induction may improve the cell adaptability to severe stress. In this manner, we noticed that harvesting the cells through centrifugation prior to osmotic shocks enhanced their resistance to severe stresses. Cells were centrifuged at 5000 rpm for 2 min and the phosphorylation and the nuclear accumulation of Hog1 were measured. For stresses below 2 M sorbitol the dynamics of Hog1 were similar with or without centrifugation (Figure A2A-B). However, at the concentration of 2.5 M sorbitol, centrifuged cells triggered an activation of Hog1 whereas non-centrifuged cells could not. Similarly, centrifuged cells presented a higher capacity to import Hog1 inside the nucleus. Indeed, at 2.5 M sorbitol, only 40% of pre-stressed cells were non-responsive while for the same concentration, 100% of non-centrifuged cells were non-responsive. The transition between responsive and non-responsive cells shifted from 2 M to 2.6 M sorbitol (Figure A2C). Yet, the response kinetics remained identical with or without pre-stress (Figure A2D). Therefore, pre-stressing the cells through centrifugation allows a higher resistance to further stresses but the time to activate the cascade is still delayed to the same extent.

## Appendix

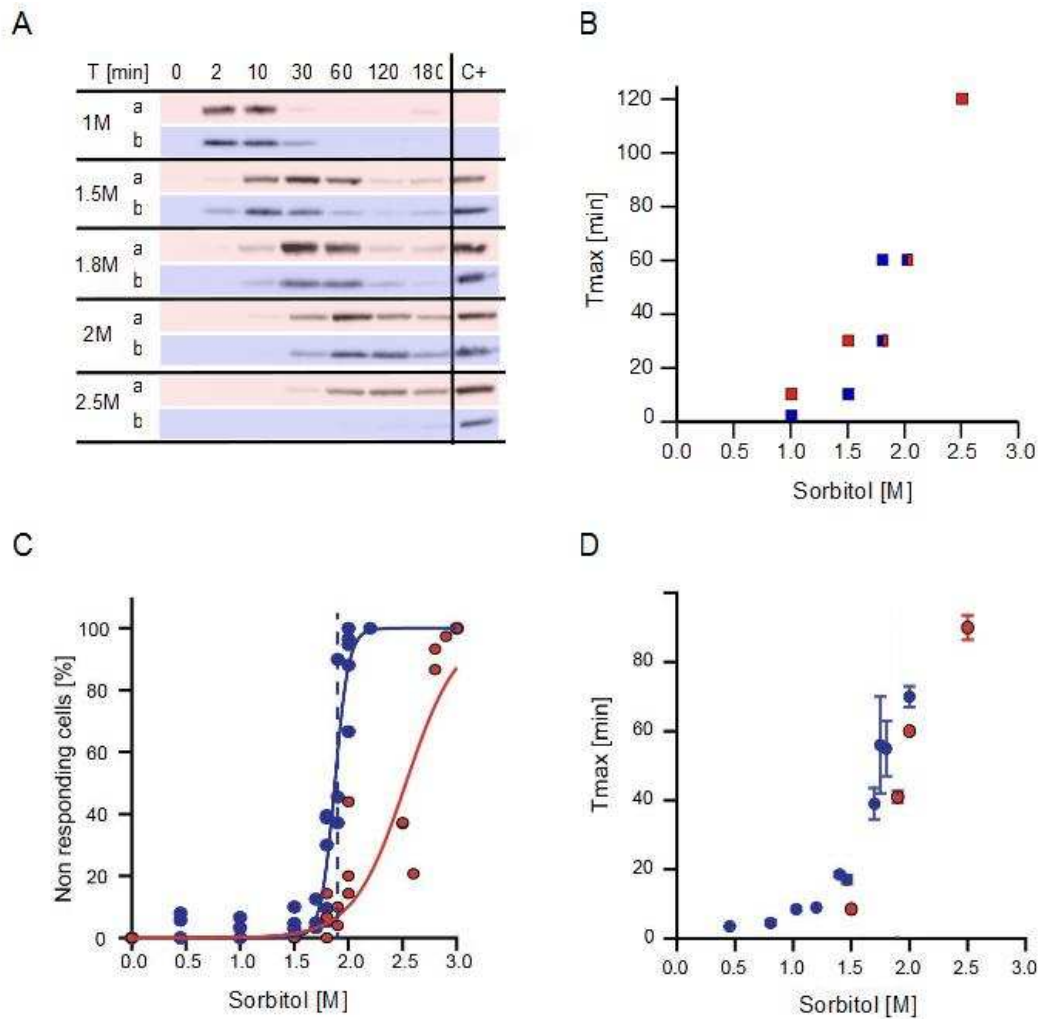


Figure A2. Comparison of the HOG pathway response ability with and without pre-stimulations. Hog1 phosphorylation (A-B) and nuclear translocation (C-D) kinetics and ability are represented in function of the stress intensity applied. (A) Western blot comparison of phosphorylated Hog1 between preliminary centrifuged cells (a: red blots, 5000 rpm for 2 min) and normal cells (b: blue plots). A marked difference is observable for the 2.5 M sorbitol blots for which centrifuged cells are able to trigger Hog1 activation while directly stressed one cannot. (B) Despite this resistance to severe stress, the kinetics (red squares) are similar to non-centrifuged cells (blue squares). (C) The percentage of cells able to respond after a direct stress (blue circle, figure 7), is compared with pre-stressed cells (red circles, 5000 rpm for 2 min). At severe osmolarities, the response transition is shifted from 2 M to 2.6 M sorbitol. (D) Although the threshold depends on how cells were prepared, the delay of the cascade followed the predicted trend: Hog1 nuclear translocation is delayed when the osmotic compression increases.

### The cells sense the rate of increase of the input intensity

We now address if the rate of input induction could also influence cellular adaptability. All along this work, the stress was applied quickly, in less than 10 sec. However in the wild, cells are not necessary exposed to such abrupt variation of

concentration. This raises the question of whether the observed jamming transition depends on the absolute level of the osmotic stress or on its rate of variation. Using the nuclear accumulation of Hog1 as a readout, we performed an experiment with an up-staircase input. The sorbitol concentration was increased by step of 1 M to a final concentration of 3 M. The time interval between steps was respectively 1 min (Figure A3B), 2 min (Figure A3C) and 5 min (Figure A3D). We previously showed that abrupt 3 M sorbitol stimulation inhibits Hog1 nuclear localization (Figure A1). In contrast, we observed here a rapid Hog1 import in 3 to 5 min, similarly to a single 1 M sorbitol stress (Figure A3A). The level of maximum nuclear import strongly depended on the intervals duration. Indeed, with only 1 min interval time, the nuclear accumulation reached half of the mean value upon 1 M sorbitol stimulation. However, for both 2 min and 5 min duration, the rate of Hog1 translocation was similar to a 1 M sorbitol step shock. If the induction time of the osmotic stress is slower than the nuclear translocation of Hog1, the osmotic compression is no more a limiting factor for Hog1 activation. Surprisingly, we observed that Hog1 stayed nuclear over time while it was quickly exported after a gentle osmotic single step shock stimulation (Figure A3A). Consequently, for a progressive stress the absolute value of the input is ineffective on the protein import but seems to impact its export mechanism.

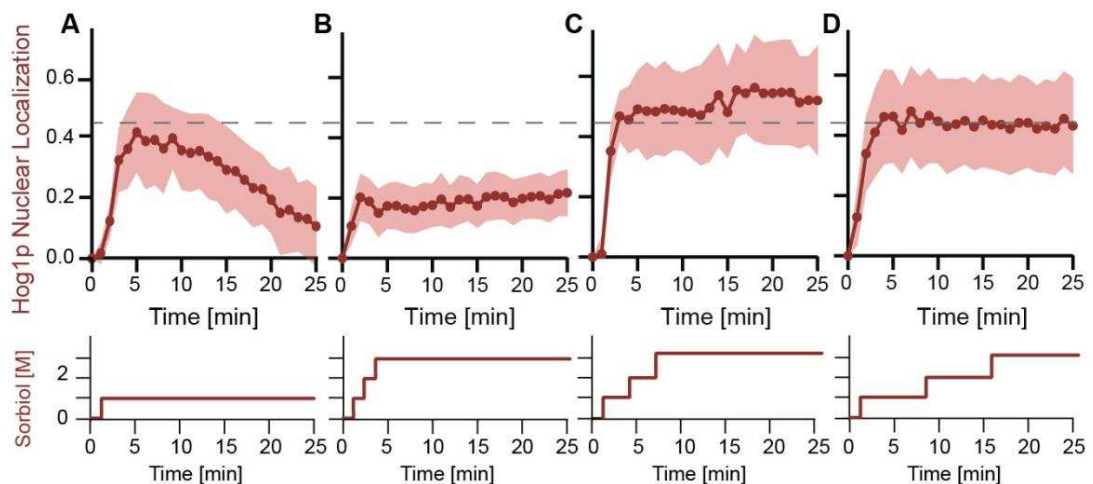


Figure A3. The ability to import Hog1 inside the nucleus depends on the rate of environmental change. Cells are subjected to up-staircase inputs. The environment increases by step of 1 M sorbitol to reach 3 M final sorbitol concentration. The interval time between each step is respectively 1 min (B), 2 min (C) and 5 min (D). In (A) is shown the response to a single pulse of 1 M sorbitol. The amount of Hog1 nuclear translocation strongly depends on the rate of osmotic change. (C) and (D) demonstrate that while Hog1 has enough time to translocate into the nucleus, further adaptation and nuclear export of Hog1 are blocked.

## Appendix

We reached a similar conclusion using the microfluidic chip developed by Uhlendorf and coworkers [149]. In their device, cells are trapped in chambers slightly smaller than the yeast cell ( $3.1\ \mu\text{m}$  high) and the change of media occurs slowly by diffusion ( $\sim 2\ \text{min}$ ) (Figure A4A). Instead of up-staircase input scenarios with different sorbitol concentrations as previously used, this system provides a ramp input. In this condition, we applied a single strong stress of 2 M sorbitol and observed a maximum nuclear localization around 60 to 65 min after the shock (Figure A4B). This kinetics is similar to what has been previously obtained upon a sharp 2 M sorbitol stress ( $\sim 70\ \text{min}$ ) (Figure 29). Yet a marked difference is obtained concerning the proportion of cells able to respond. While only 50% of suddenly stressed cells triggered a response (Figure A1), 100% of cells imported Hog1 in the nucleus upon a slow ramp input. Although the dynamics are similar between experiments, slow change of environment triggers a higher capacity to respond to severe stresses.

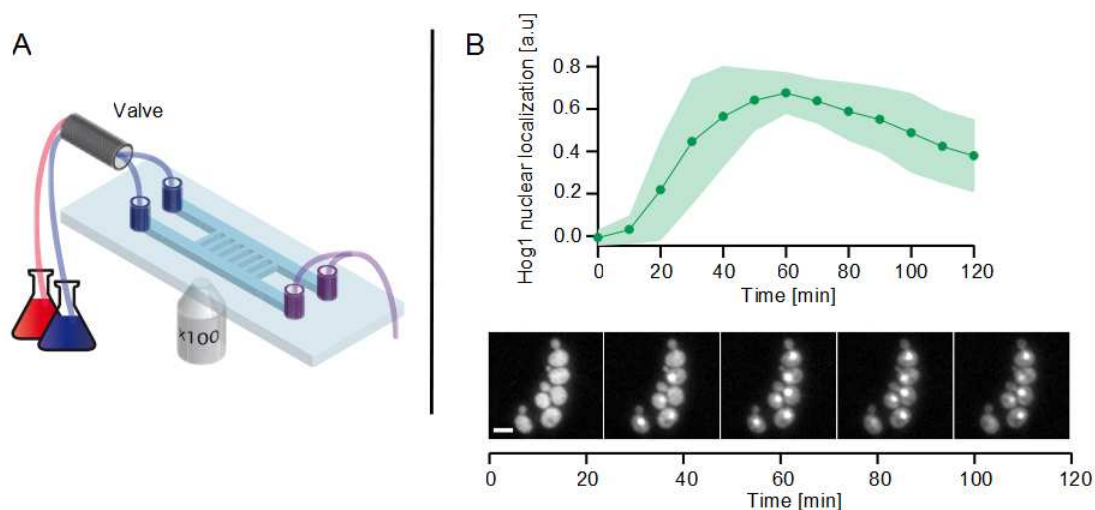


Figure A4. Effects of a severe osmotic stress (sorbitol 2 M) on the nuclear localization of Hog1 using the microfluidic device developed by Uhlendorf *et al.* [149]. (A) The microfluidic device is composed by two channels in which the media flow. The change of medium is controlled by a valve and occurs in about 2 min. (B) 100% of cells triggers the nuclear localization of Hog1 upon slow induction ( $\sim 2\ \text{min}$ ) of severe osmotic stress (sorbitol 2 M). Bottom panel: GFP (Hog1) images of 2 M sorbitol experiment over time. The scale bar represents  $4\ \mu\text{m}$ .

## Cell death after long periods of severe stresses

We previously observed that short periods of severe stresses did not alter the cell ability to import Hog1 inside the nucleus (Figure 46-Figure 47). However, upon a long period of severe stress (3 hours), a high percentage of cells (> 90%) stay non-responsive. We wonder whether this inability to recover a long timescale of strong stress can be attributed to cell death. Colony Forming Unit (CFU) is an indirect method of viable cell counting based on their capacity to form colonies. We applied 2 M and 3 M sorbitol concentrations from 5 min to 4 hours and then plated the cells on SC plates and waited to observe colonies (Figure A5). After respectively 1 hour and 4 hours of 2 M sorbitol incubation, 80% and 60% of cells were viable (Figure A5). Consequently, 2 M sorbitol triggered a slow decrease in viability in function of time. We similarly analyzed the effect of 3 M sorbitol on cell viability. After 1 hour of incubation, less than 10% of viability was observed while after 4 hours, almost all cells were dead (Figure A5). Therefore, 3 M sorbitol triggered a sharp decrease in viability upon long periods of incubation. Our results suggest that the intensity of the stress and/or the time of incubation are factors of yeast viability alterations.

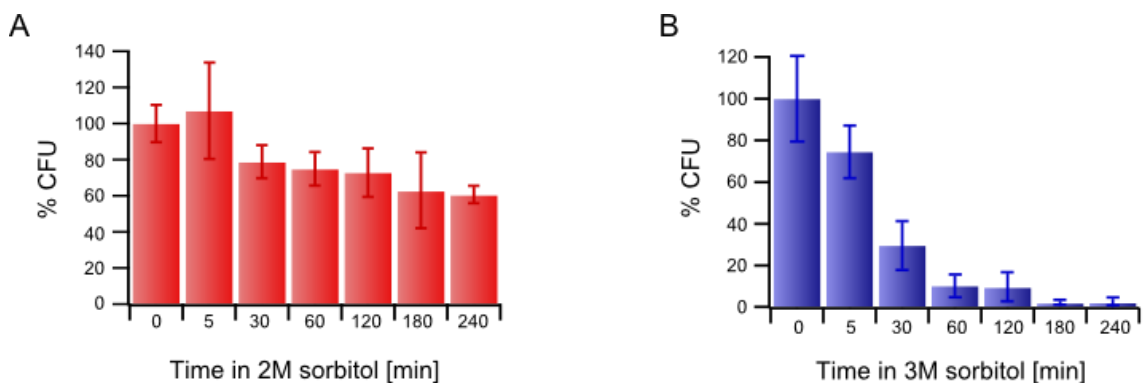


Figure A5. Prolonged exposition to severe osmotic stress impairs the reversibility of biological processes. Percentage of Colonies Forming Units (CFU) after different periods of incubation in 2 M sorbitol (A) and 3 M sorbitol (B). Each experiment is realized in triplicate and averaged.

## 13. Supplementary Data

### Bionumbers

Table A1. Key numbers in *S. cerevisiae*

Categories	Properties	Values	References
Yeast proportions	Diameter of haploid cell	4 $\mu\text{m}$	[196]
	Mean haploid cell volume	37 $\mu\text{m}^3$	[197]
	nuclear/cell volume	7%	[198]
	Fraction of cell mass that is water	60.4 $\pm$ 0.2%	[199]
	Cell density	1.1 g/ml	[200]
	Fraction of cell wall out of total cell mass	24.5%	[201]
Yeast timescales	Doubling time haploid cell	99 min	[202]
	Time of protein diffusion across the cell	$\sim$ 0.5 sec	Bionumbers
	Protein production rate in haploid cell	13000 proteins/cell/sec	[203]
Yeast concentrations	Protein density in cytoplasm	332.4 g/L	This study
	Average concentration of a protein in cell	$\sim$ 1 $\mu\text{M}$	[204]
	Range of protein concentrations	5-13.107 proteins/cell	[205]
Yeast osmosis	Yeast turgor pressure	0.6 $\pm$ 0.2 MPa	[67]
	Internal yeast osmolarity	$\geq$ 600 mOsm	[85]
	YPD media osmolarity	250 mOsm	[85]

### Osmotic Pressure: order of magnitude

Hyper-osmotic stress triggers an osmotic pressure which can be estimated using the Van't Hoff equation (Equation 5). For reminder, this equation is expressed as:

$$\pi = RTC_i \quad (\text{A1})$$

R is the perfect gas constant,  $C_i$  the molar concentration of solute  $i$  and  $T$  the temperature (in kelvin), set at 30°C for yeast ( $\sim$ 303 kelvin). The Table A2 compiles the range of concentrations and their respective osmotic pressures used in this study. Those osmotic pressures are compared with iso-osmotic conditions and natural environment variations.

Table A2. List of osmotic pressures used in this study and find in the wild

Environments	Osmolytes	Concentrations (M)	Osmotic Pressures (MPa)
Wild	sucrose/glucose	0.83 - 1.38	2.1 – 3.5
Iso-osmotic	glucose	0.11	0.28
Moderate hyper-osmotic	sorbitol	1	2.5
Strong hyper-osmotic	sorbitol	3	7.55

## 14. Materials and Methods

### Yeast strains

Table A3. List of yeast strains used in this study

Name	Background	Genotype	Source
yPH015	BY4742	<i>HOG1-GFP-HIS3; HTB2-mCherry-URA3</i>	[138]
yPH016	yPH15	<i>HOG1-GFP-HIS3; HTB2-mCherry-URA3; pbs2Δ-Kan</i>	[138]
yPH033	BY4741	<i>MSN2-GFP-HIS3MX6; HTB2-mCherry-KanMX4</i>	This study
yPH069	BY4741	<i>CRZ1-GFP-HIS3MX6; HTB2-mCherry-KanMX4</i>	This study
yPH107	BY4741	<i>MIG1-GFP-HIS3MX6; HTB2-mCherry-KanMX4</i>	This study
yPH082	BY4742	<i>YAP1-GFP-HIS3 + plasmid pRS316-mCherry</i>	Devaux's lab
yPH114	BY4741	<i>ABP1-GFP-HIS3</i>	Haguenauer-Tsapis' lab
yPH115	BY4741	<i>SEC7-mCherry-KanMX4</i>	Haguenauer-Tsapis' lab
yPH34	BY4741	<i>MSN2-GFP-HIS3, hog1Δ::Kan</i>	This study
yPH110	BY4741	<i>CRZ1-GFP-HIS3; HTB2-mCherry; hog1Δ::hph</i>	This study
yPH38	W303	<i>can1-100;his3Δ::prACT1-ymCitrine-tADH1-His3MX6</i>	Murray's lab
yPH12	-	<i>leu2::pADH1-YFP</i>	O'Shea's lab
yPH14	BY4741	<i>URA1::GFP-HIS3</i>	Ramanathan's lab

### Culture conditions and media

Cultures were maintained on YPD medium (1% yeast extract, 2% Bacto Peptone, 2% glucose) or on Synthetic Complete (SC) medium (0.67% yeast nitrogen base without amino acids, 2% glucose, 0.08% Complete Supplement Mixture dropout mix). We mainly used glucose as carbon source. We also used galactose for the strain *MIG1-GFP* since Mig1 is activated through the addition of glucose. When necessary, we used the Complete Supplement Mixture without one or several amino acids. For microfluidic experiments, cells were grown overnight at 30°C in synthetic complete

## Appendix

medium, re-inoculated the morning into fresh SC medium and grown at 30°C for 4-5 hours before microscopy. For osmotic stress, we used solution of sorbitol ranging from 0.45 M to 3 M. We prepared stock solutions of sorbitol at the concentrations of 4 M and 6 M. The 4 M solution was used for 0.45 M to 2 M working solutions preparation, while the 6 M stock solution was used for 2.5 M to 3 M sorbitol working solutions. Working solutions were prepared by mixing sorbitol stock solutions with SC solution 2-times concentrated (2X). We performed our experiments in SC medium because of its low auto-fluorescence. The preparation for NaCl, H<sub>2</sub>O<sub>2</sub> and CaCl<sub>2</sub> solution was identical to sorbitol (Table A4).

Table A4. List of osmotic solutions used in this study

	Stock solutions (M)	Working solutions (M)
Sorbitol	4 and 6	From 0.45 to 3
NaCl	5	From 0.25 to 1.5
CaCl <sub>2</sub>	3	0.2
H <sub>2</sub> O <sub>2</sub>	30.10 <sup>-3</sup>	0.3.10 <sup>-3</sup>

## Strains list

Strains from this study (Table A3) have been constructed using the transformation protocol from Sébastien Léon. Cells were grown in SC medium to OD<sub>600</sub> = 1 and were centrifuged twice for 1 min at 3000 g. The supernatant was removed and the cells were resuspended in a solution of TEL 1X (10 µl for 1 OD). TEL 1X preparation includes TE (Tris-HCl 1 M, pH 8; EDTA 0.5 M pH 8) and TEL 5X (5 mL TE 10 x + 5 mL LiAc 10X). Cells were then conserved on ice. One cell aliquot was used for one transformation. Janck *et al.* developed a versatile protocol for tagging or deleting yeast genes [206]. Using this method, we generated a PCR product from an initial plasmid containing the desire cassette (Table A5). In cells previously aliquoted, we added 20 µg of carrier DNA previously boiled, 5 µl of the PCR product and 300 µL of TEL-PEG solution. The final solution was mixed by pipetting up and down and incubated at 30°C for 30 min. It was then transferred at 42°C for 15 min. The preparation was briefly centrifuged, the supernatant was replaced by YPD and cells were plated on specific selection plates. For antibiotic selection, the cells need to settle for 30 min at 30°C in order to express the selective marker. Once colonies

## Appendix

formed, insertion verification was performed either by PCR or by fluorescent microscopy.

Table A5. List of plasmids used for strains construction

Name	Genotype	Source
pRS316-mCherry	URA3 CEN6 ARSH4 mCherry	Devaux's lab
pFA6-hphNT1	hphNT1	PCR-toolbox (EUROSCARF)
pYM35	DsRed1 KanMX4	PCR-Toolbox (EUROSCARF)
pFA6-HIS3MX6	<i>HIS3MX6</i> marker for gene deletion	PCR-Toolbox (EUROSCARF)
pYM35-mCherry	C-terminal tagging with mCherry, <i>KanMX4</i>	Haguenauer-Tsapis' lab

### Mammalian cell lines

We used two human cell lines. A549 cells are human alveolar basal epithelial cells and MCF-7 is a human breast cancer cell line. Both cell lines stably express GFP. The gene was introduced using lentivirus (Figure A6).

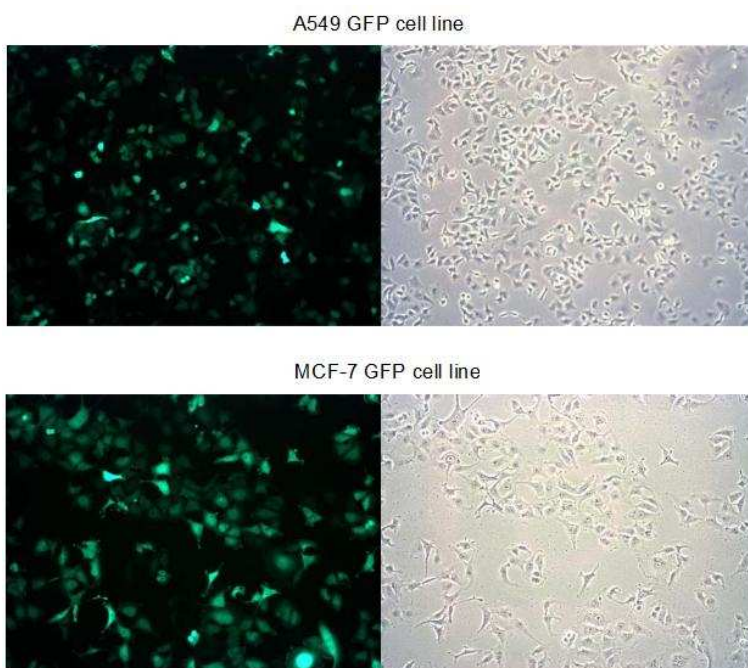


Figure A6. GFP fluorescence (left) or bright field (right) pictures of the two cell lines A549 (top) and MCF-7 (bottom) used in this study.

## Appendix

These human cell lines were cultured in DMEM solution and incubated at 37°C with 5% CO<sub>2</sub>. DMEM contains 1% Antibiotics (from stock solution of 100X stock of Penicillin, Streptomycin, L-glutamine) and 10% Fetal Bovine Serum (FBS). Cells were cultured in 10 ml DMEM between 2 and 4 days before microscopy experiments. For imaging, a low-fluorescence medium called Leibovitz's L-15, supplemented with 1% Antibiotics and 10% FBS was used. For hyper-osmotic stress induction, we used 40% (w/w) polyethylene glycol 400 diluted in the Leibovitz's L-15 solution.

### **Inverted fluorescent microscopy**

The cells were observed using an Olympus IX81 inverted fluorescent microscope with a QuantEM 512SC camera and a x100 1.40 NA immersion oil objective. Emission from GFP was visualized at 528 nm (38-nm bandwidth) upon excitation at 490 nm (20-nm bandwidth); emission of mCherry was visualized at 617 nm (73-nm bandwidth) upon excitation at 555 nm (28-nm bandwidth). Images were acquired through MetaMorphR software

### **FRAP and FLIP microscopy**

FRAP and FLIP experiments on strain *HOG1-GFP, pbs2Δ* were performed at the Nikon Imaging Centre of the Curie Institute. Experiments were done at 30°C on a Total Internal Reflection Fluorescence (TIRF) Nikon eclipse Ti inverted fluorescent microscope equipped with a QuantEM 512SC camera, a Piezo Flexure Objective Scanner (P-721 PIFOC) and a x100 1.45 NA DIC Oil objective. Emission filter is 525 nm and excitation filter 470 nm wavelength. For bleaching, we used a 491 nm pulse generated by a FRAP 4D module (Roper). A cytoplasmic area of typically 2 μm diameter was photo-bleached by a 50 ms Laser pulse. A single focal plane was then recorded every 50 ms with 5 ms exposure time. FLIP experiments were performed with the same system and conditions except that pictures were recorded every 250 ms. For the three yeast strains *pACT1-citrine*, *pADH1-YFP* and *URA1-GFP* and for the mammalian cells lines MCF-7 and A549, FRAP experiments were conducted at the Mechanobiology Institute of the National University of Singapore.

## Appendix

Experiments were performed at 30°C for yeast strains and at 37°C with 5% CO<sub>2</sub> for mammalian cells. We used a Perkin Elmer Spinning disk equipped with a Hamamatsu C9100 camera and an x100 1.40 NA DIC Oil objective. Emission filter is 615 nm and excitation filter 445 nm wavelength. For bleaching, we used a 488 nm pulse. A cytoplasmic area of typically 2 μm diameter was photo-bleached by a 50 ms Laser pulse. A single focal plane was then recorded every 200 ms.

### Western blot

Cells were grown in appropriate synthetic medium to OD<sub>600</sub> = 1. They were either centrifuged at 5000 rpm for 2 min or collected by filtration on a porous membrane with pore diameter inferior at 1 μm. The cells were then stressed with different sorbitol concentrations (1 M to 2.5 M) for different periods of time. To prepare protein extracts, cultures were rapidly suspended in 10% Trichloroacetic acid and maintained in ice at least 10 min. Cells were centrifuged and the supernatant was discarded to leave around 100 μl in the tubes. Cells were then broken by bead-beating the samples (10 min at 4°C) with glass beads (425–600 μm). The samples were centrifuged, the supernatant discarded and the pellet re-suspended in SDS Buffer (1X NuPage buffer, 10% β mercaptoethanol and 200 mM Tris) to a final volume of 100 μl. Samples were loaded on 10% SDS-PAGE NuPage pre-cast gel in 1X NuPage running buffer and run at 180 V for 1 hour. Proteins were transferred to PVDF membranes at 30 V at 4°C overnight. Dual phosphorylation of Hog1 on Thr-174 and Tyr-176 was observed using an anti-dually phosphorylated p38 antibody 1:1000. The positive control corresponds to Phosphoglycerate Kinase Monoclonal (PGK) detection using PGK primary antibody 1:1000. The detection for both proteins was performed using the secondary antibodies goat anti-rabbit-HRP at 1:10000 (Figure A7). The bands were then visualized using ECL-plus system in a Fujifilm LAS 4000 imaging system. Membranes were stripped between Hog1PP and PGK antibodies incubations using Tris-HCl 62.5 mM, pH 6.8 with 2% SDS.

## Appendix

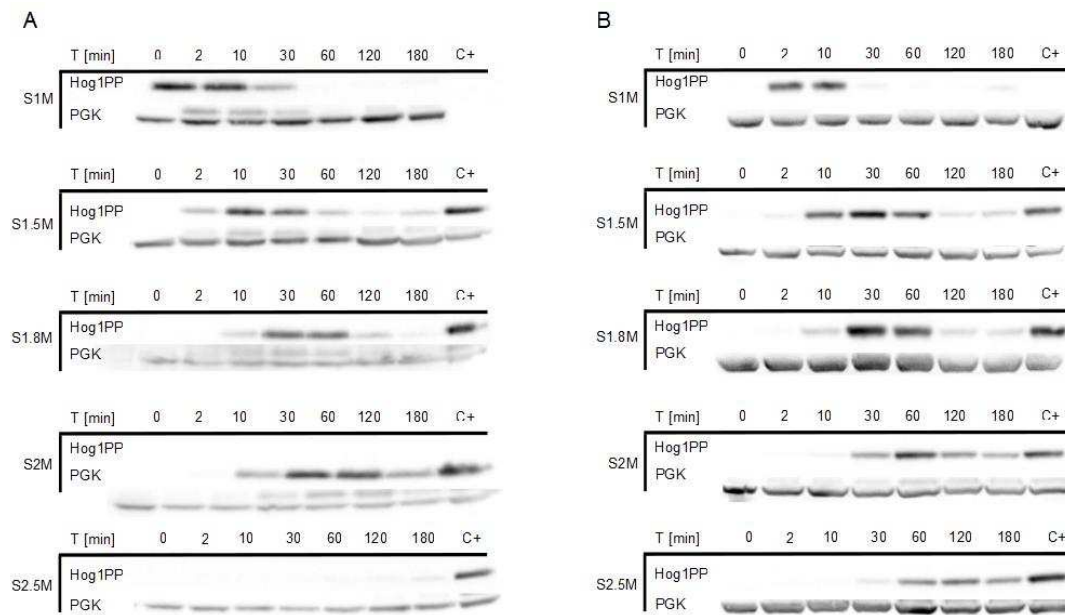


Figure A7. Western blots incubated successively with Hog1PP and PGK antibodies. Prior to the western experiment, proteins were either filtered (A) or centrifuged (B) and then stressed with different concentrations of sorbitol.

### Images analyses / Quantification of the relative nuclear localization

Quantification of the nuclear co-localization was obtained by using a combination of classic software to display stack of images (Metamorph), analyze them (ImageJ) and plot them (Igor Pro). The analysis consisted in monitoring the co-localization of a protein labeled GFP in the nucleus with the histone 2B as a nuclear marker (Htb2-mCherry). Image acquisition was performed in phase contrast, GFP and RFP channels at different time points (Figure A8).

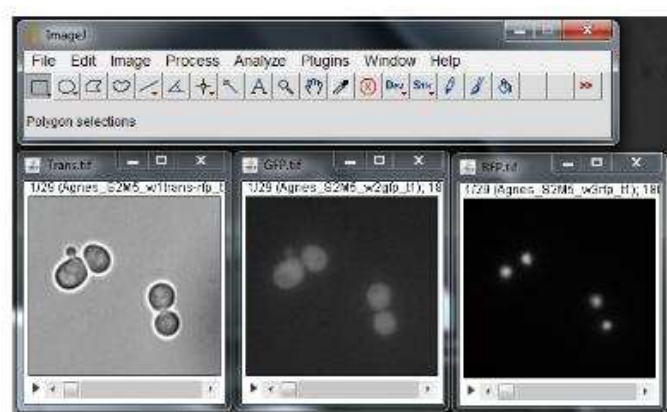


Figure A8. Stacks obtained from image acquisition: phase contrast, GFP (Hog1) and RFP (Htb2-mCherry).

A typical field of view contained at least 10 cells. The analysis was then performed using ImageJ. It consisted in extracting data about the contour of the cells, the cytoplasm GFP fluorescence, the nuclear localization and the GFP inside the nucleus. The background of the GFP stack was subtracted using the *Rolling ball* subtraction (200 pixels) command based on the rolling ball algorithm. The GFP stack was then filtered using the *Gaussian blur* program (1 pixel) in order to reduce image noise. We thresholded the pictures and then segmented the cells with a watershed algorithm to avoid cell fusion. Then we used the *Analyze particles* command on this binary stack and assigned a ROI to each cell. The whole GFP cell fluorescence (GFPc) was measured using the ROI manager (Figure A9).

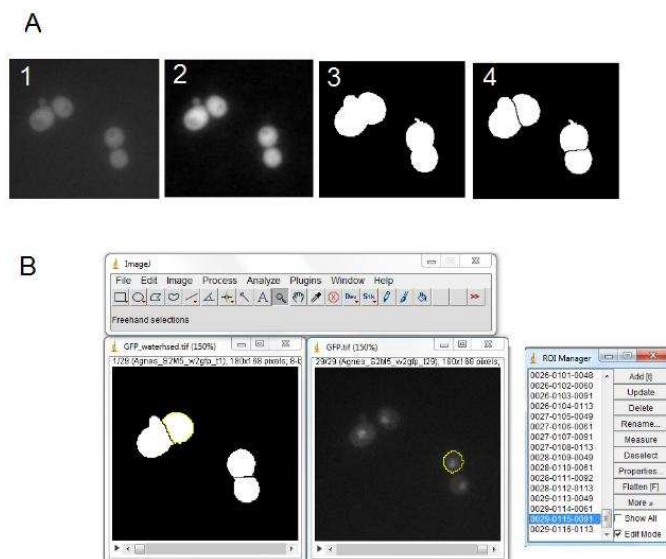


Figure A9. GFP cell fluorescence measurement. (A) The GFP stack was first treated through four steps: 1- Background subtraction, 2- Stack filtering, 3- Picture threshold 4- Cells segmentation. (B) Using *Analyze particle*, a ROI was assigned to each cell. Using these ROI measurements, the whole GFP fluorescence was measured on the original GFP stack.

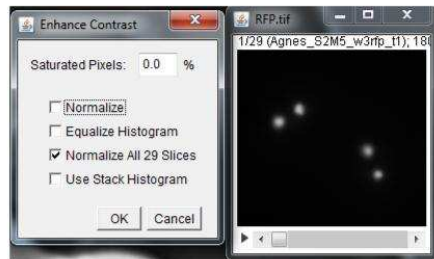
We performed similar treatments on the RFP stack to get the position of the nucleus. The intensity of the RFP stack was corrected from photobleaching using the *Enhanced contrast* command for every pictures of the stack. The nucleus position data were added to the ROI manager. From the GFP stack, the nucleus fluorescence was measured: The RFP segmentation stack was used on the GFP stack in order to measure the fluorescence of the interest protein at the nucleus position. The new measurement was called GFPn (Figure A10). This dataset was then used to compute the nuclear amount of GFP inside the nucleus. In a second step, those data were treated using IgorPro to compute the ratio of the total fluorescence intensity of the nucleus to the cell.

## Appendix

$$\text{Nuclear localization} = \frac{GFP_n - GFP_c}{GFP_c} \quad (\text{A2})$$

At the end of the procedure, the ratio of the nuclear intensity on the total cell is obtained for each cell of the movie. Experiments were made in triplicate. We then performed the mean and standard deviation from the total cell number.

A



B

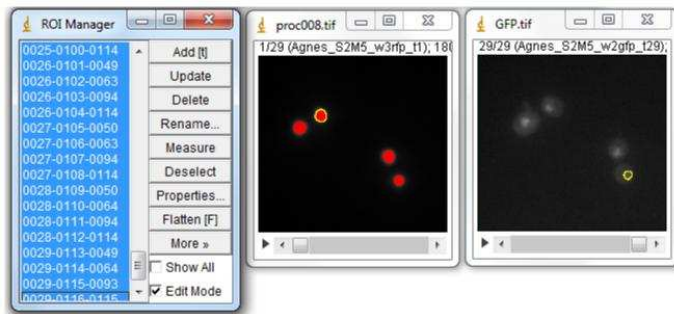


Figure A10. GFP nuclear fluorescence measurement. (A) The fluorescence intensity of the RFP stack was first normalized using the *Enhance contrast* command. (B) Using *Analyze particle*, a ROI was assigned to each nucleus. From these ROI measurements, the nuclear GFP fluorescence was measured on the original GFP stack.

## Quantification of the cellular volume

Using ImageJ, we manually measured the cell's area by fitting ellipses to the cells contour. The analysis was performed on at least 10 cells per image acquisition. From the cell area, we computed the equivalent volume assuming that cells are spheres. Presuming that the area of cells are  $A=4\pi R^2$ , the radius was extracted and the volume calculated from  $V= 4/3 \pi R^3$ . Since we were interested in volume variations, we measured for each cell the relative volume,  $V/V_{\max}$  in which  $V_{\max}$  is the volume of the cell before the osmotic compression. The mean and standard deviation were then calculated for each sorbitol condition.

## FRAP and FLIP analysis

FRAP and FLIP images obtained from the low-fluorescence strain *HOG1-GFP; pbs2Δ* were denoised using the ND-Safir procedure. This method, developed by Boulanger *et al.* [207], improves the signal to noise ratio. As the pictures obtained at the Mechanobiology Institute of the National University of Singapore presented high fluorescence values, it was not necessary to denoise the pictures. We then analyzed all the images the same way. The images were normalized on ImageJ by dividing the intensity of the whole bleached area fluorescence,  $I_{frap}(t)$ , by the intensity of the bleached area fluorescence just before the bleach,  $I_{frap-pre}$ . This operation was performed using the function *Image calculator* on ImageJ.

$$I_{\text{norm}}(t) = \frac{I_{frap}(t)}{I_{frap-pre}} \quad (\text{A3})$$

After this operation, the bleached area becomes visible due to the difference of intensity created by the division. An ellipse was fitted on this area and its intensity of fluorescence was measured for every time point, for each cell and condition. Files were imported to Igor Pro and the results were plotted.

## Quantification of the diffusion coefficient

From FRAP experiments, the diffusion coefficients were calculated for Hog1 (*HOG1-GFP, pbs2Δ*) in iso-osmotic and sorbitol 1 M conditions. To obtain adequate estimation of the diffusion coefficient, 2D theoretical model developed by Braga *et al.* was used [153]. During the time of photobleaching, diffusion can occur but is neglected by most of the FRAP models. Instead, Braga *et al.* took into account this parameter by analyzing the profile width of the bleached zone during the fluorescence recovery. Those intensity profiles were measured on the first picture of the experiment through a rotating line of 5-10 pixels width centered on the bleached area. The mean of every pixel of the line is calculated. The rotation angle increment was 5° giving a total of 72 lines (Figure A11). Intensity profiles were plotted for one cell per condition, assuming that every cell presented the same intensity profile. This measurement allowed the extraction of the width,  $\omega_m$ , and depth,  $k_m$ , of the bleached area. The initial chosen radius of the bleached area corresponds to  $\omega_s$ . It

## Appendix

was assumed to be the radius of the bleached area at half the depth,  $k_m$ . With those parameters, the typical timescale of photo-bleaching recovery,  $\tau$ , was extracted from the fluorescence recovery curves (Figure A12).

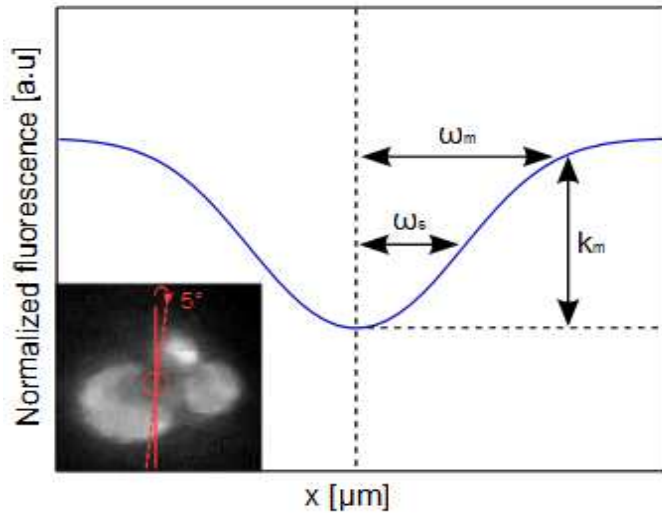


Figure A11. Representation of the fluorescence intensity profile. The picture on the bottom shows the method for the profile measurement on a bleached cell. From the bleached area (red circle) a  $5^\circ$  increment rotating line measures the profile on the first picture of the FRAP movie. From the fluorescence intensity profile, parameters such as  $\omega_s$  and  $\omega_m$  are extracted.

The diffusion coefficient  $D$  was then estimated by taking into account that particles diffuse over the bleached area radius,  $\omega_m$ , in the typical time,  $\tau$ , with a diffusion coefficient  $D = \omega_m^2/4\tau$ . The parameters and diffusion coefficients we obtained are shown in the Table A6.

Table A6. FRAP parameters and coefficients of diffusion

Osmotic conditions	$\omega_m$ ( $\mu\text{m}$ )	$\tau$ (sec)	$D$ ( $\mu\text{m}^2\text{s}^{-1}$ )
SC	2.4	0.091	15.8
Sorbitol 1 M	2.4	0.85	1.7

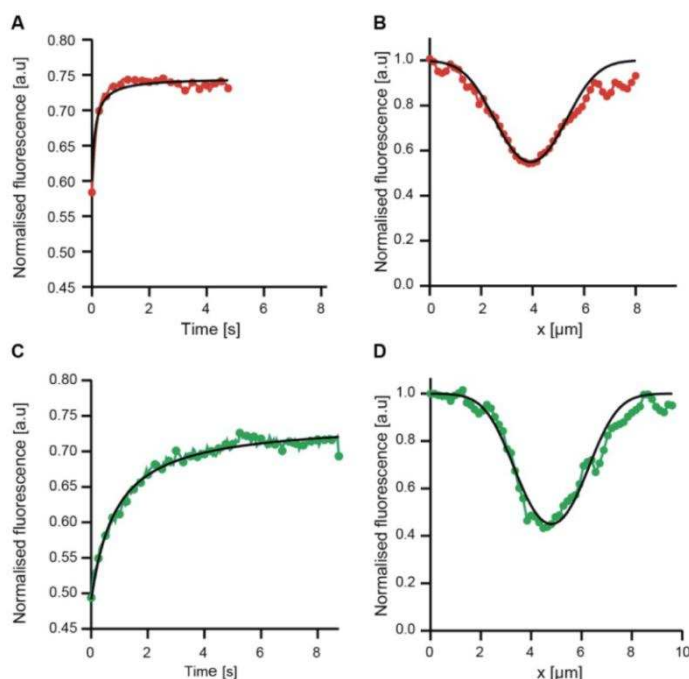


Figure A12. Recovery curves and fluorescence profiles after FRAP experiments performed on the yeast strain *HOG1-GFP; pbs2Δ* (A-B) in normal SC conditions and (C-D) in sorbitol 1 M conditions. Left panels: Average profiles of fluorescence recovery. Right panels: Transverse sections of the average photobleached area.

## BIBLIOGRAPHY

1. Fulton AB: **How crowded is the cytoplasm?** *Cell* 1982, **30**:345–347.
2. Medalia O, Weber I, Frangakis AS, Nicastro D, Gerisch G, Baumeister W: **Macromolecular architecture in eukaryotic cells visualized by cryoelectron tomography.** *Science* 2002, **298**:1209–13.
3. Minton AP: **Excluded volume as a determinant of macromolecular structure and reactivity.** *Biopolymers* 1981, **20**.
4. Minton AP: **Holobiochemistry: the effect of local environment upon the equilibria and rates of biochemical reactions.** *The International journal of biochemistry* 1990, **22**:1063–7.
5. Minton AP: **The influence of macromolecular crowding and macromolecular confinement on biochemical reactions in physiological media.** *The Journal of biological chemistry* 2001, **276**:10577–80.
6. Minton AP: **Influence of macromolecular crowding upon the stability and state of association of proteins: predictions and observations.** *Journal of pharmaceutical sciences* 2005, **94**:1668–75.
7. Ghaemmaghami S, Oas TG: **Quantitative protein stability measurement in vivo.** *Nature Structural Biology* 2001, **8**:879–882.
8. Weiss M, Elsner M, Kartberg F, Nilsson T: **Anomalous subdiffusion is a measure for cytoplasmic crowding in living cells.** *Biophysical journal* 2004, **87**:3518–24.
9. Jurkowitz-Alexander MS, Altschuld RA, Hohl CM, Johnson JD, McDonald JS, Simmons TD, Horrocks LA: **Cell swelling, blebbing, and death are dependent on ATP depletion and independent of calcium during chemical hypoxia in a glial cell line (ROC-1).** *Journal of neurochemistry* 1992, **59**:344–52.
10. Vom Dahl S, Hallbrucker C, Lang F, Häussinger D: **Regulation of cell volume in the perfused rat liver by hormones.** *The Biochemical journal* 1991, **280** ( Pt 1):105–9.
11. Handler JS, Kwon HM: **Kidney cell survival in high tonicity.** *Comparative biochemistry and physiology. Part A, Physiology* 1997, **117**:301–6.
12. Chowdhury S, Smith KW, Gustin MC: **Osmotic stress and the yeast cytoskeleton : Phenotype-specific suppression of an actin mutation.** *The Journal of cell biology* 1992, **118**:561–571.
13. Whitacre J, Davis D, Toenjes K, Brower S, Adams a: **Generation of an isogenic collection of yeast actin mutants and identification of three interrelated phenotypes.** *Genetics* 2001, **157**:533–43.

## Bibliography

14. Finan JD, Leddy HA, Guilak F: **Osmotic stress alters chromatin condensation and nucleocytoplasmic transport.** *Biochemical and biophysical research communications* 2011, **408**:230–5.
15. Elcock AH: **Models of Macromolecular Crowding Effects & the Need for Quantitative Comparisons with Experiment.** *Curr Opin Struct Biol* 2010, **20**:196–206.
16. Zimmerman SB, Trach SO: **Estimation of macromolecule concentrations and excluded volume effects for the cytoplasm of Escherichia coli.** *Journal of molecular biology* 1991, **222**:599–620.
17. Ridgway D, Broderick G, Lopez-Campistrous A, Ru'aini M, Winter P, Hamilton M, Boulanger P, Kovalenko A, Ellison MJ: **Coarse-grained molecular simulation of diffusion and reaction kinetics in a crowded virtual cytoplasm.** *Biophysical journal* 2008, **94**:3748–59.
18. Lanni F, Waggoner AS, Taylor DL: **Structural organization of interphase 3T3 fibroblasts studied by total internal reflection fluorescence microscopy.** *The Journal of cell biology* 1985, **100**:1091–102.
19. Rivas G, Ferrone F, Herzfeld J: **Life in a crowded world.** *EMBO reports* 2004, **5**:23–7.
20. Chebotareva NA, Kurganov BI, Livanova NB: **Biochemical effects of molecular crowding.** *Biochemistry* 2004, **69**:1239–51.
21. Tellam RL, Sculley MJ, Nichol LW, Wills PR: **The influence of poly(ethylene glycol) 6000 on the properties of skeletal-muscle actin.** *The Biochemical journal* 1983, **213**:651–9.
22. Lavery PE, Kowalczykowski SC: **Enhancement of recA protein-promoted DNA strand exchange activity by volume-occupying agents.** *The Journal of biological chemistry* 1992, **267**:9307–14.
23. Sunshine HR, Hofrichter J, Eaton WA: **Gelation of sickle cell hemoglobin in mixtures with normal adult and fetal hemoglobins.** *Journal of molecular biology* 1979, **133**:435–67.
24. Batra J, Xu K, Zhou H-X: **Nonadditive effects of mixed crowding on protein stability.** *Proteins* 2009, **77**:133–8.
25. Van den Berg B, Wain R, Dobson CM, Ellis RJ: **Macromolecular crowding perturbs protein refolding kinetics: implications for folding inside the cell.** *The EMBO journal* 2000, **19**:3870–5.
26. Van den Berg B, Ellis RJ, Dobson CM: **Effects of macromolecular crowding on protein folding and aggregation.** *The EMBO journal* 1999, **18**:6927–33.

## Bibliography

27. Uversky VN, M Cooper E, Bower KS, Li J, Fink AL: **Accelerated alpha-synuclein fibrillation in crowded milieu.** *FEBS letters* 2002, **515**:99–103.
28. Zimmerman SB, Trach SO: **Effects of macromolecular crowding on the association of E. coli ribosomal particles.** *Nucleic acids research* 1988, **16**:6309–26.
29. Wilf J, Gladner JA, Minton AP: **Acceleration of fibrin gel formation by unrelated proteins.** *Thrombosis research* 1985, **37**:681–8.
30. Zimmerman SB: **Macromolecular crowding effects on macromolecular interactions: some implications for genome structure and function.** *Biochimica et biophysica acta* 1993, **1216**:175–85.
31. Leduc C, Padberg-Gehle K, Varga V, Helbing D, Diez S, Howard J: **Molecular crowding creates traffic jams of kinesin motors on microtubules.** *Proceedings of the National Academy of Sciences of the United States of America* 2012, **109**:6100–5.
32. Banks DS, Fradin C: **Anomalous diffusion of proteins due to molecular crowding.** *Biophysical journal* 2005, **89**:2960–71.
33. Amsden B: **Solute diffusion in hydrogels.** *Polymer Gels and Networks* 1998, **6**:13–43.
34. Ignatova Z, Gierasch LM: **Effects of osmolytes on protein folding and aggregation in cells.** *Methods in enzymology* 2007, **428**:355–72.
35. Muzzey D, Van Oudenaarden A: **Quantitative time-lapse fluorescence microscopy in single cells.** *Annual review of cell and developmental biology* 2009, **25**:301–27.
36. Kao HP, Abney JR, Verkman AS: **Determinants of the Translational Mobility of a Small Solute in Cell Cytoplasm.** *The Journal of Cell Biology* 1993, **120**:175–184.
37. Konopka MC, Shkel IA, Cayley S, Record MT, Weisshaar JC: **Crowding and confinement effects on protein diffusion in vivo.** *Journal of bacteriology* 2006, **188**:6115–23.
38. Zieger M, Mayer A: **Yeast vacuoles fragment in an asymmetrical two-phase process with distinct protein requirements.** *Mol Biol Cell* 2012, **23**:3438–3449.
39. Finan JD, Chalut KJ, Wax A, Guilak F: **Nonlinear osmotic properties of the cell nucleus.** *Ann Biomed Eng* 2009, **37**:477–491.
40. Petelenz-Kurdziel E: **Quantification of cell volume changes upon hyperosmotic stress in *Saccharomyces cerevisiae*.** *Integrative biology* 2011, **3**:1120–1126.
41. Moran U, Phillips R, Milo R: **SnapShot: key numbers in biology.** *Cell* 2010, **141**:1262–1262.e1.

## Bibliography

42. Wood V, Gwilliam R, Rajandream M-A, Lyne M, Lyne R, Stewart A, Sgouros J, Peat N, Hayles J, Baker S, Basham D, Bowman S, Brooks K, Brown D, Brown S, Chillingworth T, Churcher C, Collins M, Connor R, Cronin A, Davis P, Feltwell T, Fraser A, Gentles S, Goble A, Hamlin N, Harris D, Hidalgo J, Hodgson G, Holroyd S, et al.: **The genome sequence of *Schizosaccharomyces pombe***. *Nature* 2002, **415**.
43. Wu J-Q, Pollard TD: **Counting cytokinesis proteins globally and locally in fission yeast**. *Science* 2005, **310**:310–4.
44. Dill KA, Ghosh K, Schmit JD: **Physical limits of cells and proteomes**. *Proc Natl Acad Sci U S A* 2011, **108**:17876–82.
45. Ellis RJ: **Macromolecular crowding: obvious but underappreciated**. *Trends in biochemical sciences* 2001, **26**:597–604.
46. Vazquez A: **Optimal macromolecular density in the cell**. *Proc Natl Acad Sci U S A* 2012, **109**:E533; author reply E534.
47. Zhou EH, Trepatt X, Park CY, Lenormand G, Oliver MN, Mijailovich SM, Hardin C, Weitz D a, Butler JP, Fredberg JJ: **Universal behavior of the osmotically compressed cell and its analogy to the colloidal glass transition**. *Proc Natl Acad Sci U S A* 2009, **106**:10632–7.
48. Angell CA: **Formation of glasses from liquids and biopolymers**. *Science* 1995, **267**:1924–35.
49. Eide JL, Chakraborty AK: **Effects of quenched and annealed macromolecular crowding elements on a simple model for signaling in T lymphocytes**. *The journal of physical chemistry. B* 2006, **110**:2318–24.
50. Lipkow K, Andrews SS, Bray D: **Simulated Diffusion of Phosphorylated CheY through the Cytoplasm of *Escherichia coli***. *Journal of bacteriology* 2005, **187**:45–53.
51. Takahashi K, Arjunan SNV, Tomita M: **Space in systems biology of signaling pathways--towards intracellular molecular crowding in silico**. *FEBS letters* 2005, **579**:1783–8.
52. Takahashi K, Yugi K, Hashimoto K, Yamada Y, Pickett CJF, Tomita M: **Computational Challenges in Cell Simulation : A Software Engineering Approach**. *IEEE Intelligent Systems* 2002, **17**:64–71.
53. Rohwer JM, Postma PW, Kholodenko BN, Westerhoff H V: **Implications of macromolecular crowding for signal transduction and metabolite channeling**. *Proceedings of the National Academy of Sciences of the United States of America* 1998, **95**:10547–52.
54. Van Wuytswinkel O, Reiser V, Siderius M, Kelders MC, Ammerer G, Ruis H, Mager WH: **Response of *Saccharomyces cerevisiae* to severe osmotic stress**:

**evidence for a novel activation mechanism of the HOG MAP kinase pathway.** *Mol Microbiol* 2000, **37**:382–397.

55. Strange K: **Cellular volume homeostasis.** *Advances in physiology education* 2004, **28**:155–9.

56. Grattoni A, Canavese G, Montevicchi FM, Ferrari M: **Fast membrane osmometer as alternative to freezing point and vapor pressure osmometry.** *Analytical chemistry* 2008, **80**:2617–22.

57. Beitz E: *Aquaporins*. Springer; 2009, **06**:424.

58. O'Neill WC: **Physiological significance of volume-regulatory transporters.** *The American journal of physiology* 1999, **276**:C995–C1011.

59. Staverman AJ: **The theory of measurement of osmotic pressure.** *Recueil des Travaux Chimiques des Pays-Bas* 1951, **70**:344–352.

60. Pritchard J: *Turgor Pressure*. 2001:1–3.

61. Boyer JS: *Measuring the Water Status of Plants and Soils*. Academic Press; 1995:178.

62. Walsby AE: **Gas vesicles.** *Microbiological reviews* 1994, **58**:94–144.

63. Minc N, Boudaoud A, Chang F: **Mechanical forces of fission yeast growth.** *Current biology* 2009, **19**:1096–101.

64. Stock JB, Rauch B, Roseman S: **Periplasmic space in Salmonella typhimurium and Escherichia coli.** *The Journal of biological chemistry* 1977, **252**:7850–61.

65. Whatmore AM, Reed RH: **Determination of turgor pressure in Bacillus subtilis: a possible role for K<sup>+</sup> in turgor regulation.** *Journal of general microbiology* 1990, **136**:2521–6.

66. Gervais P, Molin P, Marechal PA, Herail-Foussereau C: **Thermodynamics of yeast cell osmoregulation: Passive mechanisms.** *Journal of Biological Physics* 1996, **22**:73–86.

67. Schaber J, Adrover MA, Eriksson E, Pelet S, Petelenz-Kurdziel E, Klein D, Posas F, Goksor M, Peter M, Hohmann S, Klipp E: **Biophysical properties of Saccharomyces cerevisiae and their relationship with HOG pathway activation.** *Eur Biophys J* 2010, **39**:1547–1556.

68. Meikle AJ, Reed RH, Gadd GM: **Osmotic adjustment and the accumulation of organic solutes in whole cells and protoplasts of Saccharomyces cerevisiae.** *Journal of general microbiology* 1988, **134**:3049–60.

## Bibliography

69. Shabala SN, Lew RR: **Turgor Regulation in Osmotically Stressed Arabidopsis Epidermal Root Cells . Direct Support for the Role of Cell Turgor Measurements.** *Plant physiology* 2002, **129**:290–299.
70. Pinette MF, Koch AL: **Variability of the turgor pressure of individual cells of the gram-negative heterotroph *Ancylobacter aquaticus*.** *Journal of bacteriology* 1987, **169**:4737–42.
71. Martinez de Maranon I, Tourdot-Marechal R, Gervais P: **Involvement of osmotic cell shrinkage on the proton extrusion rate in *Saccharomyces cerevisiae*.** *International journal of food microbiology* 2001, **67**:241–246.
72. Arnold WN, Lacy JS: **Permeability of the cell envelope and osmotic behavior in *Saccharomyces cerevisiae*.** *Journal of bacteriology* 1977, **131**:564–71.
73. Cosgrove DJ: **Wall relaxation and the driving forces for cell expansive growth.** *Plant physiology* 1987, **84**:561–4.
74. Borghetti P, Della Salda L, De Angelis E, Maltarello MC, Petronini PG, Cabassi E, Marcato PS, Maraldi NM, Borghetti AF: **Adaptive cellular response to osmotic stress in pig articular chondrocytes.** *Tissue & cell* 1995, **27**:173–83.
75. Mongin AA, Orlov SN: **Mechanisms of cell volume regulation and possible nature of the cell volume sensor.** *Pathophysiology : the official journal of the International Society for Pathophysiology / ISP* 2001, **8**:77–88.
76. Kempf B, Bremer E: **Uptake and synthesis of compatible solutes as microbial stress responses to high-osmolality environments.** *Archives of microbiology* 1998, **170**:319–30.
77. Hochachka PW, Somero GN: *Biochemical Adaptation: Mechanism and Process in Physiological Evolution.* Oxford University Press, New York.; 2002, **2002**.
78. Atwell BJ, Kriedemann PE, Turnbull CGN: *Plants in Action: Adaptation in Nature, Performance in Cultivation.* Macmillan Education AU; 1999:664.
79. Brown AD: *Microbial water stress.* 1976, **40**:803–846.
80. Blomberg A, Adler L: **Physiology of osmotolerance in fungi.** *Advances in microbial physiology* 1992, **33**:145–212.
81. Horikoshi K, Grant WD: *Extremophiles: Microbial Life in Extreme Environments.* 1998.
82. Onishi H: **Osmophilic yeasts.** *Advances in food research* 1963, **12**:53–94.
83. Madigan M, Martinko J, Parker J: *Antibiotics: isolation and characterization.* In: *Brock Biology of Microorganisms.* 8th edition. Prentice-Hall International Inc. New Jersey; 1997:440–442.

## Bibliography

84. Ariño J, Ramos J, Sychrová H: **Alkali metal cation transport and homeostasis in yeasts.** *Microbiology and molecular biology reviews* 2010, **74**:95–120.
85. Gustin MC, Albertyn J, Alexander M, Davenport K: **MAP kinase pathways in the yeast *Saccharomyces cerevisiae*.** *Microbiol Mol Biol Rev* 1998, **62**:1264–1300.
86. Smith DA, Morgan BA, Quinn J: **Stress signalling to fungal stress-activated protein kinase pathways.** *FEMS microbiology letters* 2010, **306**:1–8.
87. Martín H, Flández M, Nombela C, Molina M: **Protein phosphatases in MAPK signalling: we keep learning from yeast.** *Molecular microbiology* 2005, **58**:6–16.
88. Rodríguez de Mier SR: **Systems and synthetic biology studies in *Saccharomyces cerevisiae*.** 2011:164.
89. Neiman AM: **Ascospore formation in the yeast *Saccharomyces cerevisiae*.** *Microbiology and molecular biology reviews : MMBR* 2005, **69**:565–84.
90. Gagiano M, Bauer FF, Pretorius IS: **The sensing of nutritional status and the relationship to filamentous growth in *Saccharomyces cerevisiae*.** *FEMS yeast research* 2002, **2**:433–70.
91. Posas F, Takekawa M, Saito H: **Signal transduction by MAP kinase cascades in budding yeast.** *Current opinion in microbiology* 1998, **1**:175–82.
92. Davenport KR, Sohaskey M, Kamada Y, Levin DE, Gustin MC: **A second osmosensing signal transduction pathway in yeast. Hypotonic shock activates the PKC1 protein kinase-regulated cell integrity pathway.** *The Journal of biological chemistry* 1995, **270**:30157–61.
93. Hohmann S: **Osmotic stress signaling and osmoadaptation in yeasts.** *Microbiol Mol Biol Rev* 2002, **66**:300–372.
94. Kofahl B, Klipp E: **Modelling the dynamics of the yeast pheromone pathway.** *Yeast* 2004, **21**:831–50.
95. Yi T-M, Kitano H, Simon MI: **A quantitative characterization of the yeast heterotrimeric G protein cycle.** *Proc Natl Acad Sci U S A* 2003, **100**:10764–9.
96. Klipp E, Nordlander B, Krüger R, Gennemark P, Hohmann S: **Integrative model of the response of yeast to osmotic shock.** *Nature biotechnology* 2005, **23**:975–82.
97. O'Rourke SM, Herskowitz I: **The Hog1 MAPK prevents cross talk between the HOG and pheromone response MAPK pathways in *Saccharomyces cerevisiae*.** *Genes & development* 1998, **12**:2874–86.
98. McClean MN, Mody A, Broach JR, Ramanathan S: **Cross-talk and decision making in MAP kinase pathways.** *Nat Genet* 2007, **39**:409–414.

## Bibliography

99. Patterson JC, Klimenko ES, Thorner J: **Single-cell analysis reveals that insulation maintains signaling specificity between two yeast MAPK pathways with common components.** *Science signaling* 2010, **3**:ra75.
100. Gasch AP, Spellman PT, Kao CM, Carmel-Harel O, Eisen MB, Storz G, Botstein D, Brown PO: **Genomic expression programs in the response of yeast cells to environmental changes.** *Molecular biology of the cell* 2000, **11**:4241–57.
101. Brown JL, Bussey H, Stewart RC: **Yeast Skn7p functions in a eukaryotic two-component regulatory pathway.** *The EMBO journal* 1994, **13**:5186–94.
102. Levin DE: **Cell wall integrity signaling in *Saccharomyces cerevisiae*.** *Microbiology and molecular biology reviews* 2005, **69**:262–91.
103. Capaldi AP, Kaplan T, Liu Y, Habib N, Regev A, Friedman N, O'Shea EK: **Structure and function of a transcriptional network activated by the MAPK Hog1.** *Nature genetics* 2008, **40**:1300–6.
104. Tamas MJ, Rep M, Thevelein JM, Hohmann S: **Stimulation of the yeast high osmolarity glycerol (HOG) pathway: evidence for a signal generated by a change in turgor rather than by water stress.** *FEBS Lett* 2000, **472**:159–165.
105. Bilslund E, Molin C, Swaminathan S, Ramne A, Sunnerhagen P: **Rck1 and Rck2 MAPKAP kinases and the HOG pathway are required for oxidative stress resistance.** *Molecular microbiology* 2004, **53**:1743–56.
106. Winkler A, Arkind C, Mattison CP, Burkholder A, Knoche K, Ota I: **Heat stress activates the yeast high-osmolarity glycerol mitogen-activated protein kinase pathway, and protein tyrosine phosphatases are essential under heat stress.** *Eukaryotic cell* 2002, **1**:163–73.
107. Thorsen M, Di Y, Tängemo C, Morillas M, Ahmadpour D, Van der Does C, Wagner A, Johansson E, Boman J, Posas F, Wysocki R, Tamás MJ: **The MAPK Hog1p modulates Fps1p-dependent arsenite uptake and tolerance in yeast.** *Molecular biology of the cell* 2006, **17**:4400–10.
108. Martinez de Marañon I, Marechal PA, Gervais P: **Passive response of *Saccharomyces cerevisiae* to osmotic shifts: cell volume variations depending on the physiological state.** *Biochemical and biophysical research communications* 1996, **227**:519–23.
109. Ferrigno P, Posas F, Koepp D, Saito H, Silver PA: **Regulated nucleo/cytoplasmic exchange of HOG1 MAPK requires the importin beta homologs NMD5 and XPO1.** *The EMBO journal* 1998, **17**:5606–14.
110. Reiser V, Ruis H, Ammerer G: **Kinase activity-dependent nuclear export opposes stress-induced nuclear accumulation and retention of Hog1 mitogen-**

**activated protein kinase in the budding yeast *Saccharomyces cerevisiae*.** *Molecular biology of the cell* 1999, **10**:1147–61.

111. Westfall PJ, Ballon DR, Thorner J: **When the stress of your environment makes you go HOG wild.** *Science* 2004, **306**:1511–2.

112. Hoffmann EK, Lambert IANH, Pedersen SF: **Physiology of Cell Volume Regulation in Vertebrates.** *Physiol Rev* 2009, **89**:193–277.

113. Saito H: *The Sln1-Ypd1-Ssk1 multistep phosphorelay system that regulates an osmosensing MAP kinase cascade in yeast. in: Histidine Kinases in Signal Transduction.* Academic Press, San Diego; 2003:397–419.

114. Tatebayashi K, Tanaka K, Yang H-Y, Yamamoto K, Matsushita Y, Tomida T, Imai M, Saito H: **Transmembrane mucins Hkr1 and Msb2 are putative osmosensors in the SHO1 branch of yeast HOG pathway.** *The EMBO journal* 2007, **26**:3521–33.

115. Maeda T, Takekawa M, Saito H: **Activation of yeast PBS2 MAPKK by MAPKKs or by binding of an SH3-containing osmosensor.** *Science* 1995, **269**:554–8.

116. Saito H, Tatebayashi K: **Regulation of the osmoregulatory HOG MAPK cascade in yeast.** *Journal of biochemistry* 2004, **136**:267–72.

117. O'Rourke SM, Herskowitz I, O'Shea EK: **Yeast go the whole HOG for the hyperosmotic response.** *Trends Genet* 2002, **18**:405–412.

118. Brewster J, De Valoir T, Dwyer N, Winter E, Gustin M: **An osmosensing signal transduction pathway in yeast.** *Science* 1993, **259**:1760–1763.

119. Zapater M, Clotet J, Escoté X, Posas F: **Control of Cell Cycle Progression by the Stress-Activated Hog1 MAPK.** *Cell Cycle* 2005, **4**:6–7.

120. Clotet J, Escoté X, Adrover MA, Yaakov G, Garí E, Aldea M, De Nadal E, Posas F: **Phosphorylation of Hsl1 by Hog1 leads to a G2 arrest essential for cell survival at high osmolarity.** *The EMBO journal* 2006, **25**:2338–46.

121. Proft M, Struhl K: **MAP kinase-mediated stress relief that precedes and regulates the timing of transcriptional induction.** *Cell* 2004, **118**:351–61.

122. Bilsland-Marchesan E, Ariño J, Saito H, Sunnerhagen P, Posas F: **Rck2 kinase is a substrate for the osmotic stress-activated mitogen-activated protein kinase Hog1.** *Molecular and cellular biology* 2000, **20**:3887–95.

123. Nordlander B, Krantz M, Hohmann S: **Hog1-mediated metabolic adjustments following hyperosmotic shock in the yeast *Saccharomyces cerevisiae*.** *Topics in current genetics* 2008, **20**:141–158.

## Bibliography

124. Westfall PJ, Patterson JC, Chen RE, Thorner J: **Stress resistance and signal fidelity independent of nuclear MAPK function.** *Proc Natl Acad Sci U S A* 2008, **105**:12212–12217.
125. Mettetal JT, Muzzey D, Gómez-Uribe C, Van Oudenaarden A: **The frequency dependence of osmo-adaptation in *Saccharomyces cerevisiae*.** *Science* 2008, **319**:482–4.
126. Rep M, Reiser V, Gartner U, Thevelein JM, Hohmann S, Ammerer G, Ruis H: **Osmotic stress-induced gene expression in *Saccharomyces cerevisiae* requires Msn1p and the novel nuclear factor Hot1p.** *Molecular and cellular biology* 1999, **19**:5474–85.
127. Proft M, Pascual-Ahuir A, De Nadal E, Ariño J, Serrano R, Posas F: **Regulation of the Sko1 transcriptional repressor by the Hog1 MAP kinase in response to osmotic stress.** *The EMBO journal* 2001, **20**:1123–33.
128. Nadal D, Casadome L, Posas F: **Targeting the MEF2-Like Transcription Factor Smp1 by the Stress-Activated Hog1 Mitogen-Activated Protein Kinase.** *Mol Cell Biol* 2003, **23**:229–237.
129. Schüller C, Brewster JL, Alexander MR, Gustin MC, Ruis H: **The HOG pathway controls osmotic regulation of transcription via the stress response element (STRE) of the *Saccharomyces cerevisiae* CTT1 gene.** *The EMBO journal* 1994, **13**:4382–9.
130. Rep M, Krantz M, Thevelein JM, Hohmann S: **The Transcriptional Response of *Saccharomyces cerevisiae* to osmotic shock.** *The Journal of biological chemistry* 2000, **275**:8290–8300.
131. Yaakov G, Duch A, Garcia-Rubio M, Clotet J, Jimenez J, Aquilera A, Posas F: **The Stress-activated Protein Kinase Hog1 Mediates S Phase Delay in Response to Osmostress.** *Molecular Biology of the Cell* 2009, **20**:3572–3582.
132. Ansell R, Granath K, Hohmann S, Thevelein JM, Adler L: **The two isoenzymes for yeast NAD<sup>+</sup>-dependent glycerol 3-phosphate dehydrogenase encoded by GPD1 and GPD2 have distinct roles in osmoadaptation and redox regulation.** *The EMBO journal* 1997, **16**:2179–87.
133. Pahlman AK, Granath K, Ansell R, Hohmann S, Adler L: **The yeast glycerol 3-phosphatases Gpp1p and Gpp2p are required for glycerol biosynthesis and differentially involved in the cellular responses to osmotic, anaerobic, and oxidative stress.** *The Journal of biological chemistry* 2001, **276**:3555–63.
134. Young C, Mapes J, Hanneman J, Al-Zarban S, Ota I: **Role of Ptc2 type 2C Ser/Thr phosphatase in yeast high-osmolarity glycerol pathway inactivation.** *Eukaryotic cell* 2002, **1**:1032–40.

135. Maeda T, Tsai AY, Saito H: **Mutations in a protein tyrosine phosphatase gene (PTP2) and a protein serine/threonine phosphatase gene (PTC1) cause a synthetic growth defect in *Saccharomyces cerevisiae*.** *Molecular and cellular biology* 1993, **13**:5408–17.
136. Jacoby T, Flanagan H, Faykin A, Seto AG, Mattison C, Ota I: **Two protein-tyrosine phosphatases inactivate the osmotic stress response pathway in yeast by targeting the mitogen-activated protein kinase, Hog1.** *The Journal of biological chemistry* 1997, **272**:17749–55.
137. Siderius M, Van Wuytswinkel O, Reijenga KA, Kelders M, Mager WH: **The control of intracellular glycerol in *Saccharomyces cerevisiae* influences osmotic stress response and resistance to increased temperature.** *Molecular microbiology* 2000, **36**:1381–90.
138. Hersen P, McClean MN, Mahadevan L, Ramanathan S: **Signal processing by the HOG MAP kinase pathway.** *Proc Natl Acad Sci U S A* 2008, **105**:7165–7170.
139. Balagaddé FK, You L, Hansen CL, Arnold FH, Quake SR: **Long-term monitoring of bacteria undergoing programmed population control in a microchemostat.** *Science (New York, N.Y.)* 2005, **309**:137–40.
140. Peixoto A, Monteiro M, Rocha B, Veiga-Fernandes H: **Quantification of multiple gene expression in individual cells.** *Genome research* 2004, **14**:1938–47.
141. Bengtsson M, Ståhlberg A, Rorsman P, Kubista M: **Gene expression profiling in single cells from the pancreatic islets of Langerhans reveals lognormal distribution of mRNA levels.** *Genome Research* 2005, **15**:1388–1392.
142. Upadhyaya S, Selvaganapathy PR: **Microfluidic devices for cell based high throughput screening.** *Lab on a chip* 2010, **10**:341–8.
143. Harrison D., Fluri K, Seiler K, Fan Z, Effenhauser CS, Manz A: **Micromachining a miniaturized capillary electrophoresis-based chemical analysis system on a chip.** *science* 1993, **261**:895–897.
144. Whitesides GM, Ostuni E, Takayama S, Jiang X, Ingber DE: **Soft lithography in biology and biochemistry.** *Annu Rev Biomed Eng* 2001, **3**:335–373.
145. Weigl BH, Bardell RL, Cabrera CR: **Lab-on-a-chip for drug development.** *Advanced Drug Delivery Reviews* 2003, **55**:349–377.
146. Beebe DJ, Mensing GA, Walker GM: **Physics and applications of microfluidics in biology.** *Annual review of biomedical engineering* 2002, **4**:261–86.
147. Therriault D, White SR, Lewis JA: **Chaotic mixing in three-dimensional microvascular networks fabricated by direct-write assembly.** *Nature materials* 2003, **2**:265–71.

## Bibliography

148. Zi Z, Liebermeister W, Klipp E: **A quantitative study of the Hog1 MAPK response to fluctuating osmotic stress in *Saccharomyces cerevisiae*.** *PloS one* 2010, **5**:e9522.
149. Uhlenendorf J, Miermont A, Delaveau T, Charvin G, Fages F, Bottani S, Batt G, Hersen P: **Long-term model predictive control of gene expression at the population and single-cell levels.** *Proc Natl Acad Sci U S A* 2012, **109**:14271–6.
150. Liebman PA, Entine G: **Lateral diffusion of visual pigment in photoreceptor disk membranes.** *Science* 1974, **185**:457–9.
151. Giese B, Au-Yeung C-K, Herrmann A, Diefenbach S, Haan C, Küster A, Wortmann SB, Roderburg C, Heinrich PC, Behrmann I, Müller-Newen G: **Long term association of the cytokine receptor gp130 and the Janus kinase Jak1 revealed by FRAP analysis.** *The Journal of biological chemistry* 2003, **278**:39205–13.
152. Mueller F, Mazza D, Stasevich TJ, McNally JG: **FRAP and kinetic modeling in the analysis of nuclear protein dynamics: what do we really know?** *Current opinion in cell biology* 2010, **22**:403–11.
153. Braga J, Desterro JMP, Carmo-fonseca M: **Intracellular macromolecular mobility measured by Fluorescence Recovery after Photobleaching with confocal laser scanning microscopes.** *Molecular biology of the cell* 2004, **15**:4749–4760.
154. Axelrod D, Koppel DE, Schlessinger J, Elson E, Webb WW: **Mobility measurement by analysis of fluorescence photobleaching recovery kinetics.** *Biophysical journal* 1976, **16**:1055–69.
155. Swaminathan R, Hoang CP, Verkman AS: **Photobleaching Recovery and Anisotropy Decay of Green Fluorescent Protein GFP-S65T in Solution and Cells : Cytoplasmic Viscosity Probed by Green Fluorescent Protein Translational and Rotational Diffusion.** *Biophysical Journal* 1997, **72**:1900–1907.
156. Kelley JB, Paschal BM: **Hyperosmotic stress signaling to the nucleus disrupts the Ran gradient and the production of RanGTP.** *Mol Biol Cell* 2007, **18**:4365–4376.
157. Stochaj U, Rassadi R, Chiu J: **Stress-mediated inhibition of the classical nuclear protein import pathway and nuclear accumulation of the small GTPase Gsp1p.** *FASEB J* 2000, **14**:2130–2132.
158. Angelides KJ, Elmer LW, Loftus D, Elson E: **Distribution and lateral mobility of voltage-dependent sodium channels in neurons.** *The Journal of cell biology* 1988, **106**:1911–25.
159. Paul-Gilloteaux P, Waharte F: **Influence of spatial confinement on 2D diffusion measurements by several fluorescence microscopy techniques (SPT, TICS, FRAP).** *International Symposium on Biomedical*

160. Görner W, Durchschlag E, Martinez-Pastor MT, Estruch F, Ammerer G, Hamilton B, Ruis H, Schuller C: **Nuclear localization of the C2H2 zinc finger protein Msn2p is regulated by stress and protein kinase A activity.** *Genes & Development* 1998, **12**:586–597.
161. Garreau H, Hasan RN, Renault G, Estruch F, Boy-Marcotte E, Jacquet M: **Hyperphosphorylation of Msn2p and Msn4p in response to heat shock and the diauxic shift is inhibited by cAMP in *Saccharomyces cerevisiae*.** *Microbiology (Reading, England)* 2000, **146 ( Pt 9)**:2113–20.
162. Beck T, Hall MN: **The TOR signalling pathway controls nuclear localization of nutrient-regulated transcription factors.** *Nature* 1999, **402**:689–92.
163. Delaunay A, Pflieger D, Barrault MB, Vinh J, Toledano MB: **A thiol peroxidase is an H<sub>2</sub>O<sub>2</sub> receptor and redox-transducer in gene activation.** *Cell* 2002, **111**:471–81.
164. Delaunay A, Isnard AD, Toledano MB: **H<sub>2</sub>O<sub>2</sub> sensing through oxidation of the Yap1 transcription factor.** *The EMBO journal* 2000, **19**:5157–66.
165. Okazaki S, Tachibana T, Naganuma A, Mano N, Kuge S: **Multistep disulfide bond formation in Yap1 is required for sensing and transduction of H<sub>2</sub>O<sub>2</sub> stress signal.** *Molecular cell* 2007, **27**:675–88.
166. Stathopoulos AM, Cyert MS: **Calcineurin acts through the CRZ1/TCN1-encoded transcription factor to regulate gene expression in yeast.** *Genes Dev* 1997, **11**:3432–3444.
167. Boustany LM, Cyert MS: **Calcineurin-dependent regulation of Crz1p nuclear export requires Msn5p and a conserved calcineurin docking site.** *Genes Dev* 2002, **16**:608–619.
168. Polizotto RS, Cyert MS: **Calcineurin-dependent nuclear import of the transcription factor Crz1p requires Nmd5p.** *The Journal of cell biology* 2001, **154**:951–60.
169. Cunningham KW, Fink GR: **Calcineurin inhibits VCX1-dependent H<sup>+</sup>/Ca<sup>2+</sup> exchange and induces Ca<sup>2+</sup> ATPases in *Saccharomyces cerevisiae*.** *Molecular and cellular biology* 1996, **16**:2226–37.
170. DeVit MJ, Johnston M: **The nuclear exportin Msn5 is required for nuclear export of the Mig1 glucose repressor of *Saccharomyces cerevisiae*.** *Current biology : CB* 1999, **9**:1231–41.
171. Rubenstein EM, McCartney RR, Zhang C, Shokat KM, Shirra MK, Arndt KM, Schmidt MC: **Access denied: Snf1 activation loop phosphorylation is controlled by availability of the phosphorylated threonine 210 to the PP1 phosphatase.** *The Journal of biological chemistry* 2008, **283**:222–30.

## Bibliography

172. Nehlin JO, Carlberg M, Ronne H: **Control of yeast GAL genes by MIG1 repressor: a transcriptional cascade in the glucose response.** *The EMBO Journal* 1991, **10**:3373–7.
173. Hohmann S: **Osmotic adaptation in yeast-control of the yeast osmolyte system.** *International review of cytology* 2002, **215**:149–187.
174. Bose S, Dutko JA, Zitomer RS: **Genetic factors that regulate the attenuation of the general stress response of yeast.** *Genetics* 2005, **169**:1215–26.
175. Isoyama T, Murayama A, Nomoto A, Kuge S: **Nuclear import of the yeast AP-1-like transcription factor Yap1p is mediated by transport receptor Pse1p, and this import step is not affected by oxidative stress.** *The Journal of biological chemistry* 2001, **276**:21863–9.
176. Steinman RM, Mellman IS, Muller WA, Cohn ZA: **Endocytosis and the recycling of plasma membrane.** *The Journal of cell biology* 1983, **96**:1–27.
177. Wendland B, Emr SD, Riezman H: **Protein traffic in the yeast endocytic and vacuolar protein sorting pathways.** *Current opinion in cell biology* 1998, **10**:513–22.
178. Dautry-Varsat A: **Receptor-mediated endocytosis: the intracellular journey of transferrin and its receptor.** *Biochimie* 1986, **68**:375–81.
179. Olazabal IM, Machesky LM: **Abp1p and cortactin, new “hand-holds” for actin.** *The Journal of cell biology* 2001, **154**:679–82.
180. Kaksonen M, Sun Y, Drubin DG: **A pathway for association of receptors, adaptors, and actin during endocytic internalization.** *Cell* 2003, **115**:475–87.
181. Franzusoff A, Redding K, Crosby J, Fuller RS, Schekman R: **Localization of components involved in protein transport and processing through the yeast Golgi apparatus.** *The Journal of cell biology* 1991, **112**:27–37.
182. Cyert MS: **Calcineurin signaling in *Saccharomyces cerevisiae*: how yeast go crazy in response to stress.** *Biochemical and Biophysical Research Communications* 2003, **311**:1143–1150.
183. Ozcan S, Johnston M: **Function and regulation of yeast hexose transporters.** *Microbiology and molecular biology reviews* 1999, **63**:554–69.
184. Al-Mohanna FA, Pettit EJ, Hallett MB: **Does actin polymerization status modulate Ca<sup>2+</sup> storage in human neutrophils? Release and coalescence of Ca<sup>2+</sup> stores by cytochalasins.** *Experimental cell research* 1997, **234**:379–87.
185. Lange K, Brandt U: **Calcium storage and release properties of F-actin: evidence for the involvement of F-actin in cellular calcium signaling.** *FEBS letters* 1996, **395**:137–42.

186. Erickson GR, Alexopoulos LG, Guilak F: **Hyper-osmotic stress induces volume change and calcium transients in chondrocytes by transmembrane, phospholipid, and G-protein pathways.** *Journal of biomechanics* 2001, **34**:1527–35.
187. Pintsch T, Satre M, Klein G, Martin J, Schuster SC: **Cytosolic acidification as a signal mediating hyperosmotic stress responses in Dictyostelium discoideum.** *BMC Cell Biology* 2001, **2**.
188. Mulholland J, Preuss D, Moon a, Wong a, Drubin D, Botstein D: **Ultrastructure of the yeast actin cytoskeleton and its association with the plasma membrane.** *The Journal of cell biology* 1994, **125**:381–91.
189. Kojima A, Toshima JY, Kanno C, Kawata C, Toshima J: **Localization and functional requirement of yeast Na<sup>+</sup>/H<sup>+</sup> exchanger, Nhx1p, in the endocytic and protein recycling pathway.** *Biochimica et biophysica acta* 2012, **1823**:534–543.
190. Hoson T, Nishitani K, Miyamoto K, Ueda J, Kamisaka S, Yamamoto R, Masuda Y: **Effects of hypergravity on growth and cell wall properties of cress hypocotyls.** *Journal of experimental botany* 1996, **47**:513–7.
191. Soto T, Núñez A, Madrid M, Vicente J, Gacto M, Cansado J: **Transduction of centrifugation-induced gravity forces through mitogen-activated protein kinase pathways in the fission yeast Schizosaccharomyces pombe.** *Microbiology* 2007, **153**:1519–29.
192. Silva RD, Sotoca R, Johansson B, Ludovico P, Sansonetty F, Silva MT, Peinado JM, Côrte-Real M: **Hyperosmotic stress induces metacaspase- and mitochondria-dependent apoptosis in Saccharomyces cerevisiae.** *Molecular microbiology* 2005, **58**:824–34.
193. Morris G, Winters L, Coulson G, Clarke K: **Effect of Osmotic Stress on the Ultrastructure and Viability of the Yeast Saccharomyces cerevisiae.** *Journal of General Microbiology* 1986, **129**:2023–2034.
194. Wu F-S, Cahoon AB: **Plasmolysis facilitates the accumulation of protein and DNA into extra-plasmalemma spaces of intact plant cells.** *Plant science* 1995, **104**:201–214.
195. Mille Y, Beney L, Gervais P: **Viability of Escherichia coli after combined osmotic and thermal treatment : a plasma membrane implication.** *Biochimica et biophysica acta* 2002, **1567**:41–48.
196. Sherman BF, Sherman MF, Enzymol M: **Getting Started with Yeast.** *Methods Enzymol* 2002, **350**:3–41.
197. Tyson CB, Lord PG, Wheals AE: **Dependency of size of Saccharomyces cerevisiae cells on growth rate.** *Journal of bacteriology* 1979, **138**:92–8.

## Bibliography

198. Jorgensen P, Edgington NP, Schneider BL, Rupes I, Tyers M, Futcher B: **The Size of the Nucleus Increases as Yeast Cells Grow.** *Molecular Biology of the Cell* 2007, **18**:3523–3532.
199. Illmer P, Erlebach C, Schinner F: **A practicable and accurate method to differentiate between intra- and extracellular water of microbial cells.** *FEMS microbiology letters* 1999, **178**:135–9.
200. Reuß M, Josić D, Popović M, Bronn WK: **Viscosity of yeast suspensions.** *European Journal of Applied Microbiology and Biotechnology* 1979, **8**:167–175.
201. Aguilar-Uscanga B, François JM: **A study of the yeast cell wall composition and structure in response to growth conditions and mode of cultivation.** *Letters in applied microbiology* 2003, **37**:268–74.
202. Di Talia S, Skotheim JM, Bean JM, Siggia ED, Cross FR: **The effects of molecular noise and size control on variability in the budding yeast cell cycle.** *Nature* 2007, **448**:947–51.
203. Von der Haar T: **A quantitative estimation of the global translational activity in logarithmically growing yeast cells.** *BMC systems biology* 2008, **2**:87.
204. Ghaemmaghani S, Huh W-K, Bower K, Howson RW, Belle A, Dephoure N, O'Shea EK, Weissman JS: **Global analysis of protein expression in yeast.** *Nature* 2003, **425**:737–41.
205. Picotti P, Kuemmel A, Costenoble R, Lam H, Campbell D, Mueller L, Heinemann M, Deutsch E, Sauer U, Domon B, Aebersold R: **Analysis of the *S. cerevisiae* metabolic network by targeted proteomics.** 2008.
206. Janke C, Magiera MM, Rathfelder N, Taxis C, Reber S: **A versatile toolbox for PCR-based tagging of yeast genes : new fluorescent proteins , more markers and promoter substitution cassettes.** *Yeast* 2004, **21**:947–962.
207. Boulanger J, Kervrann C, Bouthemy P, Elbau P, Sibarita J-B, Salamero J: **Patch-based nonlocal functional for denoising fluorescence microscopy image sequences.** *IEEE transactions on medical imaging* 2010, **29**:442–54.
208. Agre P, Bonhivers M, Borgnia MJ: **The aquaporins, blueprints for cellular plumbing systems.** *The Journal of biological chemistry* 1998, **273**:14659–62.
209. Carbrey JM, Bonhivers M, Boeke JD, Agre P: **Aquaporins in *Saccharomyces*: Characterization of a second functional water channel protein.** *Proc Natl Acad Sci U S A* 2001, **98**:1000–5.

## Appended Articles

**A. Miermont**, J. Uhlendorf, M. McClean and P. Hersen, “The Dynamical Systems Properties of the HOG Signaling Cascade”, Review article, *Journal of Signal Transduction*, Vol. 2011, 2011

J. Uhlendorf, **A. Miermont**, T. Delaveau, G. Charvin, F. Fages, S. Bottani, G. Batt, P. Hersen, “Long-term model predictive control of gene expression at the population and single-cell levels”, *PNAS*, 2012 Aug 28;109 (35):14271-6

**A. Miermont**, F. Waharte, S. Hu, M. N. McClean, S. Bottani, S. Léon and P. Hersen, “Severe osmotic compression triggers a slow-down of intracellular signaling which can be explained by molecular crowding”, accepted in *PNAS* (2013).

## Appended Articles

**Article #1:**

**Review: The Dynamical Systems Properties  
of the HOG Signaling Cascade.**

Agnès Miermont, Jannis Uhlendorf, Megan McClean and  
Pascal Hersen.

Journal of Signal Transduction, 2011

## Review Article

# The Dynamical Systems Properties of the HOG Signaling Cascade

**Agnès Miermont,<sup>1</sup> Jannis Uhlendorf,<sup>1,2</sup> Megan McClean,<sup>3</sup> and Pascal Hersen<sup>1,4</sup>**

<sup>1</sup>Laboratoire Matière et Systèmes Complexes, UMR7057, CNRS and Université Paris Diderot, 10 rue Alice Domon et Léonie Duquet, 75013 Paris, France

<sup>2</sup>Contraintes Research Group, Institut National de Recherche en Informatique et en Automatique, INRIA Paris—Rocquencourt, France

<sup>3</sup>Lewis-Sigler Institute for Integrative Genomics, Princeton University, Princeton, NJ 08540, USA

<sup>4</sup>The Mechanobiology Institute, National University of Singapore, 5A Engineering Drive 1, Singapore 117411, Singapore

Correspondence should be addressed to Pascal Hersen, pascal.hersen@univ-paris-diderot.fr

Received 14 August 2010; Revised 19 October 2010; Accepted 12 November 2010

Academic Editor: Johannes Boonstra

Copyright © 2011 Agnès Miermont et al. This is an open access article distributed under the Creative Commons Attribution License, which permits unrestricted use, distribution, and reproduction in any medium, provided the original work is properly cited.

The High Osmolarity Glycerol (HOG) MAP kinase pathway in the budding yeast *Saccharomyces cerevisiae* is one of the best characterized model signaling pathways. The pathway processes external signals of increased osmolarity into appropriate physiological responses within the yeast cell. Recent advances in microfluidic technology coupled with quantitative modeling, and techniques from reverse systems engineering have allowed yet further insight into this already well-understood pathway. These new techniques are essential for understanding the dynamical processes at play when cells process external stimuli into biological responses. They are widely applicable to other signaling pathways of interest. Here, we review the recent advances brought by these approaches in the context of understanding the dynamics of the HOG pathway signaling.

## 1. Introduction

Living organisms have evolved specialized biochemical pathways to cope with stressful, often changing environments. Even in simple cells such as yeast, thousands of specialized sets of sensing and signaling proteins form modules used to monitor and adapt to the environmental state and its variations. Such modules can be insulated or, on the contrary, connected to one another. Whereas insulation allows for robust and sensitive response, the interconnection of modules allows for higher-level behavior such as multiple input sensing and decision making through cross-talk [1]. For a given stimulus, the biochemical components of the different modules that play a role in the cellular response are usually well described in the literature. Their biological functions and interactions are known in detail, especially in model organisms such as the budding yeast. This knowledge comes from decades of complex, tedious, and elegant experiments. Genetic techniques such as gene deletion, mutation, and overexpression have been used to infer the connection patterns between proteins and the architectures of many modular functions.

Biochemical assays provided crucial information on protein phosphorylation and kinase activity. Microarrays revealed the role of these modules in determining global gene expression.

Signaling pathways are naturally dynamic [2] in that cells must respond to external signals in a timely manner, and indeed, the cellular response is often affected by the temporal properties of the external signal. In addition, the internal dynamics and timing of events in the signaling pathway determine the cellular response. These internal dynamics determine the information flow, allowing cells to process and convey information from a sensory input to a specific protein in charge of orchestrating the cellular response [3]. Until recently, experimental techniques have been limited such that most studies have examined the response of a signaling pathway to a stationary stimulus. Accordingly, adaptation and cellular responses to environmental cues were usually studied only with respect to the magnitude of the stimulus without seriously taking into account dynamical aspects. Identification of the components of a signaling pathway through the techniques mentioned above, combined with studies of simple stationary stimuli, is not enough to

understand the dynamics or systems-level properties of a complex biological network.

With the emergence of systems biology, there has been an important paradigm shift, and it is becoming increasingly clear that the temporal variations of stimulatory inputs can be directly sensed by cells [5] and that studying cells in time-variable environments is a powerful way to determine signaling pathway architecture and to understand how they process information [6, 7]. Experimental microfluidics-based strategies have matured to allow for excellent control of the cellular environment both in time and space [8, 9]. This technology coupled with genetic engineering to fluorescently tagged proteins allows for real-time observation of the system's response using fluorescence microscopy. Finally, quantitative real-time measurements form the basis for the development of mathematical models and the use of signal analysis tools, such as reverse engineering, to model the dynamical aspects of signaling pathways [10]. These models in turn provide testable experimental predictions.

This review describes the recent strategies that have been developed to assess quantitatively the dynamics of the canonical HOG MAP kinase (MAPK) pathway in the yeast, *Saccharomyces cerevisiae*. We shall first briefly review the key characteristics of the organization of the HOG pathway. We then discuss the novel experimental and modeling tools [10, 11, 16–18] that are allowing new insights into the pathway's dynamics and systems-level behavior.

## 2. MAPK Cascades in Yeast

Among signaling pathways, the Mitogen Activated Protein Kinases (MAPK) family has received considerable attention. MAPK pathways are very well conserved from yeasts to mammals [19–21] and several comprehensive reviews are available in the recent literature [22, 23]. MAP Kinase pathways are involved in many cellular processes such as stress response, the regulation of differentiation and proliferation. These pathways contain a canonical module of three protein kinases that act in series (Figure 1). Upon phosphorylation by an upstream protein, a MAP kinase kinase (MAPKKK) phosphorylates a MAP kinase kinase (MAPKK) on conserved serine and threonine residues, which in turn phosphorylates a MAP kinase (MAPK) on a threonine (sometimes serine) and a tyrosine residue located adjacent to each other and separated by a single amino acid (Thr/Ser-X-Tyr). This dual phosphorylation site is located in the activation loop of the catalytic domain and its dual phosphorylation is needed for activation of the MAP kinase.

There are five MAPK modules in yeast (Table 1) [22]. The hyperosmotic glycerol (HOG) pathway is activated in response to a hyperosmotic stress [24–28]. The Cell Wall Integrity (CWI) module controls the cell wall integrity and is triggered in response to numerous stresses including cell wall deterioration, temperature shifts, and hypo osmotic shocks [29–31]. The pheromone pathway [32, 33] controls the mating response which involves an important morphological deformation of yeast cells. Finally, the filamentous growth pathway [33, 34] and the sporulation pathway [22] control

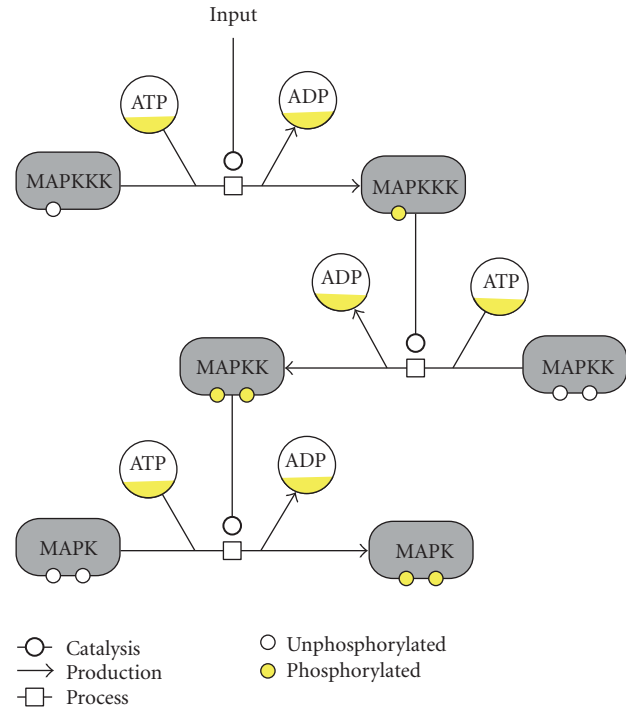


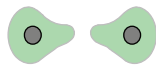
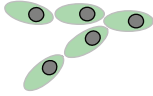
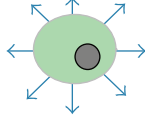
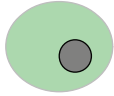
FIGURE 1: The canonical structure of a MAPK cascade. We used the Systems Biology Graphical Notation (SBGN) [4] to represent the interactions between the MAP Kinases. Activations of MAPK occur through enzymatic phosphorylation and ATP consumption. Interactions with other components and in particular with phosphatases are not shown. In the case of the HOG pathway in yeast, dual phosphorylation of the final MAPK (Hog1p) occurs within a few minutes after an hyper-osmotic stimulus.

the response to starvation for haploid and diploid cells although the sporulation pathway is not as well known as the other four MAPK pathways. Only its MAPK has been identified in diploid cells (Smk1p), and it is thought to drive the spore cell wall assembly [22]. Though they share numerous components, the five MAPK pathways of the yeast *Saccharomyces cerevisiae* are tightly regulated by cross-talk and mutual inhibition which permit faithful signaling, adaptation to their environment, and regulation of growth and morphogenesis [22]. Among these MAPK pathways, the HOG pathway (Figure 2) is particularly well suited to study signaling dynamics, since it can be reliably activated through increasing the osmolarity of the environment.

## 3. The HOG MAPK Signaling Pathway

Water homeostasis is fundamental for life. In nature, the environment can vary rapidly from isotonic to hyper or hypo osmotic conditions, and yeast cells have to adapt quickly [23, 47]. The first response after a hyperosmotic shock is the rapid loss in few seconds of cell volume due to water efflux and the activation of membrane sensory receptors followed by the activation of the HOG pathway which is completed after a few minutes (Figure 2) [11, 48]. Two distinct branches of the pathway detect changes in osmolarity and activate the

TABLE 1: The MAPK pathways in *S. cerevisiae*. The morphological adaptation corresponds to the cell behavior in response to each specific signaling input. The major molecular actors for each pathway are indicated below. Spore cell wall assembly during sporulation is another morphogenetic process driven by a MAPK protein (Smk1p), but with little knowledge on the other proteins involved and the structure of the pathway.

External Stress	Pheromone	Starvation	Hyperosmolarity	Cell wall Stress
Morphological Adaptation				
Membrane Sensors	Ste2/3	Sho1	Sln1, Sho1, Msb2, Hkr1, Opy2	Wsc1, Mid2
MAPKKK	Ste11	Ste11	Ssk2/22 & Ste11	Bck1
MAPKK	Ste7	Ste7	Pbs2	Mkk1/Mkk2
MAPK	Fus3/Kss1	Kss1	Hog1	Slr2
Transcription factors	Ste12 [22, 35]	Ste12, Tec1 [22, 35, 36]	Hot1, Sko1, Smp1, Msn2/4 [22, 28, 37, 38]	Rlm1, Swi4/6 [22, 39, 40]
Inhibition	Msg5, Ptp2, Ptp3 [21, 41, 42]	— [21]	Ptcs, Ptp2, Ptp3 [21, 43–45]	Msg5, Ptp2, Ptp3, Sdp1 [21, 30, 46]

pathway. These branches converge at the level of the MAPKK Pbs2p. The first branch is referred to as the SHO1 branch [23, 49], while the second is referred to as the SLN1 branch [50, 51].

Sln1p negatively regulates the HOG signaling pathway and deletion of *SLN1* is lethal due to pathway overactivation. This lethality is suppressed by knocking out any of the downstream components *SSK1*, *SSK2/SSK22*, *PBS2*, or *HOG1*. Sln1p contains two transmembrane domains, a histidine kinase domain and a receiver sequence. Sln1p autophosphorylates on its histidine kinase domain. The phosphate group is then transferred to its receiver domain, then to Ypd1p and finally to Ssk1p. This set of three proteins forms a phosphorelay [50, 51], a very common signaling motif in prokaryotes [51], but rare in eukaryotic cells such as yeast. The phosphorylated form of Ssk1p is inactive and the downstream MAPK pathway is usually not activated. However, after a hyperosmotic stress, Sln1p is inactivated by an unknown mechanism (though it has been proposed that Sln1p is sensitive to membrane tension [23, 52]) leading to the inactivation of Ypd1p and derepression of Ssk1p. Finally, unphosphorylated Ssk1p binds to the MAPKKKs Ssk2p and Ssk22p, which autophosphorylate, and then can phosphorylate the MAPKK Pbs2p. Sln1p seems to dominate the kinetic response of the pathway while also ensuring its robustness by inducing high basal Hog1p expression counteracted by a fast-acting negative feedback to allow rapid pathway response [53]. Thus, this tightly tuned signaling branch allows rapid and sensitive responses to environmental changes.

Sho1p consists of four transmembrane domains and an SH3 domain. This domain permits the recruitment of molecular actors, notably the MAPKK Pbs2p, to the plasma membrane [54]. The upstream kinase Ste20p, the G-protein Cdc42p, and the MAPKKK Ste11p needed for the activation of the protein Pbs2p are also recruited to the membrane [55]. Since it is a transmembrane protein, Sho1p has long been considered an osmosensor [56]. However, recent studies

suggest that Sho1p is more an anchor protein than a sensor for osmolarity [55]. Hkr1p and Msb2p, two mucin-like [57–60] proteins that form heterooligomeric complexes with Sho1p [58, 59] have recently been proposed as osmosensors of the SHO1 branch. Components of the SHO1 branch also take part in pseudohyphal development and mating, indicating that Sho1p might not have a specific role in osmosensing but a more general role related to cell shape measurement [61].

MAPKKKs of these two initiating branches induce the phosphorylation of the MAP kinase kinase Pbs2p on the conserved residues Ser514 and Thr518 [62]. Pbs2p is a cytoplasmic protein essential for the activation of Hog1p by dual phosphorylation on the conserved Thr174 and Tyr176 [62]. *PBS2* and *HOG1* are essential for osmoadaptation as null mutations in both genes induce osmosensitivity [23, 63]. Pbs2p also plays the role of a scaffold for the SHO1 branch [49, 54, 56, 64] by anchoring the different components, promoting signal propagation between proper protein partners and preventing improper cross-talk between the Pheromone pathway and the HOG pathway. Once Pbs2p phosphorylates Hog1p, Hog1PP translocates to the nucleus in a manner that is dependent upon the karyopherin Nmd5p [65]. Localization of Hog1p-GFP to the nucleus can be used as a reliable reporter of pathway activity.

#### 4. Sequential Response after a Hyperosmotic Shock

The activation of the Hog1p MAPK triggers several responses on different time-scales (Figure 3) [48]. A rapid non-transcriptional response in the cytoplasm corresponds to the closure of Fps1p [66] and the activation of several kinases (e.g., Rck2p [67], Pfk2p [68]). Fps1p belongs to the ubiquitous Major Intrinsic Protein (MIP) [69] family and is known to play a central role in yeast osmoadaptation by controlling both uptake and efflux of the osmolyte

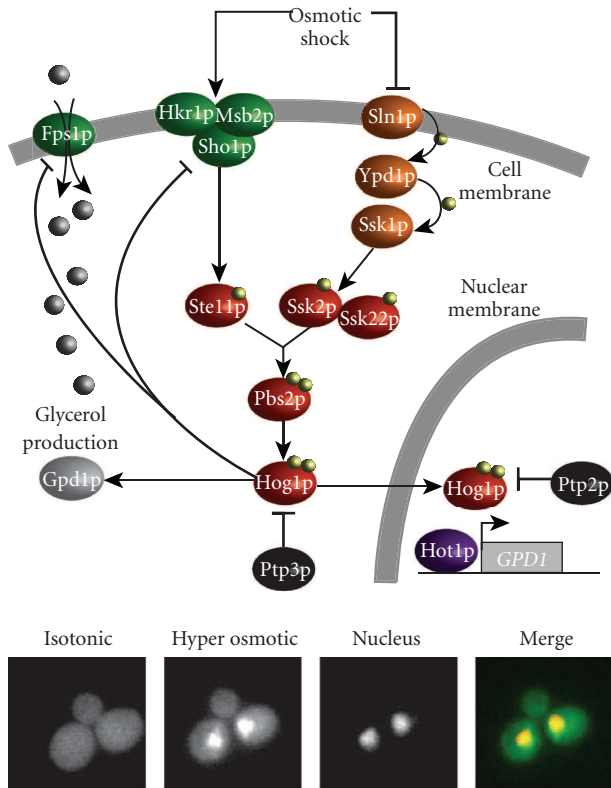


FIGURE 2: The HOG pathway. View of the main molecular actors involved in the hyperosmotic glycerol pathway (see text for more details). Two branches led by Sho1p and Sln1p are sensitive to high osmolarity and lead to the activation of Pbs2p and Hog1p after a hyperosmotic shock. Hog1p has both a cytoplasmic and a nuclear role, with different timescales, that correspond to a fast non transcriptional response and a longer response involving transcription when dealing with strong hyper osmotic shock. The yeast pictures at the bottom show nuclear localization of Hog1p tagged by GFP after a moderate hyper-osmotic shock (Sorbitol, 1 M). Colocalization with the nucleus is seen on the overlay pictures between the GFP channel (Hog1p) and the RFP channel (Htb2p). Note that localization is transient and reversible if the cell is put back into isotonic conditions.

glycerol [70]. Importantly, Fps1p is gated by osmotic changes [66, 71]. Indeed, this channel protein is closed under hyperosmotic stress to enable intracellular accumulation of glycerol, whereas it is open under low-osmolarity conditions to allow for glycerol efflux.

On a longer time scale, several minutes after an osmotic shock, Hog1p induces the modification of expression of nearly 600 genes [72–75]. This transcriptional response is driven by intermediate transcriptional factors: Hot1p, Sko1p, Smp1p, and Msn2/4p [37, 38, 74, 76, 77]. Importantly, Hog1p initiates glycerol biosynthesis via the transcriptional factor Hot1p [38]. Glycerol production is due to the expression of glycerol-3-phosphate dehydrogenase and glycerol-3-phosphatase. Both enzymes are encoded by two similar isogenes, *GPD1*, *GPD2* and *GPP1*, *GPP2*, respectively, [78, 79]. The accumulation of glycerol results in an increase of the internal osmolarity, leading to water influx and cell

size recovery. Hot1p is also involved in regulating glycerol influx by inducing a strong and transient expression of *STL1*, which codes for a glycerol proton symporter located in the plasma membrane [80]. Hog1p is dephosphorylated and exported from the nucleus via the karyopherin Xpo1p [65] 20 to 30 minutes after an osmotic shock depending on the severity of the shock. This is concomitant with the onset of glycerol production and restoration of osmotic balance. Dephosphorylation of Hog1p is due to nuclear phosphatases. Phosphatases have a critical role in down-regulation of MAPK proteins whose excessive activation can be lethal for the cell. In yeast, three classes of protein phosphatases are known to downregulate MAPK pathways. The dual specificity phosphatases (DSPs) dephosphorylate both phosphotyrosine (pY) and phosphothreonine (pT). The protein tyrosine phosphatases (PTPs) dephosphorylate only tyrosine residues. Finally, protein phosphatases type 2C (PTC) dephosphorylate threonine, serine, and sometimes tyrosine residues. For the HOG pathway, the serine-threonine phosphatases Ptc1p, Ptc2p, and Ptc3p act on both the Pbs2p (MAPKK) and Hog1p (MAPK), while the tyrosine phosphatases, Ptp2p and Ptp3p strictly control Hog1p [43, 44, 49]. Ptp2p is predominantly localized in the nucleus, Ptp3p in the cytoplasm, while the protein phosphatases types 2C are located both in the cytoplasm and in the nucleus. Simultaneous knockout of both *PTP2* and *PTC1* is lethal for the cell [45]. Deletion of *PTP3* induces overactivation of Hog1p but is not lethal because it predominantly acts on other MAPK proteins involved in the mating pathway.

### 5. Towards a Model of the HOG Pathway

Years of genetic and biochemical analysis have provided us with an extraordinarily precise description of the key players in the HOG pathway. What about the signaling dynamics of the pathway? How does the architecture determine the pathway’s signal processing ability? Classic molecular biology experiments were based on step shock experiments with an osmotic agent, such as NaCl or sorbitol at various concentrations. Phosphorylation states of key proteins have been measured at different time points after a step shock at the population level, showing a transient increase of phosphorylation (lasting several minutes) concomitant with nuclear enrichment of Hog1p [81]. Nuclear cytoplasmic shuttling of Hog1p was also observed qualitatively, indicating a fast deactivation of the pathway when cells are returned to an isotonic environment [81]. Levels of gene expression have been measured at different timepoints after an osmotic shock using microarrays [73]. Although done with a low resolution in time compared to biophysical experiments, these measurements give an idea of the dynamics of the activation of the pathway.

Based on such measurements, several models have been proposed to describe mathematically the HOG signaling pathway and more generally osmoadaptation in yeast [82]. The most comprehensive and the first integrative one is due to Klipp et al. [81]. Their model takes not only the HOG signaling cascade into account (only the *SLN1* branch), but

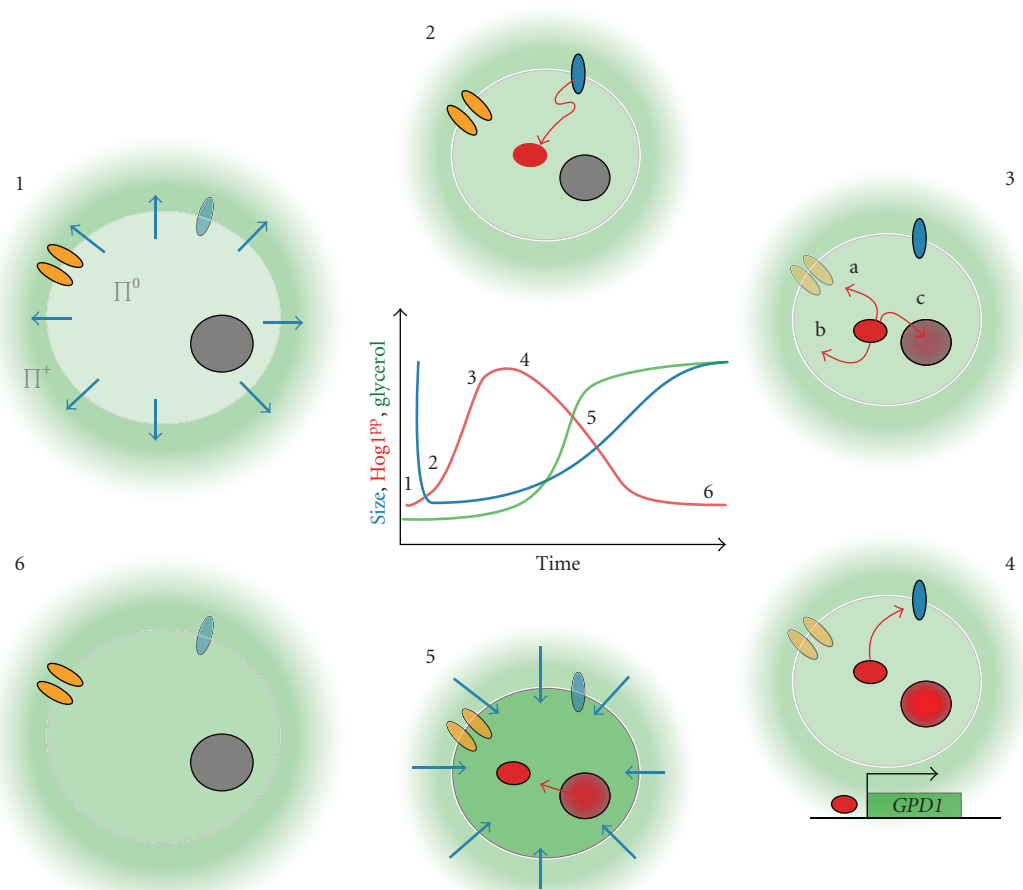


FIGURE 3: Sequential sketch of yeast adaptation to a hyperosmotic shock. The evolution with time of the size, phosphorylation of Hog1p, and internal concentration of glycerol are schematically represented in the center of the picture. (1) After an increase of the external osmolarity (green), a first mechanical response corresponds to a rapid loss of water (blue arrow). It leads to a decrease of the cell size and a loss of turgor pressure. (2) HOG osmosensors (blue) activate the pathway and eventually lead to the phosphorylation of Hog1p. (3) Hog1PP induces several processes: (a) Inactivation of the glycerol channel Fps1p preventing glycerol leakage; (b) direct or indirect activation of cytoplasmic actors, for example, 6-phosphofructo-2-kinase (Pfk2p) involved in glycerol synthesis; (c) translocation in the nucleus. Note that there are other targets of Hog1p such as Sic1p, Hsl1p, Nha1p, and Tok1p. (4) Nuclear Hog1PP induces a large transcriptional response. In particular, the gene *GPD1* leading to glycerol synthesis is upregulated. Negative feedbacks (glycerol production, phosphorylation of Sho1p, etc.) allow inhibition of the pathway activity. (5) Increase of the internal glycerol leads to water influx and progressive cell size recovery while Hog1p is exported from the nucleus. (6) Pathway is off, and turgor pressure and cell size are restored. The cell is adapted to its new environment.

also includes a description for the metabolic production of glycerol, as well as an elementary gene expression model for the enzymes involved in glycerol production. The model also includes the closure of the membrane glycerol transporter Fps1p and takes the dephosphorylation of nuclear Hog1p by Ptp2p into account. Most reactions in the model were described by the mass action rate law. The model consisted of 70 parameters, of which 24 had to be estimated. To estimate this number of parameters with the limited data available, the authors divided the model in modules and fitted them separately to data points. Their model reproduced accurately the transient response of the HOG pathway after a single hyperosmotic shock. This included the phosphorylation states of Hog1p and Pbs2p, as well as glycerol production and cell-size recovery. In addition, the model was able to correctly predict the effect of different mutations of proteins

involved in the pathway. Mutants unable to produce glycerol (*gpd1Δ*, *gpd2Δ*) [83] or to close the Fps1p channel showed an increased duration of HOG activity. Mutants with an increased phosphatase Ptp2p activity showed a lower level of phosphorylated Hog1p but a similar period of HOG activity.

Although very promising, such an approach is still extremely difficult to fine tune since it relies on many unknown parameters. Comparison of the model outputs to experimental data is crucial. To further constrain and test complex models one needs quantitative, time-resolved experiments at the single-cell level in response to complex input signals.

As engineers do with electronic circuits and chips, a very powerful way to explore the dynamics of a given system is to observe its response to complex input signals. Such an approach lends itself to developing minimal models that

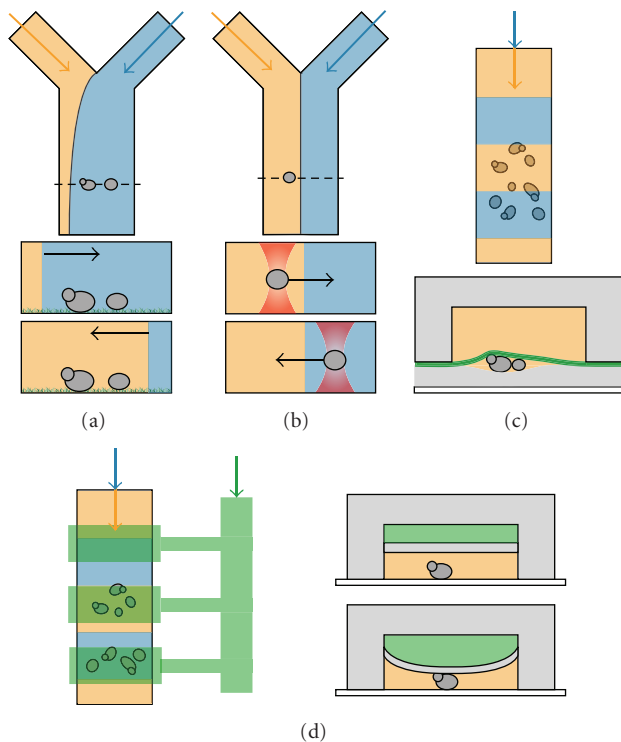


FIGURE 4: Different microfluidics techniques to control the chemical environment of single yeast cells while imaging them through microscopy. (a) Microfluidic system as described in Hersen et al. [11]. Yeast cells are fixed in the channel by the lectin protein Concanavalin A. One inlet is filled with an iso-osmotic media (blue) and the other with a hyperosmotic media (orange). By tightly controlling the pressure in each inlet, it is possible to create a periodic shock on the cells. (b) Optical tweezers system (red) as described by Eriksson et al. permits to control the cells position in the channel with two fluids flowing side by side [12]. (c) The system developed by Charvin et al. uses a dialysis membrane (green) to trap cells on top of a soft PDMS slice [13]. (d) Multilayer microfluidic device [14]. The top layer (green) is used to capture cells. By controlling the pressure inside this channel, cells can be optimally trapped while subjected to periodic shocks. The bottom layer is used to culture cells.

capture the dynamical properties of the pathway, such as feedback loops and signal processing abilities, without taking into account all the details of the biochemical reactions. These approaches require designing experimental systems in which the extracellular environment can be quickly and precisely varied. We will now review the innovative methodologies that have been recently used to study single yeast cells in time varying environments. Then, we will review how those measurements have been integrated into minimal modeling to further study the dynamics of the HOG pathway.

## 6. Fast Control of the Chemical Environment of Single Cells

Several approaches, using microfluidics [8, 9, 84, 85], have been recently proposed to allow for a fast and reliable control

of the chemical environment of yeast cells [7]. Hersen et al. [11] designed a fast binary switch to repeatedly change the environment of single yeast cells between two chemical conditions as fast as every second (Figure 4(a)). They used a Y-shaped flow chamber,  $50\ \mu\text{m}$  high and  $500\ \mu\text{m}$  wide, with two inlets. One inlet was filled with an isotonic medium, and the other with the same culture medium complemented with sorbitol to increase its osmolarity. At such small scales, flows are laminar and fluids do not mix but rather simply flow side by side. The lateral position of the fluids interface is set by the relative hydrostatic pressure—or the relative flux—of the two inlets. Changing this pressure difference displaces the interface laterally in less than a second. Yeast cells, previously fixed in the channel through concanavalin-A coating were then repeatedly switched from an isotonic to a hyperosmotic environment. An interesting alternative developed by Eriksson et al. [12] consists of moving the cells with optical tweezers (Figure 4(b)) rather than moving fluids over fixed cells. This strategy removes the potential influence of cell adhesion on signaling dynamics related to morphological changes, but at the cost of technological complexity. Also, such a strategy is very time consuming. Holographic tweezers—a sophisticated version of optical tweezers—can help to increase the number of cells that can be observed in real time [86]. Another strategy was proposed by Charvin et al. [13, 87]. Yeast cells are fixed between a permeable dialysis membrane and a cover slip coated with a very thin layer of soft PDMS (Poly-Di-MethylSiloxane). A channel is placed on top of the membrane and allows flow of fresh media and exchange within a few minutes. Nutrients and other chemicals can freely diffuse through the membrane. With this device, environmental exchange happens more slowly, but cells can grow over several generations in a monolayer simplifying their observation through microscopy. Indeed, Charvin et al. used it to force periodic expression of cyclins in yeast growing exponentially up to 8–10 generations.

More complex devices have been proposed, though they require a high degree of expertise to fabricate and manipulate. Bennet et al. [88] developed an environmental switcher capable of generating sinusoidal inputs. Their multilayer device was composed of a microchemostat, with a depth of  $4\ \mu\text{m}$  to force yeast cells to grow in a monolayer, and a fluid mixer to generate complex time varying environmental signals for the cells in the chemostat chamber. They used this device, in a particularly elegant work, to revisit the wiring of the GAL system in yeast, by subjecting cells to sinusoidal inputs of carbon source over a range of frequencies. Taylor et al. [14] described a high throughput microfluidics single-cell imaging platform to study the dynamics of the pheromone response in yeast. They combined a fluidic multiplexer, an array of channels, and many sieve valves to trap cells and to control fluid delivery. They were able to perform simultaneous time lapse imaging of 256 chambers with 8 different genotypes with several dynamical inputs. Such a strategy, although very sophisticated, can enhance dramatically the quantity of data gathered to improve our knowledge and refine modeling of MAPK pathways in yeast [7].

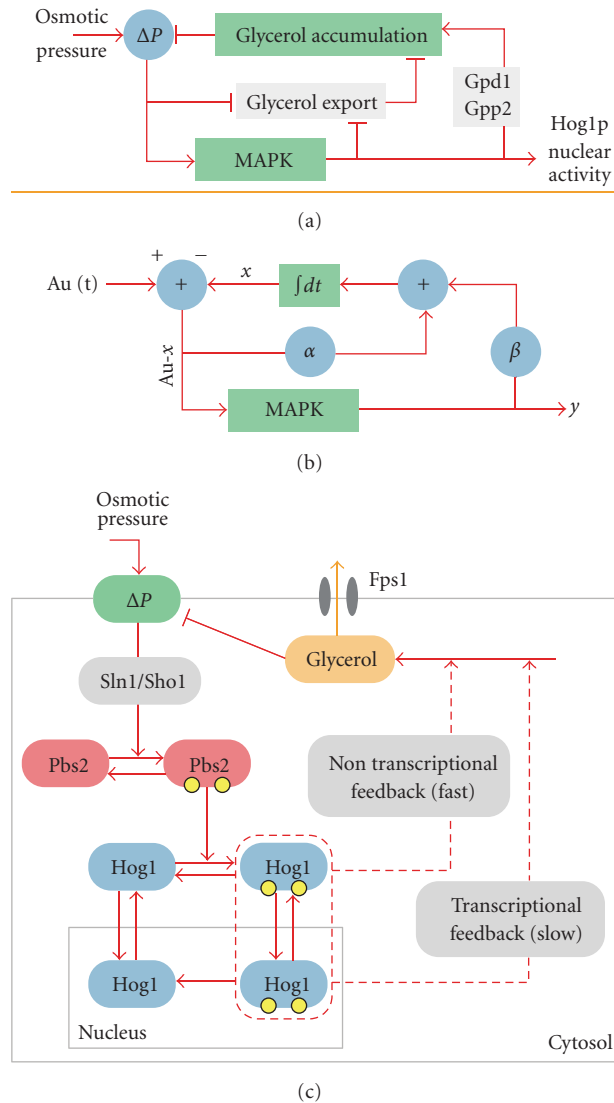


FIGURE 5: Schematic representation of the Hog pathway models of Mettetal et al. [10] and Zi et al. [15]. Pictures are redrawn from original figures of these papers. Top: (a) Diagrammatic representation of Mettetal’s model.  $Au(t)$  represents the osmolarity applied at time  $t$  and the variables  $x$  and  $y$  can be identified with the intracellular glycerol concentration and the enrichment of Hog1 in the nucleus. The model contains a feedback depending on Hog1p (with strength  $\beta$ ) and one, which is independent of Hog1p (strength  $\alpha$ ). The equations for this model read  $\dot{y} = (A_0u - x) - \gamma y$  and  $\dot{x} = \alpha(A_0u - x) + \beta y$ . (b) The same model, interpreted in biological terms. The export of osmolytes is regulated by a mechanism, which does not depend on the MAPK pathway (e.g., closure of Fps1p) and by a mechanism depending on Hog1p activation. (c) Diagram of the model structure proposed by Zi et al. The model includes a simplified version of the MAPK pathway as well as two different feedbacks induced by activated Hog1p (a slow transcriptional and a fast nontranscriptional). Both of these feedbacks act by increasing the production of glycerol.

### 7. New Insights from Coupling Complex Stimulus and Reverse Systems Engineering

Using such microfluidics strategies (Figure 4(a)), Hersen et al. studied the HOG pathway response to periodical osmotic stimulation over a range of frequencies. Interestingly, the HOG pathway acts as a low-pass filter, meaning that the output of the pathway (Hog1p nuclear localization) does not follow a fast varying input precisely, but rather integrates fast fluctuations over time. For wild-type strains, when the input signal varies slower than once every 200 s, Hog1p

cytoplasmic—nuclear shuttling follows the input variations faithfully [11, 17]. However, when the input varies more rapidly than every 200 s, Hog1p nuclear translocation no longer follows the input faithfully, but instead integrates over the input fluctuations [11, 17]. This typical time is also the slowest time (or limiting step) of activation of the pathway although it was not possible from these experiments to point out which biochemical step was limiting. By genetic removal of one of the two branches, the contribution of each branch was also measured by Hersen et al., and it was found that the SHO1 branch is slower than the SLN1 branch by

almost a factor two. The SHO1 branch was actually unable to integrate the too fast variations of the input whereas the SLN1 branch, when taken alone, was displaying a similar behavior than wild-type cells [11]. Those investigations clearly evidenced that the pathway can be turned off very quickly and repeatedly, suggesting the existence of several feedback loops acting on different timescales.

An attempt to decipher the dynamical aspects of these feedback loops has been done by Mettetal et al. [10], who also examined the response of the Hog1p nuclear localization in response to an oscillating input. They constructed, based on these frequency experiments, a simple predictive model, which was not based on biological knowledge (Figure 5(a)). Subsequently, they identified the two variables of their model with the intercellular osmolyte concentration and the phosphorylation state of Hog1p and concluded that the pathway contains a Hog1-dependent and a Hog1-independent feedback mechanism. By underexpressing Pbs2p, thereby reducing the sensitivity of the Hog1-response to the input, they were able to isolate the Hog1-independent feedback from the Hog1-dependent feedback. Based on this they concluded that the Hog1-dependent feedback is required for fast pathway inactivation. By inhibiting translation, they showed indeed that the slow transcriptional response triggered by Hog1p is only necessary for the adaptation to multiple osmotic shocks, while for a single osmotic shock faster nontranscriptional feedback mechanisms dominate the response. Their conclusion is in perfect agreement with recent experimental investigations showing that even cells with Hog1p anchored to the membrane present an increase of glycerol production after a hyperosmotic shock [89]. Although the details are not known, Hog1p directly or indirectly activates the 6-Phosphofructo-2-kinase (PFK2) [68] which leads to an increase production of glycerol through Gpd1p activity.

Hao et al. also focused on rapid non-transcriptional feedback loops. First, they noticed that the response of the SHO1 branch is more transient than that of the SLN1 branch. Then, based on previous observations, they constructed three simple mathematical models, each describing another possible mechanism of HOG inactivation. One model was based on Hog1p mediating activation of a negative regulator (phosphatases), while the other two models focused on the negative control of a positive regulator. Analysis of the different models suggested a Hog1p-dependent feedback mechanism occurring early in the response. Their experimental analysis confirmed this and suggested that Hog1p acts negatively on Sho1p by phosphorylation, thereby implementing a direct negative feedback loop.

Muzzey et al. [18] followed a similar approach to study the feedback mechanisms within the pathway. They identified the transient activation of Hog1p with a feature called perfect adaptation, which states that the steady state output of the pathway does not depend on the strength of the osmotic shock. They argued that robust perfect adaptation requires at least one negative feedback loop containing an integrating component [90] and they analyzed the location of this integrator. They defined an integrating component as a dynamic variable whose rate of change does not

depend on itself. They monitored multiple system quantities (cell volume, Hog1p, and glycerol) and used varied input waveforms to analyze the pathway. Similar to Hao et al. [16], they constructed different variants of a mathematical model, each with a different location of the integrating component. The authors found that the integral feedback property is Hog1p dependent and regulates glycerol uptake.

More recently, Zi et al. [15] analyzed the experimental frequency response of the HOG pathway done by Hersen et al. and Mettetal et al. They constructed a minimal model that can reproduce the response of the pathway to oscillating inputs (Figure 5(b)) [15]. They defined a signal response gain, which is defined as the ratio of the integrated change of the output of the pathway to the integrated input change and represents a measurement for the efficiency of signal transduction. They concluded that yeast cells have optimized this signal response gain with respect to certain durations and frequencies of osmotic variations.

These different analyses have shown that the HOG signaling cascade can be described in a very simple and modular way with several feedback loops operating to deactivate the pathway: two operating on short time scales through Hog1p activity (Sho1p deactivation and glycerol production increase), and one depending on transcriptional activation of *GPD1*. The dynamics of the pathway was also precisely measured and it was shown that it behaves as a low-pass filter with a cutoff frequency, probably set by protein concentration. Interestingly, the SHO1 branch which is known to be involved in other cellular processes was shown to be slower in activating the Hog1p MAPK than the SLN1 branch. Finally, those approaches have provided us with an easily tractable mathematical model of the HOG pathway that can be efficiently coupled to detailed mechanistic models to study *in silico* the behavior of this MAPK pathway. Taken together, the coupling between mathematical modeling and experimental frequency analysis of the HOG pathway has given very important insights into the HOG pathway dynamics and more generally its functioning, demonstrating the interest of developing such strategies for studying signaling pathways in yeast.

## 8. Future Directions

Although the structure and the dynamics of the HOG signaling pathway are now well understood, several key points remain to be elucidated, the most elusive one being the mechanistic functioning of the two osmosensors, Sln1p and the Sho1p complex. Another important aspect of a better understanding of the HOG pathway is to integrate its behavior with other cellular processes. In particular, in 2000, Gasch et al. [73] compiled genome expression profiles of *S. cerevisiae* yeast subjected to several stress conditions and discovered that genes normally induced after a hyperosmotic shock are downregulated in response to a hypo-osmotic shock and vice versa. The CWI pathway is activated by hypo-osmotic stimulation [29], its physiological role being to reinforce the cell wall and prevent the cell from bursting. HOG and CWI do not share direct components but were

seen to interact with each other [91, 92]. During cell growth both pathways may well be activated and deactivated within short intervals to balance between cell expansion and cell wall development. The Sln1p-dependent response regulator Skn7p [93, 94] could have a role in linking the cell-integrity pathway to the HOG pathway. Skn7p also interacts with Rho1p an upstream component of the CWI pathway. The evidence that Skn7p is apparently controlled by sensors of both the HOG pathway and the cell-integrity pathway makes Skn7p an excellent candidate for a regulator that coordinates osmoregulation and cell wall biogenesis [23, 93, 94]. More work is needed to better understand the putative role of Skn7p in coordinating different aspects of turgor pressure control and cell surface assembly. Using minimal models and fluctuating environments to activate periodically the CWI and/or the HOG pathway is one interesting way to explore their interactions. Similarly, it is known that the HOG pathway and the Pheromone pathway can interact [95–98]. For example, a *hog1Δ* strain will respond to a hyperosmotic shock by activating the response to pheromone pathway. Again, the dynamics of such cross-talk has not been intensely studied. Performing time varying inputs with both pheromone and hyperosmotic medium will provide invaluable experimental data to probe the dynamical aspects of cross-talk between MAPK in yeast.

Since MAPKs pathways are highly conserved from yeast to mammalian cells, it would be interesting to test higher eukaryotic cells, in single cell experiments, for similar system level properties. Although more difficult to implement than for yeast cells, microfluidic technics can also be used to control the external environments of mammalian cells both in time and space. Transposing the approaches described here to mammalian cells will probably give further insights in their signaling pathways dynamics.

## 9. Conclusion

Since its initial discovery in 1993 [24], extensive molecular and genetic research has uncovered the molecular actors, interactions, and functions of the components in the HOG signaling pathway. However, these methods are limited in that one cannot predict the behavior of a complex system from the analysis of isolated components. Understanding of the entire system requires the use of novel techniques borrowed from engineering, physics, and mathematics. Microfluidic technologies combined with live-cell microscopy have allowed the use of temporally complex stimuli to interrogate pathway function. Kinetic information obtained through biochemistry combined with knowledge of the molecular components has allowed for complex quantitative models of the HOG pathway to be constructed. These models in turn provide experimentally testable predictions about pathway behavior and function. Simple “black-box” models designed to mimic only key components of the pathway have proven useful for understanding specific phenomena. Thus, genetic and biochemical data combined with novel experimental approaches and modeling have allowed for the prediction of the dynamics and systems-level

properties of HOG pathway signaling processes. These techniques are easily extended to other signaling pathways of interests with the final goal being to understand the relationships between structure, kinetics, and dynamics at the systems-level in complex biological networks.

## Acknowledgment

P. Hersen is supported by the ANR program of the French Government (ANR-JCh-DiSiP). A. Miermont and J. Uhlen-dorf are students of the Frontier in Life Sciences PhD program (Paris, France).

## References

- [1] L. H. Hartwell, J. J. Hopfield, S. Leibler, and A. W. Murray, “From molecular to modular cell biology,” *Nature*, vol. 402, no. 6761, pp. C47–C52, 1999.
- [2] P. Nurse, “Life, logic and information,” *Nature*, vol. 454, no. 7203, pp. 424–426, 2008.
- [3] R. Brent, “Cell signaling: what is the signal and what information does it carry?” *FEBS Letters*, vol. 583, no. 24, pp. 4019–4024, 2009.
- [4] N. L. Novère, M. Hucka, H. Mi et al., “The systems biology graphical notation,” *Nature Biotechnology*, vol. 27, no. 8, pp. 735–741, 2009.
- [5] A. Jovic, B. Howell, and S. Takayama, “Timing is everything: using fluidics to understand the role of temporal dynamics in cellular systems,” *Microfluidics and Nanofluidics*, vol. 6, no. 6, pp. 717–729, 2009.
- [6] O. Lipan and W. H. Wong, “The use of oscillatory signals in the study of genetic networks,” *Proceedings of the National Academy of Sciences of the United States of America*, vol. 102, no. 20, pp. 7063–7068, 2005.
- [7] S. Paliwal, J. Wang, and A. Levchenko, “Pulsing cells: how fast is too fast?” *HFSP Journal*, vol. 2, no. 5, pp. 251–256, 2008.
- [8] G. M. Whitesides, E. Ostuni, S. Takayama, X. Jiang, and D. E. Ingber, “Soft lithography in biology and biochemistry,” *Annual Review of Biomedical Engineering*, vol. 3, pp. 335–373, 2001.
- [9] M. R. Bennett and J. Hasty, “Microfluidic devices for measuring gene network dynamics in single cells,” *Nature Reviews Genetics*, vol. 10, no. 9, pp. 628–638, 2009.
- [10] J. T. Mettetal, D. Muzzey, C. Gómez-Urbe, and A. van Oudenaarden, “The frequency dependence of osmo-adaptation in *Saccharomyces cerevisiae*,” *Science*, vol. 319, no. 5862, pp. 482–484, 2008.
- [11] P. Hersen, M. N. McClean, L. Mahadevan, and S. Ramanathan, “Signal processing by the HOG MAP kinase pathway,” *Proceedings of the National Academy of Sciences of the United States of America*, vol. 105, no. 20, pp. 7165–7170, 2008.
- [12] E. Eriksson, J. Enger, B. Nordlander et al., “A microfluidic system in combination with optical tweezers for analyzing rapid and reversible cytological alterations in single cells upon environmental changes,” *Lab on a Chip*, vol. 7, no. 1, pp. 71–76, 2007.
- [13] G. Charvin, F. R. Cross, and E. D. Siggia, “A microfluidic device for temporally controlled gene expression and long-term fluorescent imaging in unperturbed dividing yeast cells,” *PLoS One*, vol. 3, no. 1, Article ID e1468, 2008.
- [14] R. J. Taylor, D. Falconnet, A. Niemistö et al., “Dynamic analysis of MAPK signaling using a high-throughput microfluidic

- single-cell imaging platform,” *Proceedings of the National Academy of Sciences of the United States of America*, vol. 106, no. 10, pp. 3758–3763, 2009.
- [15] Z. Zi, W. Liebermeister, and E. Klipp, “A quantitative study of the Hog1 MAPK Response to fluctuating osmotic stress in *Saccharomyces cerevisiae*,” *PLoS One*, vol. 5, no. 3, Article ID e9522, 2010.
- [16] N. Hao, M. Behar, S. C. Parnell et al., “A systems-biology analysis of feedback inhibition in the Sho1 osmotic-stress-response pathway,” *Current Biology*, vol. 17, no. 8, pp. 659–667, 2007.
- [17] M. N. McClean, P. Hersen, and S. Ramanathan, “In vivo measurement of signaling cascade dynamics,” *Cell Cycle*, vol. 8, no. 3, pp. 373–376, 2009.
- [18] D. Muzzey, C. A. Gómez-Uribe, J. T. Mettetal, and A. van Oudenaarden, “A systems-level analysis of perfect adaptation in yeast osmoregulation,” *Cell*, vol. 138, no. 1, pp. 160–171, 2009.
- [19] C. Widmann, S. Gibson, M. B. Jarpe, and G. L. Johnson, “Mitogen-activated protein kinase: conservation of a three-kinase module from yeast to human,” *Physiological Reviews*, vol. 79, no. 1, pp. 143–180, 1999.
- [20] D. Sheikh-Hamad and M. C. Gustin, “MAP kinases and the adaptive response to hypertonicity: functional preservation from yeast to mammals,” *American Journal of Physiology*, vol. 287, no. 6, pp. F1102–F1110, 2004.
- [21] R. E. Chen and J. Thorner, “Function and regulation in MAPK signaling pathways: lessons learned from the yeast *Saccharomyces cerevisiae*,” *Biochimica et Biophysica Acta*, vol. 1773, no. 8, pp. 1311–1340, 2007.
- [22] M. C. Gustin, J. Albertyn, M. Alexander, and K. Davenport, “Map kinase pathways in the yeast *Saccharomyces cerevisiae*,” *Microbiology and Molecular Biology Reviews*, vol. 62, no. 4, pp. 1264–1300, 1998.
- [23] S. Hohmann, “Osmotic stress signaling and osmoadaptation in yeasts,” *Microbiology and Molecular Biology Reviews*, vol. 66, no. 2, pp. 300–372, 2002.
- [24] J. L. Brewster, T. De Valoir, N. D. Dwyer, E. Winter, and M. C. Gustin, “An osmosensing signal transduction pathway in yeast,” *Science*, vol. 259, no. 5102, pp. 1760–1763, 1993.
- [25] S. M. O’Rourke, I. Herskowitz, and E. K. O’Shea, “Yeast go the whole HOG for the hyperosmotic response,” *Trends in Genetics*, vol. 18, no. 8, pp. 405–412, 2002.
- [26] P. J. Westfall, D. R. Ballon, and J. Thorner, “When the stress of your environment makes you go HOG wild,” *Science*, vol. 306, no. 5701, pp. 1511–1512, 2004.
- [27] S. Hohmann, “Control of high osmolarity signalling in the yeast *Saccharomyces cerevisiae*,” *FEBS Letters*, vol. 583, no. 24, pp. 4025–4029, 2009.
- [28] S. Hohmann, M. Krantz, and B. Nordlander, “Yeast osmoregulation,” *Methods in Enzymology*, vol. 428, pp. 29–45, 2007.
- [29] K. R. Davenport, M. Sohaskey, Y. Kamada, D. E. Levin, and M. C. Gustin, “A second osmosensing signal transduction pathway in yeast: hypotonic shock activates the PKC1 protein kinase-regulated cell integrity pathway,” *Journal of Biological Chemistry*, vol. 270, no. 50, pp. 30157–30161, 1995.
- [30] H. Martín, J. M. Rodríguez-Pachón, C. Ruiz, C. Nombela, and M. Molina, “Regulatory mechanisms for modulation of signaling through the cell integrity Slt2-mediated pathway in *Saccharomyces cerevisiae*,” *Journal of Biological Chemistry*, vol. 275, no. 2, pp. 1511–1519, 2000.
- [31] J. C. Harrison, E. S. G. Bardes, Y. Ohya, and D. J. Lew, “A role for the Pkc1p/Mpk1p kinase cascade in the morphogenesis checkpoint,” *Nature Cell Biology*, vol. 3, no. 4, pp. 417–420, 2001.
- [32] E. A. Elion, “Pheromone response, mating and cell biology,” *Current Opinion in Microbiology*, vol. 3, no. 6, pp. 573–581, 2000.
- [33] K. Tedford, S. Kim, D. Sa, K. Stevens, and M. Tyers, “Regulation of the mating pheromone and invasive growth responses in yeast by two MAP kinase substrates,” *Current Biology*, vol. 7, no. 4, pp. 228–238, 1997.
- [34] F. Banuett, “Signaling in the yeasts: an informational cascade with links to the filamentous fungi,” *Microbiology and Molecular Biology Reviews*, vol. 62, no. 2, pp. 249–274, 1998.
- [35] B. Ren, F. Robert, J. J. Wyrick et al., “Genome-wide location and function of DNA binding proteins,” *Science*, vol. 290, no. 5500, pp. 2306–2309, 2000.
- [36] V. Gavrias, A. Andrianopoulos, C. J. Gimeno, and W. E. Timberlake, “*Saccharomyces cerevisiae* TEC1 is required for pseudohyphal growth,” *Molecular Microbiology*, vol. 19, no. 6, pp. 1255–1263, 1996.
- [37] M. Proft, A. Pascual-Ahuir, E. de Nadal, J. Arño, R. Serrano, and F. Posas, “Regulation of the Sko1 transcriptional repressor by the Hog1 MAP kinase in response to osmotic stress,” *The EMBO Journal*, vol. 20, no. 5, pp. 1123–1133, 2001.
- [38] P. M. Alepuz, E. de Nadal, M. Zapater, G. Ammerer, and F. Posas, “Osmostress-induced transcription by Hot1 depends on a Hog1-mediated recruitment of the RNA Pol II,” *The EMBO Journal*, vol. 22, no. 10, pp. 2433–2442, 2003.
- [39] P. Shore and A. D. Sharrocks, “The MADS-box family of transcription factors,” *European Journal of Biochemistry*, vol. 229, no. 1, pp. 1–13, 1995.
- [40] K. Madden, Y. J. Sheu, K. Baetz, B. Andrews, and M. Snyder, “SBF cell cycle regulator as a target of the yeast PKC-MAP kinase pathway,” *Science*, vol. 275, no. 5307, pp. 1781–1784, 1997.
- [41] K. Doi, A. Gartner, G. Ammerer et al., “MSG5, a novel protein phosphatase promotes adaptation to pheromone response in *S.cerevisiae*,” *The EMBO Journal*, vol. 13, no. 1, pp. 61–70, 1994.
- [42] X. L. Zhan, R. J. Deschenes, and K. L. Guan, “Differential regulation of FUS3 map kinase by tyrosine-specific phosphatases PTP2/PTP3 and dual-specificity phosphatase MSG5 in *Saccharomyces cerevisiae*,” *Genes & Development*, vol. 11, no. 13, pp. 1690–1702, 1997.
- [43] C. P. Mattison and I. M. Ota, “Two protein tyrosine phosphatases, Ptp2 and Ptp3, modulate the subcellular localization of the Hog1 MAP kinase in yeast,” *Genes & Development*, vol. 14, no. 10, pp. 1229–1235, 2000.
- [44] J. Warmka, J. Hanneman, J. Lee, D. Amin, and I. Ota, “Ptc1, a type 2C Ser/Thr phosphatase, inactivates the HOG pathway by dephosphorylating the mitogen-activated protein kinase Hog1,” *Molecular and Cellular Biology*, vol. 21, no. 1, pp. 51–60, 2001.
- [45] T. Maeda, A. Y. M. Tsai, and H. Saito, “Mutations in a protein tyrosine phosphatase gene (PTP2) and a protein serine/threonine phosphatase gene (PTC1) cause a synthetic growth defect in *Saccharomyces cerevisiae*,” *Molecular and Cellular Biology*, vol. 13, no. 9, pp. 5408–5417, 1993.
- [46] H. Martín, M. Flández, C. Nombela, and M. Molina, “Protein phosphatases in MAPK signalling: we keep learning from yeast,” *Molecular Microbiology*, vol. 58, no. 1, pp. 6–16, 2005.
- [47] E. de Nadal, P. M. Alepuz, and F. Posas, “Dealing with osmotic stress through MAP kinase activation,” *EMBO Reports*, vol. 3, no. 8, pp. 735–740, 2002.

- [48] P. D'Haeseleer, "Closing the circle of osmoregulation," *Nature Biotechnology*, vol. 23, no. 8, pp. 941–942, 2005.
- [49] H. Saito and K. Tatebayashi, "Regulation of the osmoregulatory HOG MAPK cascade in yeast," *Journal of Biochemistry*, vol. 136, no. 3, pp. 267–272, 2004.
- [50] T. Maeda, S. M. Wurgler-Murphy, and H. Saito, "A two-component system that regulates an osmosensing MAP kinase cascade in yeast," *Nature*, vol. 369, no. 6477, pp. 242–245, 1994.
- [51] F. Posas, S. M. Wurgler-Murphy, T. Maeda, E. A. Witten, T. C. Thai, and H. Saito, "Yeast HOG1 MAP kinase cascade is regulated by a multistep phosphorelay mechanism in the SLN1-YPD1-SSK1 "two-component" osmosensor," *Cell*, vol. 86, no. 6, pp. 865–875, 1996.
- [52] V. Reiser, D. C. Raitt, and H. Saito, "Yeast osmosensor Sln1 and plant cytokinin receptor Cre1 respond to changes in turgor pressure," *Journal of Cell Biology*, vol. 161, no. 6, pp. 1035–1040, 2003.
- [53] J. Macia, S. Regot, T. Peeters, N. Conde, R. Solé, and F. Posas, "Dynamic signaling in the Hog1 MAPK pathway relies on high basal signal transduction," *Science Signaling*, vol. 2, no. 63, p. ra13, 2009.
- [54] T. Maeda, M. Takekawa, and H. Saito, "Activation of yeast PBS2 MAPKK by MAPKKKs or by binding of an SH3-containing osmosensor," *Science*, vol. 269, no. 5223, pp. 554–558, 1995.
- [55] V. Reiser, S. M. Salah, and G. Ammerer, "Polarized localization of yeast Pbs2 depends on osmotic stress, the membrane protein Sho1 and Cdc42," *Nature Cell Biology*, vol. 2, no. 9, pp. 620–627, 2000.
- [56] B. T. Seet and T. Pawson, "MAPK signaling: Sho business," *Current Biology*, vol. 14, no. 17, pp. R708–R710, 2004.
- [57] E. de Nadal, F. X. Real, and F. Posas, "Mucins, osmosensors in eukaryotic cells?" *Trends in Cell Biology*, vol. 17, no. 12, pp. 571–574, 2007.
- [58] K. Tatebayashi, K. Tanaka, H. Y. Yang et al., "Transmembrane mucins Hkr1 and Msb2 are putative osmosensors in the SHO1 branch of yeast HOG pathway," *The EMBO Journal*, vol. 26, no. 15, pp. 3521–3533, 2007.
- [59] S. M. O'Rourke and I. Herskowitz, "A third osmosensing branch in *Saccharomyces cerevisiae* requires the Msb2 protein and functions in parallel with the Sho1 branch," *Molecular and Cellular Biology*, vol. 22, no. 13, pp. 4739–4749, 2002.
- [60] T. Yabe, T. Yamada-Okabe, S. Kasahara et al., "HKR1 encodes a cell surface protein that regulates both cell wall  $\beta$ -glucan synthesis and budding pattern in the yeast *Saccharomyces cerevisiae*," *Journal of Bacteriology*, vol. 178, no. 2, pp. 477–483, 1996.
- [61] M. Hayashi and T. Maeda, "Activation of the HOG pathway upon cold stress in *Saccharomyces cerevisiae*," *Journal of Biochemistry*, vol. 139, no. 4, pp. 797–803, 2006.
- [62] S. J. Mansour, K. A. Resing, J. M. Candi et al., "Mitogen-activated protein (MAP) kinase phosphorylation of MAP kinase kinase: determination of phosphorylation sites by mass spectrometry and site-directed mutagenesis," *Journal of Biochemistry*, vol. 116, no. 2, pp. 304–314, 1994.
- [63] M. Krantz, D. Ahmadpour, L. G. Ottosson et al., "Robustness and fragility in the yeast high osmolarity glycerol (HOG) signal-transduction pathway," *Molecular Systems Biology*, vol. 5, article no. 281, 2009.
- [64] A. Zarrinpar, R. P. Bhattacharyya, M. P. Nittler, and W. A. Lim, "Sho1 and Pbs2 act as scaffolds linking components in the yeast high osmolarity MAP kinase pathway," *Molecular Cell*, vol. 14, no. 6, pp. 825–832, 2004.
- [65] P. Ferrigno, F. Posas, D. Koepf, H. Saito, and P. A. Silver, "Regulated nucleo/cytoplasmic exchange of HOG1 MAPK requires the importin  $\beta$  homologs NMD5 and XPO1," *The EMBO Journal*, vol. 17, no. 19, pp. 5606–5614, 1998.
- [66] M. Mollapour and P. W. Piper, "Hog1 mitogen-activated protein kinase phosphorylation targets the yeast Fps1 aquaglyceroporin for endocytosis, thereby rendering cells resistant to acetic acid," *Molecular and Cellular Biology*, vol. 27, no. 18, pp. 6446–6456, 2007.
- [67] E. Bilsland-Marchesan, J. Ariño, H. Saito, P. Sunnerhagen, and F. Posas, "Rck2 kinase is a substrate for the osmotic stress-activated mitogen-activated protein kinase Hog1," *Molecular and Cellular Biology*, vol. 20, no. 11, pp. 3887–3895, 2000.
- [68] H. Dihazi, R. Kessler, and K. Eschrich, "High osmolarity glycerol (HOG) pathway-induced phosphorylation and activation of 6-phosphofructo-2-kinase are essential for glycerol accumulation and yeast cell proliferation under hyperosmotic stress," *Journal of Biological Chemistry*, vol. 279, no. 23, pp. 23961–23968, 2004.
- [69] M. J. Tamás, K. Luyten, F. C. W. Sutherland et al., "Fps1p controls the accumulation and release of the compatible solute glycerol in yeast osmoregulation," *Molecular Microbiology*, vol. 31, no. 4, pp. 1087–1104, 1999.
- [70] M. Siderius, O. Van Wuytswinkel, K. A. Reijenga, M. Kelders, and W. H. Mager, "The control of intracellular glycerol in *Saccharomyces cerevisiae* influences osmotic stress response and resistance to increased temperature," *Molecular Microbiology*, vol. 36, no. 6, pp. 1381–1390, 2000.
- [71] S. E. Beese, T. Negishi, and D. E. Levin, "Identification of positive regulators of the yeast Fps1 glycerol channel," *PLoS Genetics*, vol. 5, no. 11, Article ID e1000738, 2009.
- [72] J. Yale and H. J. Bohnert, "Transcript expression in *Saccharomyces cerevisiae* at high salinity," *Journal of Biological Chemistry*, vol. 276, no. 19, pp. 15996–16007, 2001.
- [73] A. P. Gasch, P. T. Spellman, C. M. Kao et al., "Genomic expression programs in the response of yeast cells to environmental changes," *Molecular Biology of the Cell*, vol. 11, no. 12, pp. 4241–4257, 2000.
- [74] M. Rep, M. Krantz, J. M. Thevelein, and S. Hohmann, "The transcriptional response of *Saccharomyces cerevisiae* to osmotic shock. Hot1p and Msn2p/Msn4p are required for the induction of subsets of high osmolarity glycerol pathway-dependent genes," *Journal of Biological Chemistry*, vol. 275, no. 12, pp. 8290–8300, 2000.
- [75] P. M. Alepuz, A. Jovanovic, V. Reiser, and G. Ammerer, "Stress-induced MAP kinase Hog1 is part of transcription activation complexes," *Molecular Cell*, vol. 7, no. 4, pp. 767–777, 2001.
- [76] E. de Nadal, L. Casadomé, and F. Posas, "Targeting the MEF2-like transcription factor Smp1 by the stress-activated Hog1 mitogen-activated protein kinase," *Molecular and Cellular Biology*, vol. 23, no. 1, pp. 229–237, 2003.
- [77] M. Rep, M. Proft, F. Remize et al., "The *Saccharomyces cerevisiae* Sko1p transcription factor mediates HOG pathway-dependent osmotic regulation of a set of genes encoding enzymes implicated in protection from oxidative damage," *Molecular Microbiology*, vol. 40, no. 5, pp. 1067–1083, 2001.
- [78] A. Valadi, K. Granath, L. Gustafsson, and L. Adler, "Distinct intracellular localization of Gpd1p and Gpd2p, the two yeast isoforms of NAD-dependent glycerol-3-phosphate dehydrogenase, explains their different contributions to redox-driven glycerol production," *Journal of Biological Chemistry*, vol. 279, no. 38, pp. 39677–39685, 2004.
- [79] J. Albertyn, S. Hohmann, J. M. Thevelein, and B. A. Prior, "GPD1, which encodes glycerol-3-phosphate dehydrogenase,

- is essential for growth under osmotic stress in *Saccharomyces cerevisiae*, and its expression is regulated by the high-osmolarity glycerol response pathway,” *Molecular and Cellular Biology*, vol. 14, no. 6, pp. 4135–4144, 1994.
- [80] C. Ferreira, F. Van Voorst, A. Martins et al., “A member of the sugar transporter family, Stt1p is the glycerol/H symporter in *Saccharomyces cerevisiae*,” *Molecular Biology of the Cell*, vol. 16, no. 4, pp. 2068–2076, 2005.
- [81] E. Klipp, B. Nordlander, R. Krüger, P. Gennemark, and S. Hohmann, “Integrative model of the response of yeast to osmotic shock,” *Nature Biotechnology*, vol. 23, no. 8, pp. 975–982, 2005.
- [82] P. Gennemark, B. Nordlander, S. Hohmann, and D. Wedelin, “A simple mathematical model of adaptation to high osmolarity in yeast,” *In Silico Biology*, vol. 6, no. 3, pp. 193–214, 2006.
- [83] S. Karlgren, N. Pettersson, B. Nordlander et al., “Conditional osmotic stress in yeast: a system to study transport through aquaglyceroporins and osmotic stress signaling,” *Journal of Biological Chemistry*, vol. 280, no. 8, pp. 7186–7193, 2005.
- [84] P. Wilding, J. Pfahler, H. H. Bau, J. N. Zemel, and L. J. Kricka, “Manipulation and flow of biological fluids in straight channels micromachined in silicon,” *Clinical Chemistry*, vol. 40, no. 1, pp. 43–47, 1994.
- [85] Y. Xia and G. M. Whitesides, “Soft lithography,” *Annual Review of Materials Science*, vol. 28, no. 1, pp. 153–184, 1998.
- [86] A. Lafong, W. J. Hossack, J. Arlt, T. J. Nowakowski, and N. D. Read, “Time-Multiplexed Laguerre-Gaussian holographic optical tweezers for biological applications,” *Optics Express*, vol. 14, no. 7, pp. 3065–3072, 2006.
- [87] G. Charvin, F. R. Cross, and E. D. Siggia, “Forced periodic expression of G cyclins phase-locks the budding yeast cell cycle,” *Proceedings of the National Academy of Sciences of the United States of America*, vol. 106, no. 16, pp. 6632–6637, 2009.
- [88] M. R. Bennett, W. L. Pang, N. A. Ostroff et al., “Metabolic gene regulation in a dynamically changing environment,” *Nature*, vol. 454, no. 7208, pp. 1119–1122, 2008.
- [89] P. J. Westfall, J. C. Patterson, R. E. Chen, and J. Thorner, “Stress resistance and signal fidelity independent of nuclear MAPK function,” *Proceedings of the National Academy of Sciences of the United States of America*, vol. 105, no. 34, pp. 12212–12217, 2008.
- [90] T. M. Yi, Y. Huang, M. I. Simon, and J. Doyle, “Robust perfect adaptation in bacterial chemotaxis through integral feedback control,” *Proceedings of the National Academy of Sciences of the United States of America*, vol. 97, no. 9, pp. 4649–4653, 2000.
- [91] R. Alonso-Monge, E. Real, I. Wojda, J. P. Bebelman, W. H. Mager, and M. Siderius, “Hyperosmotic stress response and regulation of cell wall integrity in *Saccharomyces cerevisiae* share common functional aspects,” *Molecular Microbiology*, vol. 41, no. 3, pp. 717–730, 2001.
- [92] R. García, J. M. Rodríguez-Peña, C. Bermejo, C. Nombela, and J. Arroyo, “The high osmotic response and cell wall integrity pathways cooperate to regulate transcriptional responses to zymolyase-induced cell wall stress in *Saccharomyces cerevisiae*,” *Journal of Biological Chemistry*, vol. 284, no. 16, pp. 10901–10911, 2009.
- [93] J. L. Brown, H. Bussey, and R. C. Stewart, “Yeast Skn7p functions in a eukaryotic two-component regulatory pathway,” *The EMBO Journal*, vol. 13, no. 21, pp. 5186–5194, 1994.
- [94] J. L. Brown, S. North, and H. Bussey, “SKN7, a yeast multicopy suppressor of a mutation affecting cell wall  $\beta$ -glucan assembly, encodes a product with domains homologous to prokaryotic two-component regulators and to heat shock transcription factors,” *Journal of Bacteriology*, vol. 175, no. 21, pp. 6908–6915, 1993.
- [95] A. Mody, J. Weiner, and S. Ramanathan, “Modularity of MAP kinases allows deformation of their signalling pathways,” *Nature Cell Biology*, vol. 11, no. 4, pp. 484–491, 2009.
- [96] L. Rensing and P. Ruoff, “How can yeast cells decide between three activated MAP kinase pathways? A model approach,” *Journal of Theoretical Biology*, vol. 257, no. 4, pp. 578–587, 2009.
- [97] M. N. McClean, A. Mody, J. R. Broach, and S. Ramanathan, “Cross-talk and decision making in MAP kinase pathways,” *Nature Genetics*, vol. 39, no. 3, pp. 409–414, 2007.
- [98] S. M. O’Rourke and I. Herskowitz, “The Hog1 MAPK prevents cross talk between the HOG and pheromone response MAPK pathways in *Saccharomyces cerevisiae*,” *Genes & Development*, vol. 12, no. 18, pp. 2874–2886, 1998.

## Appended Articles

**Article #2:**

**Long-term model predictive control of gene  
expression at the population and  
single-cell levels.**

Jannis Uhlendorf, Agnès Miermont, Thierry Delaveau,  
Gilles Charvin, François Fages, Samuel Bottani, Gregory Batt and  
Pascal Hersen

PNAS 2012 Aug 28;109(35):14271-6

# Long-term model predictive control of gene expression at the population and single-cell levels

Jannis Uhlenдорff<sup>a,b</sup>, Agnès Miermont<sup>b</sup>, Thierry Delaveau<sup>c</sup>, Gilles Charvin<sup>d</sup>, François Fages<sup>a</sup>, Samuel Bottani<sup>b</sup>, Gregory Batt<sup>a,1,2</sup>, and Pascal Hersen<sup>b,e,1,2</sup>

<sup>a</sup>Contraintes Research Group, Institut National de Recherche en Informatique et en Automatique, INRIA Paris-Rocquencourt, 78150 Rocquencourt, France; <sup>b</sup>Laboratoire Matière et Systèmes Complexes, Unité Mixte de Recherche 7057 Centre National de la Recherche Scientifique and Université Paris Diderot, 75013 Paris, France; <sup>c</sup>Laboratoire de Génomique des Microorganismes, Unité Mixte de Recherche 7238 Centre National de la Recherche Scientifique and Université Pierre et Marie Curie, 75006 Paris, France; <sup>d</sup>Institut de Génétique et Biologie Moléculaire et Cellulaire, 67400 Illkirch, France; and <sup>e</sup>Mechanobiology Institute, National University of Singapore, Singapore 117411

Edited by David A. Weitz, Harvard University, Cambridge, MA, and approved July 16, 2012 (received for review April 23, 2012)

Gene expression plays a central role in the orchestration of cellular processes. The use of inducible promoters to change the expression level of a gene from its physiological level has significantly contributed to the understanding of the functioning of regulatory networks. However, from a quantitative point of view, their use is limited to short-term, population-scale studies to average out cell-to-cell variability and gene expression noise and limit the nonpredictable effects of internal feedback loops that may antagonize the inducer action. Here, we show that, by implementing an external feedback loop, one can tightly control the expression of a gene over many cell generations with quantitative accuracy. To reach this goal, we developed a platform for real-time, closed-loop control of gene expression in yeast that integrates microscopy for monitoring gene expression at the cell level, microfluidics to manipulate the cells' environment, and original software for automated imaging, quantification, and model predictive control. By using an endogenous osmolarity responsive promoter and playing with the osmolarity of the cells environment, we show that long-term control can, indeed, be achieved for both time-constant and time-varying target profiles at the population and even the single-cell levels. Importantly, we provide evidence that real-time control can dynamically limit the effects of gene expression stochasticity. We anticipate that our method will be useful to quantitatively probe the dynamic properties of cellular processes and drive complex, synthetically engineered networks.

model based control | computational biology |  
high osmolarity glycerol pathway | quantitative systems biology

Understanding the information processing abilities of biological systems is a central problem for systems and synthetic biology (1–6). The properties of a living system are often inferred from the observation of its response to static perturbations. Time-varying perturbations have the potential to be much more informative regarding the dynamics of cellular functions (7–12). Currently, it is not possible to precisely perturb protein levels in an analogous manner, even though this perturbation would be instrumental in our understanding of gene regulatory networks. Indeed, despite the development of novel regulatory systems, including various RNA-based solutions (13), transcriptional control by means of inducible promoters is still the preferred method for manipulating protein levels (14, 15). Unfortunately, inducible promoters have several generic limitations. First, there is a significant delay between gene expression activation and effective protein synthesis. Second, many cellular processes can interfere with gene expression through internal feedback loops whose effects are hard to predict. Third, the process of gene expression shows significant levels of noise (16–18). Given these limitations, novel experimental strategies are required to gain quantitative, real-time control of gene expression *in vivo*.

Here, we see the problem of manipulating gene expression to obtain given temporal profiles of protein levels as a model-based control problem. More precisely, we investigate the effectiveness of computerized closed-loop control strategies to control gene expression *in vivo*. In model-based closed-loop control, a model of the

system is used to constantly update the control strategy based on real-time observations. We propose an experimental platform that implements such an *in silico* closed loop in the budding yeast *Saccharomyces cerevisiae*. We show that gene expression can be controlled by repeatedly stimulating a native endogenous promoter over many cell generations (>15 h) for both time-constant and time-varying target profiles and at both the population and single-cell levels. Recently, Miliadis-Argeitis et al. (19) also proposed an approach for feedback control of gene expression in yeast. In contrast to their work, we propose a method that is effective at the single-cell level, for time-varying target profiles, and robust despite the presence of strong internal feedback loops. We start by describing the gene induction system and the experimental platform before discussing its efficiency.

## Results and Discussion

**Controlled System.** We based our approach on the well-known response of yeast to an osmotic shock, which is mediated by the high osmolarity glycerol (HOG) signaling cascade. Its activation leads to the phosphorylation of the protein Hog1 (Fig. 1A), which orchestrates cell adaptation through glycerol accumulation. Phosphorylated Hog1 promotes glycerol production by activating gene expression in the nucleus as well as stimulating glycerol-producing enzymes in the cytoplasm. After they are adapted, the cells do not sense the hyperosmotic environment anymore, the HOG cascade is turned off, and the transcriptional response stops (20–22). In control terms, yeast cells implement several short-term (non transcriptional) and long-term (transcriptional) negative feedback loops that ensure perfect adaptation to the osmotic stress (10, 23). Because of these adaptation mechanisms, it is a priori challenging to control gene expression induced by osmotic stress. It is, thus, an excellent system to show that one can robustly control protein levels, even in the presence of internal negative feedback loops. Several genes are up-regulated in response to a hyperosmotic stress. These genes include the nonessential gene *STL1*, which codes for a glycerol proton symporter (24, 25). We decided to use its native promoter (pSTL1) to drive the expression of yECitrine, a fluorescent reporter. Applying an osmotic stress transiently activated the HOG cascade (Fig. 1B), and yECitrine levels reached modest values (600 fluorescence units) (Fig. 1B). Importantly, when short but repeated stresses were applied, pSTL1 could be repeatedly activated, and much higher levels could be reached (Fig. 1C).

Author contributions: J.U., G.B., and P.H. designed research; J.U. performed research; J.U., A.M., T.D., G.C., F.F., S.B., G.B., and P.H. contributed new reagents/analytic tools/software; J.U., G.B., and P.H. analyzed data; and J.U., G.B., and P.H. wrote the paper.

The authors declare no conflict of interest.

This article is a PNAS Direct Submission.

Freely available online through the PNAS open access option.

<sup>1</sup>To whom correspondence may be addressed. E-mail: gregory.batt@inria.fr or pascal.hersen@univ-paris-diderot.fr.

<sup>2</sup>G.B. and P.H. contributed equally to this work.

This article contains supporting information online at [www.pnas.org/lookup/suppl/doi:10.1073/pnas.1206810109/-DCSupplemental](http://www.pnas.org/lookup/suppl/doi:10.1073/pnas.1206810109/-DCSupplemental).

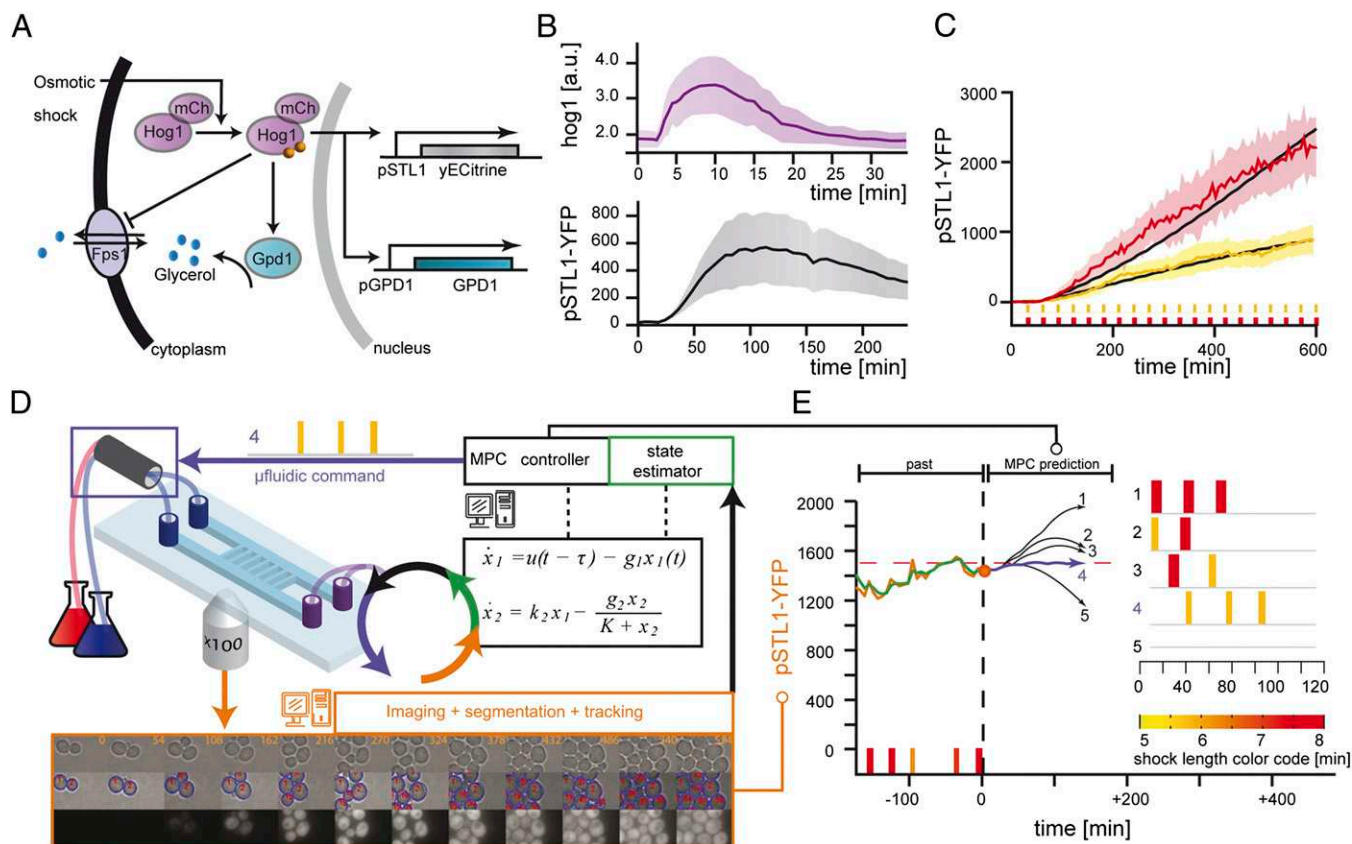


**Fig. 1.** A platform for real-time control of gene expression in yeast. (A) A hyperosmotic stress triggers the activation and nuclear translocation of Hog1. Short-term adaptation is mainly implemented by cytoplasmic activation of the glycerol-producing enzyme Gpd1 and closure of the aqua-glyceroporin channel Fps1. Long-term adaptation occurs primarily through the production of Gpd1. (B) When maintained in a hyperosmotic environment (1 M sorbitol), the HOG cascade was quickly activated, which is seen by Hog1 nuclear enrichment. This transient signaling response lasted typically <20 min. The expression level of pSTL1-yECitrine (YFP) increased after an ~20-min delay, peaked around 600 fluorescence units after 100 min, and then decayed. (C) In contrast, the fluorescence level showed a continuous increase when stimulated periodically ( $T = 30$  min). The increase rate was larger for longer pulses (red, 8 min; yellow, 5 min). Black curves are the expected behaviors based on our model of the pSTL1 induction. Solid lines and their envelopes are the experimental means and SDs of the cells' fluorescence. (D) Yeast cells grew as a monolayer in a microfluidic device that was used to rapidly change the cells' osmotic environment (blue frame) and image their response. Segmentation and cell tracking were done using a Hough transform (orange frame). The measured yECitrine fluorescence, either of a single cell or of the mean of all cells, was then sent to a state estimator connected to an MPC controller. A model (black frame) of pSTL1 induction was used to find the best possible series of osmotic pulses to apply in the future so that the predicted yECitrine level follows a target profile. (E) At the present time point (orange circle), the system state is estimated (green), and the MPC searches for the best input (pulse duration and number of pulses) (see text and *SI Materials and Methods*), which minimizes the distance of the MPC predictions (black curves) to the target profile (red dashed line) for the next 2 h. Here, the osmotic series of pulses that corresponds to the blue curve (4) was selected and sent to the microfluidic command. This control loop is iterated every 6 min.

A closed-loop control of the pSTL1 activity requires the acquisition and analysis of live cell images, the computation of the input (i.e., osmolarity) to be applied in the near future, and the ability to change the cells' osmotic environment accordingly (Fig. 1D and E).

**Experimental Platform.** To observe the cells and control their environment, we designed a versatile platform made of standard microscopy and microfluidic parts. The microfluidic device contained several 3.1- $\mu\text{m}$ -high chambers that were connected by both ends to large channels through which liquid media could be perfused (Fig. 1D). Because the typical diameter of an *S. cerevisiae* cell is 4–5  $\mu\text{m}$ , the cells were trapped in the chamber and grew as a monolayer. Their motion was limited to slow lateral displacement due to cell growth (Fig. S1). This design allowed for long-term cell tracking (>15 h) and relatively rapid media exchanges (~2 min). The HOG pathway was activated by switching between normal and sorbitol-enriched (1 M) media.

**Model of pSTL1 Induction.** To decide what osmotic stress to apply at a given time, we used an elementary model of pSTL1 induction. Many models have been proposed for the hyperosmotic

stress response in yeast (10, 26–30). We used a generic model of gene expression written as a two-variable delay differential equation system, where the first variable denotes the recent osmotic stress felt by the cell and the second variable is the protein fluorescence level (Fig. 1D, *Materials and Methods*, Table S1, and *SI Materials and Methods*). Because our goal was to show robust control, despite the presence of unmodeled feedback loops, the adaptation mechanisms described above were purposefully neglected. The choice of this model was also motivated by the tradeoff between its ability to quantitatively predict the system's behavior (favors complexity) and the ease of solving state estimation problems (favors simplicity). Despite its simplicity, we found a fair agreement between model predictions and calibration data corresponding to fluorescence profiles obtained by applying either isolated or repeated osmotic shocks of various durations (Fig. 1C and Fig. S2).

**Closing the Loop.** The fluorescence intensity of a single cell arbitrarily chosen at the start of the experiment, or the average fluorescence intensity of the cell population, was sent to a state estimator (extended Kalman filter discussed in *SI Materials and Methods*) connected to a model predictive controller (31). Model Predictive Control (MPC) is an efficient framework well-adapted

to constrained control problems. Schematically, given a model of the system and desired temporal profiles for the system's outputs, MPC aims at finding inputs to minimize the deviation between the outputs of the model and the desired outputs. The control strategy is applied for a (short) period. Then, the new state of the system is observed, and this information is used to compute the control strategy to be applied during the next time interval. This receding horizon strategy yields an effective feedback control. In practice, every 6 min, given the current estimate of the system state, past osmotic shocks, and our model of gene expression, the controller searched for the optimal number of osmotic pulses to apply within the next 2 h and their optimal start times and durations (Fig. 1E). If a shock had to be applied within the next 6 min, then it was applied. Otherwise, the same computation was reiterated 6 min later based on new observations, thus effectively closing the feedback loop. Here, we dealt with short-term cell adaptation by imposing a maximal stress duration of 8 min and a 20-min relaxation period between consecutive shocks. Under such conditions, cells stay responsive to osmotic stress at all times (Fig. 1C). This can be explained by the fact that, in absence of stress, the glycerol channel Fps1 opens (21, 32) and lets the glycerol leak out of the cell, thus effectively resetting the osmotic state of the cells (29).

Note that a proportional integral (PI) controller would have been an attractive alternative, because it would not have required the development of a model of the system. With PI controllers, the applied input (i.e., stress) is simply the weighted sum of the current error (deviation between target and measured outputs) and the integral of the (recent) past errors. Consequently,

using a PI controller to reach high levels of fluorescence would lead to a control strategy in which high stress is maintained over extended periods of time. This condition would trigger cell adaptation and eventually lead to a stalled situation in which the maximal stress is applied without any effect.

**Closed-Loop Population Control Experiments.** Our first goals were to maintain the average fluorescence level of a cell population at a given constant value (set-point experiment) and force it to follow a time-varying profile (tracking experiment). Both types of experiments lasted at least 15 h, starting with a few cells and ending with 100–300 cells in the field of view (Fig. S3). The control objective was to minimize the mean square deviations (MSDs) between the mean fluorescence of the population of cells and the target profile. We succeeded in maintaining the average fluorescence level at a given constant value or forcing it to follow several given time-varying profiles (Fig. 2 A–D, Figs. S3, S4, and S5, and Movies S1, S2, and S3). Admissible time-varying target profiles were obviously constrained by the intrinsic timescales of the system, such as the maximal protein production and degradation rates. However, within these constraints, graded responses could be obtained. In Fig. 2C, for example, the trapeze slope is less steep than what maximal pSTL1 induction can deliver (Fig. 2A and B). Note that our control strategy opened the possibility to reach higher fluorescence levels than what full induction with a step shock would allow (compare with Fig. 1B). Indeed, because of cell perfect adaptation to hyperosmotic stresses, a sustained 1 M sorbitol shock triggers only a transient gene expression and fluorescence peaks at moderate levels (Fig. 1B). By using repeated, well-separated pulses,

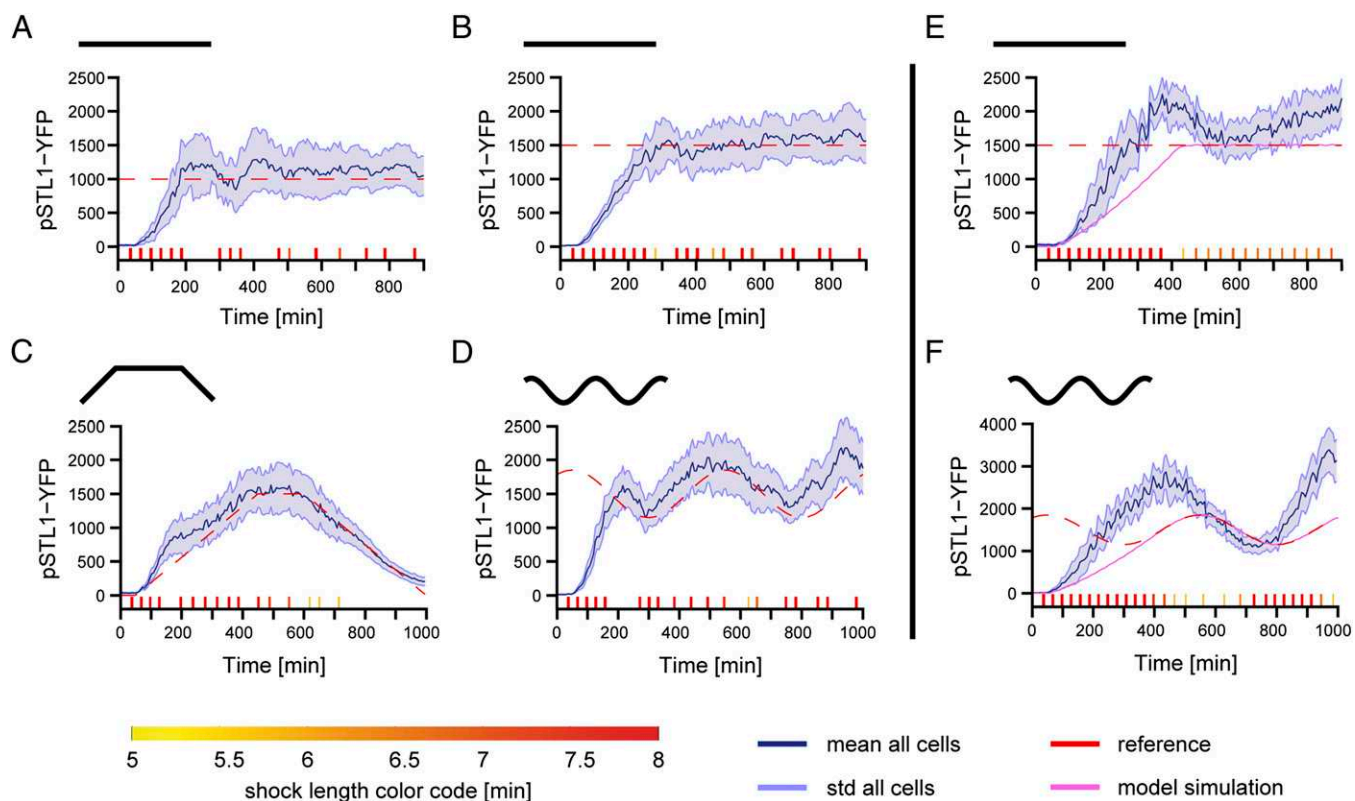


**Fig. 2.** Real-time control of gene expression can be achieved at the population level. (A and B) Set-point control experiments with target values 1,000 and 1,500 fluorescence units (f.u.; red dashed line). This unit is the same across all graphs (no renormalization). To avoid desensitizing the HOG pathway, the controller repeatedly applied short osmotic pulses (durations between 5 and 8 min). The timeline of osmotic events is shown at the bottom of each graph (color code along the bottom). Shock starting times and durations were computed in real time. The measured mean cell fluorescence is shown as solid blue lines. The envelopes indicate SD of the fluorescence distribution across the yeast population. (C and D) Tracking control experiments. In C, the target has a trapezoidal shape (maximum at 1,500 f.u.). In D, the target is sinusoidal (average value at 1,500 f.u.). In both cases, the mean level of fluorescence successfully follows the time-varying target profile. (E and F) Open-loop control experiments. Two examples of open-loop control (the osmotic inputs were computed using our model before starting the experiments) showing poor control quality. Errors accumulate over time. The simulated behavior of the system is represented in violet.

pSTL1 was iteratively activated (Fig. 1C and Movie S4). To assess the effective control range, we performed additional control experiments with target values spanning an order of magnitude (200–2,000 fluorescence units) (Fig. S5). Despite an initial overshoot for the lower target (200 fluorescence units), our results showed good control accuracy over time.

Quantitative limitations of our experimental platform can originate from the model, the state estimator, the control algorithm, and the intrinsic biological variability of gene expression. In silico analysis showed that applying the proposed control strategy to the (estimated state of the) system resulted in control performances that were significantly better than those obtained experimentally (Fig. 2 E and F and Fig. S4). Therefore, the control algorithm performed well, and future improvements should focus on system modeling and state estimation to better represent the experimental state of the system. To assess the importance of biological variability and modeling limitations, we carried out open-loop control experiments with the same objectives and the same model of the system. A time series of osmotic pulses was computed before the experiment and then sent to yeast cells without performing real-time corrections. Important deviations were found, indicating clear discrepancies between model predictions and the long-term system behavior (Fig. 2 E and F). As expected, open-loop strategies cannot result in a quantitative, robust control of gene expression. In contrast, closed-loop control performs well, despite significant biological variability and/or limited model accuracy.

**Closed-Loop Single-Cell Control Experiments.** In a second set of experiments, we focused on the real-time control of gene expression at the single-cell level. We tracked one single cell over at least 15 h and used its fluorescence to feed the MPC controller. As shown

in Fig. 3, we obtained results with quality that is out of reach of any conventional gene induction system, both for constant and time-varying target profiles (Movies S5, S6, and S7). Because of intrinsic noise in gene expression, single-cell control was a priori more challenging than population control. Indeed, compared with the mean fluorescence levels in population control experiments, the fluorescence levels of controlled cells in single-cell control experiments showed larger fluctuations around the target values. However, at the cell level, the MSDs of controlled cells obtained in single-cell control experiments were significantly smaller than the MSDs of a cell in population control experiments (Fig. 4B, SI Materials and Methods, Table S2, and Fig. S6). For set-point control experiments in which fluctuations happen around a fixed reference value, we also defined the fluorescence noise level as the standard deviation (SD) over the mean. Again, we found that single-cell control significantly decreased noise at the cell level (Fig. 4C, SI Materials and Methods, Table S2, and Fig. S6). Taken together, these results show that real-time control effectively improves control quality and counteracts the effects of noise in gene expression when performed at the single-cell level. Interestingly, single-cell control experiments showed that, in few cases, the controlled cell behaved significantly differently from the rest of the population over extended periods of time (e.g., see Fig. 3A), suggesting long-term memory effects for gene expression spanning many cell generations. Lastly, the fact that, for different controlled cells but the same control objective, the decisions of the closed-loop controller were markedly different (Fig. 3E) highlights the fact that feedback control was critical to achieve good control performance at the single-cell level. This suggests that cell-to-cell variability and noise in gene expression fundamentally limit the quality of any open-loop inducible system.

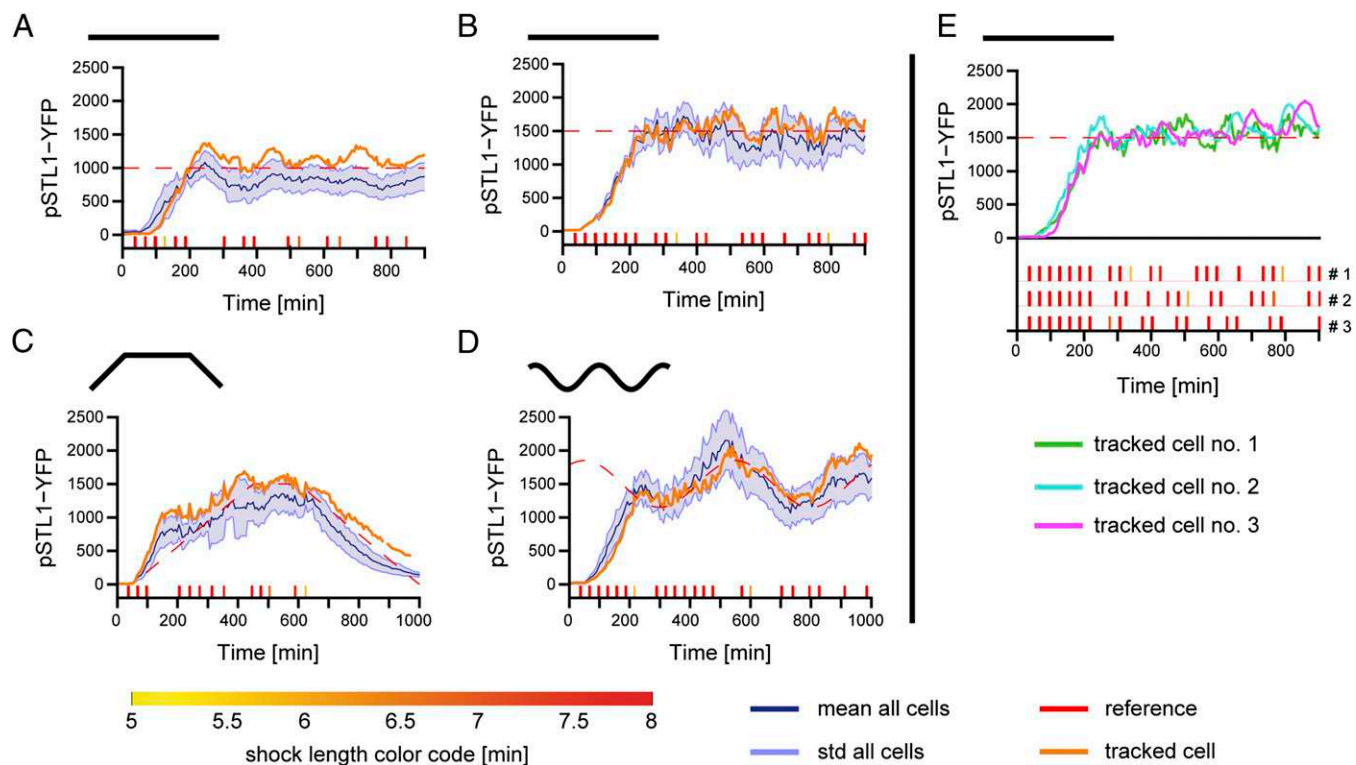


**Fig. 3.** Real-time control of gene expression can be achieved at the single-cell level. (A and B) Set-point control experiments at values 1,000 and 1,500 f.u. The yECitrine fluorescence of the controlled cells is shown as orange lines. The blue line and its envelope indicate the mean fluorescence across the cell population. The population follows the target profile but with less accuracy than the controlled single cell. (C and D) Tracking control experiments. In C, the target has a trapezoidal shape (maximum at 1,500 f.u.). In D, the target is sinusoidal (average at 1,500 f.u.). (E) The fluorescence of the controlled cell in three different single-cell control experiments is represented together with the osmolarity profiles that were applied. Different experiments are labeled with different colors, and therefore, their corresponding osmotic inputs can be identified. It appears that, for each cell, the controller decisions were markedly different, showing that cell-to-cell variability was at play and that feedback control was critical when performing single-cell control.

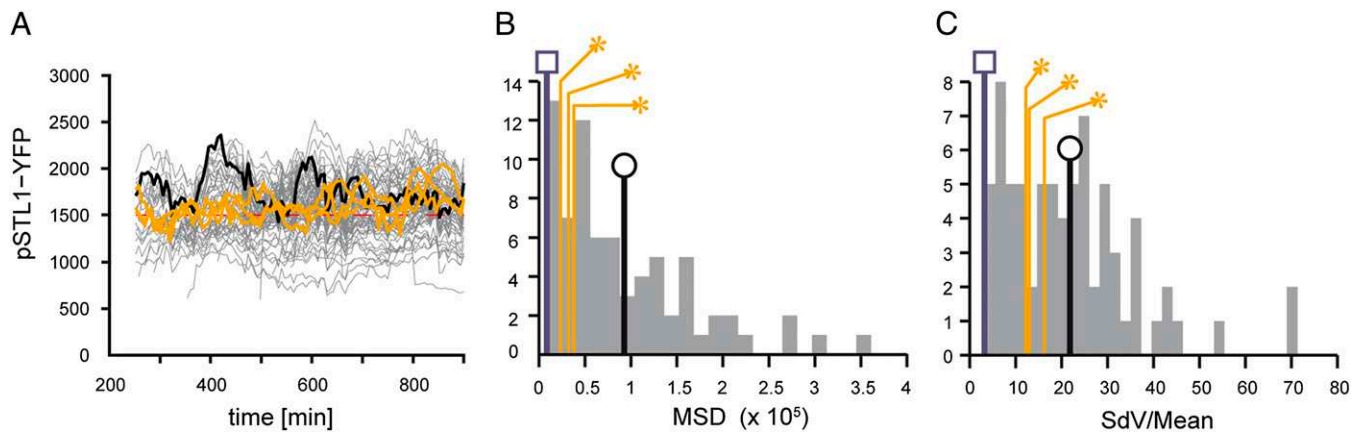


**Fig. 4.** Effectiveness of closed-loop control. (A) Single-cell fluorescence time profiles in two population control experiments (thin gray lines) and three single-cell control experiments (thick orange lines). One representative trace of a single cell in a population control experiment is shown in black. (B) Distribution of the MSDs of individual cells in population control experiments (gray). MSDs are defined with respect to the target profiles. The orange bars (stars) show the MSDs of the controlled cells in three single-cell control experiments. These data are compared with the mean MSD of single cells when controlling the population (black line, circle), which shows lower control quality. As expected, the control quality of the population is better (blue line, square), because noise in gene expression is averaged out. (C) Distribution of the noise levels defined as the ratio of the SD to the mean. Lower noise levels are observed for controlled cells in single-cell control experiments (orange, star) than a random cell in population control experiments (black line).

## Conclusions

We showed that gene expression can be controlled in real time with quantitative accuracy at both the population and single-cell levels by interconnecting conventional microscopy, microfluidics, and computational tools. Importantly, we provided evidence that real-time control can dynamically limit the effects of gene expression stochasticity when applied at the single-cell level. This model predictive control framework overcame the presence of a significant delay between the environmental change and the fluorescent protein observation and the action of strong non-modeled endogenous negative feedback loops. The fact that good control results can be obtained in a closed-loop setting with a relatively coarse model of an endogenous promoter (compare with open-loop results) suggests that extensive modeling will not be required to transpose our approach to other endo- and exogenous induction systems (e.g., the galactose, methionine, or tetracycline inducible promoters). To appreciate the difficulty of the control problems that we addressed, one should keep in mind that the controlled system, a yeast cell, is an extremely complex and partially known dynamical system and that the controlled process, gene expression, is intrinsically stochastic.

Despite the fact that the importance of control theory for systems and synthetic biology has been widely recognized for more than a decade (33, 34), the actual use of *in silico* feedback loops to control intracellular processes has only been proposed recently. In 2011, we showed that the signaling activity in live yeast cells can be controlled by an *in silico* feedback loop (35). Using a PI controller, we controlled the output of a signal transduction pathway by modulating the osmotic environment of cells in real time. A similar framework has been proposed by Menolascina et al. (36). More recently, Toettcher et al. (37) used elaborate microscopy techniques and optogenetics to control (in real time and the single-cell level) the localization and activity of a signal transduction protein (PI3K) in eukaryotic cells. Interestingly, they were able to buffer external stimuli and clamp phosphatidylinositol (3,4,5)-triphosphate (PIP3) levels for short time scales. Because these two frameworks necessitate image acquisition at a high frequency, they are not suitable for long-term experiments. The most closely related work is the work by Miliadis-Argeitis et al. (19). Using optogenetic techniques, Miliadis-Argeitis et al. (19) managed to control the expression of a yeast gene to a constant target value over a few hours. Their approach is based on a chemostat culture and well-adapted for biotechnological applications, such as the production of biofuels or small-molecules. However, because it does not allow for single-cell tracking and control, it is less adapted to probe biological processes in single-cell

quantitative biology applications. Controlling small cell populations, or even single cells, may be needed in multicellular systems, where cells differ by their genotype (38) or physical location (39).

Connecting living cells to computers is a promising field of research both for applied and fundamental research. By maintaining a system around specific operating points or driving it out of its standard operating regions, our approach offers unprecedented opportunities to investigate how gene networks process dynamical information at the cell level. We also anticipate that our platform will be used to complement and help the development of synthetic biology through the creation of hybrid systems resulting from the interconnection of *in vivo* and *in silico* computing devices.

## Material and Methods

**Yeast Strains and Plasmids.** All experiments were performed using a pSTL1::yECitrine-HIS5, Hog1::mCherry-hph yeast strain derived from the S288C background. Cells were cultured overnight in synthetic complete (SC) medium at 30 °C; 4 h before loading them into the microfluidic chip, 60  $\mu$ L overnight culture were diluted into 5 mL SC, thus obtaining an OD of  $\sim$ 0.19. During the experiment, cell growth continued, with a doubling time between 100 and 250 min (*SI Materials and Methods* and *Movies S1, S2, S3, S4, S5, S6, and S7*).

**Microfluidics.** We microfabricated a master wafer by standard soft lithography techniques. A microfluidic chip was made by casting polydimethylsiloxane (PDMS) (Sylgard 184 kit; Dow Corning) on the master wafer, curing it at 65 °C overnight, peeling it off, and bonding it to a glass coverslip after plasma activation. Cells were loaded into the imaging chamber by syringe injection. This created a positive pressure, which let the cells enter the trap. Liquid medium was flown by aspiration into the device using a peristaltic pump (IPC-N; Ismatec) placed after the microfluidic device. We used a flow rate of 230  $\mu$ L/min. A computer-controlled three-way valve (LFA series; The Lee Company) was used to select between regular medium (SC) or the same medium supplemented with 1 M sorbitol. A switch of the valve state did not lead to an instantaneous change of the cells' environment inside the microfluidic device: a certain time (depending on the flow rate) was needed for the fluid to pass from the valve to the channels and the imaging chamber (*Fig. S1*).

**Microscopy and Experimental Setup.** We used an automated inverted microscope (IX81; Olympus) equipped with an X-Cite 120PC fluorescent illumination system (EXFO) and a QuantEM 512 SC camera (Roper Scientific). The YFP filters used were HQ500/20 $\times$  (excitation filter; Chroma), Q515LP (dichroic; Chroma), and HQ535/30M (emission; Chroma). All these components were driven by the open-source software  $\mu$ Manager (40), a plug-in of ImageJ (41), which we interfaced with Matlab using in-house-developed code. The temperature of the microscope chamber, which also contained the media reservoirs, was constantly held at a temperature of 30 °C by a temperature control

system (Life Imaging Services). Images were taken with a 100× objective (PlanApo 1.4 NA; Olympus). The fluorescence exposure time was 200 ms, with fluorescence intensity set to 50% of maximal power. The fluorescence exposure time was chosen such that the fluorescent illumination did not cause noticeable effects on cellular growth over extended periods of time. Importantly, illumination, exposure time, and camera gain were not changed between experiments, and no data renormalization was done. Therefore, the fluorescence intensities can be directly compared across experiments.

**Image Analysis.** The cellular boundaries were identified on the bright-field image using a circular Hough transform implemented in Matlab (42). For tracking, we compared the current image with the previous one, defined a cell-to-cell distance matrix, and used linear optimization to match pairs of cells. The tracking process was made more robust by also considering the last but one image if a gap was detected (caused by rare segmentation errors). The YFP fluorescence level in each cell was defined as the mean fluorescence level taken over the cell area after subtraction of the background fluorescent level. The signaling activity of the Hog1 cascade can be estimated by measuring the Hog1 nuclear enrichment. We defined the nuclear enrichment of Hog1::mCherry as the difference between the minimal and maximal fluorescence intensities within a cell. Maximal and minimal Hog1::mCherry intensities were computed by averaging the fluorescence of the 15 brightest and 15 dimmest pixels, respectively.

**Modeling.** The controller used a two dimensional ordinary differential equation (ODE) model to predict the behavior of the system:

$$\dot{x}_1 = u(t - \tau) - g_1 x_1$$

and

$$\dot{x}_2 = k_2 x_1 - g_2 \frac{x_2}{K + x_2},$$

where  $x_1$  denotes the recent osmotic stress and  $x_2$  denotes the protein fluorescence level. The osmotic input ( $u$ ) is shifted by  $\tau = 20$  min to account for the observed delay in the system. The remaining parameters have been estimated based on several calibration experiments:  $g_1 = 4.02 \times 10^{-3}$ ,  $k_2 = 0.58$ ,  $g_2 = 37.5$ ,  $K = 750$ , and  $\tau = 20$  (SI Materials and Methods, Table S1, and Fig. S2).

**State Estimation.** We implemented an extended Kalman filter, which estimates the system state based on fluorescent observations and the model of the system. The parameters of the filter (measurement noise  $R$  and process noise  $Q$ ) were set to  $R = 2,500$  and  $Q = \text{diag}(0.37, 925)$ .

**Model Predictive Control.** The controller searches for osmolarity profiles that minimize the squared deviations between model output and target profile within the next 120 min, while fulfilling the input constraints (pulse duration of 5 to 8 min separated by at least 20 min). In practice, this problem is recast into a parameter search problem, in which parameters are used for encoding stress starting times and shock durations and solved using the global optimization tool CMAES. Because image analysis and parameter search may take up to 3 min, the input to be applied is not immediately available at the time of the measurement. Consequently, we apply at time  $t$  the input that was computed at time  $t - 3$  min.

**ACKNOWLEDGMENTS.** The authors acknowledge discussions with D. di Bernardo (Tigem), P.-Y. Bourguignon (Max Planck), S. Léon (Institut Jacques Monod & Centre National de la Recherche Scientifique), F. Devaux, M. Garcia (Université Pierre et Marie Curie), J. M. di Meglio, A. Prastowo (Matière et Systèmes Complexes), R. Bourdais (Supélec), A. Kabla (Cambridge University), E. Cinquemani, H. de Jong, D. Ropers, J. Schaul, and S. Stoma (Institut National de Recherche en Informatique et en Automatique). We acknowledge the support of the Agence Nationale de la Recherche (under the references DiSiP-ANR-07-JCJC-0001 and ICEBERG-ANR-10-BINF-06-01), of the Région Ile de France (C’Nano-ModEnv), of the Action d’Envergure ColAge from INRIA/INSERM (Institut Nationale de la Santé et de la Recherche Médicale), of the MechanoBiology Institute, and of the Laboratoire International Associé CAFS (Cell Adhesion France-Singapour).

1. Bhalla US, Ram PT, Iyengar R (2002) MAP kinase phosphatase as a locus of flexibility in a mitogen-activated protein kinase signaling network. *Science* 297:1018–1023.
2. Hooshangi S, Thiberge S, Weiss R (2005) Ultrasensitivity and noise propagation in a synthetic transcriptional cascade. *Proc Natl Acad Sci USA* 102:3581–3586.
3. Cai L, Dalal CK, Elowitz MB (2008) Frequency-modulated nuclear localization bursts coordinate gene regulation. *Nature* 455:485–490.
4. Celani A, Vergassola M (2010) Bacterial strategies for chemotaxis response. *Proc Natl Acad Sci USA* 107:1391–1396.
5. Baumgartner BL, et al. (2011) Antagonistic gene transcripts regulate adaptation to new growth environments. *Proc Natl Acad Sci USA* 108:21087–21092.
6. O’Shaughnessy EC, Palani S, Collins JJ, Sarkar CA (2011) Tunable signal processing in synthetic MAP kinase cascades. *Cell* 144:119–131.
7. Walter E, Pronzato L (1997) *Identification of Parametric Models from Experimental Data* (Springer, Berlin).
8. Bennett MR, et al. (2008) Metabolic gene regulation in a dynamically changing environment. *Nature* 454:1119–1122.
9. Hersen P, McClean MN, Mahadevan L, Ramanathan S (2008) Signal processing by the HOG MAP kinase pathway. *Proc Natl Acad Sci USA* 105:7165–7170.
10. Muzzey D, Gómez-Urbe CA, Mettetal JT, van Oudenaarden A (2009) A systems-level analysis of perfect adaptation in yeast osmoregulation. *Cell* 138:160–171.
11. Shimizu TS, Tu Y, Berg HC (2010) A modular gradient-sensing network for chemotaxis in *Escherichia coli* revealed by responses to time-varying stimuli. *Mol Syst Biol* 6:382.
12. Pelet S, et al. (2011) Transient activation of the HOG MAPK pathway regulates bimodal gene expression. *Science* 332:732–735.
13. Rao CV (2012) Expanding the synthetic biology toolbox: Engineering orthogonal regulators of gene expression. *Curr Opin Biotechnol*, 10.1016/j.copbio.2011.12.015.
14. Voigt CA (2006) Genetic parts to program bacteria. *Curr Opin Biotechnol* 17:548–557.
15. Khalil AS, Collins JJ (2010) Synthetic biology: Applications come of age. *Nat Rev Genet* 11:367–379.
16. Elowitz MB, Levine AJ, Siggia ED, Swain PS (2002) Stochastic gene expression in a single cell. *Science* 297:1183–1186.
17. Balázsi G, van Oudenaarden A, Collins JJ (2011) Cellular decision making and biological noise: From microbes to mammals. *Cell* 144:910–925.
18. Munsky B, Neuert G, van Oudenaarden A (2012) Using gene expression noise to understand gene regulation. *Science* 336:183–187.
19. Miliás-Argeitis A, et al. (2011) In silico feedback for in vivo regulation of a gene expression circuit. *Nat Biotechnol* 29:1114–1116.
20. de Nadal E, Alepuz PM, Posas F (2002) Dealing with osmotic stress through MAP kinase activation. *EMBO Rep* 3:735–740.
21. Hohmann S (2002) Osmotic stress signaling and osmoadaptation in yeasts. *Microbiol Mol Biol Rev* 66:300–372.
22. Miermont A, Uhlendorf J, McClean M, Hersen P (2011) The dynamical systems properties of the HOG signaling cascade. *J Signal Transduct* 2011:930940.
23. Yi TM, Huang Y, Simon MI, Doyle J (2000) Robust perfect adaptation in bacterial chemotaxis through integral feedback control. *Proc Natl Acad Sci USA* 97:4649–4653.
24. Ferreira C, et al. (2005) A member of the sugar transporter family, Stl1p is the glycerol/H+ symporter in *Saccharomyces cerevisiae*. *Mol Biol Cell* 16:2068–2076.
25. O’Rourke SM, Herskowitz I (2004) Unique and redundant roles for HOG MAPK pathway components as revealed by whole-genome expression analysis. *Mol Biol Cell* 15:532–542.
26. Klipp E, Nordlander B, Krüger R, Gennemark P, Hohmann S (2005) Integrative model of the response of yeast to osmotic shock. *Nat Biotechnol* 23:975–982.
27. Hao N, et al. (2007) A systems-biology analysis of feedback inhibition in the Sho1 osmotic-stress-response pathway. *Curr Biol* 17:659–667.
28. Mettetal JT, Muzzey D, Gómez-Urbe C, van Oudenaarden A (2008) The frequency dependence of osmo-adaptation in *Saccharomyces cerevisiae*. *Science* 319:482–484.
29. Zi Z, Liebermeister W, Klipp E (2010) A quantitative study of the Hog1 MAPK response to fluctuating osmotic stress in *Saccharomyces cerevisiae*. *PLoS ONE* 5:e9522.
30. Zechner C, et al. (2012) Moment-based inference predicts bimodality in transient gene expression. *Proc Natl Acad Sci USA* 109:8340–8345.
31. Findeisen R, Imsland L, Allgower F, Foss BA (2003) State and output feedback nonlinear model predictive control: An overview. *Eur J Control* 9:179–195.
32. Tamás MJ, et al. (1999) Fps1p controls the accumulation and release of the glycerol soluble glycerol in yeast osmoregulation. *Mol Microbiol* 31:1087–1104.
33. Csete ME, Doyle JC (2002) Reverse engineering of biological complexity. *Science* 295:1664–1669.
34. Iglesias PA, Ingalls BP (2009) *Control Theory and Systems Biology* (MIT Press, Cambridge, MA).
35. Uhlendorf J, Bottani S, Fages F, Hersen P, Batt G (2011) Towards real-time control of gene expression: Controlling the hog signaling cascade. *Pac Symp Biocomput* 2011:338–349.
36. Menolascina F, di Bernardo M, di Bernardo D (2011) Analysis, design and implementation of a novel scheme for in-vivo control of synthetic gene regulatory network. *Automatica* 47:1265–1270.
37. Toettcher JE, Gong D, Lim WA, Weiner OD (2011) Light-based feedback for controlling intracellular signaling dynamics. *Nat Methods* 8:837–839.
38. Regot S, et al. (2011) Distributed biological computation with multicellular engineered networks. *Nature* 469:207–211.
39. Sprinzak D, et al. (2010) Cis-interactions between Notch and Delta generate mutually exclusive signalling states. *Nature* 465:86–90.
40. Edelstein A, Amodaj N, Hoover K, Vale R, Stuurman N (2010) Computer control of microscopes using µManager. *Curr Protoc Mol Biol*, 10.1002/0471142727.mb1420s92.
41. Rasband WS (1997–2012) *ImageJ* (US National Institutes of Health, Bethesda, MD). Available at <http://imagej.nih.gov/ij/>. Accessed July 29, 2012.
42. Ballard DH (1981) Generalizing the Hough transform to detect arbitrary shapes. *Pattern Recognit* 13(2):111–122.

# Supporting Information

Uhlendorf et al. 10.1073/pnas.1206810109

## SI Materials and Methods

**Mathematical Model.** The hyperosmotic stress response is one of the best-studied adaptation processes in yeast (1). Many mathematical models with various levels of complexity have been developed (2–6). In particular, the work by Mettetal et al. (2) showed that essential aspects of the high osmolarity glycerol signaling cascade (amplitude and temporal profile of the protein Hog1 nuclear localization) can be captured by an extremely simple two dimensional linear model. Because simplicity is critical for state estimation (see below), we took inspiration from this minimalistic model, and we propose the following ordinary differential equation (ODE) model:

$$\dot{x}_1 = u(t - \tau) - g_1 x_1$$

and

$$\dot{x}_2 = k_2 x_1 - g_2 \frac{x_2}{K + x_2}.$$

The two variables  $x_2$  and  $x_1$  denote the protein fluorescence level and the recent osmotic stress felt by the cell, respectively, whereas  $u$  denotes the osmolarity in the imaging chamber. The recent osmotic stress  $x_1$  is modeled by a term integrating the osmotic stress  $[u(t - \tau)]$  and a linear decay term  $(-g_1 x_1)$ , which lets the influence of past osmotic stresses diminish exponentially with time. The term describing the osmolarity ( $u$ ) is computed based on (a piecewise linearization of) the profile shown in Fig. S1 and the valve status. A delay in  $u$  aggregates times for signal transduction, gene expression, and protein synthesis. The fluorescence level increases linearly with the integrator with rate  $k_2$ . Because we did not observe any saturation of the protein fluorescence levels, even for long time experiments (>10 h), in characterization experiments (Fig. S2), we deduced that protein degradation should not be modeled as a term proportional to its concentration as usually assumed. A good fit altogether was obtained using a saturating term for its degradation rate. To fit our model parameters, we designed two types of experiments to probe different aspects of the cell response dynamics: repeated or isolated osmotic shocks. For both cases, we performed experiments with shocks lasting 5, 6, 7, or 8 min (Fig. S2). Based on these observations, we manually set the delay  $\tau$  to 20 min and the protein level corresponding to degradation half-saturation  $K$  to 750. In these conditions, degradation does not saturate in single shocks experiments. The three other parameters have been set using the global optimization tool CMAES (7) so that they minimize the mean squared deviation between model predictions and observations over all experiments. All parameters are summarized in Table S1. Despite its extreme simplicity, we were able to obtain an acceptable fit to the data (Fig. 1 and Fig. S2).

**State Estimation.** For linear systems, the standard approach for state estimation is to use a Kalman filter. Using a linear model, the past control inputs, and (noisy) measurements, it gives an estimate of the system state together with its uncertainty. For each estimate, the filter chooses a weighted average between observation and model prediction, the weight of each term depending on its associated uncertainty. Kalman filters can be extended to nonlinear systems (EKF) by linearizing the nonlinear model around the operating points (8). Note that the delay in the model only concerns the input. In consequence, a classical EKF can be used without the need for specific delayed system state estimation techniques. An EKF requires the tuning of few parameters,

the covariance matrix of the measurement error ( $R$ ), and the covariance matrix of the process noise ( $Q$ ), where errors in both cases are assumed to be Gaussian-distributed with zero mean. Although it is very difficult to evaluate the quality of the state estimation process, we were able to obtain good control performances after setting  $R$  to 2,500 and  $Q$  to  $\text{diag}(0.37, 925)$ . The value of  $R$  has been chosen by estimating the variance of the observations from experimental data. The ratio of the diagonal values in  $Q$  has been determined by the steady-state values of  $x_1$  and  $x_2$ . Then, the actual values of  $Q$  have been determined by ensuring consistency between the innovation residuals (the difference between model prediction and observation) and the variance of the innovation residuals, which is estimated by the Kalman filter.

## Comparison Between Single-Cell Control and Population Control

**Quality.** To compare the control quality of the control loop across different experiments, we consider the mean square deviation (MSD) of the measured signal with respect to the target profile. For single-cell control experiments, the signal is simply the fluorescence of the controlled cell. For population control experiments, signals can either be the mean of the fluorescence across the population of cells or the fluorescence of any cell within the controlled population. In the first case, we refer to the MSD of the mean, and in the second case, we refer to single-cell MSDs in a population experiment. The mean MSD is then the mean of the single-cell MSDs. Note the difference between the MSD of the mean and the mean MSD (Fig. 4 and Fig. S6). In set-point and sine wave experiments, only the time period for which the cells effectively follow the target has been considered (the first 250 min of the initialization phase were disregarded). To allow for a proper quantification of control performance, only cells that have been tracked continuously for at least 5 (set point) or 7 (tracking) hours were considered.

For set-point experiments, in which the fluorescence of the cells remained around a fixed target value, we defined the noise level of a measured signal as its SD over its mean. As for control quality, we compared (in Fig. S6) the single-cell noise level in single-cell and population control experiments with the noise level of the mean and the mean noise level for population control experiments.

We wondered whether controlling cells individually gives statistically better results than controlling them as members of a population. The null assumption ( $H_0$ ) was, therefore, that MSDs (or noise levels) of cells in single-cell control experiments or population control experiments follow the same distribution. The alternative assumption ( $H_1$ ) was that the MSDs (or noise levels) in single-cell control experiments are statistically smaller than in population control experiments. Because we worked with samples of small sizes and could not a priori assume that MSDs or noise levels follow a known probability distribution, we used a nonparametric method (9), the Fligner–Policello (FP) test (10). Like the Wilcoxon–Mann–Whitney test, the FP test is one of the most powerful nonparametric tests used to check whether two independent samples have been drawn from the same distribution. However, in contrast to the Wilcoxon–Mann–Whitney test, the FP test allows for comparison of samples having different variances (Behrens–Fisher problem) (9). This difference is important, because we expected that single-cell control reduced the variance of MSDs. In its one-sided form, the FP test addresses precisely the question stated above ( $H_0$  vs.  $H_1$ ). As shown in Table S2, the test revealed that single-cell control does statistically improve control performances for both MSDs (at least in one case) and noise levels.

- Hohmann S, Mager WH (2003) *Yeast Stress Responses* (Springer, Berlin).
- Mettetal JT, Muzzey D, Gómez-Urbe C, van Oudenaarden A (2008) The frequency dependence of osmo-adaptation in *Saccharomyces cerevisiae*. *Science* 319:482–484.
- Muzzey D, Gómez-Urbe CA, Mettetal JT, van Oudenaarden A (2009) A systems-level analysis of perfect adaptation in yeast osmoregulation. *Cell* 138:160–171.
- Zi Z, Liebermeister W, Klipp E (2010) A quantitative study of the Hog1 MAPK response to fluctuating osmotic stress in *Saccharomyces cerevisiae*. *PLoS One* 5:e9522.
- Klipp E, Nordlander B, Krüger R, Gennemark P, Hohmann S (2005) Integrative model of the response of yeast to osmotic shock. *Nat Biotechnol* 23:975–982.
- Hao N, et al. (2007) A systems-biology analysis of feedback inhibition in the Sho1 osmotic-stress-response pathway. *Curr Biol* 17:659–667.
- Hansen N, Ostermeier A (2001) Completely derandomized self-adaptation in evolution strategies. *Evol Comput* 9:159–195.
- Jazwinski AH (1970) *Stochastic Processes and Filtering Theory*, ed Bellman R (Academic, London).
- Siegel S, Castellan NJ (1988) *Nonparametric Statistics for the Behavioral Sciences* (McGraw-Hill, New York).
- Fligner MA, Policello GE (1981) Robust rank procedures for the Behrens-Fisher problem. *J Am Stat Assoc* 76:162–168.

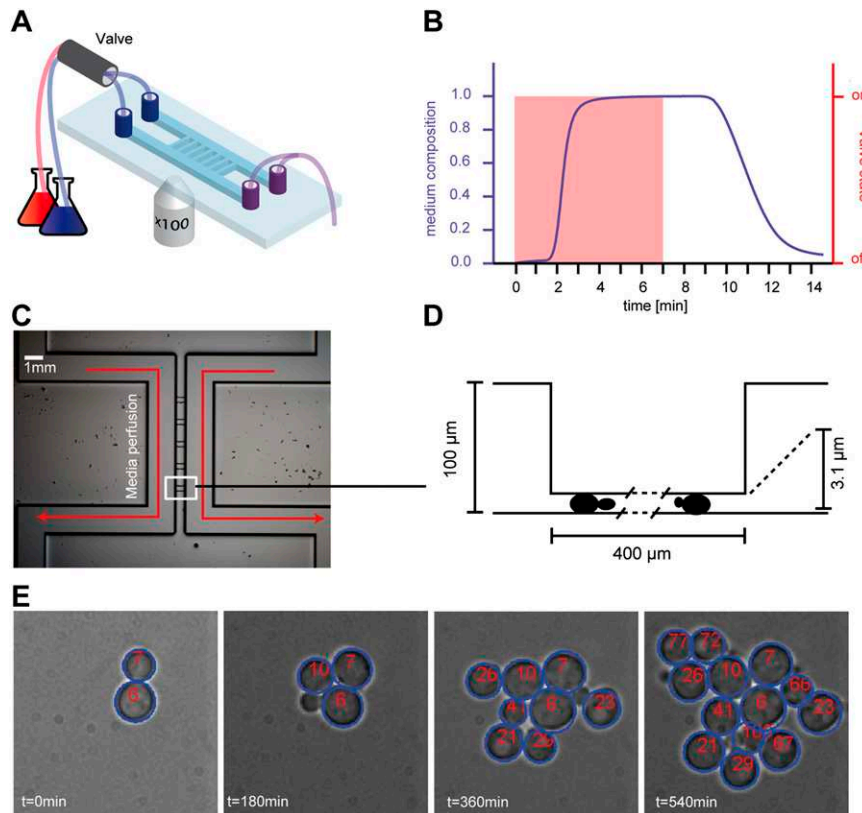


**Fig. S1.** The microfluidic device. (A) Schematic representation of the microfluidic device. A flow is created in the channels thanks to a peristaltic pump placed downstream. Upstream, a valve allows switching between the two media. (B) Using ink, we measured the dynamics of fluid exchange. This switching profile was obtained in a robust manner. (C) Close up of the microfluidic device. (D) Cells are captured within thin chambers. The media in the imaging chamber are exchanged by diffusion. (E) An example of cell imaging, segmentation, and tracking is shown.

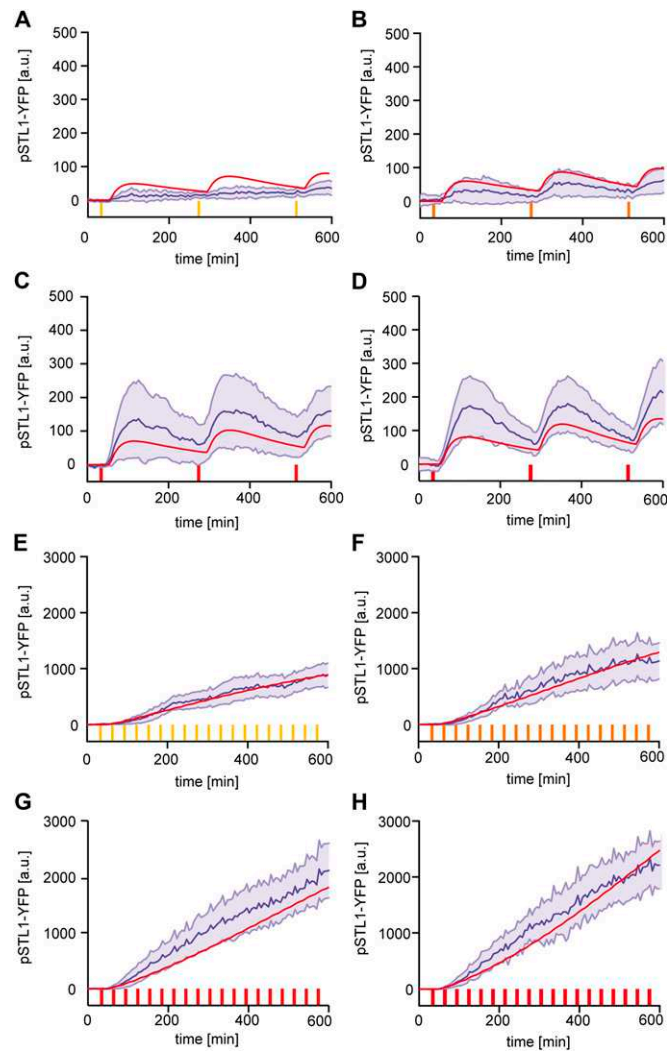


**Fig. S2.** Calibration experiments. (A–D) Isolated osmotic shocks lasting 5, 6, 7, and 8 min were applied every 4 h. (E–H) Osmotic shocks lasting 5, 6, 7 and 8 min were applied every 30 min. The fluorescence of yECitrine, controlled by the *STL1* promoter, was quantified. Experimental means and SDs are represented as blue lines and blue envelopes. Model predictions using the parameters of Table S1 are represented in red. Note that the scales for fluorescence intensities in repeated or isolated shock experiments are significantly different.

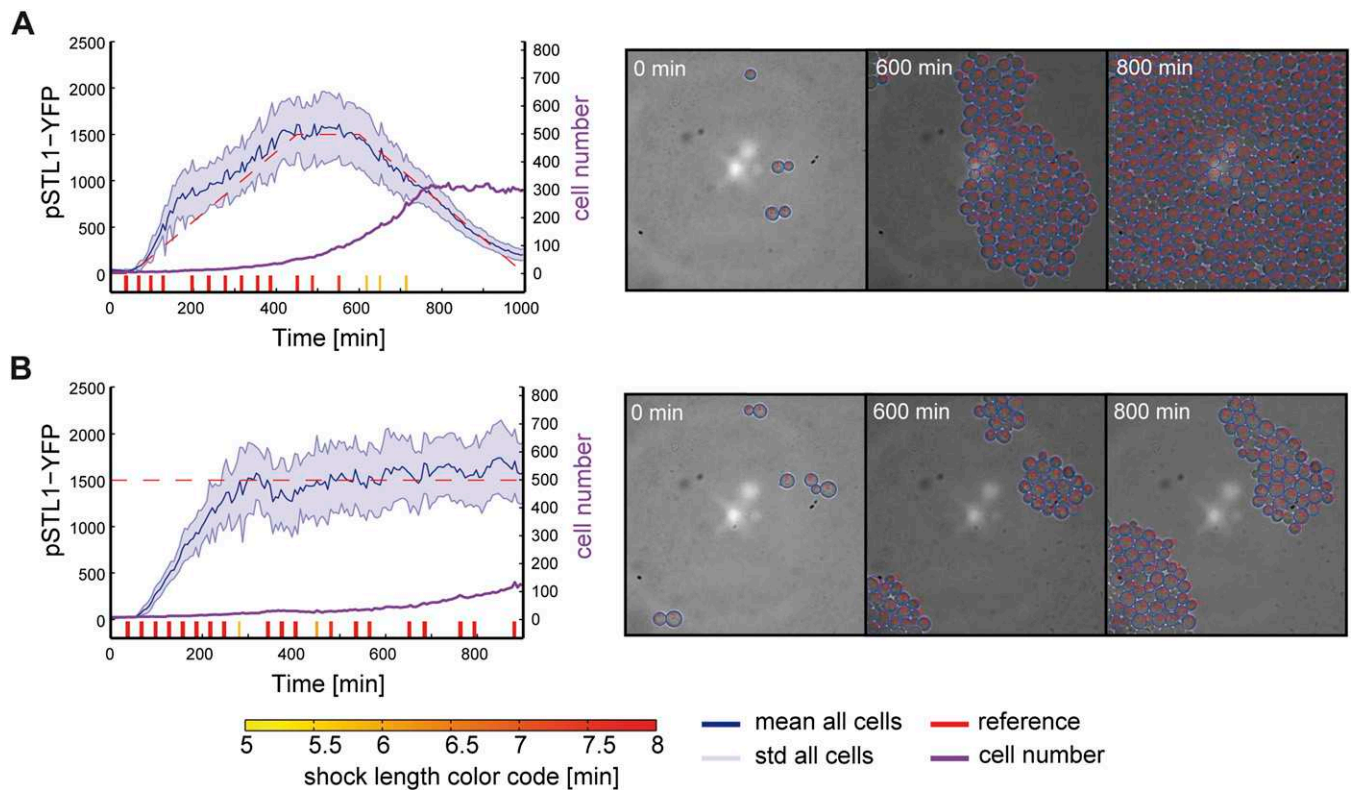


**Fig. S3.** Cell growth during experiments. (A) Cell growth in the field of view. The number of cells detected in the field of view is depicted in violet. In most experiments, the field of view is completely covered with cells after 800–900 min. Cells growing out of the imaging chamber are washed away by the flow, and the number of cells detected in the field of view reaches a plateau (the maximal number of cells in the field of view is around 300). (B) Strong osmotic shocks are known to transiently stop the cell cycle. In this experiment, repeated strong osmotic inputs were applied to reach the target value of 1,500 fluorescence units (f.u.). These inputs led to a slowdown of the cell cycle, and the cells grew slower compared with the experiment shown in A.

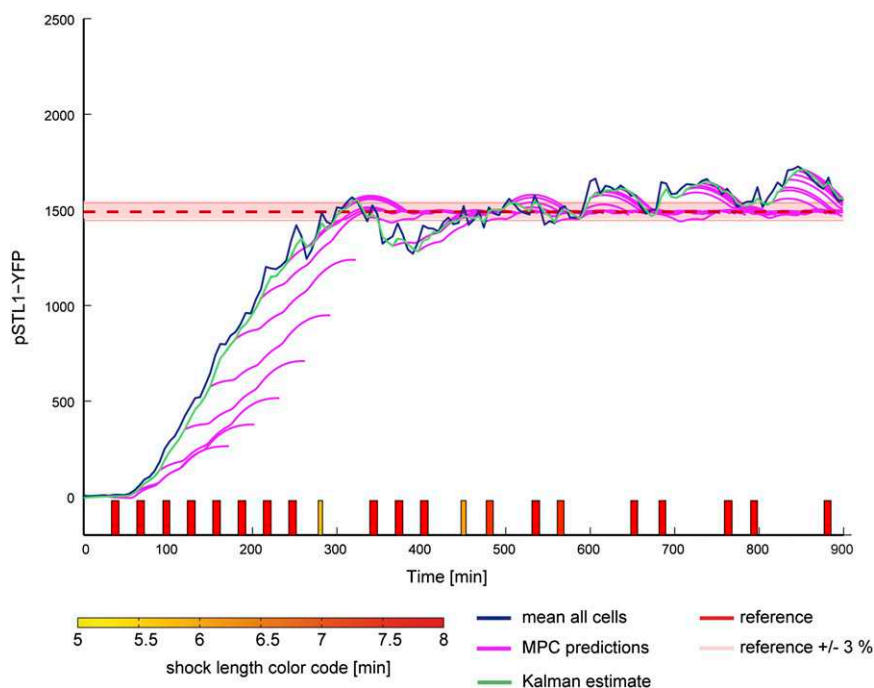


**Fig. S4.** Performance of the model predictive control algorithm. In this plot of the population control experiments from Fig. 2B, the Kalman estimation is indicated as a green line, and the predictions of the best control strategy found at each iteration of the model predictive controller are plotted as violet lines. It shows that good (theoretical) control strategies were found by the controller. Limitations are, therefore, likely to come essentially from model inaccuracies and biological variability. The red envelope around the reference indicates a region close to the reference ( $\pm 3\%$ ).

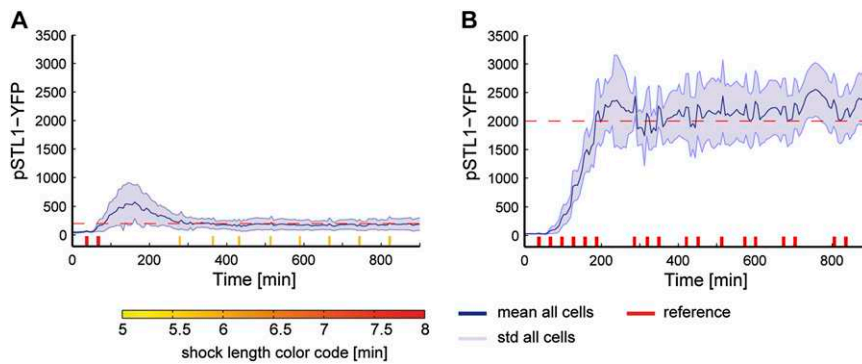


**Fig. S5.** Assessing control capabilities of the proposed platform. We investigated the lower and higher limits for set-point control using the proposed platform. (A) In the first experiment, we set the target value at a very low level: 200 f.u. The control result shows a significant overshoot at the beginning, but after ~300 min, the observed fluorescence level follows the target value faithfully. Lower control objectives are hardly possible with our experimental setting, because these control targets would be within the background fluorescence level of a cell (around 30 f.u.). (B) In the second experiment, we tested the upper limits of the control platform by setting the target value at 2,000 f.u. The control works but shows significant levels of noise. These results show that one can control gene expression within a 10-fold range using the proposed experimental setting.

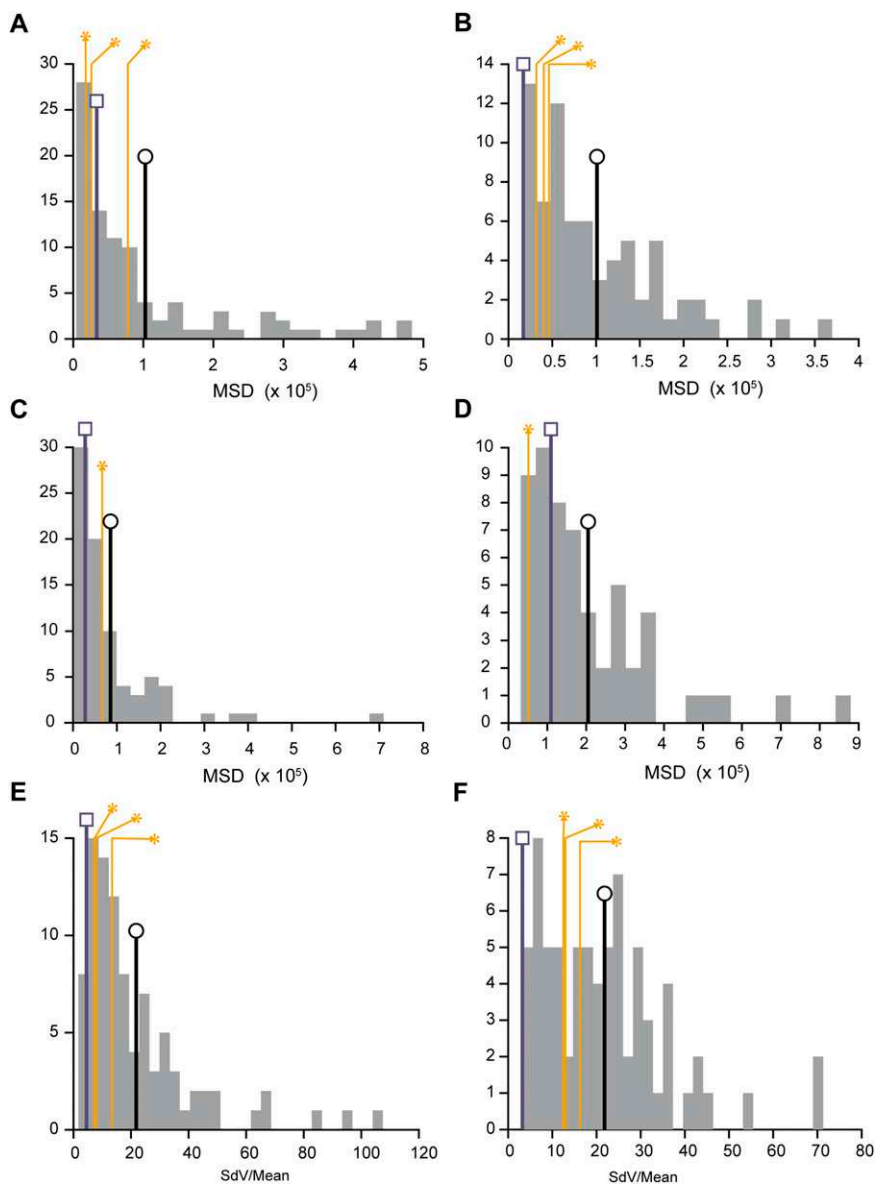


**Fig. S6.** Comparison of the control qualities and the noise levels between single-cell and population control experiments. (A–D) Histograms showing the distribution of single-cell MSDs in population control experiments. MSD of the mean (blue bar, square), mean MSD (black bar, circle), and MSD of the controlled cells in three single-cell control experiments (orange, star). (A) Target control at 1,000 f.u. (B) Target control at 1,500 f.u. (C) Trapeze control (Fig. 2). (D) Sine wave control (Fig. 2). (E and F) Histograms showing the noise levels of single-cell fluorescence in population control experiments. Noise level of the mean (blue bar, square), mean noise level (black bar, circle), and noise levels of the controlled cell in three single-cell control experiments (orange, star). E and F correspond to set-point control experiments at a value 1,000 and 1,500, respectively.

**Table S1. List of parameter values**

Name	Value
$g_1$	$4.02 \cdot 10^{-3}$
$g_2$	37.5
$\tau$	20
$k_2$	0.581
$K$	750

**Table S2. Computation of the  $\dot{U}$  statistic, its associated  $P$  value for MSDs and noise levels, and the two set-point control experiments using the FP test**

Experiment	N1	N2	$\dot{U}$	$P$ value*
MSD, $T = 1,000$ f.u. (Fig. S6A)	92	3	171	0.15
MSD, $T = 1,500$ f.u. (Fig. S6B)	73	3	172	$1.7 \cdot 10^{-7}$
Noise level, $T = 1,000$ f.u. (Fig. S6E)	92	3	202	$3.7 \cdot 10^{-3}$
Noise level, $T = 1,500$ f.u. (Fig. S6F)	73	3	144	$8.5 \cdot 10^{-3}$

N1 and N2 are sample sizes.  
 \*As standard for the FP test, the  $P$  value computation uses the normal approximation.

**SM 1 : Real time yeast population control to a constant target profile**

Long-term model predictive control of gene expression at the population and single-cell levels

J. Uhlendorf, A. Miermont, T. Delaveau, G. Charvin, F. Fages, S. Bottani, G. Batt\* & P. Hersen\*

✉ pascal.hersen@univ-paris-diderot.fr    🔗 <http://tinyurl.com/TeamHersen>  
 ✉ gregory.batt@inria.fr    🔗 <http://www-rocq.inria.fr/~batt/>

UNIVERSITÉ PARIS DIDEROT CIFS Inria

**Movie S1.** Population control I. The target profile is constant ( $T = 1,500$  f.u.).

[Movie S1](#)





**SM 6 : Real time yeast single cell control to a sine wave target profile**

Long-term model predictive control of gene expression at the population and single-cell levels

J. Uhlendorf, A. Miermont, T. Delaveau, G. Charvin, F. Fages, S. Bottani, G. Batt\* & P. Hersen\*

✉ pascal.hersen@univ-paris-diderot.fr    🔗 <http://tinyurl.com/TeamHersen>  
✉ gregory.batt@inria.fr    🔗 <http://www-rocq.inria.fr/~batt/>

PARIS DIDEROT  

Movie S6. Single-cell control II. The target profile is a sine wave.

[Movie S6](#)

**SM 7 : Real time yeast single cell control to a trapeze target profile**

Long-term model predictive control of gene expression at the population and single-cell levels

J. Uhlendorf, A. Miermont, T. Delaveau, G. Charvin, F. Fages, S. Bottani, G. Batt\* & P. Hersen\*

✉ pascal.hersen@univ-paris-diderot.fr    🔗 <http://tinyurl.com/TeamHersen>  
✉ gregory.batt@inria.fr    🔗 <http://www-rocq.inria.fr/~batt/>

PARIS DIDEROT  

Movie S7. Single-cell control III. The target profile is a trapeze.

[Movie S7](#)

## Appended Articles

**Article #3:**

**Severe osmotic compression triggers a slow-down of intracellular signaling which can be explained by molecular crowding.**

Agnès Miermont, François Waharte, Shiqiong Hu, Megan N. McClean, Samuel Bottani, Sébastien Léon and Pascal Hersen

Accepted in PNAS, 2013.

# Severe osmotic compression triggers a slowdown of intracellular signaling, which can be explained by molecular crowding

Agnès Miermont<sup>a</sup>, François Waharte<sup>b</sup>, Shiqiong Hu<sup>c</sup>, Megan Nicole McClean<sup>d</sup>, Samuel Bottani<sup>a</sup>, Sébastien Léon<sup>e</sup>, and Pascal Hersen<sup>a,c,1</sup>

<sup>a</sup>Laboratoire Matière et Systèmes Complexes, Unité Mixte de Recherche (UMR) 7057, Centre National de la Recherche Scientifique (CNRS), Université Paris Diderot, 75013 Paris, France; <sup>b</sup>Biolmaging Cell and Tissue Core Facility (PICT-IBISA), UMR 144, CNRS, Institut Curie, 75005 Paris, France; <sup>c</sup>Mechanobiology Institute, National University of Singapore, Singapore 117411; <sup>d</sup>Lewis-Sigler Institute for Integrative Genomics, Princeton University, Princeton, NJ 08544; and <sup>e</sup>Institut Jacques Monod, CNRS, Université Paris Diderot, 75013 Paris, France

Edited by David A. Weitz, Harvard University, Cambridge, MA, and approved February 15, 2013 (received for review September 4, 2012)

**Regulation of the cellular volume is fundamental for cell survival and function. Deviations from equilibrium trigger dedicated signaling and transcriptional responses that mediate water homeostasis and volume recovery. Cells are densely packed with proteins, and molecular crowding may play an important role in cellular processes. Indeed, increasing molecular crowding has been shown to modify the kinetics of biochemical reactions in vitro; however, the effects of molecular crowding in living cells are mostly unexplored. Here, we report that, in yeast, a sudden reduction in cellular volume, induced by severe osmotic stress, slows down the dynamics of several signaling cascades, including the stress-response pathways required for osmotic adaptation. We show that increasing osmotic compression decreases protein mobility and can eventually lead to a dramatic stalling of several unrelated signaling and cellular processes. The rate of these cellular processes decreased exponentially with protein density when approaching stalling osmotic compression. This suggests that, under compression, the cytoplasm behaves as a soft colloid undergoing a glass transition. Our results shed light on the physical mechanisms that force cells to cope with volume fluctuations to maintain an optimal protein density compatible with cellular functions.**

biophysics | HOG pathway | protein diffusion

The evolutionary adaptations of cells and organisms to specific environments are well characterized. Physiological adaptations to environmental variations are also important for cell survival and growth. Environmental challenges such as changes in temperature, pH, and osmolarity are known to alter cellular function. For example, temperature variations impact protein folding, the kinetics of biochemical reactions, and protein-binding specificities (1). The balance of water activity is a critical requirement for a wide range of cellular functions (2–5). On the one hand, a shift to a lower osmotic environment increases cell volume, threatening the integrity of the cellular membrane (4, 6, 7). To counteract such stress, bacteria and yeast are surrounded by highly resistant cell walls that mechanically protect them from bursting (4). On the other hand, high osmolarity causes water efflux and cell shrinkage (4, 8). In yeast, osmotic shrinkage is completed within a few tens of seconds after exposure to increased osmolarity (9). The final cell volume is set by the mechanical equilibration of external, internal, and turgor pressures (10, 11). Hyperosmotic stress alters a variety of cellular processes, such as disrupting the cytoskeleton structure (12, 13), inducing chromatin remodeling (14, 15), and triggering cell cycle arrest (16, 17) and apoptosis (18, 19). The high-osmolarity glycerol (HOG) pathway of the budding yeast *Saccharomyces cerevisiae* (Fig. 1A) orchestrates adaptation (20) to hyperosmotic shock to ensure water homeostasis and volume recovery, notably through glycerol production (4, 21). Several studies have provided a comprehensive, quantitative understanding of the dynamics of the HOG pathway (9–11, 20, 22–25). Membrane sensors (Sln1p, Msb2p, Hkr1p) are activated by osmotic stress and induce

successive phosphorylation of the HOG mitogen-activated protein kinases (MAPKs), culminating in dual phosphorylation of the Hog1p kinase (4) and leading to the Nmd5p-dependent nuclear import of Hog1p, which accumulates in the nucleus (Fig. 1A) and orchestrates a large transcriptional response.

One of the main physiological changes that occurs immediately after hyperosmotic stress is an increase in the intracellular protein concentrations and the total protein density, thus leading to molecular crowding. This may alter the mobility, folding, stability, and association rates of several proteins inside the cell. Molecular crowding has received little attention in living cells, although it is usually invoked to explain why biochemical reactions rates may vary in vivo and in vitro (26–29). For instance, the diffusion coefficient of the green fluorescent protein is typically 10 times lower in cells than in vitro (30).

Cells are densely packed with proteins. An estimate in yeast gives a typical protein density of a few hundred grams per liter for a volume fraction of typically 20–30%. Osmotically compressed cells will be even more crowded. However, the effects of increasing molecular crowding on cell signaling have not been experimentally investigated and are difficult to predict (1, 26, 28). Increasing the protein concentration increases the probability of protein interactions and protein association rates and may lead to more rapid biochemical kinetics. However, the diffusion of proteins may be reduced in an overcrowded cytoplasm (31, 32), thus slowing down biochemical kinetics.

Changing the cell volume by altering the osmotic pressure is a simple strategy to study the effect of increasing molecular crowding on active processes in living cells. Such strategy can be conveniently applied to yeast, and the HOG pathway is a natural candidate for study. The HOG pathway has been extensively studied in response to gentle and mild osmotic stresses (<1 M sorbitol). In such cases, the stronger the osmotic stimulation, the more potent and longer the duration of Hog1p nuclear localization (4, 11, 20, 24). A preliminary hint of what happens under more severe osmotic stresses, and thus stronger compression, came from a study by Van Wuytswinkel et al., who reported that Hog1p nuclear import and phosphorylation were surprisingly delayed under severe osmotic stress (1.4 M NaCl) (33); however, no satisfying explanation was given for this observation. Delayed nuclear import

Author contributions: A.M., S.L., and P.H. designed research; A.M., F.W., and S.H. performed research; S.H., M.N.M., S.B., S.L., and P.H. contributed new reagents/analytic tools; A.M., F.W., M.N.M., S.B., S.L., and P.H. analyzed data; and A.M. and P.H. wrote the paper.

The authors declare no conflict of interest.

This article is a PNAS Direct Submission.

Freely available online through the PNAS open access option.

<sup>1</sup>To whom correspondence should be addressed. E-mail: pascal.hersen@univ-paris-diderot.fr.

This article contains supporting information online at [www.pnas.org/lookup/suppl/doi:10.1073/pnas.1215367110/-DCSupplemental](http://www.pnas.org/lookup/suppl/doi:10.1073/pnas.1215367110/-DCSupplemental).

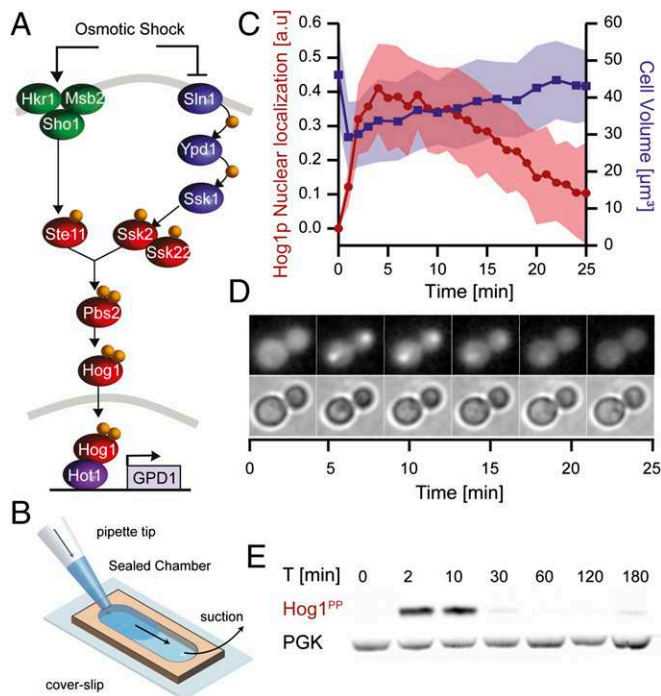


**Fig. 1.** Dynamics of the HOG cascade. (A) HOG cascade. (B) Illustration of the sealed gasket chambers used to experimentally regulate the cells' environment. (C) Osmotic stimulation (1 M sorbitol) induced immediate cell shrinkage (blue curve) followed by nuclear accumulation of Hog1p (red curve). Data are represented as the mean of several cells  $\pm$  1 SD ( $n > 20$ ). Cells progressively recovered their size and switched off the HOG cascade through negative-feedback loops. (D) Nuclear accumulation of Hog1p was rapid and robust after a 1 M sorbitol osmotic stress. (E) Phosphorylation levels of Hog1p after a 1 M sorbitol osmotic stress followed the same pattern with a rapid induction and then a slow decay. Typically, within 30 min, nuclear Hog1p was no longer observed, and Hog1p returned to basal phosphorylation levels. Phosphoglycerate kinase (PGK) was used as a positive control.

and phosphorylation of Hog1p under severe osmotic stress could be attributable to a loss of the activity of a sensor or a kinase, a decrease in the nucleocytoplasmic transport of Hog1p, salt toxicity, or, alternatively, the effects of molecular crowding attributable to osmotic compression, as discussed above. In this article, we set out to address the effects of osmotic compression on signaling dynamics by monitoring several signaling processes in yeast over a range of osmotic stresses.

**Results**

**Both Phosphorylation and Nuclear Import of Hog1p Are Slowed Down During Severe Osmotic Compression.** To study the dynamics of activation of the HOG cascade, we measured changes in the nuclear fluorescence of Hog1p-GFP yeast cells immobilized in a sealed gasket chamber (Fig. 1B). The environment of the cells was rapidly changed (typically in less than 10 s; Fig. S1) from normal yeast media to the same media supplemented with sorbitol. After 1 M sorbitol treatment, Hog1p became phosphorylated and was imported into the nucleus within a few minutes (Fig. 1C–E). The cell volume immediately decreased after osmotic stimulation with 1 M sorbitol and then restored progressively over time (Fig. 1C). The dynamics of Hog1p nuclear translocation and phosphorylation under these conditions were very reproducible and in agreement with the literature (9, 23).

We then studied the behavior of the HOG pathway in response to stronger osmotic stresses (Fig. 2). Both the time taken to observe Hog1p phosphorylation and the time needed to reach maximal Hog1p nuclear localization increased when osmotic compression

increased (Fig. 2). Under gentle stimulation (1 M sorbitol), the maximum nuclear intensity was reached after  $\sim$ 2–3 min, whereas for severe shock ( $\sim$ 1.8 M sorbitol), maximum nuclear intensity was reached after  $\sim$ 55 min (Fig. 2B and F and Movie S1). Thus, increasing the sorbitol concentration from 1 M to 1.8 M reduced the nuclear import rate of Hog1p by one order of magnitude. Similar results were obtained when using NaCl as an osmotic agent (Fig. S2). As the sorbitol concentration increased, the rate of Hog1p phosphorylation also reduced (Fig. 2D) and correlated well with the time taken for nuclear localization of Hog1p to be observed (Fig. 2E and F). Note that Hog1p nuclear translocation was synchronously observed for all cells subjected to osmotic shock lower than 1.8 M sorbitol. However, the proportion of cells that displayed nuclear enrichment of Hog1p quickly decreased when the intensity of osmotic stress increased above 1.8 M sorbitol (Fig. S2). When exposed to 2 M sorbitol, only 25% of the cells displayed nuclear localization of Hog1p, even after several hours of observation; this effect was not related to cell death, because most cells remained viable even after several hours of osmotic treatment (Fig. S3).

**Timing of Hog1p Nuclear Import Is Correlated with the Decrease in Cell Volume.** Cell volume decreased with increasing osmotic stress, reaching a plateau at around 40% of the initial cell volume for sorbitol concentrations above  $\sim$ 2 M (Fig. 2C). This is in

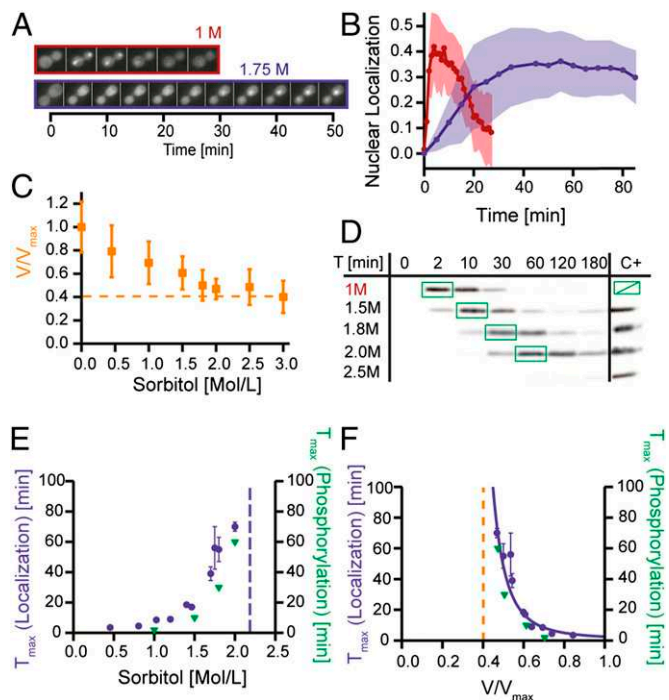


**Fig. 2.** Severe osmotic stress reduces the kinetics of HOG activation and nuclear translocation. (A) Time-lapse imaging of the nuclear localization of Hog1p in cells exposed to 1 M (red) and 1.75 M (blue) sorbitol. (B) The rate of Hog1p nuclear translocation was reduced by severe osmotic shock (red, 1 M sorbitol; blue, 1.75 M sorbitol). Maximal nuclear accumulation was observed  $\sim$ 45–60 min after 1.75 M sorbitol treatment (E). (C) Cell volume decreased with increasing concentrations of sorbitol, down to a plateau at around  $\sim$ 40% of the initial volume. (D) Western blots showing Hog1p phosphorylation over time and under increasing osmotic stress. Phosphorylation of Hog1p after 2 min at 1 M sorbitol is used as a positive control (C+). (E) Time at which the Hog1p nuclear concentration and phosphorylation levels reached a maximum increased with the strength of the osmotic shock. Above 2.2 M sorbitol (blue dashed), no cells displayed nuclear accumulation of Hog1p (Fig. S2). (F) Same data as in E, shown as a function of relative cell volume compression. The blue line is a fit consistent with what is expected for a soft colloid near a glassy transition,  $T = T_0 \frac{V}{V_{max}} e^{\alpha V_{max}/V}$ , where  $T_0 = 0.065$  and  $\alpha = 3.6$ .

agreement with Schaber et al., who proposed the minimum compression volume for yeast cells to be between 33% and 49% of their normal volume (10). The delays in both Hog1p phosphorylation and nuclear translocation correlated with the changes in cell volume: the smaller the cell volume (measured immediately after osmotic stress), the slower the dynamics of Hog1p phosphorylation and nuclear translocation (Fig. 2*F*). More precisely, the timing of Hog1p activation displayed a divergent behavior when the cell volume approached  $V/V_{\max} \approx 0.4$  (Discussion and Fig. S4).

**Diffusion of Hog1p Reduces in Osmotically Compressed Cells.** We conducted fluorescence recovery after photobleaching (FRAP) experiments to investigate whether the reduced rate of Hog1p translocation in a crowded cytoplasm could be explained by a decrease in protein mobility. We used *HOG1-GFP pbs2Δ* cells (Fig. 3 and Movie S2). In a *pbs2Δ* background, the HOG pathway is genetically disrupted, and Hog1p-GFP cannot be phosphorylated or imported into the nucleus. FRAP experiments can thus be performed in any osmotic environment without triggering nuclear enrichment of Hog1p-GFP. We observed that the diffusion of Hog1p-GFP (Fig. 3 and Movie S2) decreased with increasing osmotic compression. Fluorescence recovery took less than a second in isotonic conditions, and around 5 s after a gentle osmotic stress (1 M sorbitol; Fig. S5). We obtained a diffusion coefficient of  $\sim 15 \mu\text{m}^2\cdot\text{s}^{-1}$  in isotonic conditions and  $\sim 1.7 \mu\text{m}^2\cdot\text{s}^{-1}$  after stress with 1 M sorbitol (Fig. S5). However, no recovery after photobleaching was observed after treatment with 2 M sorbitol (Fig. 3*A*), and it was not possible to quantify the diffusion coefficient. Fluorescence loss in photobleaching (FLIP) experiments (Fig. 3*D* and *E*, Fig. S6, and Movie S2) confirmed this result: cells continuously bleached at the same location entirely lost their fluorescence in isotonic conditions, but not after a sudden, severe osmotic stress. Similar results were obtained when using other fluorescently tagged proteins in a wild-type background (Fig. S6). These results are also in good agreement with previous measurements of the effect of molecular crowding on

diffusion (28, 31, 32) and indicate that severe osmotic compression decreases the mobility of Hog1p.

**Nuclear Translocation of Msn2p Is also Delayed During Severe Hyperosmotic Compression.** To further test whether the observed slowdowns in nuclear translation, phosphorylation and protein mobility were specific to components of the HOG pathway, we examined the dynamics of the nuclear translocation of Msn2p (34–36), a key transcription factor in the general stress response of yeast. After hyperosmotic stress, Msn2p is hyperphosphorylated and imported into the nucleus (37). Nuclear import of Msn2p is achieved via a different mechanism to Hog1p; Msn2p contains a nuclear localization signal and does not interact a priori with Nmd5p (36). We nevertheless observed the same scenario as for Hog1p: the rate of nuclear translocation of Msn2p progressively reduced as osmotic compression increased (Fig. 4*A* and *E* and Movie S3); this effect was not dependent on alterations to the dynamics of Hog1p, as a similar behavior was observed in a *hog1Δ* background (Fig. S7).

**Dynamics of the Nuclear Translocation of Yap1p, Crz1p, and Mig1p Are Delayed When Cells Are Osmotically Compressed.** We further tested the nuclear-translocation dynamics of transcription factors that are not specifically activated by osmotic stress: Yap1p, Crz1p, and Mig1p (Fig. 4 and Movies S4, S5, and S6). Yap1p is involved in the oxidative stress response and contains a nuclear localization signal but is constantly exported from the nucleus by Crm1p (38). The addition of 300  $\mu\text{M}$  hydrogen peroxide ( $\text{H}_2\text{O}_2$ ) triggers oxidation of the cysteine residues in Yap1p, leading to a conformational change that blocks its nuclear export by Crm1p. Hence, Yap1p accumulates in the nucleus upon oxidative stress. The transcription factor Crz1p is a cytoplasmic protein involved in the regulation of calcium ion homeostasis. Upon stimulation with calcium, Crz1p is dephosphorylated and imported into the nucleus (39). In the presence of glucose, Mig1p is dephosphorylated by the Reg1p-Glc7p protein phosphatase complex and imported into the nucleus, where it binds to the promoters of glucose-repressed genes (40).

In the following experiments, the objective was to reduce the cell volume using severe hyperosmotic shock and, simultaneously, to activate and measure the nuclear translocation of these transcription factors. We applied a dual input of a severe hyperosmotic shock and a stimulus of either 300  $\mu\text{M}$   $\text{H}_2\text{O}_2$  (Yap1p), 200 mM  $\text{Ca}^{2+}$  (Crz1p), or 2% (wt/wt) glucose, which were added to cells initially grown in galactose (Mig1p). In isotonic conditions, Crz1p localized to the nucleus within a few minutes of the addition of  $\text{Ca}^{2+}$  (Fig. 4*B*). This burst of nuclear translocation was delayed by several minutes when the cells were stimulated with  $\text{Ca}^{2+}$  in combination with severe hyperosmotic shock (1.4 M sorbitol; Fig. 4*B* and *F*). Interestingly, Crz1p was also partially activated to undergo nuclear translocation by mild osmotic stress alone (Fig. 4*B*); this effect may be attributable to variations in the internal calcium concentration following cell shrinkage. Note that when stimulated by a severe hyperosmotic stress alone, the dynamics of Crz1p nuclear translocation was also slowed down, in agreement with our hypothesis that increasing osmotic compression reduces the rate of intracellular signaling (Fig. 4*B*). Similarly, we observed a marked reduction in the rate of nuclear import of Yap1p (Fig. 4*C* and *G*) and Mig1p (Fig. 4*D* and *H*) when the cells were both stimulated and osmotically compressed; these slowdowns became more pronounced with increasing volumetric compression (Fig. 4*J* and Fig. S4). Taken together, these results suggest that a nonspecific slowdown in the kinetics of nuclear translocation occurs when cellular volume is reduced through a severe osmotic compression.

**Dynamics of Endocytosis and Vesicular Trafficking Are Reduced During Osmotic Shock.** To gain further insight into the effect of osmotic compression, we investigated the effects of osmotic compression on the dynamics of three additional processes. We

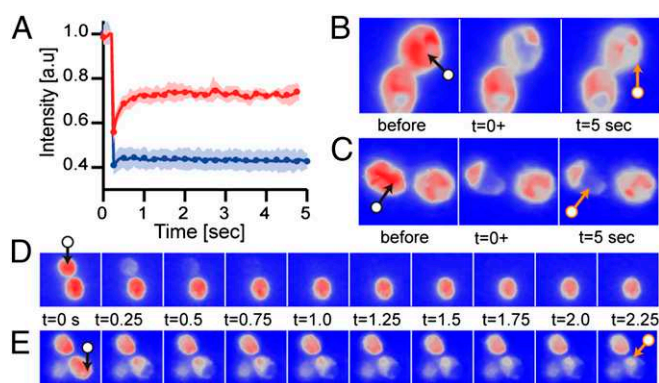


**Fig. 3.** Diffusion of Hog1p-GFP in the cytoplasm is decreased by osmotic compression. (A) FRAP experiments on the *HOG1-GFP pbs2Δ* strain in SC medium (red curve) and after 2 M sorbitol stress (blue curve). (B) FRAP images of *HOG1-GFP pbs2Δ* cells in SC medium before bleaching (Left), immediately after bleaching (Center), and 5 s later (Right). The bleached area is indicated by the black arrow, and its recovery is indicated by the orange arrow. (C) FRAP images of a *HOG1-GFP pbs2Δ* cell in a severe osmotic environment (2 M sorbitol). In contrast to B, the bleached area did not recover after 5 s. (D) FLIP time series for a *HOG1-GFP pbs2Δ* cell in SC medium. The same spot was continuously bleached (black arrow), and total cell fluorescence rapidly decreased compared with the unbleached neighboring cell. (E) After severe osmotic compression, the cell maintained some cytoplasmic fluorescence over a long time (orange arrow), indicating that the diffusion of fluorescent protein was very limited. Pictures are color-coded to improve visualization (blue for low intensity and red for high intensity).

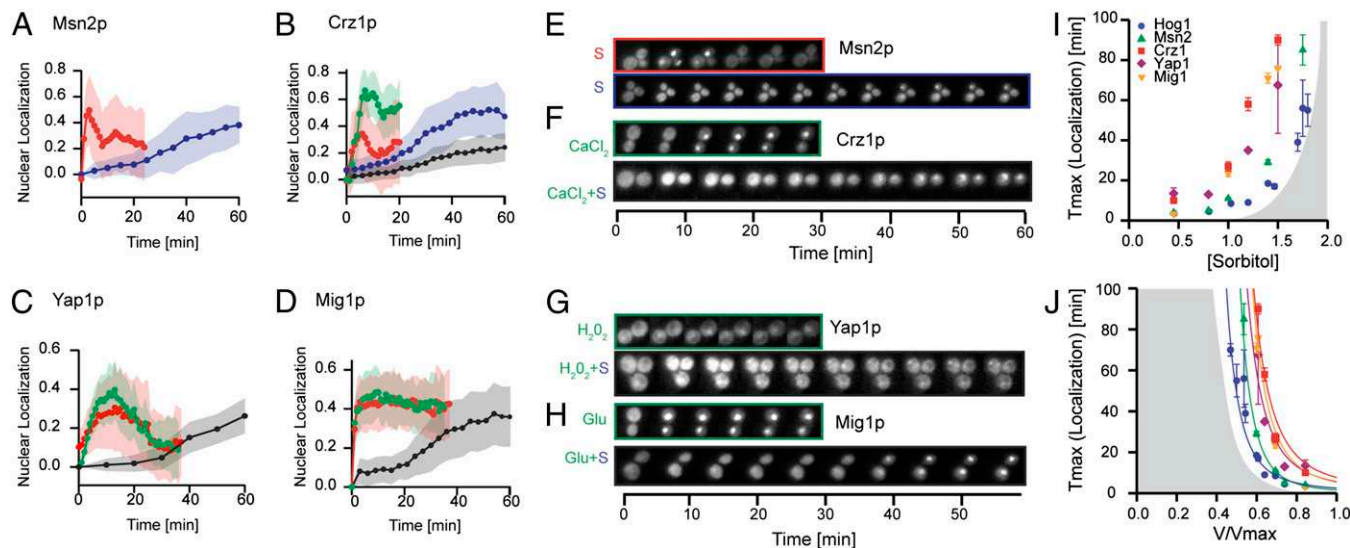


**Fig. 4.** Several signaling cascades are delayed when the cell volume is suddenly decreased by osmotic compression. (A) Nuclear localization of Msn2p in response to gentle osmotic stress (0.45 M sorbitol, red) and severe osmotic stress (1.75 M sorbitol, blue). (B) Nuclear localization of Crz1p in response to calcium shock (200 mM, green), gentle osmotic stress (0.45 M sorbitol, red), severe osmotic stress (1.75 M sorbitol, blue), and combined calcium shock and severe volume reduction by osmotic stress (200 mM  $\text{Ca}^{2+}$  plus 1.4 M sorbitol, black). (C) Nuclear localization of Yap1p in response to oxidative stress (300  $\mu\text{M}$   $\text{H}_2\text{O}_2$ , green), oxidative stress and gentle osmotic compression (300  $\mu\text{M}$   $\text{H}_2\text{O}_2$  plus 0.45 M sorbitol, red), and combined oxidative stress and severe osmotic stress ( $\text{H}_2\text{O}_2$  plus 1.4 M sorbitol, black). (D) Nuclear localization of Mig1p in response to glucose (20 g/L, green), combined glucose and gentle osmotic stress (glucose plus 0.45 M sorbitol, red), and combined glucose and severe osmotic stress (glucose plus 1.4 M sorbitol, black). Cells were precultured in galactose without glucose. For A–D, data are represented as the mean of many cells ( $n > 20$ )  $\pm$  1 SD. (E–H) Time-lapse images of the nuclear localization of Msn2p (E), Yap1p (F), Crz1p (G), and Mig1p (H). “S” indicates sorbitol, and the concentrations used and color code are the same as for A–D. (I and J) Measurement of the time to reach maximum nuclear localization of Msn2p (sorbitol), Yap1p ( $\text{H}_2\text{O}_2$ ), Crz1p ( $\text{Ca}^{2+}$ ), Mig1p (glucose), and Hog1p (sorbitol) as a function of either the additional sorbitol concentration used (I) or the relative cell volume (J). The curves fit the function  $T = T_0 \frac{V}{V_{\text{max}}} e^{\alpha V_{\text{max}}/V}$  that models the behavior of a soft colloid. For Msn2p,  $T_0 = 0.035$  and  $\alpha = 3.9$ ; for Crz1p,  $T_0 = 0.096$  and  $\alpha = 4.4$ ; for Yap1p,  $T_0 = 0.077$  and  $\alpha = 4.3$ ; for Mig1p,  $T_0 = 0.043$  and  $\alpha = 4.8$ .

first analyzed the mobility of the protein Abp1p, an actin-binding protein that dynamically partitions between the plasma membrane and endosomes under normal conditions (41). After sudden and severe osmotic stress (3 M sorbitol), Abp1p patches suddenly stopped their random motion (Fig. S8 and Movie S7). We also examined Sec7p, which is involved in protein transport and is found in the cytoplasm and Golgi-associated coated vesicles (42). The mobility of Sec7p was drastically impaired by osmotic compression (Fig. S8 and Movie S8). Finally, using a tracer of bulk endocytosis, the fluorescent dye FM4-64 (43), we observed that the active internalization and transport of vesicles stalled after sudden osmotic compression (Fig. S8).

**Signaling Dynamics Quickly Recover When Cell Volume Is Restored.** If the reductions observed in the dynamics of cell signaling were only attributable to a reduction in cell volume, the cells should be able to recover their normal signaling activity upon the restoration of cell volume. Hence, we investigated signaling dynamics after the recovery of cell volume, as illustrated in Fig. 5A. Hog1p-GFP or Msn2p-GFP cells were subjected to a severe osmotic stress and then returned to a less hyperosmotic environment, to relax the osmotic compression (Fig. 5B and C). We did not return the cells to isotonic conditions, because we wanted to determine whether Hog1p and Msn2p translocated to the nucleus, which does not happen in isotonic conditions. Whereas cells did not show any nuclear localization during the first 5 min of severe osmotic stress, marked, rapid localization of Hog1p and Msn2p became visible when the cells were returned to a less hyperosmotic environment (1 M sorbitol). Thus, the cells were still alive and could function properly as soon as the osmotic clamp was mechanically relaxed. Similar experiments were performed for Crz1p, Mig1p, and Yap1p (Fig. 5D–F). Initially, in the presence of severe osmotic stress, the cells did not display any localization activity for any of these pathways. However, relaxation of the osmotic constraint led to the rapid

activation of these pathways. Therefore, although decreasing the cell volume inhibited the signal-processing ability of the cells, their signal-processing ability was recovered as soon as the cell volume was restored.

**Discussion**

Taken together, our experiments demonstrate that severe osmotic compression drastically reduces the rate of several dynamic processes in living cells. Reducing the volume of yeast cells led to a lower diffusion coefficient and slower rates of Hog1p phosphorylation and nuclear import. The dynamics of the nuclear translocation of other transcription factors (Yap1p, Crz1p, Msn2p, and Mig1p) were similarly delayed by osmotic compression. Importantly, release of the osmotic clamp on the cells led to a rapid recovery of signaling. Each of the proteins tested is activated by a different process (phosphorylation, dephosphorylation, and oxidation) and undergoes nuclear import via a different mechanism, and yet the kinetics of their nuclear translocation displayed a similar dependence on osmotic compression. In addition, the kinetics of actin-binding protein mobility, vesicular trafficking, and endocytosis were also reduced by osmotic compression. These observations argue in favor of a general, nonspecific, physical slowdown process.

The cytoplasm is a dense assembly of proteins in a liquid, namely a colloid. Interestingly, when a colloid becomes too dense, its relaxation dynamics are dramatically slowed down, and its viscosity increases dramatically. Similarly, if the cytoplasm becomes too crowded, it becomes very difficult for proteins to diffuse, and their mobility drastically reduces. Zhou et al. (44) recently demonstrated that higher eukaryotic cells behave as soft colloids: colloids made of deformable particles. During the glassy transition of soft colloids, the viscosity diverges exponentially with the colloid volume fraction,  $\phi$  (45). Assuming that the diffusion coefficient of a protein,  $D$ , scales as the inverse of the cytoplasmic viscosity, and that the rates of diffusion limited reactions scale with  $\phi D$ , the

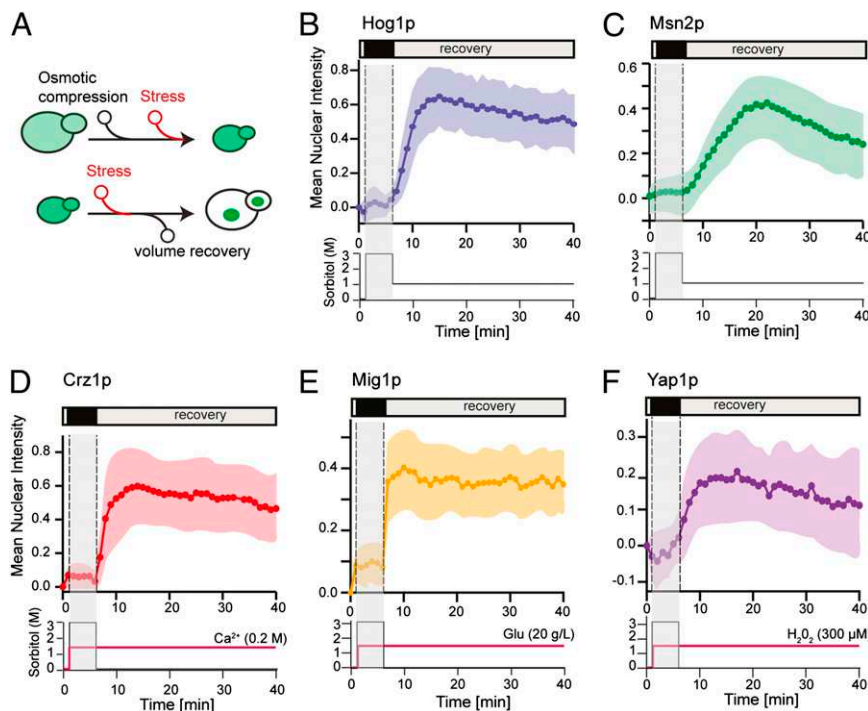


**Fig. 5.** Signaling-cascade dynamics are immediately restored upon recovery of the cell volume. (A) Principle of signaling activation by volume recovery. Cells are stressed and, at the same time, osmotically compressed by severe osmotic stress (3 M sorbitol). The osmotic compression was then relaxed by a return to a lower osmotic stress conditions, and we investigated whether the cells could detect and respond to the chemical stress that was still present in the cells' environment. (B–F) Time courses of the nuclear localization of Hog1p (B), Msn2p (C), Crz1p (D), Mig1p (E), and Yap1p (F) under these experimental conditions. As soon as the volume of the cell was restored, the studied signaling cascades could function normally, as indicated by nuclear localization of their respective transcription factors.

typical timescale of a diffusion limited reaction should scale as  $e^{c\phi}/\phi$ . This scaling is in good agreement with our measurements (see the fitting curve in Figs. 2F and 4J and Fig. S4). This suggests that osmotically compressed yeast cells behave as soft colloids and undergo a glassy transition under too-severe compression. This also supports our hypothesis that osmotic compression leads to a decrease in the mobility of proteins in the cytoplasm, because of an increase in molecular crowding. Our results emphasize the importance of molecular crowding, induced by hyperosmotic compression in our experiments, in determining the kinetics of biochemical reactions within cells.

Recently, Dill et al. (1) outlined that cellular function should be analyzed within the context of the mechanical and thermodynamic constraints exerted by the environment. Dill et al. argued that an optimal protein density must exist, which originates from the competition between the two counteracting effects discussed at the beginning of this article: increasing molecular crowding enhances the rate of biochemical reactions but only up to the point where the negative effects of molecular crowding on protein diffusion become dominant. Our results in living cells support this view. We hypothesize that the size of cells was determined by evolution, so that cells usually function at a protein density that enables them to resist mild and sudden changes in osmolarity. Thus, the total protein density is likely to be smaller than the optimum proposed by Dill et al., because cells with too high of a protein density would be at risk for the complete arrest of key cellular processes upon sudden osmotic shock: a behavior obviously not favored by evolution. Our results outline why the protein density, or the cell volume, must be regulated in order for cells to function properly. We propose that the effects of molecular crowding should be taken into account when considering the biological (gene networks, signaling) and physical (cellular mechanics) properties that constrain cellular dynamics.

## Materials and Methods

**Yeast Strains and Maintenance.** Cultures were maintained in YPD medium [1% yeast extract (Difco; 0127-17), 2% Bacto Peptone (Difco; 0118-17), 2% glucose (VWR; 24379.294)] or in Synthetic Complete (SC) medium (0.67% yeast nitrogen base without amino acids; Fisher; W1706W), 2% glucose (VWR; 24379.294), and 0.08% Complete Supplement Mixture dropout mixture (MP Biomedicals; 114500012). Cells were grown overnight at 30 °C in SC, reinoculated into fresh SC, and grown at 30 °C for 4–6 h before microscopy. See Tables S1 and S2 for details on the yeast strains. Details on the preparation of protein extracts and Western blotting are given in SI Materials and Methods.

**Sudden Osmotic Stimulation.** Perfusion chamber gaskets from Invitrogen (4 chambers, 19 mm × 6 mm, 80 μL; C-18128) were used as an inexpensive and simple system to switch the cells from one environment to another. A solution of Con A (2 mg/mL; MP Biomedicals; 2150710.2) was added into the chamber, and, after 15 min of incubation, yeast cells were injected and allowed 10–15 min to adhere to the coverslip before starting the experiment.

**Microscopy and Image Analysis.** The cells were observed using an Olympus IX81 inverted fluorescent microscope with a QuantEM 5125C camera and a 100×/1.40 NA immersion oil objective. GFP emission was visualized at 528 nm (38-nm bandwidth) upon excitation at 490 nm (20-nm bandwidth); mCherry was visualized at 617 nm (73-nm bandwidth) upon excitation at 555 nm (28-nm bandwidth). Images were acquired using MetaMorph software (Molecular Devices), and image analysis was performed with ImageJ (46). The fluorescence intensity of transcription factors in the nucleus was obtained by measuring the intensity of GFP colocalized with the nuclear marker Htb2p-mCherry. We removed the background from the GFP channel (rolling ball method with a radius of 200 pixels), applied a Gaussian blur (1 pixel) to reduce noise, found a threshold to separate the cells from the background (Otsu thresholding), and segmented the cells using the “analyze particles” and “watershed” plugins of ImageJ. We computed the relative nuclear intensity as  $[GFP(\text{nucleus}) - GFP(\text{cytoplasm})]/GFP(\text{cytoplasm})$  and renormalized all cells by subtracting the value for first measurement performed before osmotic compression. The area of the cell was measured by fitting ellipses to the contour of the cells. From the cell area, we computed the equivalent cell volume assuming that cells are spheres with

a radius  $r = (\text{area}/\pi)^{1/2}$ . We measured the relative volume for each cell using  $V/V_{\text{max}}$  in which  $V_{\text{max}}$  is the volume of the cell before osmotic compression.

**FRAP and FLIP Experiments.** FRAP and FLIP experiments were performed at the Nikon Imaging Centre of the Institut Curie. Experiments were performed at 30 °C on a total internal reflection fluorescence Nikon Eclipse Ti inverted fluorescent microscope equipped with a QuantEM 512SC camera, and a 100× 1.45 NA immersion oil objective. The emission filter wavelength was 525 nm, and the excitation filter was 470 nm. For bleaching, we used a 491-nm pulse generated by a FRAP 4D module (Roper). A cytoplasmic area of typically 2 μm in diameter was photo-bleached by a 50-ms laser pulse. A single focal plane was then recorded every 50 ms with a 50-ms exposure time. FLIP experiments were performed using the same system; however, the images were recorded every 250 ms. FRAP images were denoised using the ND-Safir software on 10 cells for each condition. This procedure, developed by Boulanger et al.

(47), improves the signal to noise ratio and is crucial for the quantitative analysis of FRAP data. Once denoised, the images were normalized by the fluorescence intensity of the bleached area just before the bleach. Additional FRAP experiments were performed using a spinning disk microscope at the Mechanobiology Institute of Singapore (Fig. S6 C, D, F, and G).

**ACKNOWLEDGMENTS.** We thank J. Uhlendorf, G. Batt, G. Charvin, S. Rutherford, C. Dargemont, and J.-M. Di Meglio for insightful discussions on and critical reading of the manuscript. We also thank J. Salamero for advice on the “FRAP 4D module” and the FRAP/FLIP experiments, and the Nikon Imaging Center of the Institut Curie. A.M. is a student of the Frontiers of Living Systems doctoral program. We acknowledge the support of the Agence Nationale de la Recherche (DISIP-ANR-07-JCJC-0001 and ICEBERG-ANR-10-BINF-06-01), the C’Nano(ModEnv) program, the “Who am I?” Laboratory of Excellence (ANR-11-LABX-0071 and ANR-11-IDEX-0005-01), the Mechanobiology Institute, and the Laboratoire International Associé Cell Adhesion France-Singapour (CAFS).

1. Dill KA, Ghosh K, Schmit JD (2011) Physical limits of cells and proteomes. *Proc Natl Acad Sci USA* 108(44):17876–17882.
2. Strange K (2004) Cellular volume homeostasis. *Adv Physiol Educ* 28(1-4):155–159.
3. Ho SN (2006) Intracellular water homeostasis and the mammalian cellular osmotic stress response. *J Cell Physiol* 206(1):9–15.
4. Hohmann S (2002) Osmotic stress signaling and osmoadaptation in yeasts. *Microbiol Mol Biol Rev* 66(2):300–372.
5. Häussinger D (1996) The role of cellular hydration in the regulation of cell function. *Biochem J* 313(Pt 3):697–710.
6. Grant WD (2004) Life at low water activity. *Philos Trans R Soc Lond B Biol Sci* 359(1448):1249–1266.
7. Lang F, et al. (1998) Functional significance of cell volume regulatory mechanisms. *Physiol Rev* 78(1):247–306.
8. Petelenz-Kurdziel E, et al. (2011) Quantification of cell volume changes upon hyperosmotic stress in *Saccharomyces cerevisiae*. *Integr Biol (Camb)* 3(11):1120–1126.
9. Hersen P, McClean MN, Mahadevan L, Ramanathan S (2008) Signal processing by the HOG MAP kinase pathway. *Proc Natl Acad Sci USA* 105(20):7165–7170.
10. Schaber J, et al. (2010) Biophysical properties of *Saccharomyces cerevisiae* and their relationship with HOG pathway activation. *Eur Biophys J* 39(11):1547–1556.
11. Klipp E, Nordlander B, Krüger R, Gennemark P, Hohmann S (2005) Integrative model of the response of yeast to osmotic shock. *Nat Biotechnol* 23(8):975–982.
12. Chowdhury S, Smith KW, Gustin MC (1992) Osmotic stress and the yeast cytoskeleton: Phenotype-specific suppression of an actin mutation. *J Cell Biol* 118(3):561–571.
13. Slaninová I, Sesták S, Svoboda A, Farkas V (2000) Cell wall and cytoskeleton reorganization as the response to hyperosmotic shock in *Saccharomyces cerevisiae*. *Arch Microbiol* 173(4):245–252.
14. Kültz D, Chakravarty D (2001) Maintenance of genomic integrity in mammalian kidney cells exposed to hyperosmotic stress. *Comp Biochem Physiol A Mol Integr Physiol* 130(3):421–428.
15. Mas G, et al. (2009) Recruitment of a chromatin remodelling complex by the Hog1 MAP kinase to stress genes. *EMBO J* 28(4):326–336.
16. Escoté X, Zapater M, Clotet J, Posas F (2004) Hog1 mediates cell-cycle arrest in G1 phase by the dual targeting of Sic1. *Nat Cell Biol* 6(10):997–1002.
17. Clotet J, et al. (2006) Phosphorylation of Hsl1 by Hog1 leads to a G2 arrest essential for cell survival at high osmolarity. *EMBO J* 25(11):2338–2346.
18. Silva RD, et al. (2005) Hyperosmotic stress induces metacaspase- and mitochondria-dependent apoptosis in *Saccharomyces cerevisiae*. *Mol Microbiol* 58(3):824–834.
19. Galvez A, et al. (2001) A rapid and strong apoptotic process is triggered by hyperosmotic stress in cultured rat cardiac myocytes. *Cell Tissue Res* 304(2):279–285.
20. Muzzey D, Gómez-Urbe CA, Mettetal JT, van Oudenaarden A (2009) A systems-level analysis of perfect adaptation in yeast osmoregulation. *Cell* 138(1):160–171.
21. Miermont A, Uhlendorf J, McClean MN, Hersen P (2011) The Dynamical Systems Properties of the HOG Signaling Cascade. *J Signal Transduct* 2011:930940.
22. O’Rourke SM, Herskowitz I (2004) Unique and redundant roles for HOG MAPK pathway components as revealed by whole-genome expression analysis. *Mol Biol Cell* 15(2):532–542.
23. Mettetal JT, Muzzey D, Gómez-Urbe C, van Oudenaarden A (2008) The frequency dependence of osmo-adaptation in *Saccharomyces cerevisiae*. *Science* 319(5862):482–484.
24. Zi Z, Liebermeister W, Klipp E (2010) A quantitative study of the Hog1 MAPK response to fluctuating osmotic stress in *Saccharomyces cerevisiae*. *PLoS ONE* 5(3):e9522.
25. Pelet S, et al. (2011) Transient activation of the HOG MAPK pathway regulates bimodal gene expression. *Science* 332(6030):732–735.
26. Minton AP (2001) The influence of macromolecular crowding and macromolecular confinement on biochemical reactions in physiological media. *J Biol Chem* 276(14):10577–10580.
27. Ellis RJ (2001) Macromolecular crowding: Obvious but underappreciated. *Trends Biochem Sci* 26(10):597–604.
28. Zhou H-X, Rivas G, Minton AP (2008) Macromolecular crowding and confinement: Biochemical, biophysical, and potential physiological consequences. *Annu Rev Biophys* 37:375–397.
29. Schoen I, Kramer H, Braun D (2009) Hybridization kinetics is different inside cells. *Proc Natl Acad Sci USA* 106(51):21649–21654.
30. Konopka MC, Shkel IA, Cayley S, Record MT, Weisshaar JC (2006) Crowding and confinement effects on protein diffusion in vivo. *J Bacteriol* 188(17):6115–6123.
31. Dorsaz N, De Michele C, Piazza F, De Los Rios P, Foffi G (2010) Diffusion-limited reactions in crowded environments. *Phys Rev Lett* 105(12):120601.
32. Roosen-Runge F, et al. (2011) Protein self-diffusion in crowded solutions. *Proc Natl Acad Sci USA* 108(29):11815–11820.
33. Van Wuytswinkel O, et al. (2000) Response of *Saccharomyces cerevisiae* to severe osmotic stress: Evidence for a novel activation mechanism of the HOG MAP kinase pathway. *Mol Microbiol* 37(2):382–397.
34. Garreau H, et al. (2000) Hyperphosphorylation of Msn2p and Msn4p in response to heat shock and the diauxic shift is inhibited by cAMP in *Saccharomyces cerevisiae*. *Microbiology* 146(Pt 9):2113–2120.
35. Beck T, Hall MN (1999) The TOR signalling pathway controls nuclear localization of nutrient-regulated transcription factors. *Nature* 402(6762):689–692.
36. Görner W, et al. (1998) Nuclear localization of the C2H2 zinc finger protein Msn2p is regulated by stress and protein kinase A activity. *Genes Dev* 12(4):586–597.
37. Capaldi AP, et al. (2008) Structure and function of a transcriptional network activated by the MAPK Hog1. *Nat Genet* 40(11):1300–1306.
38. Delaunay A, Isnard AD, Toledano MB (2000) H2O2 sensing through oxidation of the Yap1 transcription factor. *EMBO J* 19(19):5157–5166.
39. Polizzotto RS, Cyert MS (2001) Calcineurin-dependent nuclear import of the transcription factor Crz1p requires Nmd5p. *J Cell Biol* 154(5):951–960.
40. Nehlin JO, Carlberg M, Ronne H (1991) Control of yeast GAL genes by MIG1 repressor: A transcriptional cascade in the glucose response. *EMBO J* 10(11):3373–3377.
41. Kaksonen M, Sun Y, Drubin DG (2003) A pathway for association of receptors, adaptors, and actin during endocytic internalization. *Cell* 115(4):475–487.
42. Franzusoff A, Redding K, Crosby J, Fuller RS, Schekman R (1991) Localization of components involved in protein transport and processing through the yeast Golgi apparatus. *J Cell Biol* 112(1):27–37.
43. Vida TA, Emr SD (1995) A new vital stain for visualizing vacuolar membrane dynamics and endocytosis in yeast. *J Cell Biol* 128(5):779–792.
44. Zhou EH, et al. (2009) Universal behavior of the osmotically compressed cell and its analogy to the colloidal glass transition. *Proc Natl Acad Sci USA* 106(26):10632–10637.
45. Mattsson J, et al. (2009) Soft colloids make strong glasses. *Nature* 462(7269):83–86.
46. Rasband WS (1997–2012) ImageJ (National Institutes of Health, Bethesda). Available at <http://imagej.nih.gov/ij/>. Accessed December 18, 2012.
47. Boulanger J, et al. (2010) Patch-based nonlocal functional for denoising fluorescence microscopy image sequences. *IEEE Trans Med Imaging* 29(2):442–454.

# Supporting Information

Miermont et al. 10.1073/pnas.1215367110

## SI Materials and Methods

For western blotting and protein extract, cells were grown in appropriate synthetic medium to  $OD_{600} = 1$ . They were collected by filtration and then stressed with different sorbitol concentrations (1–2.5 M) for the indicated time period. To prepare protein extracts, cultures were rapidly suspended in 10% trichloroacetic acid (Sigma; T0699) and maintained in ice for at least 10 min. Cells were centrifuged, and maximum supernatant was discarded to leave around 100  $\mu$ L in the tubes. Cells were broken by bead-beating the samples (10 min at 4 °C) with glass beads (425–600  $\mu$ m) (Sigma; G8772). The samples were centrifuged, the supernatant was discarded, and the pellet was resuspended in SDS buffer (1 $\times$  NuPage buffer, 10%  $\beta$  mercaptoethanol, and 200 mM Tris) to a final volume of 100  $\mu$ L. Samples were loaded on 10% SDS/PAGE NuPage

precast gel (Invitrogen; NP0315BOX) in 1 $\times$  NuPage running buffer (Invitrogen; NP0001) and run at 180 V for 1 h. Proteins were transferred to PVDF membranes (Invitrogen; LC2005) at 30 V at 4 °C overnight. Dual phosphorylation of Hog1p on Thr-174 and Tyr-176 was examined in a Western blot analysis using an anti-dually phosphorylated p38 antibody 1:1,000 (Cell Signaling Technologies; 9211L), and the positive control was examined using phosphoglycerate kinase monoclonal primary antibody 1:1,000 (Invitrogen; 22C5D8). Goat anti-rabbit-HRP secondary antibodies (Jackson ImmunoResearch; 111-035-003) were used at a dilution of 1:10,000. Antibody binding was visualized using ECL-plus system (Amersham; GE RPN2132) in a Fujifilm LAS 4000 imaging system. Membranes were stripped between both primary antibodies using 62.5 mM Tris-HCl (pH 6.8) with 2% SDS.

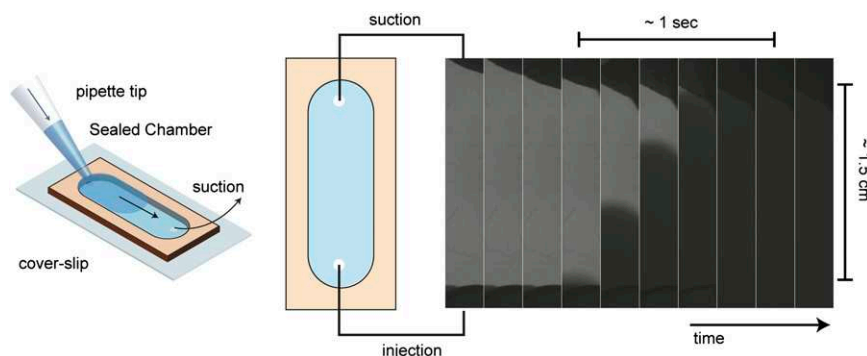


**Fig. S1.** Quick exchange of fluids in a gasket sealed chamber. Using a pipette at one inlet of the gasket and a paper filter (black area at the top) at the outlet to generate a flow, it is possible to replace the entire volume of liquid contained in the chamber within a few seconds. The actual time it takes to replace water (light gray) with a liquid containing a dye (seen as a dark gray area rising vertically) is of the order of 1 s (there is 0.2 s between each images). A few additional seconds are required to get the pipette and the filter correctly aligned with the inlet and outlet of the gasket chamber. In practice, one needs typically 10 s to complete this operation.

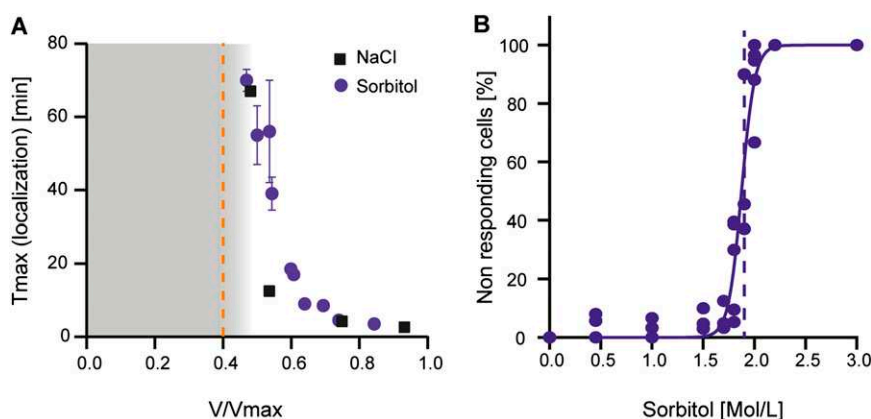


**Fig. S2.** Additional data regarding Hog1p slowdown by osmotic compression. (A) Both NaCl and sorbitol triggered similar slowdown of the HOG cascade when plotted as a function of the relative cell volume variation. (B) For mild osmotic stresses (<1.5 M sorbitol), all cells eventually displayed a Hog1p nuclear localization. However, there was an abrupt transition around 2 M sorbitol, above which almost no cells displayed Hog1p nuclear translocation, even after more than 2 h of observation. Fitting the data with a sigmoid gave a transition at around 1.9 M sorbitol, for which 50% of the cells were not responsive.

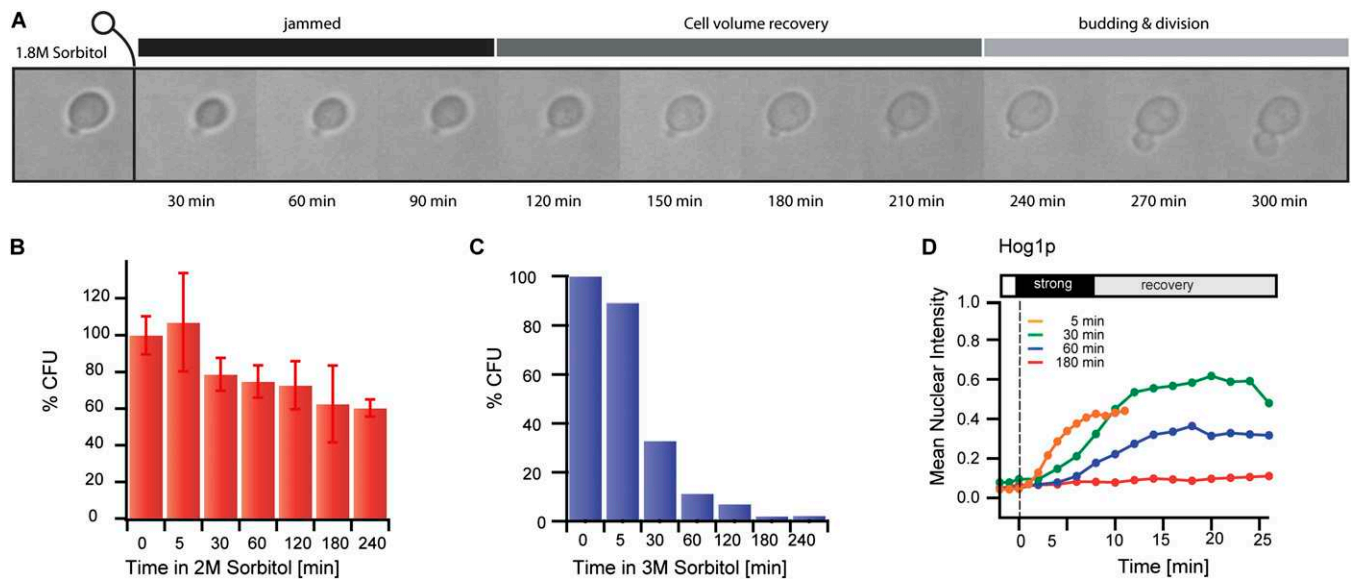


**Fig. 53.** Prolonged exposure to severe osmotic stress. (A) Cells can adapt to severe osmotic stress. Upon 1.8 M sorbitol stress, cells appear jammed at first. It took several hours for cells to eventually adapt and divide. We did not image cells for longer than ~4 h (the medium has to be changed very regularly to avoid artifacts caused by evaporation), and, thus, we did not observe cell adaptation and recovery for 2 M sorbitol shocks. However, cells can survive and adapt to such strong shocks as shown by colony-forming unit experiments. (B and C) We counted the number of colony-forming units on plates that were seeded after different periods of exposure to 2 or 3 M sorbitol. In both cases, short exposure (5 min) resulted in a high survival rate. For long exposure to 2 M sorbitol stress, the survival rate was of the order of 50%. (C) The survival rate was much lower in the case of very severe 3 M sorbitol shock. (D) Therefore, we were careful not to let the cells stay for too long in 3 M sorbitol when we performed the experiments of volume compression and recovery shown in Fig. 4. To illustrate its short-term effect on cell signaling, we applied a very severe stress (3 M sorbitol) for increasing periods of time (from 5 min to 3 h) before changing the environment back to yeast synthetic medium supplemented with 1 M sorbitol. The average dynamics of nuclear translocation of Hog1-GFP was slower and slower even if the proportion of responding cells was larger than 90% for stress shorter than 1 h. After a too-long exposition to 3 M sorbitol (>1 h), cells were unable to recover and only very few cells showed some localization (~15%). It is tempting to hypothesize that the progressive loss of efficiency in Hog1p dynamics and cell death after a too-long exposure are attributable to the arrest of internal maintenance and homeostatic processes when cells are severely osmotically compressed.

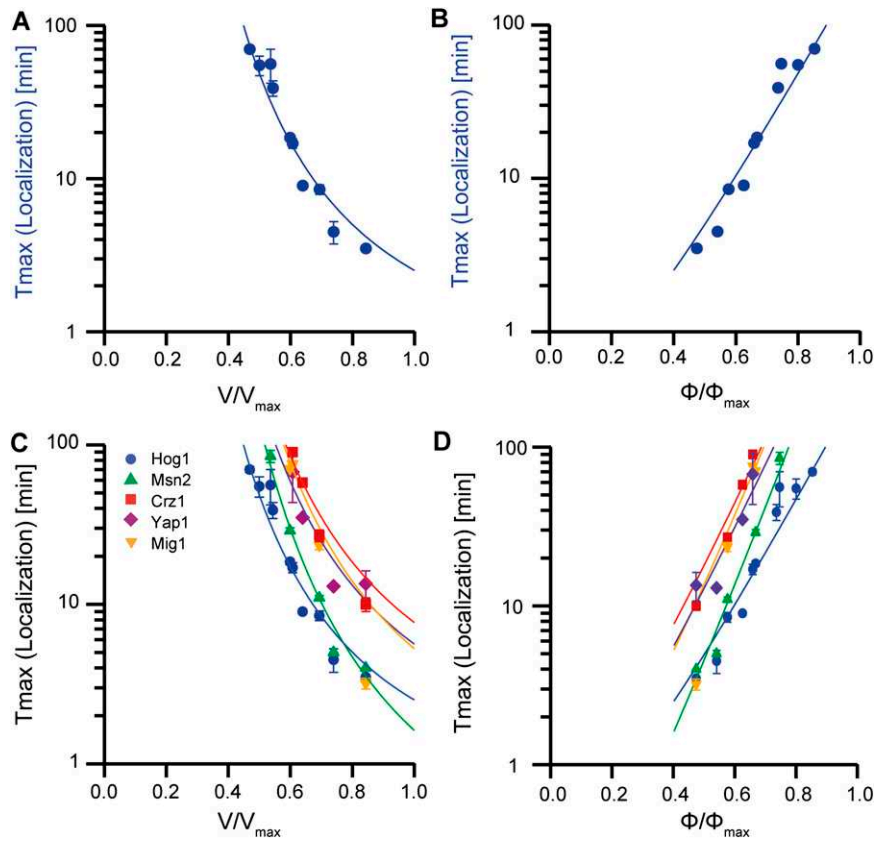


**Fig. 54.** Logarithmic plots of the signaling dynamics. This figure is based on data shown in Figs. 2F and 4J. A and C show  $\log(T_{\max})$  and the corresponding fits in function of the relative volume variation  $V/V_{\max}$ . B and D show  $\log(T_{\max})$  as a function of the relative protein density. The protein relative density,  $\phi/\phi_{\max}$ , is defined as the inverse of  $V/V_{\max}$  and normalized so that its maximum is 1 (arbitrary choice). Assuming that the cytoplasm behaves as a soft colloid, one expects to observe an exponential increase of the viscosity with the protein density:  $\eta \sim \exp(\alpha\phi)$ . Here, we do not have access to the viscosity. To link our measurements to the theoretical prediction of a soft colloid glassy transition, we assume that the diffusion coefficient of proteins vary inversely proportionally to the viscosity [as in Dill et al. (1)]. Further assuming that the rates of diffusion limited kinetics scales as  $r \sim D\phi$ , we obtain  $T_{\max} \sim 1/r \sim 1/\phi \exp(\alpha\phi)$  or, alternatively,  $T_{\max} \sim V \exp(\alpha/V)$ . The fit functions are in agreement with an exponential increase of the viscosity of the cytoplasm with the protein density as it would be the case for a soft colloid near a glassy like transition.

1. Dill KA, Ghosh K, Schmit JD (2011) Physical limits of cells and proteomes. *Proc Natl Acad Sci USA* 108(44):17876–17882.

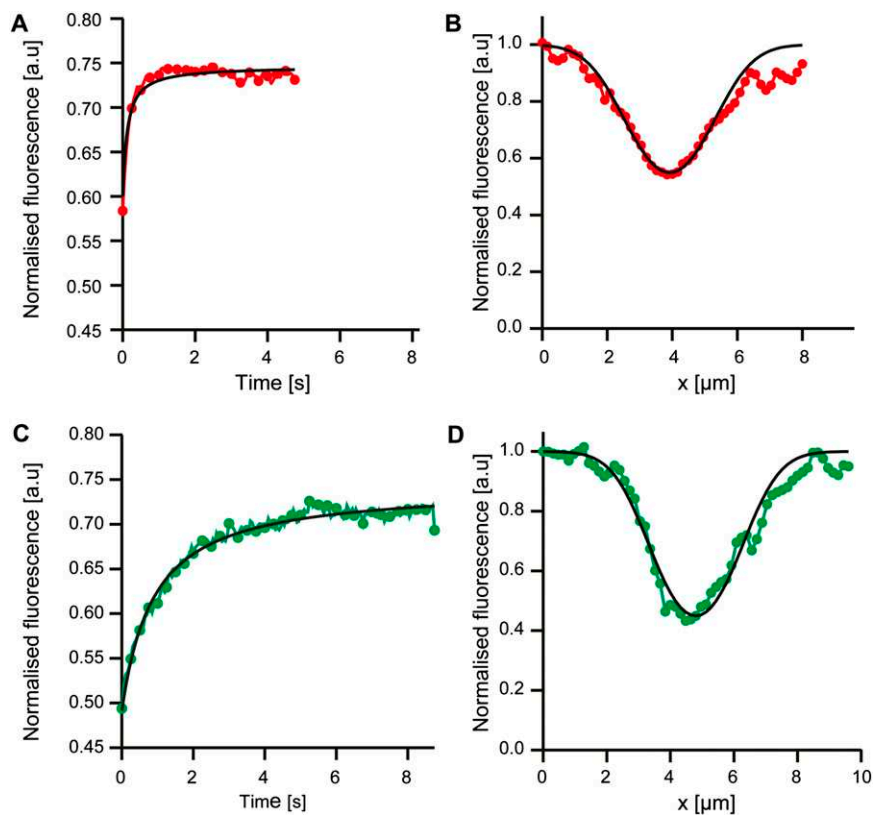


**Fig. S5.** Fluorescence recovery after photobleaching of Hog1p-GFP; *pbs2Δ* cells. (A and B) Fluorescence recovery after photobleaching (FRAP) experiments performed in Synthetic Complete (SC) medium. (A) Average profile of fluorescence recovery over six cells. (B) Transverse section of the averaged photobleached area for one cell, illustrating the size of the bleached area. (C and D) Same results but for 10 cells stimulated by a gentle osmotic shock (SC supplemented with 1 M sorbitol). Note that in both conditions, the size of the bleached area is large enough ( $\sim 1.8 \mu\text{m}$  theoretically,  $\sim 2.4 \mu\text{m}$  in practice) to prevent fluorescence recovery to the initial fluorescence value [1 in arbitrary unit (a.u.)]. It is then difficult to estimate with precision a diffusion coefficient. To estimate the diffusion coefficient, we first extracted the average Gaussian bleached fluorescent profile. Then we determined the characteristic time of diffusion ( $\tau$ ) from fluorescence recovery curves (Fig. 3 and Fig. S3). The coefficient of diffusion,  $D$ , was then estimated by taking into account that particles will diffuse over the bleached area radius,  $w_m$ , in the typical time  $\tau$  with a diffusion coefficient  $D = w_m^2/4\tau$ . From the FRAP data made in normal growth conditions (SC medium; Fig. 3 and Fig. S5), we obtained  $\tau = 0.091 \text{ s}$ ,  $w_m = 2.4 \mu\text{m}$ , and, thus,  $D = 15.8 \mu\text{m}^2\cdot\text{s}^{-1}$ . From the FRAP data made in SC supplemented with 1 M sorbitol, we found  $\tau = 0.85 \text{ s}$ ,  $w_m = 2.4 \mu\text{m}$ , and, thus,  $D = 1.7 \mu\text{m}^2\cdot\text{s}^{-1}$ . We were not able to measure it for severe osmotic stress because diffusion was apparently stalled (Fig. 3 and Fig. S6).

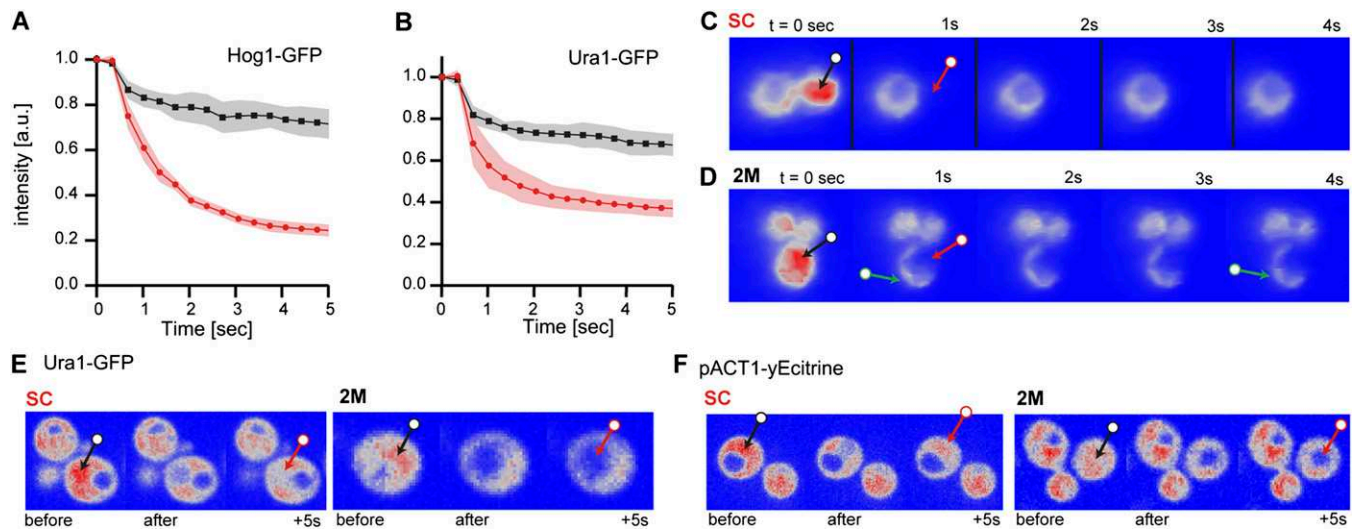


**Fig. S6.** Additional FRAP/fluorescence loss in photobleaching (FLIP) experiments. (A) FLIP data corresponding to the images shown in Fig. 3C for a Hog1-GFP, *pbs2Δ* background. Whereas the fluorescence is quickly lost outside of the continuously bleached spot (red curve) in isotonic conditions, some fluorescence remains visible outside of the bleached spot when the cell is osmotically stressed with 2 M sorbitol (black curve; see also Fig. 3). (B) FLIP data acquired on the fluorescent protein Ura1p-GFP (isotonic conditions, red; 2 M sorbitol stress, black). Severe osmotic stress led to a drastically reduced protein mobility (see also E). (C and D) Image time series of a FLIP experiment using a URA1-GFP strain. Note the green arrows that show that a residual fluorescence can be seen outside of the bleached area after a severe osmotic stress but not in isotonic conditions. (E and F) FRAP experiments using the Ura1p-GFP protein and the fluorescent protein yEctrine constitutively expressed. The difference of dynamics between isotonic and hyperosmotic conditions is obvious. Images are taken before, immediately after, and 5 s after the bleach. The arrows show the approximate location of the bleach. Whereas the bleached spot recovers (partially) its fluorescence in isotonic conditions, there is no recovery of fluorescence for strongly osmotically compressed cells, and the bleached, dark spot remains as if fluorescent proteins were “frozen.” This again shows that there is a drastic loss of protein mobility in osmotically compressed cells.

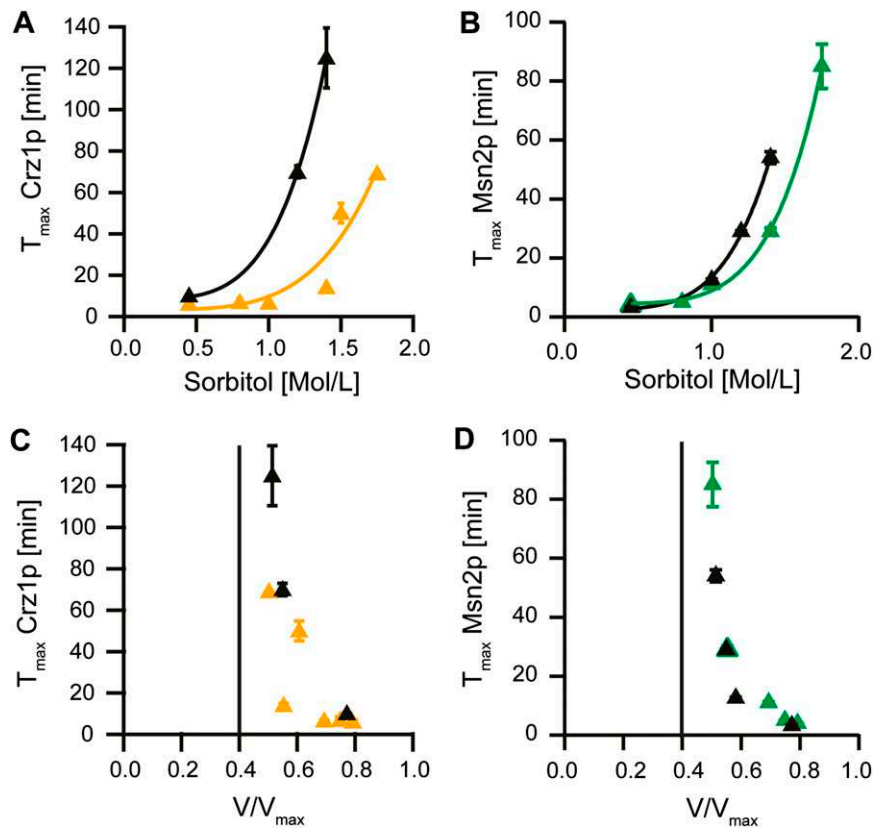


**Fig. S7.** Crz1p and Msn2p dynamics in a *hog1Δ* background. (A) We measured Crz1p nuclear-translocation dynamics in a *hog1Δ* strain (black) and compared it to a *HOG1* strain (yellow). (B) We also compared Msn2p nuclear-translocation dynamics in a *hog1Δ* strain (black) and in a *HOG1* strain (green). Both experiments showed that the slowdown is more pronounced in a *hog1Δ* strain when studied as a function of the sorbitol concentration. Because Hog1p is a key regulator of cell size regulation and cell wall integrity, it is likely that in a *hog1Δ* strain, a difference in turgor, internal osmolarity, cell wall composition, or initial cell size may be responsible for a different osmotic compressibility. Importantly, the *hog1Δ* mutant appears to behave as a *HOG1* strain when plotted in function of the volume variation (C and D). This is in agreement with our findings that pointed out the relevance of volume compression: the absolute value of the osmotic stress is not relevant here.

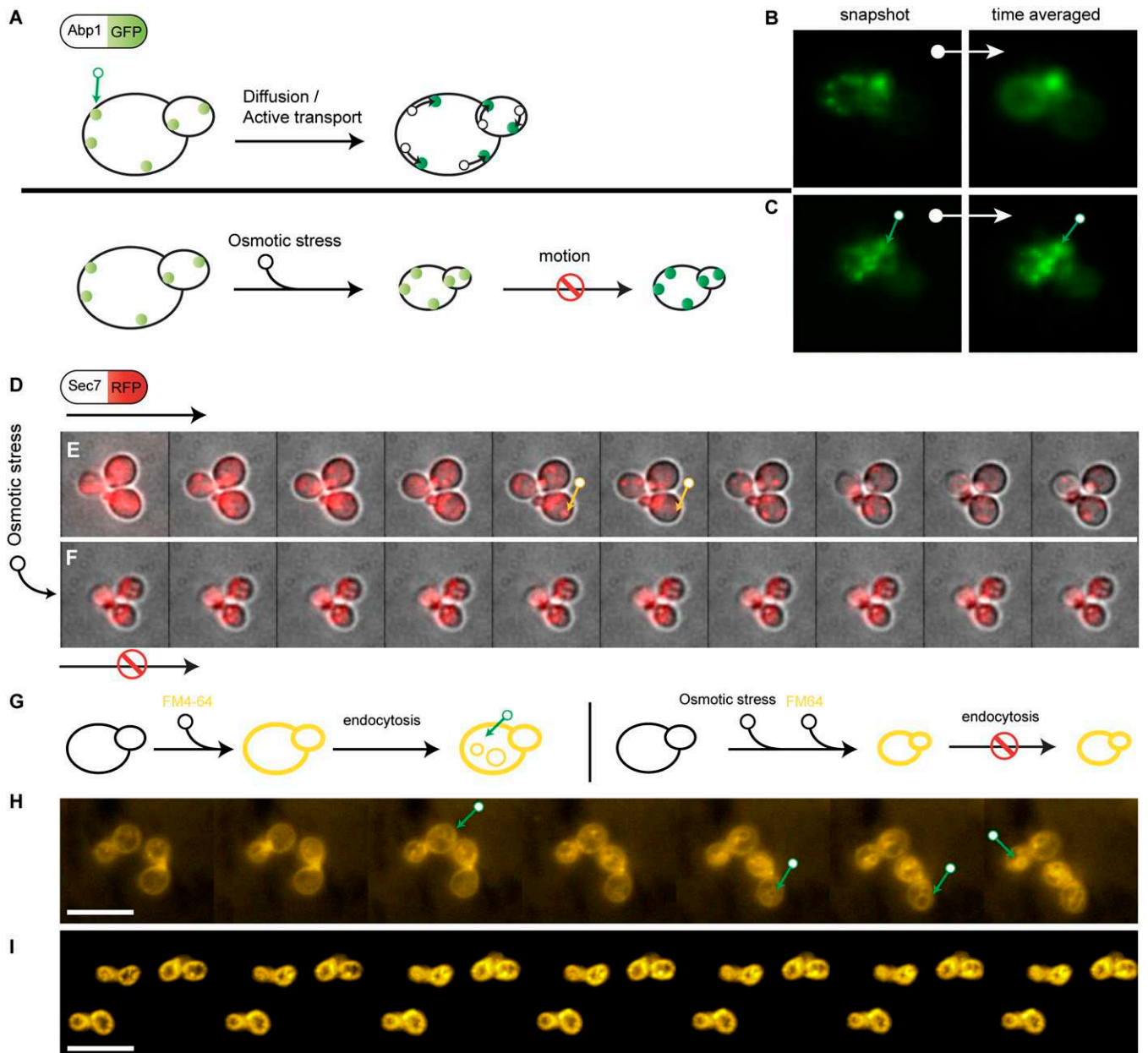


**Fig. S8.** Osmotic compression slows down Abp1p mobility, Sec7p transport, and endocytosis. (A) When Abp1p-GFP is observed by fluorescence, it displays a number of moving bright dots. As illustrated here, the effect of a sudden hyperosmotic compression is to freeze Abp1p motion. (B) Typical snapshot of Abp1p localization pattern (*Left*). The punctuated pattern is lost when averaging over time (40 min), evidencing Abp1p diffusion (*Right*). (C) Typical snapshot of Abp1p localization (*Left*; same cell as in B) after an osmotic compression (3 M sorbitol). Because the cells are in a “frozen state” (see *Results*), averaging over time does not change the localization pattern of Abp1p (see also [Movie S7](#)). (D) Sec7p is also a mobile protein that can be seen as bright dots in epifluorescence. (E and F) The dynamics of Sec7p-mCherry (E) were immediately arrested after osmotic compression by 3 M sorbitol (F). See also [Movie S8](#). (G) Endocytosis can be observed in live cells using the membrane binding dye FM4-64. (H) We observed vesicles formation and motion in normal condition (green arrows point to a few examples). (I) After a severe osmotic compression (3 M sorbitol), no FM4-64 internalization was observed, and the endocytosis appeared as if jammed.

**Table S1. List of relevant strains used in this study**

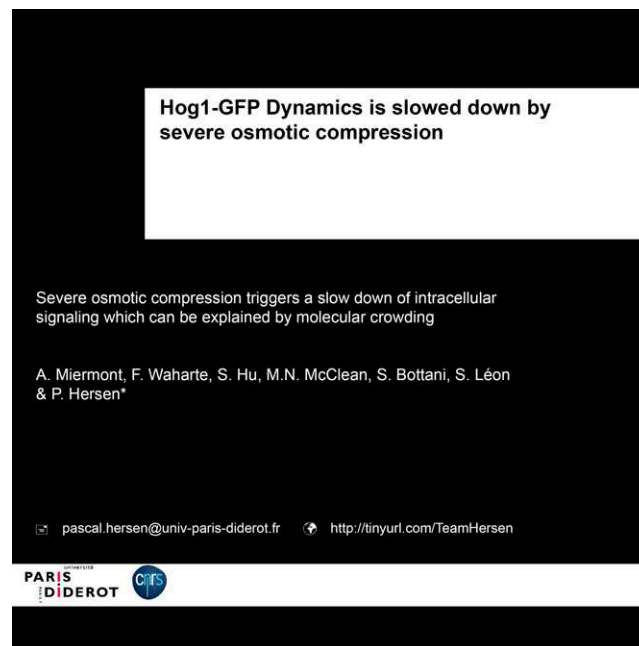
Name	Background	Genotype	Source
yPH015	BY4742	<i>HOG1-GFP-HIS3 HTB2-mCherry-URA3</i>	Hersen et al. (1)
yPH016	yPH15	<i>HOG1-GFP-HIS3 HTB2-mCherry-URA3 pbs2Δ-Kan</i>	Hersen et al. (1)
yPH033	BY4741	<i>MSN2-GFP-HIS3MX6 HTB2-mCherry-KanMX4</i>	This study
yPH069	BY4741	<i>CRZ1-GFP-HIS3MX6 HTB2-mCherry-KanMX4</i>	This study
yPH107	BY4741	<i>MIG1-GFP-HIS3MX6 HTB2-mCherry-KanMX4</i>	This study
yPH082	BY4742	<i>YAP1-GFP-HIS3</i> + plasmid pRS316-mCherry	F. Devaux, Université Pierre et Marie Curie, Paris
yPH114	BY4741	<i>ABP1-GFP-HIS3</i>	S.L. laboratory
yPH115	BY4741	<i>SEC7-mCherry_KanMX4</i>	S.L. laboratory

1. Hersen P, McClean MN, Mahadevan L, Ramanathan S (2008) Signal processing by the HOG MAP kinase pathway. *Proc Natl Acad Sci USA* 105(20):7165–7170.

**Table S2. List of relevant plasmids**

Name	Genotype	Source
pRS316-mCherry	URA3 CEN6 ARSH4 <i>mCherry</i>	F. Devaux, Université Pierre et Marie Curie, Paris
pFA6-hphNT1	<i>hphNT1</i>	PCR-toolbox Collection (1) (EUROSCARF)
pYM35	<i>DsRed1 KanMX4</i>	PCR-Toolbox Collection (1) (EUROSCARF)
pFA6-HIS3MX6	<i>HIS3MX6</i> marker for gene deletion	EUROSCARF
pYM35-mCherry	C-terminal tagging with mCherry, <i>KanMX4</i> marker	S.L. laboratory

1. Janke C, et al. (2004) A versatile toolbox for PCR-based tagging of yeast genes: New fluorescent proteins, more markers and promoter substitution cassettes. *Yeast* 21(11):947–962.



**Movie S1.** Hog1p activity in function of osmotic compression. Differential Hog1p-GFP nuclear translocation of yeast cells subjected to either 1 or 1.75 M sorbitol stress. The dynamics of translocation are slower in the case of a severe osmotic stress.

[Movie S1](#)



**Crz1-GFP Dynamics is slowed down by severe osmotic compression**

Severe osmotic compression triggers a slow down of intracellular signaling which can be explained by molecular crowding

A. Miermont, F. Waharte, S. Hu, M.N. McClean, S. Bottani, S. Léon & P. Hersen\*

✉ pascal.hersen@univ-paris-diderot.fr 🌐 <http://tinyurl.com/TeamHersen>

PARIS DIDEROT CITE

**Movie S4.** Crz1p activity in function of osmotic compression. Differential Crz1p-GFP nuclear translocation of yeast cells stimulated with  $\text{Ca}^{2+}$  alone or together with an osmotic compression. The dynamics of translocation are slower in the case of a severe osmotic compression.

[Movie S4](#)

**Yap1-GFP Dynamics is slowed down by severe osmotic compression**

Severe osmotic compression triggers a slow down of intracellular signaling which can be explained by molecular crowding

A. Miermont, F. Waharte, S. Hu, M.N. McClean, S. Bottani, S. Léon & P. Hersen\*

✉ pascal.hersen@univ-paris-diderot.fr 🌐 <http://tinyurl.com/TeamHersen>

PARIS DIDEROT CITE

**Movie S5.** Yap1p activity in function of osmotic compression. Differential Yap1p-GFP nuclear translocation of yeast cells stimulated with  $\text{H}_2\text{O}_2$  alone or together with an osmotic compression. The dynamics of translocation are slower in the case of a severe of osmotic compression. Note that Yap1p-GFP does not show a very bright nuclear localization and photobleaches quickly.

[Movie S5](#)









---

**TITLE:** SEVERE OSMOTIC COMPRESSION OF THE YEAST *SACCHAROMYCES CEREVISIAE*

**SUMMARY:** Cells have developed several signaling pathways and transcriptional regulatory networks to regulate their size and coordinate their growth with the cell division. Importantly, the interior of a cell is naturally packed with macromolecules and is said to be crowded. Macromolecular crowding has been intensely studied *in vitro* and is known to affect the kinetics of reactions. However, studying the effects of crowding *in vivo* is more challenging due to the high level of complexity and heterogeneity in the cytoplasm. In this thesis, we address the effects of changing the cellular volume on the kinetics of biochemical reactions in live *Saccharomyces cerevisiae* cells. We osmotically compressed yeast cells, thus increasing the total macromolecular density and investigated the impact of such crowding on the kinetics of signal transduction. Cell shrinkage is expected to increase the intracellular viscosity and may severely slow down the functioning of signaling pathways and cellular processes. Indeed, by progressively increasing the level of compression, we recorded a progressive slow-down of several, unrelated biological processes until a point for which cell dynamics were arrested. This was observed for the nuclear translocation of several transcription factors (Hog1, Msn2, Crz1, Mig1, and Yap1) as well as for the mobility of the proteins Abp1 and Sec7. We further showed that increasing compression decreases the ability of proteins to diffuse in both yeast and higher eukaryotic cells. We propose that this slowing down upon cellular compression is very general and is reminiscent of a soft colloidal glassy-like transition. Our results suggest the importance for cells to regulate their volume and their cytoplasmic crowding to function properly.

**KEY WORDS:** Biophysics, HOG pathway, yeast *Saccharomyces cerevisiae*, protein diffusion, macromolecular crowding, glass transition,

---